

https://dspace.org/

Preparation of magnetic nano-composite-beads and their application to remediation of Cr(VI) and U(VI) from acid mine drainage

Tavengwa, Nikita Tawanda

2013-08-07
http://hdl.handle.net/10539/13011

Downloaded from a DSpace repository. https://dspace.org/

Preparation of magnetic nano-composite-beads and their application to remediation of Cr(VI) and U(VI) from acid mine drainage



By

Nikita Tawanda Tavengwa

A dissertation submitted to the Faculty of Science, University of the Witwatersrand, Johannesburg, in fulfilment of the requirements for the degree of Master of Science

WITS University, Johannesburg, 2013

DECLARATION

I declare that this research is my own, unaided work. It is being submitted for the Degree of Master of Science at the University of the Witwatersrand, Johannesburg. It has not been submitted before for any degree or examination at any other University.



……
(Signature of Candidate)

23th April 2013
……..Day of.....

ABSTRACT

Occurring parallel to the developments in imprinting technology are magnetic materials which are being applied increasingly in environmental remediation, medicine, biotechnology and many other fields. Combining the imprinting effects of the polymer and nano magnetic particles yields composite materials which are both selective to the template and magneto responsive for easy polymer removal from aqueous solutions.

In this study, magnetic ion imprinted polymers with high recognition for uranyl ion (UO_2^{2+}) in the presence of competing ions were synthesized by bulk and precipitation polymerizations. The uranyl template was removed from the magnetic polymer matric by 1M HCl and 1M $NaHCO_3$ leachants to form cavities which were complimentary in shape and size to the template. Full characterization of the magnetite and magnetic polymers was achieved by use of the following characterization techniques: Raman spectroscopy (RS), Transmission electron microscopy (TEM), Energy dispersive spectrometry (EDS), Powder X-ray diffraction (PXRD) analysis, Brunauer, Emmett and Teller (BET) analysis, Ultraviolet visible (UV-vis) spectroscopy, Fourier-transform infrared (FTIR), Thermo-gravimetric analysis (TGA), Carbon, hydrogen, nitrogen and sulphur (CHNS) analysis, Diffuse reflectance spectroscopy (DRS) and Atomic force microscopy (AFM). Parameters which were optimized included sample pH, which gave an optimum value of 4. Magnetic IIP and NIP amounts which gave maximum adsorption capacities were found to be 50 mg for both of these adsorbents. The optimum contact time was found to be 45 minutes. The performance of all magnetic ion imprinted polymers (IIPs) was expectedly superior to that of the corresponding non imprinted polymers (NIPs) in all adsorption studies. The first rate constant (k_1) and correlation coefficient (R^2) values evaluated for the pseudo first order were found to be between 0.048-0.093 min^{-1} and 0.602-0.991 min^{-1}, respectively. For the pseudo second order, second rate constant (k_2) and correlation coefficient (R^2) were found to be between 0.273-0.678 and 0.9811-0.9992, respectively. The selectivity order observed was as follows: $UO_2^{2+} > Fe^{3+} > Pb^{2+} > Ni^{2+} > Mg^{2+}$.

The magnetic polymers selective to Cr(VI) were also synthesized and were leached with HCl to remove the template. The synthesized Cr(VI) magnetic polymers, the optimum pH obtained was 4 for both the magnetic IIP and the corresponding NIP. The amount of the adsorbent which gave the maximum adsorption was determined to be 20 and 65 mg for the magnetic IIP and NIP, respectively. A Cr(VI) concentration which was adsorbed maximally was from 5 mg L^{-1} which was therefore taken as the optimum. The maximum adsorption capacities for the magnetic polymers were 6.20 and 1.87 mg g^{-1} for the magnetic IIP and NIP, respectively. The optimum time for the adsorption of the Cr(VI) analyte was determined as 40 minutes. Investigation of the order of selectivity of anions followed the trend: $Cr_2O_7^{2-} > SO_4^{2-} > F^- > NO_3^-$.

DEDICATION

To my wife Shamiso and my daughter Tanatswa, I love you.

ACKNOWLEDGEMENTS

Firstly I would like to thank the Lord for being wonderful in all aspects of my life.

Special thanks go to Prof Luke Chimuka for his supervision, mentorship and support during my engagement with the University of the Witwatersrand. He was also able to avail financial support without which my studies were not going to be possible. Many thanks also go to Prof Ewa Cukrowska, the head of the Environmental Analytical Research group. She made it easy for me to access all the necessary instruments that I required for my research. Dr Hlanganani Tutu`s comments during our regular seminars made a great difference to my work and I want to thank him so much.

Many thanks go to Water Research Commission of South Africa for funding the project and providing experts from time to time to guid and advice me on many aspects of my work. My tuition was paid by Post graduate Merit Award, University of Witwatersrand which I would like to thank as well.

These fellow students from the Environmental Analytical Research group made my working in the laboratory an enjoyable experience: Dr J.G Lusilao, Dr E. Bakatula, Dr P. Sibiya, R. Amdany, P. Mumbiaya, T. Mavunganidze, Y. Asiedu, Thutuka, B. Camdern-Smith, D. Saad, B. Yalala and P. Matshediso. However, I would like to single out Dr Vusumzi Pakade for the fruitful constructive discussions that we had almost everyday during my studies.

This work is dedicated to my wife for her great love and patience during the course of my studies. Many thanks go to my father Orleans Muchandibaya and mother Beauty Chiadzwa for their tremendous support and encouragement they gave me throughout my studies. My sisters Alleta and Nancy together with my brother Tanaka were a great source of inspiration.

The following people were so helpful in the named analysis's: Mr T. Makgata for Atomic force microscopy analysis, Prof A. Ziegler for TEM, SEM and EDS analysis, Prof N. Coville for BET and TGA, Prof D. Billing for PXRD, Rudolph for Raman spectroscopy and DRS, Ms J. Gama for FTIR and Ms I. Khumalo for UV-Vis.

TABLE OF CONTENTS

DECLARATION i

ABSTRACT ii

DEDICATION iv

ACKNOWLEDGEMENTS v

TABLE OF CONTENTS vi

LIST OF FIGURES xiii

LIST OF TABLES xxii

ABBREVIATIONS AND ACRONYMS xxiii

CHAPTER ONE: INTRODUCTION

1.1 Background 2

1.2 Statement of the problem 6

CHAPTER TWO: LITERATURE REVIEW

2.1 Background on Uranium 10

2.1.1 Uranium mining technologies and mining in South Africa 12

2.1.2 Toxicity and fate of uranium 13

2.1.3 Uranium speciation 15

2.2 Background of chromium 17

2.2.1 Chromium mining in South Africa 18

2.2.2 Speciation and fate of chromium in the environment 18

2.2.3 Health and environmental concerns of chromium 22

2.3 South African regulation on waste and pollution 23

2.4 Water contamination and permissible limits of U and Cr(VI) 23

2.5 Conventional methods for uranium and chromium removal 24

2.5.1 Bioremediation 27

2.5.2 Permeable Reactive Barriers 28

2.5.3 Chemical precipitation 29

2.5.4 Ion exchange 30

2.5.5 Phytoextraction 30

2.5.6 Electrodialysis 31

2.6 Use of adsorbents in the removal of uranium from wastewaters 31
2.7 Magnetic nano particles 33
2.7.1 Superparamgnetism 35
2.7.2 Magnetic properties of magnetic particles 35
2.7.3 Magnetite and its magnetic properties 36
2.7.4 Synthesis of magnetic nanoparticles 38
2.7.4.1 Co-Precipitation 38
2.7.5.2 Thermal Decomposition 39
2.7.4.3 Microemulsion 39
2.7.4.4 Hydrothermal Synthesis 40
2.7.5 Coating of the magnetite 40
2.8 Ion imprinted polymers 41
2.8.1 Magnetic ion imprinted polymers 43
2.8.2 Types of template monomer interactions 44
2.8.3 Polymerization reagents 45
2.8.3.1 Functional monomers 45
2.8.3.2 Cross linkers 46
2.8.3.3 Initiators 48
2.8.3.4 Porogen 49
2.8.4 Approaches in preparation of IIPs 51
2.8.4.1 Cross-linking of bifunctional reagents 51
2.8.4.2 Chemical immobilization 51
2.8.4.3 Surface imprinting 53
2.8.4.4 Trapping 54
2.8.4.5 Metal coordination 55
2.8.5 Types of polymerizations 57
2.8.5.1 Bulk polymerization 58
2.8.5.2 Precipitation polymerization 58
2.8.5.3 Suspension polymerization 58
2.8.5.4 Emulsion polymerization 59
2.8.6 Application of imprinting technology 59

CHAPTER THREE: RESEARCH OBJECTIVES

3.1 General objectives 65
3.2 Specific objectives 65
3.3 Key questions 65
3.4 Significance of the research 66
3.5 Hypothesis 66
3.6 Novelty 66

CHAPTER FOUR: RESEARCH METHODOLOGIES

4.1 Chemicals, stock solutions and equipment **68**
4.1.1 Chemicals 68
4.1.2 Stock solutions 68
4.1.3 Equipment 69
4.2 Analytical and characterization equipment **69**
4.2.1 Ultraviolet visible spectroscopy 69
4.2.2 Raman spectroscopy 70
4.2.3 Transmission electron microscopy 70
4.2.4 Size distribution 70
4.2.5 Energy dispersive spectrometry 70
4.2.6 Powder X-ray diffraction analysis 71
4.2.7 Brunauer, Emmett and Teller analysis 71
4.2.8 Fourier-transform infrared 72
4.2.9 Thermo-gravimetric analysis 72
4.2.10 Carbon, hydrogen, nitrogen and sulphur analysis 72
4.2.11 Diffuse reflectance spectroscopy analysis 73
4.2.12 Atomic force microscopy 73
4.2.13 Ion chromatography analysis 74
4.2.14 Inductively coupled plasma-optical emission spectrometer 74
4.2.15 Atomic absorption spectroscopy 75

4.3 Research methods for U(VI) polymers 76
4.3.1 Synthesis of the magnetic-IIPs and NIPs 76
4.3.1.1 Synthesis of the magnetite 76
4.3.1.2 Coating of magnetite with γ-MPS 76
4.3.1.3 Coating of magnetite with oleic acid 77
4.3.1.4 Bulk polymerization 77
4.3.1.5 Precipitation polymerization 78
4.3.1.6 Leaching of γ-MPS and OA based polymers 78
4.3.2 Optimization of parameters for U(VI) uptake 79
4.3.2.1 Effect of initial pH 79
4.3.2.2 Effect of the amount of magnetic polymers 80
4.3.2.3 Effect of contact time 80
4.3.2.4 Effect of initial concentration 80
4.3.2.5 U(VI) selectivity of the magnetic polymers 81
4.3.2.6 Reusability of the magnetic uranyl IIPs 82
4.3.3 Kinetic modelling 83
4.3.3.1 Pseudo-first-order kinetic model 83
4.3.3.2 Pseudo-second-order kinetic model 84
4.3.4 Adsorption isotherm models 84
4.3.4.1 Freundlich isotherm model 85
4.3.4.2 Langmuir isotherm model 85
4.3.5 Sampling sites 86
4.3.6 Application of magnetic U(VI) IIPs to real samples 89
4.4 Research methods for Cr(VI) 89
4.4.1 Synthesis of polymers specific for Cr(VI) 89
4.4.1.1 Synthesis of poly(4-vinylpyridine) 89
4.4.1.2 Synthesis of magnetic poly(4-vinylpyridine) 90
4.4.1.3 Preparation of magnetic and non-magnetic poly(n-propyl-4-vinylpyridinium) bromide 90
4.4.1.4 Preparation of magnetic and non-magnetic poly(n-propyl-4-vinylpyridinium) dichromate 90
4.4.1.5 Leaching of chromium 91

4.4.2 Optimization of parameters for Cr(VI) uptake **91**
4.4.2.1 Effect of initial pH of solution 91
4.4.2.2 Effect of the amount of magnetic polymers 91
4.4.2.3 Effect of contact time 92
4.4.2.4 Effect of initial Cr(VI) concentration 92
4.4.2.5 Selectivity studies 92
4.4.2.6 Reusability of Cr(VI) IIPs 93

CHAPTER FIVE: RESULTS AND DISCUSSION

5.1 Magnetic U(VI) polymers **95**
5.1.1 Synthesis of magnetite **95**
5.1.1.1 Powder X-ray diffraction analysis 96
5.1.2 Functionalization of magnetite **97**
5.1.2.1 Carbon, hydrogen and nitrogen elemental analysis 100
5.1.2.2 Diffuse reflectance spectroscopy analysis 101
5.1.2.3 Raman spectroscopy 103
5.1.2.4 Transmission electron microscopy 105
5.1.2.5 Size distributions 106
5.1.2.6 Fourier-transforms infrared analysis 108
5.1.2.7 Dispersibility and stability of γ-MPS-Fe_3O_4 110
5.1.3 Magnetic polymer synthesis **111**
5.1.4 Leaching analysis **113**
5.1.4.1 Atomic force microscopy analysis 116
5.1.4.2 Energy-dispersive X-ray spectroscopy analysis 119
5.1.4.3 Brunauer, Emmett and Teller surface area analysis 122
5.1.4.4 Fourier-transform infrared analysis 124
5.1.4.5 Thermal gravimetric analysis 125
5.1.4.6 Magnetic response 127
5.1.5 Optimization of parameters for U(VI) adsorption **128**
5.1.5.1 Effect of pH 128
5.1.5.2 Effect of magnetic polymer quantity 131
5.1.5.3 Effect of contact time 135

5.1.5.4 Effect of concentration 138
5.1.5.5 Selectivity studies 141
5.1.5.6 Reusability studies 148
5.1.6 Adsorption kinetics 151
5.1.7 Adsorption isotherms models 152
5.1.7.1 Langmuir isotherm model 152
5.1.7.2 Freundlich isotherm model 153
5.1.8 Application to real environmental samples 154
5.2. Synthesis of magnetic polymers selective for Cr(VI) 158
5.2.1 Synthesis of magnetic poly(4-vinylpyridine) 158
5.2.2 Quartenization of magnetic poly(4vinylpyridine) 159
5.2.2.1 Quartenization study using FTIR 160
5.2.3 Addition of the dichromate imprint to the magnetic poly(4-vinylpyridine) 162
5.2.3.1 FTIR-Imprinting 162
5.2.4 Cross-linking and leaching of dichromate from the magnetic polymers 164
5.2.4.1 Brunauer, Emmett and Teller surface analysis 166
5.2.4.2 TGA analysis 168
5.2.5 Optimization of parameters for Cr(VI) adsorption 169
5.2.5.1 Effect of pH 169
5.2.5.2 Effect of magnetic polymer quantity 171
5.2.5.3 Effect of contact time 173
5.2.5.4 Effect of concentration 174
5.2.5.5 Selectivity studies 175
5.2.5.6 Reusability studies 179
5.2.6 Adsorption kinetics 180
5.2.6.1 Pseudo first order kinetics 180
5.2.6.2 Pseudo second order kinetics 180
5.2.7 Adsorption isotherms 182

CHAPTER SIX: CONCLUSIONS AND RECOMMENDATIONS

6.1 Conclusions	**186**
6.2 Recommendations for future work	**187**
REFERENCES	**191**
APPENDICES	**233**

LIST OF FIGURES

CHAPTER ONE: INTRODUCTION

Figure 1.1: Diagram showing the generation of AMD (a) before and (b) after exposure of the sulphide layer by mining activities 3

Figure 1.2: General scheme for pollutants to enter the food chain through Water pathways 4

Figure 1.3: Fusion of the magnetic materials and adsorbents to get magnetic functional material 8

CHAPTER TWO: LITERATURE REVIEW

Figure 2.1: Supply and demand of uranium 10

Figure 2.2: Species distribution of U(VI) 16

Figure 2.3: The pH-Eh diagram of stability of different chromium species 20

Figure 2.4: Species distribution diagram of chromium in an aqueous system 21

Figure 2.5: Structures of the (a) chromate and (b) dichromate anions 22

Figure 2.6: Removal efficiencies of uranium by different conventional techniques 25

Figure 2.7: Uranium(VI) reduction driven by microbial respiration 28

Figure 2.8: Orientation of domains in (a) ferromagnetism (b) aniferrimagnetism and (c) ferrimagnetism 34

Figure 2.9: Hysteresis loop of a superparamagnetic material 36

Figure 2.10: Electronic configuration in magnetite 37

Figure 2.11: Schematic diagram depicting imprinting polymerization 42

Figure 2.12: Common functional monomers used in imprinted polymerization 46

Figure 2.13: Common cross-linking monomers used in imprinted polymerization 48

Figure 2.14: An example of a linear polymer with 4-VP enchored in the polymer matrix 51

Figure 2.15: An example of the chemical immobilization approach in IIP preparation 52

Figure 2.16: An example of surface imprinting approach in IIP preparation 54
Figure 2.17: An example of trapping approach in IIP preparation 55
Figure 2.18: A scheme showing the metal coordination approach for zinc ion imprinted polymers 56
Figure 2.19: Scheme outlining the main applications envisaged for MIPs and IIPs 60

CHAPTER FOUR: MATERIALS AND METHODS

Figure 4.1: Schematic diagram of an atomic absorption spectrophotometer 75
Figure 4.2: The heating programme for uranium in the graphite furnace 76
Figure 4.3: (a) Germiston site (b) Google map of the Germiston area with pointers 26^{o}13`07.10 ``S and 28$^{o}$08`03.79``E and an elevation height of 1652 m 87
Figure 4.4: (a) Goudkoppies Wastewater Treatment Plant site (b) with pointers 25^{o}66`42.12``S and 27$^{o}$69`17.07``E and an elevation height of 1378 m 88

CHAPTER FIVE: RESULTS AND DISCUSSION

Figure 5.1: Magnetic response of magnetite 95
Figure 5.2: Magnetite showing the adsorbed hydroxyl ions 95
Figure 5.3: PXRD pattern for the synthesized magnetite 96
Figure 5.4: The hydrolysis of γ-MPS 97
Figure 5.5: Coating of the magnetite with the hydrolysed γ-MPS 98
Figure 5.6: An illustration of the arrangement of γ-MPS around the magnetic core 98
Figure 5.7: The structure of oleic acid 99
Figure 5.8: Charge delocalization on the carboxylate of the oleic acid 99
Figure 5.9: Scheme for the functionalization of magnetite with OA 100
Figure 5.10: DR spectra of magnetite as well as γ-MPS and OA coated magnetite 102

Figure 5.11: Oxidation of magnetite through two different routes 103
Figure 5.12: Raman spectrum of pure magnetite 104
Figure 5.13: Raman spectrum of the unmodified magnetite 105
Figure 5.14: Raman spectrum of the MPS modified magnetite 105
Figure 5.15: TEM images of the uncoated (a) and γ-MPS coated (b) magnetic 106
Figure 5.16: Particle size distribution of the uncoated magnetite 107
Figure 5.17: Particle size distribution of the coated magnetite 107
Figure 5.18: FTIR spectra of (a) uncoated magnetite and (b) γ-MPS coated magnetite 109
Figure 5.19: FTIR spectrum of OA-Fe_3O_4 110
Figure 5.20: UV-Vis of γ-MPS-Fe_3O_4 dispersed in water. Scans taken every after 10 min 111
Figure 5.21: Polymerization on the γ-functionalized Fe_3O_4 particles 112
Figure 5.22: Volumes of the porogenic solvent used to effect bulk and precipitation polymerization 113
Figure 5.23: The leaching of the uranyl ion from the polymeric matrix 113
Figure 5.24: Polymers leached with 1 mol dm^{-1} $NaHCO_3$: (a) bulk magnetic IIP (b) precipitate magnetic IIP 114
Figure 5.25: Polymers leached with 1 mol dm^{-1} HCl: (a) bulk magnetic IIP (b) precipitate magnetic IIP 115
Figure 5.26: Optical view of magnetic IIP with an AFM tip of width ~25 micro metres 116
Figure 5.27: AFM image of $NaHCO_3$ leached magnetic IIP 117
Figure 5.28: AFM image of HCl leached magnetic IIP 117
Figure 5.29: Image Roughness of the $NaHCO_3$ and HCl leached magnetic IIPs 118
Figure 5.30: A three dimensional AFM image of $NaHCO_3$ leached polymer 118
Figure 5.31: EDS spectra of (a) unleached bulk magnetic IIP (b) washed with1 mol dm^{-3} $NaHCO_3$ (c) and 1 mol dm^{-3} HCl 120

Figure 5.32: EDS spectra of (a) unleached precipitation magnetic IIP (b) washed with 1 mol dm^{-3} $NaHCO_3$ (c) and 1 mol dm^{-3} HCl 121
Figure 5.33: (a) The nitrogen adsorption-desorption isotherms for the unleached bulk magnetic IIP and (b) its corresponding BET plot 123
Figure 5.34: FTIR spectru for γ-MPS based polymers 127
Figure 5.35: TGA results for γ-MPS-Fe_3O_4 128
Figure 5.36: TGA of precipitation magnetic polymers 128
Figure 5.37: TGA of bulk magnetic polymers 129
Figure 5.38: Uranium imprinted polymer showing heteroatoms responsible for the uptake of uranyl ions 131
Figure 5.39: Effect of sample pH for OA IIP bulk $NaHCO_3$ leached 132
Figure 5.40: Effect of sample pH for OA NIP bulk $NaHCO_3$ leached 132
Figure 5.41: Effect of sample pH for γ-MPS IIP precipitate $NaHCO_3$ leached 133
Figure 5.42: Effect of sample pH for γ-MPS IIP precipitate HCl leached 133
Figure 5.43: Adsorption percentages obtained by varying the mass of (a) γ-MPS IIP ppt-HCl leached and (b) γ-MPS NIP ppt-HCl leached 134
Figure 5.44: Adsorption percentages obtained by varying the mass of (a) γ-MPS IIP bulk-$NaHCO_3$ leached and (b) γ-MPS NIP bulk-$NaHCO_3$ leached 135
Figure 5.45: Adsorption percentages obtained by varying the mass of (a) OA IIP bulk-$NaHCO_3$ leached and (b) OA NIP bulk-$NaHCO_3$ leached 135
Figure 5.46: Adsorption percentages obtained by varying the mass of (a) γ-MPS IIP ppt-$NaHCO_3$ leached and (b) γ-MPS NIP ppt-$NaHCO_3$ leached 136
Figure 5.47: Adsorption percentages obtained by varying the mass of (a) OA IIP ppt-$NaHCO_3$ leached and (b) OA NIP ppt-$NaHCO_3$ leached 136

Figure 5.48: Effect of contact time on the uptake of uranium by (a) γ-MPS IIP ppt-HCl leached and (b) γ-MPS NIP ppt-HCl leached 137
Figure 5.49: Effect of contact time on the uptake of uranium by (a) γ-MPS IIP bulk-$NaHCO_3$ leached and (b) γ-MPS NIP bulk-$NaHCO_3$ leached 138
Figure 5.50: Effect of contact time on the uptake of uranium by (a) OA IIP bulk-$NaHCO_3$ leached and (b) OA NIP bulk-$NaHCO_3$ leached 138
Figure 5.51: Effect of contact time on the uptake of uranium by (a) γ-MPS IIP ppt-$NaHCO_3$ leached and (b) γ-MPS NIP ppt-$NaHCO_3$ leached 139
Figure 5.52: Effect of contact time on the uptake of uranium by (a) OA IIP ppt-$NaHCO_3$ leached and (b) OA NIP ppt-$NaHCO_3$ leached 139
Figure 5.53: Effect of initial concentration on the uptake of uranium by (a) γ-MPS IIP bulk-$NaHCO_3$ leached and (b) γ-MPS NIP bulk-$NaHCO_3$ leached 140
Figure 5.54: Effect of initial concentration on the uptake of uranium by (a) OA IIP bulk-$NaHCO_3$ leached and (b) OA NIP bulk-$NaHCO_3$ leached 141
Figure 5.55: Effect of initial concentration on the uptake of uranium by (a) γ-MPS IIP ppt-$NaHCO_3$ leached and (b) γ-MPS NIP ppt-$NaHCO_3$ leached 141
Figure 5.56: Effect of initial concentration on the uptake of uranium by (a) OA IIP ppt-$NaHCO_3$ leached and (b) OA NIP ppt-$NaHCO_3$ leached 142
Figure 5.57: Extraction efficiencies of ions extracted by the magnetic IIP and NIP of γ-MPS bulk-$NaHCO_3$ leached from the spiked 2 mg L^{-1} binary mixtures of solutions 144
Figure 5.58: Extraction efficiencies of the ions extracted by the magnetic IIP and NIP of γ-MPS ppt-$NaHCO_3$ leached from the spiked 2 mg L^{-1} binary mixtures of solutions 145

Figure 5.59: Extraction efficiencies of the ions extracted by the magnetic IIP and NIP of γ-MPS ppt-HCl leached from the spiked 2 mg L^{-1} binary mixtures of solutions 146

Figure 5.60: Extraction efficiencies of the ions extracted by the magnetic IIP and NIP of OA ppt-$NaHCO_3$ leached from the spiked 2 mg L^{-1} binary mixtures of solutions 147

Figure 5.61: Extraction efficiencies of ions extracted by the magnetic IIP and NIP of OA bulk-$NaHCO_3$ leached from the spiked 2 mg L^{-1} binary mixtures of solutions 148

Figure 5.62: Reusability and stability of magnetic IIP and NIP of γ-MPS ppt-HCl leached 150

Figure 5.63: Reusability and stability of magnetic IIP and NIP of γ-MPS bulk-$NaHCO_3$ leached 151

Figure 5.64: Reusability and stability magnetic IIP and NIP of OA bulk-$NaHCO_3$ leached 151

Figure 5.65: Reusability and stability magnetic IIP and NIP of γ-MPS ppt-$NaHCO_3$ leached 152

Figure 5.66: Reusability and stability magnetic IIP and NIP of OA ppt-$NaHCO_3$ leached 152

Figure 5.67: Synthetic routes of (a) homopolymer and (b) magnetic polymer of poly(4-vinylpyridine) 160

Figure 5.68: Structure of magnetic poly(4-vinylpyridine) 160

Figure 5.69: Reaction for the quartenization of magnetic poly(4-vinylpyridinium) bromide 161

Figure 5.70: FTIR spectra of quartenized poly(4-vinylpyridine) after (a) 0 hrs, (b) 14 hrs and (c) 42 hrs 163

Figure 5.71: FTIR spectra of quartenized magnetic poly(4-vinylpyridine) after (a) 0 hrs, (b) 14 hrs and (c) 42 hrs 163

Figure 5.72: Substitution reaction of the bromide ions from magnetic poly(4-vinylpyridinium) bromide by dichromate ions 164

Figure 5.72: FTIR spectra of quartenized poly(4-vinylpyridine) after addition of $Na_2Cr_2O_7$ 165
Figure 5.74: FTIR spectra of quartenized magnetic poly(4-vinylpyridine) after addition of $Na_2Cr_2O_7$ 165
Figure 5.75: Cross-linking of the magnetic polymer 166
Figure 5.76: Leaching of the dichromate with 1 M HCl 166
Figure 5.77: Aliquots collected after leaching studies 167
Figure 5.78: Leaching of chromium and iron from the magnetic IIP 167
Figure 5.79: Washing of magnetite from magnetic NIP 168
Figure 5.80: (a) The nitrogen adsorption-desorption isotherms for the unleached non-magnetic poly(n-propyl-4-vinylpyridinium) dichromate polymer and (b) its corresponding BET plot 171
Figure 5.81: Thermogravimetric analysis of chromium magnetic polymer 174
Figure 5.82: The effect of pH and also the demonstration of the chromate/ hydroxyl competition 176
Figure 5.83: Effect of sample pH 177
Figure 5.84: Adsorption percentages obtained by varying the mass of magnetic polymers for chromium adsorption 178
Figure 5.85: Effect of contact time on the uptake of chromium by magnetic polymers 179
Figure 5.86: Effect of initial concentration on the uptake of chromium by magnetic IIP and NIP 180
Figure 5.87: A 5 mg L^{-1} anionic mixture standard 181
Figure 5.88: Calibration curve for four dichromate anionic competitors 181
Figure 5.89: An example of a fluoride ion dichromate competitor 182
Figure 5.90: Calibration curve for four dichromate anionic competitors 182
Figure 5.91: Extraction efficiencies of anions extracted by the magnetic Cr(VI) IIP and NIP from 2 mg L^{-1} spiked binary mixtures of solutions 183
Figure 5.92: Reusability and stability magnetic IIP and NIP selective to chromium 184

Figure 5.93: Pseudo first-order plots for the adsorption of chromium onto magnetic polymers 185
Figure 5.94: Pseudo second-order plots for the adsorption of chromium onto magnetic polymers 185
Figure 5.95: (a) Freundlich and (b) Langmuir isotherm model for magnetic IIP 186
Figure 5.96: (a) Freundlich and (b) Langmuir isotherm model for magnetic NIP 187

LIST OF TABLES

Table 2.1: Typical concentration ranges in different environmental Matrices 11

Table 2.2: Methods used in the mining of uranium 12

Table 2.3: Maximum allowable limits of uranium and chromium(VI) in water by different bodies 24

Table 2.4: Advantages and disadvantages of some convectional removal techniques 26

Table 2.5: Examples of the porogen used in molecular imprinting preparation and their physical properties 50

Table 2.6: Summary of some reported IIPs and polymerization techniques used 57

Table 2.7: Polymeric magnetic sorbents for the removal of U(VI) and Cr(VI) from environmental samples 63

Table 4.1: Operating conditions of the ICP-OES 74

Table 4.2: Volume composition of the polymer washing solution 77

Table 5.1: Elemental analysis of γ-MPS coated magnetite 101

Table 5.2: Elemental analysis of OA coated magnetite 101

Table 5.3: Colours of different iron oxides 102

Table 5.4: Raman bands for magnetite, maghemite and hematite 103

Table 5.5: BET constants for the bulk magnetic IIPs 124

Table 5.6: Physical properties of the uranyl ion together with those of its competitors 141

Table 5.7: K_d, K and K` values for the magnetic IIP and NIP of γ-MPS bulk-$NaHCO_3$ in binary mixtures 142

Table 5.8: K_d, K and K` values for the magnetic IIP and NIP of γ-MPS ppt-$NaHCO_3$ leached in binary mixtures 143

Table 5.9: K_d, K and K` values for the magnetic IIP and NIP of γ-MPS ppt-HCl leached in binary mixtures 144

Table 5.10: K_d, K and kKvalues for the magnetic IIP and NIP of OA ppt-$NaHCO_3$ leached in binary mixtures 145

Table 5.11: K_d, K and K` values for the magnetic IIP and NIP of OA bulk-$NaHCO_3$ leached in binary mixtures 146

Table 5.12: Summary of results of calculated kinetic parameters of pseudo-first order and pseudo-second order for U(VI) adsorption with an initial concentration of 5 mg L^{-1} 151

Table 5.13: Types of adsorption with respect to Langmuir isotherms 153

Table 5.14: The Langmuir constants and the R_L values for adsorption of U(VI) on magnetic polymers 153

Table 5.15: Freundlich constants of different uranium magnetic polymers 154

Table 5.16: Metal composition in real water samples 155

Table 5.17: Application of magnetic γ-MPS IIP bulk-$NaHCO_3$ leached and the corresponding NIP on unspiked and spiked real water samples 155

Table 5.18: Application of magnetic OA IIP bulk-$NaHCO_3$ leached and the corresponding NIP on unspiked and spiked real water samples 156

Table 5.19: Application of magnetic γ-MPS IIP ppt-$NaHCO_3$ leached and the corresponding NIP on unspiked and spiked real water samples 156

Table 5.20: Application of magnetic OA IIP bulk-$NaHCO_3$ leached and the corresponding NIP on unspiked and spiked real water samples 157

Table 5.21: Application of magnetic γ-MPS IIP ppt-$NaHCO_3$ leached and the corresponding NIP on unspiked and spiked real water samples 157

Table 5.22: BET suface areas and constants for the polymers 168

Table 5.23: K_d, K and K` values for the magnetic Cr(VI) IIP and NIP in binary mixtures 178

Table 5.24: Calculated kinetic parameters of pseudo-first and pseudo-second orders for initial Cr(VI) concentration of 5 mg L^{-1} 181

Table 5.25: The Langmuir constants and the R_L values for adsorption of Cr(VI) on magnetic polymers 183

Table 5.26: Freundlich constants for chromium magnetic polymers 184

LIST OF ABBREVIATIONS AND ACRONYMS

Acac	Acetylacetone
AMD	Acid mine drainage
AAS	Atomic absorption spectroscopy
AFM	Atomic force spectroscopy
BET	Brunauer, Emmett and Teller
CHNS	Carbon, hydrogen, nitrogen and sulphur
CNTs	Carbon nanotubes
CDs	Cyclodextrins
DU	Depleted uranium
DL	Detection limit
DRS	Diffuse reflective spectroscopy
DMRB	Dissimilatory metal reducing bacteria
DVB	Divinylbenzene
EDS	Energy dispersive spectrometry
EGDMA	Ethylene glycol dimethacrylate
F	Force
FTIR	Fourier-transform infrared
FWHM	Full width at half maximum
GTF	Glucose-tolerance factor
GFAAS	Graphite furnace atomic absorption spectroscopy
ICP-OES	Inductively coupled plasma optical emission spectroscopy
ISL	*In-situ* leaching
IIP	Ion imprinted polymer
MCL	Maximum contaminant level
MAA	Methacrylic acid
γ-MPS	γ-Methacryloxypropyltrimethoxysilane
MIP	Molecularly imprinted polymer
NEMA	National Environmental Management Act
NIP	Non imprinted polymer
NECSA	Nuclear Energy Corporation of South African
Nufcor	Nuclear Fuels Corporation of South Africa

ORNL	Oak Ridge National Laboratory
OA	Oleic acid
ppt	Precipitate
PRBs	Permeable Reactive Barriers
PXRD	Powdered X-ray diffraction
r.f	Radio frequency
rpm	Rotations per minute
SALO	Salicylaldoxime
SEM	Scanning electron microscopy
SA	South Africa
SABS	South African Bureau of Standards
SD	Standard deviation
SRB	Sulphate reducing bacteria
TEOS	Tetraethyl orthosilicate
TGA	Thermo-gravimetric analysis
t yr^{-1}	Tonnes per year
TEM	Transmission electron microscopy
TRIM	Trimethylolpropane trimethacrylate
UNSCEAR	United Nations Scientific Committee on the Effects of Atomic Radiation
4-VP	4-Vinyl pyridine
WHO	World Health Organization

Chapter 1
Introduction

This introductory chapter gives an overview of the threats and potential hazards caused by heavy metals water pollution. It also spells out the needs of removal of metal contaminants from wastewaters.

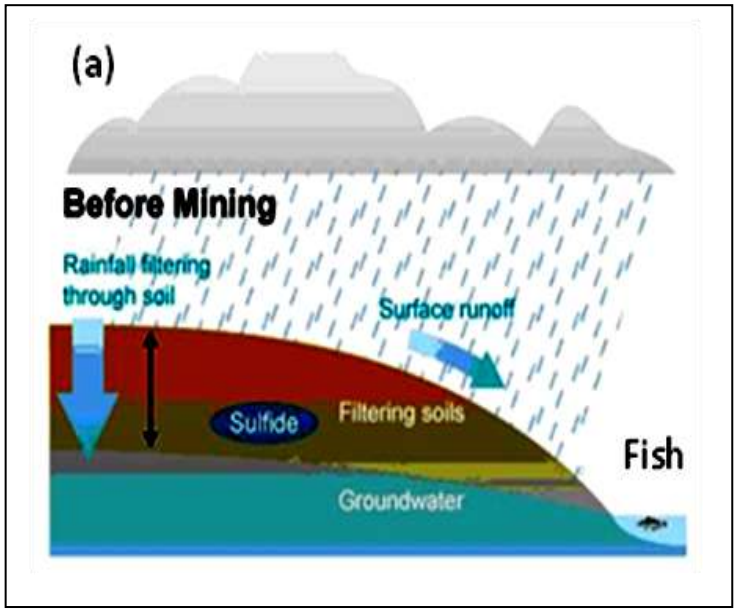
1.1 Background

One of the most critical global issues is water pollution (Ramakrishna *et al*., 2006) and it has led to alteration of the physicochemical properties of water (Richardson, 1988). Pollution of water bodies due to the indiscriminate disposal of heavy metals has been a concern for a long time. The rapid increase in the levels of environmental pollution over recent decades has resulted in increasing concern for people's well-being and for global ecosystems (Kot and Namiesnèik, 2000).

Inorganic pollutants of great physiological concern are heavy metals (Ramakrishna *et al*., 2006), because of their toxicity (Qdaisa and Moussab, 2004), towards aquatic-life, human beings and the environment (Luo *et al*., 2011). As an environmental threat, heavy metals are becoming environmental priority pollutants (Fu and Wang, 2011). Metals contamination of water supplies has become a constant area of concern (Brown, 1996).

There is a lot of evidence in literature that trace back pollution generation to anthropogenic sources in the quest for exploiting nature as a source of means of livelihood by man (Agbontalor, 2007). Industrialization and urbanization have caused excessive discharge of heavy metals into the environment (Khan *et al*., 2004). Mining industry accounts for major environmental threats in countries like South Africa because it has large reserves for several minerals (Ochieng *et al*., 2010). These mining activities are associated with environmental metals` contamination such as the one from acid mine drainage (AMD) which is highly acidic water, usually containing high concentrations of metals, sulphides and salts. AMD have been identified to be the single most significant threat to South Africa's environment. In South Africa, this is being driven home by the AMD problems being experienced at the East Rand operations of Pamodzi Gold (Naidoo, 2009). Pyrite (FeS_2) is responsible for starting acid generation. When pyrite is exposed to oxygen and water, it will be oxidized, resulting in protons release. Mining increases the exposed surface area of sulphur bearing rocks. The oxidation process occurs in undisturbed rocks as well but at a slower rate. Figure

1.1 shows that AMD is exacerbated by perturbation of the land during mining or other industrial activities. Highly acidic water then forms by reaction of the pyrite in the presence of oxygen. This acidic water leaches out other metals from rocks as it flows to water bodies.



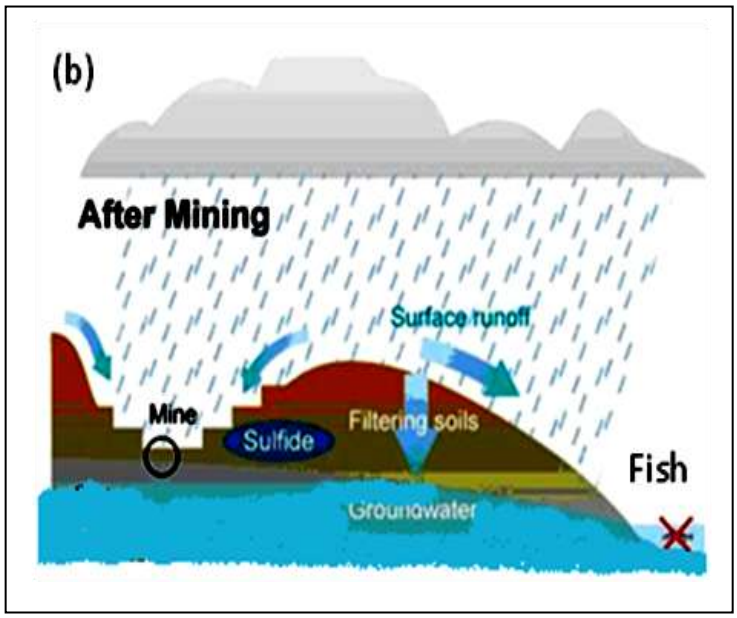


Figure 1.1: Diagram showing the generation of AMD (a) before and (b) after exposure of the sulphide layer by mining activities (Rekacewic, 2005).

These wastewaters containing heavy metals are directly or indirectly discharged into the environment (Fu and Wang, 2011), killing aquatic life. Direct water contamination also arises from many other industries such as metal cleaning, metal finishing (Luo *et al*., 2011) and textile industry (Halimoon and Yin, 2010).

Unlike organic pollutants, heavy metals are non-biodegradable (Fu and Wang, 2011) and are not subject to bacterial attack or any other break down or degradation process (Ilhan *et al*., 2004). This implies that they bioaccumulate and are a permanent addition to the marine environment. A direct consequence of this is that their concentrations often exceed the permissible levels in soil, water bodies as well as in sediments. Hence, they find their way up the food pyramid (Igwe and Abia, 2006) and this is summarized in Figure 1.2.

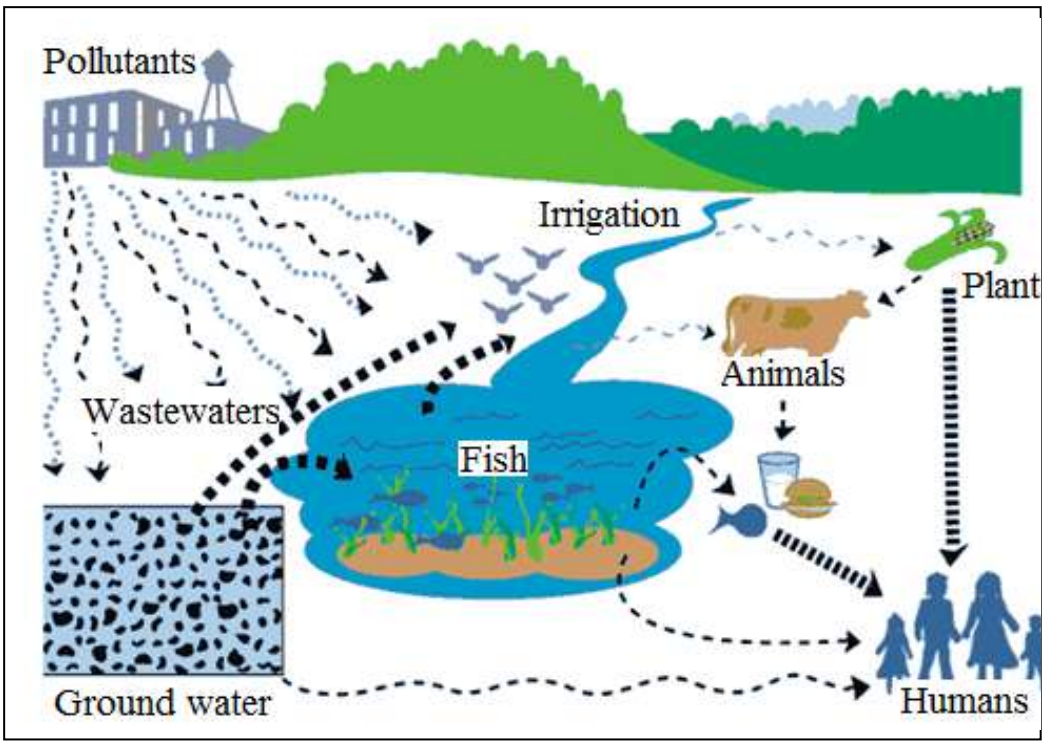


Figure 1.2: General scheme for pollutants to enter the food chain through water pathways (Nuclear Cleanup Issues, Nuclear Waste Storage Issues: http://jan.ucc.nau.edu/~doetqpp/courses/env440/env440_2/lectures/lec4/lec4.htm).

When heavy metals accumulate in the environment and in food chains, they have a potential to profoundly disrupt biological processes if they exceed certain

threshold limits (Igwe and Abia, 2006). When heavy metals are released into the environment they can cause severe damage to the human body, including accumulative poison, brain damage, and cancer (Luo *et al*., 2011) because , as mentioned earlier, they are known to be carcinogenic (Fu and Wang, 2011).

Because of the toxicity of heavy metals released into the environment, there has been an increase in the number of studies concerning removal of heavy metals from aqueous solutions (El-Sayed, 2008). Also, from the point of view of resource recovery, the removal and recovery of heavy metals is extremely important as metals are non-renewable. Presently, there are many methods that are being used to remove and recover metals from the environment (Barkhordar and Ghiasseddin, 2012).

The most common remediation techniques in the removal of heavy metals from water include chemical precipitation (Pavlović *et al*., 2007), ion exchange (Mier *et al*., 2001; Wojtówicz and Stokłosa, 2002; Bai and Bartkiewicz, 2009), electrodeposition (Meunier *et al*., 2006; Lewinsky, 2007), membrane technology (Sanga *et al*., 2008; Ahmad *et al*., 2011), reverse osmosis, nanofiltration, lime neutralization, phytoremediation (Lone *et al*., 2008; Liao and Chang, 2004; Raskin *et al*., 1997) and electrodialysis (Wang *et al*., 2010). These methods will be reviewed in chapter two of this dissertation. However, Ramakrishna *et al*. (2006) observed that metal pollutants in water cannot be removed completely by use of these conventional water purification methods. Limits for heavy metals in drinking water and wastewater have become stricter due to growing rigorous environmental regulations (Li *et al*., 2004). Due to some environmental legislation, industries are being forced to reduce the content of heavy metal in wastewaters before discharge to acceptable levels (Eisazadeh, 2008). However, the challenge to remediate hazardous metal-containing waste streams and ground waters still remains immense (Brown, 1996). There has always been need for more efficient methods for removal of metal ions from wastewaters before they are released into the environment. This is a matter of concern because of heavy metal toxicities even in low concentrations and their tendency to bioaccumulate (Pyrzyńska and Bystrzejewski, 2010).

1.2 Statement of the problem

Some governments are spending a lot of money for the remediation of heavy metals decanting in water bodies. For example, the issue of AMD is a hot subject in South Africa and is always in the media. This is because of the catastrophic effects of AMD on animals, plants and the environment. In order to assist the mining industry with the mitigation measures of AMD, the Department of Minerals and Energy (DMR) in South Africa had subsidies for the months of January, February and March 2010 amounting to R7.5 million. However, due to the extent of the problem, this amount fell well short of the funds that are necessary to treat AMD (Naidoo, 2010).

Most conventional methods require a tedious post-processing stage with secondary pollution generation and poor reusability (Luo *et al*., 2011; Zhan *et al*., 2011). Again, most of these conventional methods are non-economical and have many disadvantages such as incomplete metal removal, high reagent and energy requirements and generation of toxic sludge or other waste products that require disposal or treatment (Nameni *et al*., 2008). There is also a problem of scarcity of water resources in South Africa which has also made initiations in the research of new and efficient ways of decontaminating the available water sources. The prices of the noble materials such as heavy metals are constantly increasing. This has prompted the need of coming up with processes that are capable, in addition to wastewater purification, of recovering these metals (Qdaisa and Moussab, 2004). Luo, *et al*. (2011) noted that selective separation of heavy metal ions from water facilitates environmental protection and the reuse of a specific target precious heavy metals. However, most of the conventional methods applied are non-specific and exhibit low selectivity (Luo *et al*., 2011; Zhan *et al*., 2011). It is also known that the degree and extent of toxicity of heavy metals differs considerably from one metal to the other. Selective removal methods are therefore required to separate these metals from wastewater (Luo *et al*., 2011). There is therefore a need to develop novel adsorbents which have high selectivity (Zhan *et al*., 2011).

Adsorption was found to be an effective physicochemical treatment process in the removal of heavy metals from aqueous solutions (Kuntakapun *et al*., 2010).

Adsorption of heavy metals onto several new adsorbents has been the subject of many studies over recent years (Johnson, 1990). The use of adsorbents is the most common approach applied for decontamination of wastewater (Souag *et al*., 2009) and industrial effluents because the employed sorbent can be easily regenerated (Zhan *et al*., 2011) and because it is highly effective and economical (Pyrzyńska and Bystrzejewski, 2010). Also, the easiness of incorporation of solid sorbents into automated analytical procedures for preconcentration and determination of trace metal ions in natural waters makes adsorption a method of choice (Pyrzyńska and Bystrzejewski, 2010). The use of alternative low-cost materials as potential sorbents for the removal of heavy metals has been emphasized recently (Erdem *et al*., 2004). Some of the adsorbents used for metals` remediation include activated carbon (Kadirvelu *et al*., 2001; Al-Omair and El-Sharkawy, 2007; Ahn *et al*., 2009), chitosan (Rana *et al*., 2009; Bamgbose *et al*., 2010; Nomanbhay and Palanisamy, 2005), synthetic polymers (Saad *et al*., 2012), carbon nano tubes (Li *et al*., 2004; Moradi *et al*., 2011; Kosa *et al*., 2012) and zeolites (Shevade and Ford, 2004; Bram *et al*., 2012).

In adsorption, after sequestrating of the pollutants, filtration and centrifugation have always been used to separate the loaded adsorbents from solutions. However, this becomes very difficult when decontaminating large volumes of wastewaters. In other words, the applicability of this approach at an industrial level becomes limited. An alternative approach which has a potential of becoming popular is achieved by incorporation of magnetic materials into the adsorbent, Figure 1.3.

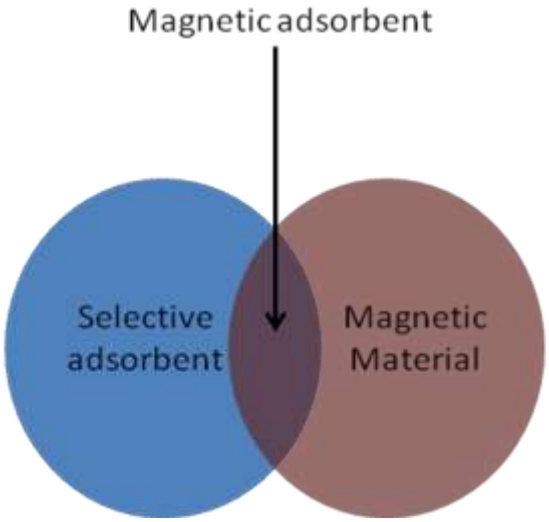


Figure 1.3: Fusion of the magnetic materials and adsorbents to get magnetic functional materials.

Most synthetic polymeric sorbents possess a uniquely attractive property that permits their rapid and highly selective removal (Oliveira *et al*., 2004) from almost any type of solutions (Franzreb *et al*., 2006) and wastewaters by application of external magnetic fields.

Chapter 2
Literature Review

This chapter presents a review of the literature relating to the chemistry of uranium and chromium. Common decontamination technologies for uranium and chromium removal from industrial wastewaters and AMD are briefly discussed and their advantages as well as disadvantages are also highlighted. A discussion on imprinting techniques then follows. Emphasis is placed on ion imprinted polymers with magnetic nanoparticles embedded in them. The chapter concludes with a brief discussion on the application of imprinting methods.

2.1 Background on uranium

The main use of uranium in the civilian sector is to fuel commercial nuclear power plants as it is commonly understood as a material storing huge amounts of energy (Sarangi and Beri, 2000). This requires uranium to be enriched with the ^{235}U isotope and the chain reaction to be controlled so that the energy is released in a manageable way (Uranuim-U). Sarangi and Beri (2000) noted that the growth of uranium mining normally follows the pattern of growth of nuclear power generation capacity in most countries. This relationship of supply and demand of uranium over time is shown in Figure 2.1.

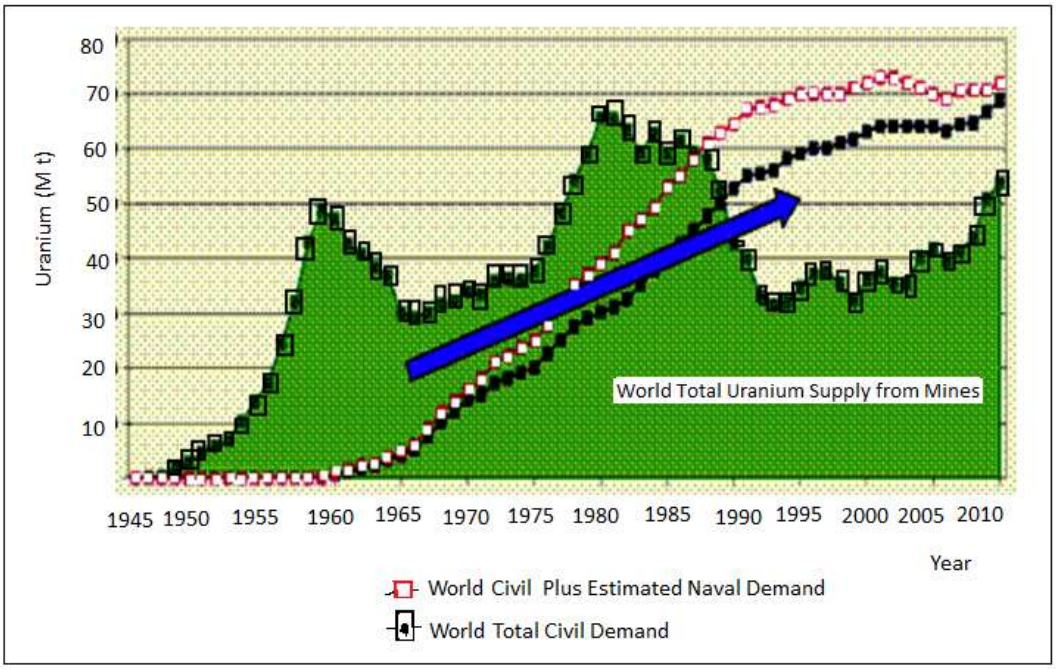


Figure 2.1: Supply and demand of uranium. Source: (*In Situ* Leach (ISL) Mining of Uranium).

Uranium is widely distributed throughout the Earth`s crust and almost all types of rocks contain some amount of uranium (Montgomery, 1995). Uranium is also present in river water, ground water and even seawater (Sarangi and Beri, 2000). The average uranium concentration in the Earth's crust is approximately 2.7 ppm (Brookins, 1988). Mining is, however, done in areas were the concentration is high enough to make profit. This is why it is restricted to certain areas of various

countries. Other countries have very little deposit and have to import enriched uranium for energy purposes. Table 2.1 shows some reported uranium concentrations in different matrices.

Table 2.1: Typical concentration ranges in different environmental matrices.

Matrix	Typical concentration range (ppm)	Reference
Soil	0.0-11.7	UNSCEAR, 1993
Air	2.2×10^{-8}-1.0×10^{-7}	NCRP, 1999
Surface water	3.0×10^{-5}-2.1×10^{-3}	WHO, 2001
Groundwater	4.0×10^{-5}-2.0×10^{-3}	WHO, 2001

Major sources of radioactive waste and contamination emanate from the production of electrical power and weapons from nuclear fuels, nuclear weapons' tests, fuel reprocessing, and nuclear accidents (Hu *at al*., 2010). Other sources of uranium include by products of mining activities of other minerals such as gold and copper (Ginder-Vogel *et al*., 2006). The process of using uranium for nuclear fuels or nuclear weapons generates a lot of uranium waste that has always been a problem for long term storage. Every 900 kg of natural uranium enriched for nuclear energy purposes contains about 120 kg of enriched uranium and the remaining 780 kg is depleted uranium (DU) (Rock Talk, 2006). In order to make a nuclear reaction occur, there has to be a greater percentage of the more fissionable ^{235}U in the fuel than occurs in nature. The enrichment process converts U_3O_8 into a gas, uranium hexafluoride (UF_6), which enables the uranium to be enriched from a ^{235}U content of 0.7% to about 3 to 4%. The enriched UF_6 is converted back into UO_2 and formed into fuel pellets. For weapons grade uranium, this content can even go up to much higher levels of up to90% ^{235}U. DU is obtained as a by-product in the enrichment process of natural uranium. DU is distinguished from natural uranium by lower relative concentrations of 0.25 to 0.30% ^{235}U (Bleise *et al*., 2003).

2.1.1 Uranium mining technologies and mining in South Africa

Various methods are available for mining of uranium as summarized in Table 2.2. These methods have been changing over time with the introduction of new technologies. Mining challenges arising from reaching deep ores also influence mining methods. In 1990, about 55% of world production came from underground mining, but this shrunk dramatically to 33% from 1999. ISL mining has been steadily increasing its share of the total. In 2010 production was as shown in Table 2.2.

Table 2.2: Methods used in the mining of uranium (World Supply of Uranium).

Method	tonnes U	%
Conventional underground	15,095	28
Conventional open pit	13,541	25
In situ leach (ISL)	22,108	41
By-product	2920	5

Until the mid-1970s, uranium was recovered exclusively through conventional underground mining and open-pit mining. The first commercial application of *in situ* recovery and *in situ* leach, ISL, techniques that used chemical agents to extract the uranium through an array of injection and recovery wells was in 1975 (Clarke and Parker, 2009). Extraction using this method is accomplished by injecting a suitable leach solution into the ore zone below the water table for desired preset period so as to dissolve the metal. The recovery of the pregnant solution is forced through other production wells. The uranium bearing solution is then pumped for further processing. The technique, wherever properly implemented, has resulted in good recovery of the metal that compares well with the recovery using conventional methods (Sarangi and Beri, 2000). Acid leach approach employs an acid based leaching system like dilute sulfuric acid to dissolve and oxidize the metal ion. Unlike conventional mining of uranium, ISL recovers the uranium in a solution rather than in ore like in the case where convectional mining is used (Manual of acid ISL uranium mining technology,

2001). Conventional mining involves removing mineralized ore from the ground, breaking it up and treating it to remove the minerals being sought. On the other hand, ISL involves leaving the ore where it is in the ground, and recovering the minerals from it by dissolving it and pumping the pregnant solution to the surface where the minerals can be recovered. Consequently, there is little surface disturbance and no tailings or waste rock generated as with other methods such as open pit.

Another type of mining method of uranium is uranium heap leaching (UHL) which is normally done if the uranium content is too low for the ore to be economically processed in uranium mills. This is achieved by placing the crushed ore on a leaching pad with a liner. The leaching agent (either alkaline or acidic) is then introduced on the top of the pile and seeps down until it reaches the liner below the pile, where it accumulates and then pumped to a processing plant (UHL, 2011).

In both ISL and UHL, after completion of the leaching process, a long term problem may result from naturally induced leaching, if the ore contains the mineral pyrite. Then, access of water and air may cause continuous bacterially induced production of sulfuric acid inside the pile known as acid mine drainage. This double effect results in the leaching of uranium and other contaminants for many years and may cause permanent contamination of ground water (UHL, 2011).

The production of uranium in South Africa has generally been a by-product of gold or copper mining. In Africa, gold and uranium mining are typically accomplished together, as both methods process large amounts of rocks for very small yields.

2.1.2 Toxicity and fate of uranium

Uranium atoms decay into other atoms that are also radioactive and commonly called "decay products." Radioactivity decay is a spontaneous process and cannot be accelerated or slowed down by any chemical or physical means (Montgomery,

2005). Uranium and its decay products primarily emit alpha radiation, however, lower levels of both beta and gamma radiations are also emitted. Alpha particles travel up to 50 mm in air and only a few microns in rocks before being absorbed and this makes them very safe. Beta particles have a travelling range of about 3 m in air and about 2 mm in rocks. Gamma rays have a high penetrating power and it can take a thick sheet of metal such as lead or concrete to reduce them significantly. ^{206}Pb, the last element on the list of uranium decay series, is stable and non-radioactive. It does not decay, and therefore has no half-life. The half live of ^{238}U is about 4.5 billion years, ^{235}U about 700 million years, and ^{234}U about 250 thousand years. In general, ^{235}U and ^{234}U pose a greater radiological health risk than ^{238}U because they have much shorter half-lives. Naturally occurring uranium contains three isotopes, namely ^{238}U, ^{235}U, and ^{234}U (Bleise *et al*., 2003). Krachler and Carbol (2011), noted that the use of uranium needs an appropriate knowledge of the isotopic composition of the material considered. Of the naturally occurring uranium radioisotopes, ^{238}U is by far the most abundant in terms of mass composition with a composition of 99.28% followed by ^{235}U at 0.72% and ^{234}U at 0.006%.

On average, approximately 90 µg of uranium exists in the human body from which about 66% is found in the skeleton, 16% in the liver, 8% in the kidneys and 10% in other tissues (WHO, 2001). Excessive exposure of uranium and its compounds cause kidney toxicity. This exposure can be through breathing air containing uranium dusts or eating substances containing uranium, which then enters the bloodstream. Once in the bloodstream, uranium compounds are filtered by the kidneys where serious damage can be inflicted at high blood concentrations. Virtually all of the observed or expected effects are from nephrotoxicity associated with deposition in the kidney tubules and glomeruli damage at high blood concentrations of uranium (ranging from about 50 to 150 mg depending on the individual) (Radiation Effects). Studies have shown that uranium causes birth defects in foetuses and infants and that the risk of leukemia is increased. Uranium also mutates human DNA and chromosomes and deforms them. Since uranium isotopes mainly emit alpha particles that have little penetrating ability, one possible radiological toxicity source can be from some of

the radioactive decay products. This is indeed the case as it was already proved in the 1920`s that contamination with radon (Schnessberger disease), a decay product of ^{238}U, can cause bronchial and lung cancer (Health Effects of Uranium Mining). For these reasons, several research groups have been stimulated for many years to investigate the chemistry and toxicology of uranium in all its chemical forms in order to assess the potential chemical and radiological risk to the environment and human health (Berto *et al*., 2011).

2.1.3 Uranium speciation

The need to determine different species of trace elements in environmental and biological materials is important since the effects or toxicity of an element and its behaviour depend to a great extent on its chemical form and concentration (Kot and Namiesnèik, 2000). The geochemical speciation of uranium influences its solubility, mobility and biological availability in the environment. Geochemical speciation information on uranium has been used to evaluate potential *in situ* remediation approaches (Lovely *et al*., 1991; U.S. DOE, 1999; Fredrickson *et al*., 2000).

Since the mobility and transport of uranium in soils occurs via water it is of great importance to investigate the aqueous chemistry of this element and its speciation in natural waters (Berto *et al*., 2011). Some previous studies underlined the importance and complexity of uranium speciation in ground waters mainly in the context of uranium milling for predicting radionuclide migration and for remediation strategies on contaminated sites (Teprat *et al*., 2009). The distribution of uranium ions in aqueous solution is dependent on both the solution pH and the total uranium concentration (Kotrba *et al*., 2011).

In nature, uranium ions normally occur in tetravalent and hexavalent form. The hexavalent form is easily soluble in acidic water (Sarangi and Beri, 2000). In oxygen-containing groundwater, uranium is most commonly found predominantly in the hexavalent oxidation state, U(VI), (Langmuir, 1978; Sandino *et al*., 1992; Farrel *et al*., 1999; Kilislioglu and Bilgin, 2003; Ginder-Vogel *et al*., 2006; Konstantinou, 2007) a highly soluble, mobile and therefore troublesome form. In

these oxidizing conditions, the uranyl predominates and behaves as strong acid in a Lewis acidity scale (Kotrba *et al*., 2011). Uranyl ions show high interaction with a variety of organic and inorganic ligands to form complex species of different stabilities (Kotrba *et al*., 2011). In systems with high dissolved carbonate concentrations, uranyl-carbonate complexes may become dominant (Gascoyne, 1992) and it forms soluble carbonate complexes in solution, Figure 2.2 (Langmuir, 1978; Pavel *et al*., 2009). These stable dissolved ternary complexes can effectively compete with mineral surfaces as "reservoirs" for U(VI) (Grenthe *et al*., 1992).

The hydrolysis of the uranyl ions in aqueous solution is significant at high pH values. A larger number of uranyl hydroxides, oxyhydrates and uranates are known, but $(UO_2)_2(OH)_2^{2+}\cdot H_2O$ is the most stable species in the presence of water at 25^{o}C. These hydrolyzed complexes represent a significant percentage of the overall speciation at high pH values (Baes and Mesmer, 1976).

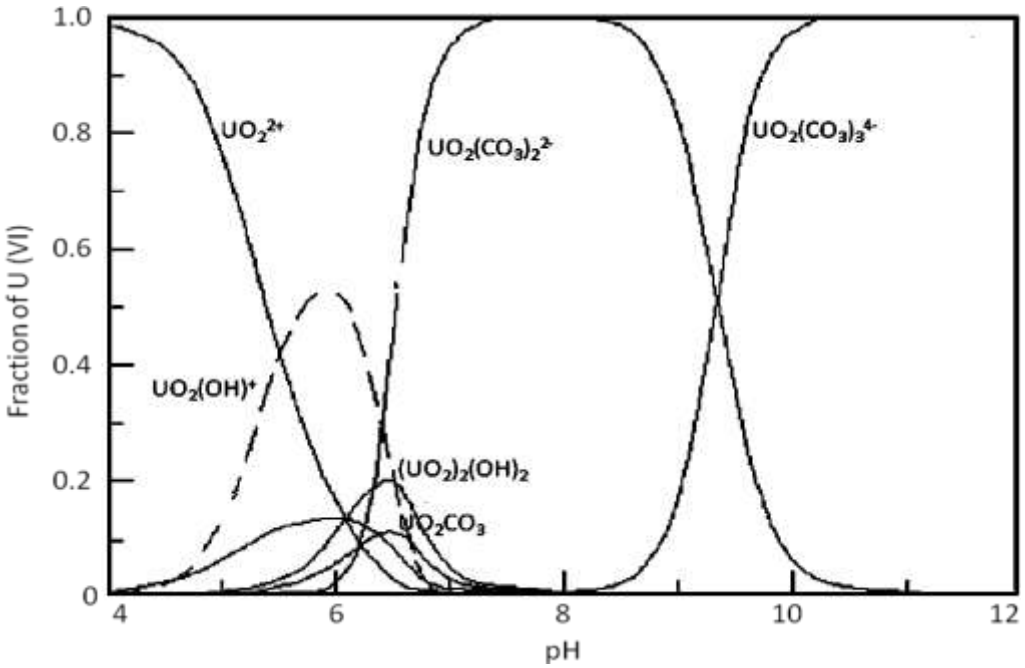


Figure 2.2: Species distribution of U(VI) (Choppin, 2006).

In concentrations below 10^{-6} M, $UO_2(OH)^+$ is the dominant hydrolysis species in solution. Above this concentration, the study of uranyl (VI) hydrolysis is

complicated due to the formation of polymeric species such as $(UO_2)_2(OH_2)_2^{2+}$, $(UO_2)_3(OH)_4^{2+}$ and $(UO_2)_3(OH)_5^{+}$. U(VI) bonds readily with minerals suspended in water and can spread easily over large areas. However, the tetravalent state, U (IV), resists combining with minerals and is highly stable and immobile (Ginder-Vogel *et al*., 2006).

2.2 Background of chromium

Chromium exists primarily in the mineral chromite, which is present in soils, waters, rocks, fauna and flora, and volcanic dust and gases. Many chromium compounds are coloured as its name means. Examples of these are ammonium dichromate (orange crystalline solid), chromium nitrate nonahydrate (purple crystals), sodium dichromate dihydrate (orange colour) and chromic sulphate which is green (Shupack, 1991).

Chromium has many industrial applications, for example, its compounds can be added to cooling water to inhibit corrosion. Chromium and its compounds are also employed in the manufacturing of inks, industrial dyes and paint pigments (Aksu *et al*., 2002). Other uses of chromium include stainless steel production, leather tanning, wood preservation, fertilizers, chrome tanning, textile, photography, *etc*., (Kannan, 1995). Chromium metal is also extensively used in ferrous alloys, mostly due to its resistance to ordinary corrosive agents. The dichromate anions can also be used to oxidize various functional groups like the aldehydes and alcohols, but their limited solubility in nonaqueous solutions has seen a continued interest in the development of new chromium(VI) reagents for the effective oxidation of organic substrates, especially under mild aprotic conditions. Considering this drawback, new polymer supported dichromates based on quaternized polyvinylpyridine were synthesized by several groups including that of Tamami and Kiasat (1997). Polymer supported solid phase organic reagents have an advantage that excess reagents and by-products can easily be separated from the reaction product which is not the case with their monomeric counterparts (Sherrington and Hodge, 1988).

2.2.1 Chromium mining in South Africa

The world has large reserves of chromite estimated to be 12 billion tons. Of this, over 95% of the world's chromium resources are concentrated in Southern Africa and Kazakhstan. The world's largest producer of ferrochrome is South Africa, having about 70% of the world's total chrome reserves. Chromium is normally mined in the form of the mineral chromite (Cammarota, 1992). These mines are located in the Bushveld Igneous Complex (BIC) in an area of approximately 12 000 square kilometres (Chromite Mining in South Africa-Overview). In total, there are 10 mining sites around South Africa (Mining Industry of South Africa). In total, the combined chromium ore reserves exceed 450 million tons, calculated to a depth of 300 metres, with an annual production capacity of more than 4 million tons. An estimation of over 200 000 jobs and a contribution of over R42 billion in Gross Domestic Product per annum by South Africa's chrome value (www.meraferesources.co.za), underscores the importance of chromium mining to the nation.

2.2.2 Speciation and fate of chromium in the environment

Chromium is one of those heavy metals which exist in variable oxidation states of which the trivalent Cr(III) and hexavalent Cr(VI) oxidation states are the most common in the environment (Toral *et al*., 2009). The oxidation states of chromium can go from -2 to +6. The electron configuration of the element in the ground state is $3d^5 4s^1$, while that for the trivalent state is $3d^3 4s^o$ and that of the hexavalent state is $3d°4s^o$. Chromium(III) oxidation state is the most stable form of chromium. Energy is required to convert the trivalent state to lower or higher states. The negative standard potential (E^o) of the Cr(III)/Cr (II) metal ion couple signifies that Cr (II) is readily oxidized to Cr(III), and Cr (II) species are stable only in the absence of any oxidant (Kotas and Stasicka, 2000). The reduction potential of Cr (II) is -0.91 V and that of Cr(III) is -0.74 V (De la Guardia and Morales-Rubio, 2003).

Just like other metals, chromium enters the environment as a result of effluents discharged from industries (Gómez and Callao, 2006). Once it enters the natural water system, chromium exists primarily in trivalent and hexavalent forms (Chen-Jen, 2002). The need to study chromium speciation emanates from drastic differences in biochemical properties of Cr(III) and Cr(VI) compounds (Panichev *et al*., 2008). For instance, Cr(III) is an essential element for humans and animals and plays an important role as the glucose-tolerance factor (GTF) in insulin metabolism (Langard and Norseth, 1990; Florence and Batley, 1980). Also Cr(III) is considered a micronutrient for many living organisms while Cr(VI) is an irritant to plants and animal tissues. The hexavalent form of chromium is also known to be very toxic to humans and causes chronic adverse effects (Langard and Norseth, 1990). Cr(VI) is carcinogenic because of its high oxidation potential and its ability to penetrate biological membranes (Udy, 1956; Lin and Huang, 2001). The toxicity of Cr(VI) is as a result of its properties as an oxidant (Katz and Salem, 1992). The Eh-pH diagram for chromium, Figure 2.3, provides a generalized depiction of the aqueous species stabilities in different redox conditions.

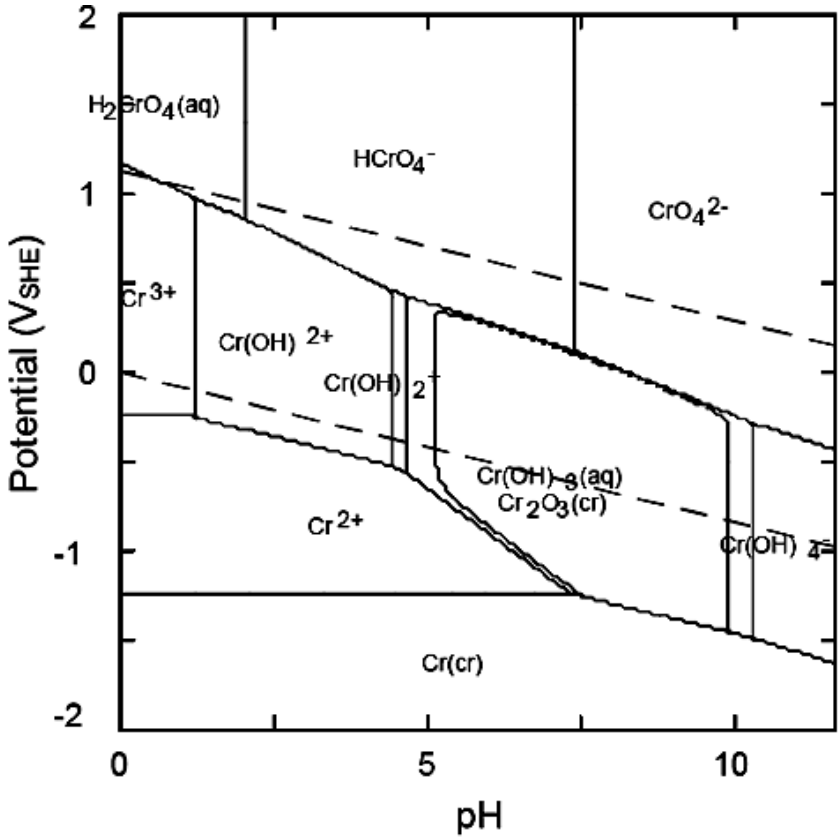


Figure 2.3: The pH-Eh diagram of stability of different chromium species (Ball and Nordstrom, 1998; Nieboer and Jusys, 1988; Richard and Bourg, 1991).

Trivalent chromium has a low solubility in aqueous medium in alkaline and neutral pH, (Petruzelli *et al*., 1995; Zhao *et al*., 1998). Low solubility of chromium(III) means it will be retained and adsorbed to solid particles or it precipitates, Johnson *et al*. (1992), thereby making it relatively immobile in the aquatic systems. On the other hand, Cr(VI) is highly soluble and can be transported over a great distance before it is reduced back to the trivalent state. In aqueous solution, the hexavalent chromium species may exist in a variety of oxospecies, namely, dichromate ($Cr_2O_7^{2-}$), hydrochromate ($HCrO_4^-$) or chromate (CrO_4^{2-}) depending on concentration and pH (Neagua and Mikhalovsky, 2010; Namasivayam and Sureshkumar, 2008; Chanda and Rempel, 1993), Figure 2.4.

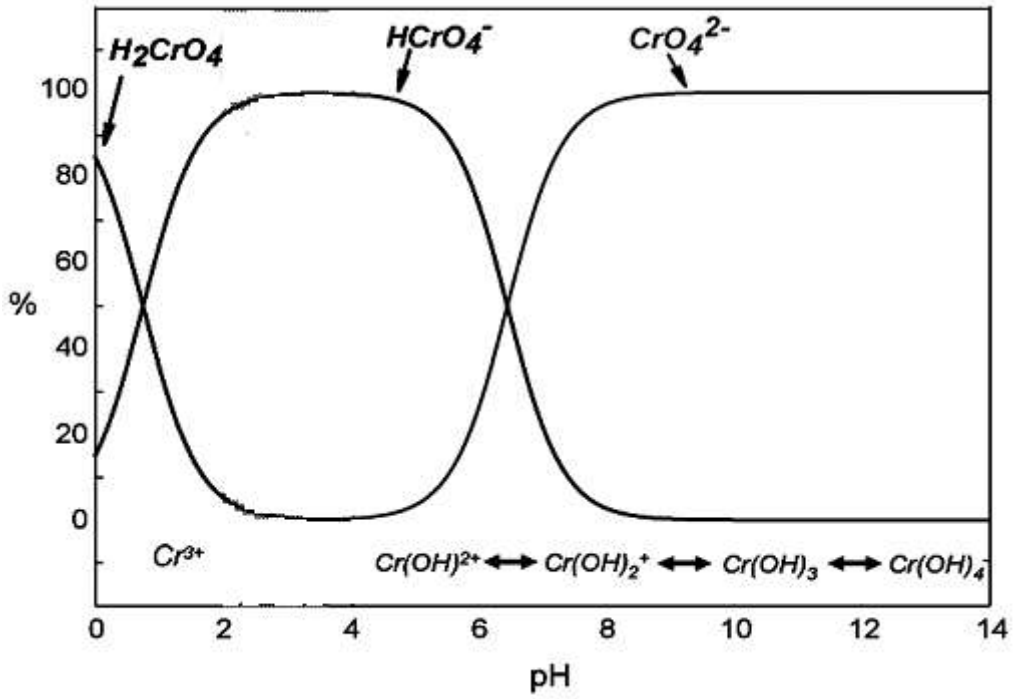


Figure 2.4: Species distribution diagram of Cr(III) and Cr(VI) in an aqueous system (Hagendorfer and Goessler, 2008).

According to Toral *et al*. (2009), the different species of Cr(VI) in aqueous solutions are given by equilibrium equations 2.1 and 2.2.

$$HCrO_4^- \rightleftharpoons H^+ + CrO_4^{2-} \qquad K = 3.2 \times 10^{-7} \qquad (2.1)$$

$$2HCrO_4^- \rightleftharpoons Cr_2O_7^{2-} + H_2O \qquad K = 33.1 \qquad (2.2)$$

Changing between the chromate and dichromate requires making the solution acidic or alkaline. In acidic solution, yellow dichromate is favoured while in alkaline solution, chromate blue colour is seen.

The structures of the chromate and dichromate anions shows that the Cr-O bond lengths are 166 pm and 163 pm, respectively, and the bridging Cr-O bond is 179 pm, while the Cr-O-Cr bond angle is 126^o (Shupack, 1991). The structures of these two anionic forms of chromium are based on the sharing of a corner of the tetrahedral structure of the chromate ion as polymerization proceeds as pH is lowered, (Figure 2.5).

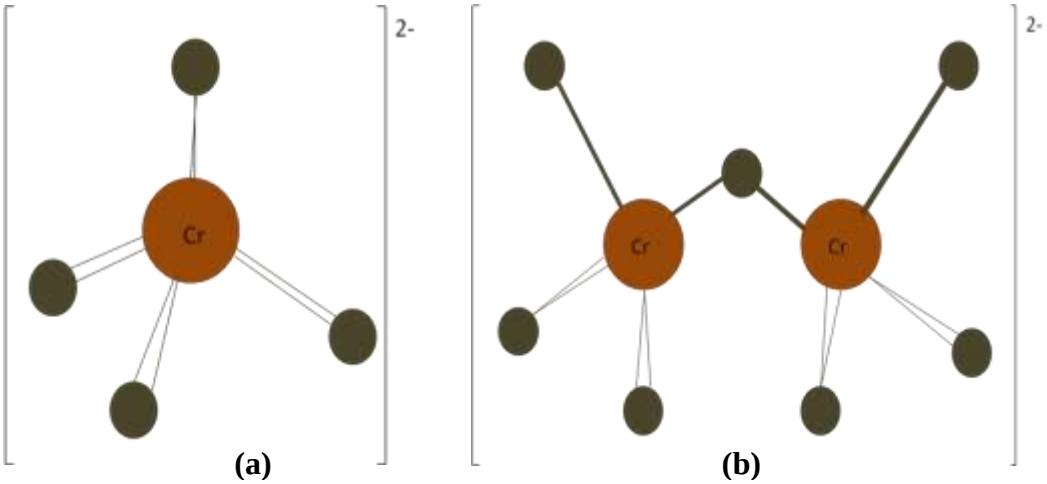


Figure 2.5: Structures of the (a) chromate and (b) dichromate anions.

2.2.3 Health and environmental concerns of chromium

One of the major causes of environmental pollution is the discharge of various heavy metals into the environment through various industrial wastewaters. These include chromium which is one of the most toxic and has become a serious health concern (Parka *et al*., 2005). The consequences of ingesting Cr(VI) are severe and will generally occur immediately after the incident. However, the likelihood of carcinogenic and cancer effects of oral exposures to Cr(VI) are dependent on the doses taken. Ingestion of very high concentrations of Cr(VI) of normally greater than 200 mg L^{-1} by humans can result in gastritis, nephrotoxicity and hepatotoxicity (Paustenbach *et al*., 2003). Because of the reductive conditions in the stomach, conversion of ingested Cr(VI) to Cr(III) prior to absorption is limited and this partly explains the lack of toxicity at lower pH (De Flora *et al*., 1987). The respiratory system has a low efficiency and capacity in the reduction of Cr(VI). This implies that cells are protected from toxic effects. However continual exposure to chromium increases the chances of lung and nasal cancer.

Owing to the corrosive nature of some chromium(VI) compounds, dermal exposure can lead to dermal ulcers and at high doses, systemic toxicity can lead to severe effects on the renal, haematological and cardiovascular system or even death.

2.3 South African regulation on waste and pollution

The National Environmental Management Act, 1998 (Act 107 of 1998) (NEMA), replacing the Environmental Conservation Act, 1989 (Act 73 of 1989), is the principal law through which environmental management is practiced and regulated in South Africa. However, NEMA is used in association with a lot of other Acts. Examples of these are the White Paper on Integrated Pollution and Waste Management (2000), the National Water Act, 1998 (Act 36 of 1998), Air Quality Act, 2004 (Act 39 of 2004) (Mining and Environmental Impact Guide, 2008). The South African Constitution (1996) also stipulates that everyone has the right to an environment that is not harmful to their health and well being. The Consumer Protection Act, CPA, which came into effect on 1 April 2011 includes the regulation of goods and services with actual or potential environmental and/or health impacts.

The South African government published, in 1999, a National Waste Management Strategy, NWMS, which presented a long-term plan for addressing key issues, needs and problems experienced with waste management. The 2008 National Radioactive Waste Disposal Institute Act provides for the establishment of a National Radioactive Waste Disposal Institute which manages radioactive waste disposal in South Africa. The responsibility for nuclear waste disposal has been discharged by the South African Nuclear Energy Corporation, NECSA. NECSA is a state corporation responsible for most nuclear energy matters including wastes and safeguards. The South African Bureau of Standards also sets regulation limits of various pollutants in different environmental compartments.

2.4 Water contamination and permissible limits of U and Cr(VI)

Most anthropogenic uranium arises from gold and copper mining (Todorov and Ilieva, 2004). Each year, large amounts of AMD containing uranium are leached into river and streams (Wang *et al*., 2011). Further, uranium contamination of groundwater is a widespread environmental problem (Riley and Zachara, 1992). Studies on groundwater at some contaminated sites have uranium contents up to 50 mg L^{-1} (Junghans and Helling, 1998; Meinrath *et al*., 2003; Jerden and Sinha,

2003). This value is more than 1600 times larger than the US EPA threshold value of 30 μg L^{-1}. Based on the risks posed by uranium and chromium, many countries and international organizations have proposed strict levels to limit discharge of these into water (Wang *et al*., 2011). Some of the limits are shown in Table 2.3.

Table 2.3: Maximum allowable limits of uranium and chromium(VI) in water by different bodies.

Body	U maximum allowed limit (μg L^{-1})	Cr(VI) maximum allowed limit (μg L^{-1})
U.S. EPA*	30	50
Canada⁂	20	50
WHO‡	20	50
South Africa⍭	≤ 15	≤ 7

* (US EPA, 1999), ⁂ (Health Canada, 1999) and ‡ (Shin *et al*., 2002), ⍭(DWA, 1999)

South Africa generally has problems of AMD from gold mining activities that also contain uranium (Tutu *et al*., 2009; Bakatula *et al*., 2012). The dust particles from tailing dumps are also blown by wind to nearby places and in the end are washed down into streams and rivers by rainfall and these contain uranium and chromium. Radionuclides contained in uranium tailings emit 20 to 100 times as much gamma-radiation as natural background levels on deposit surfaces. Some researchers have found out that gamma radiation levels decreasing rapidly with distance from the pile (Diehl, 2011).

2.5 Conventional methods of uranium and chromium removal

A number of conventional methods have been used for the removal of both chromium and uranium in various environmental compartments. Removal efficiencies for conventional treatment technologies for uranium are shown in Figure 2.6. Since this is old data, some of the reported removal efficiencies have since been improved.

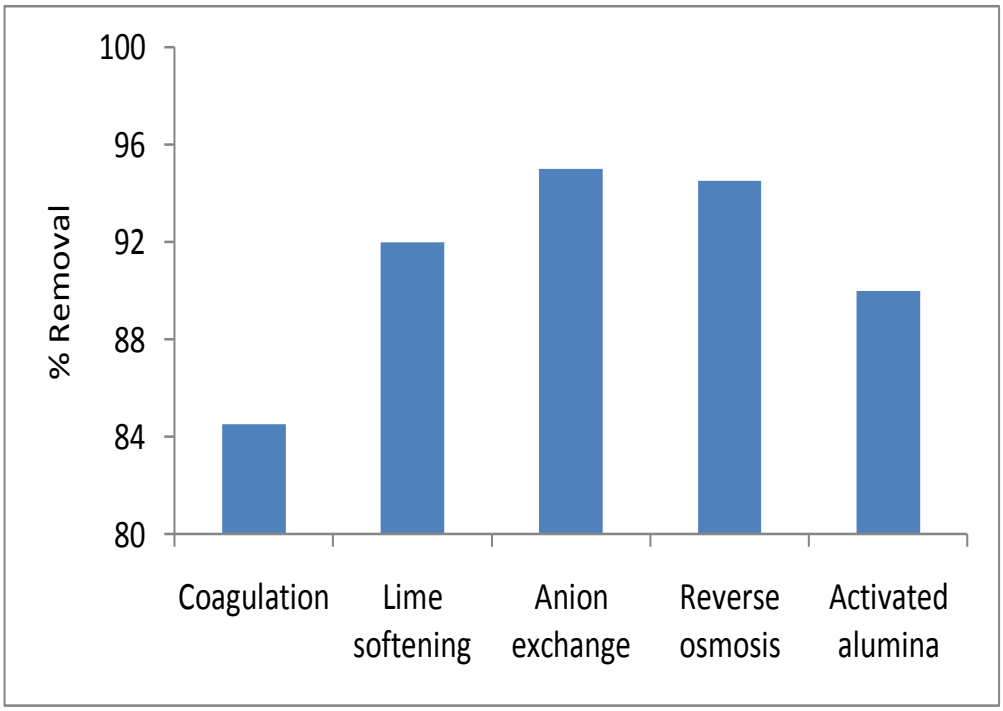


Figure 2.6: Removal of uranium by different conventional techniques.

However, the conventional methods have both advantages and disadvantages. In some cases, disadvantages exceed the advantages as seen in Table 2.4. This has therefore led to continued research in removal technologies. Current research is focused on either improving the existing ones or developing new ones altogether. Some of the conventional technologies are briefly discussed below.

Table 2.4: Advantages and disadvantages of some convectional removal techniques (Wang *et al*., 2010).

Method	Disadvantages	Advantages
Chemical precipitation	pH dependence Difficult separation Adverse effect by chelating agents Result in sludges Chemical required	Simple and cheap
Ion exchange	Sensitive to particles High operational costs No selectivity to alkaline metals Membrane fouling	No sludge generation Pure effluent recovery possible
Membrane technology	Membrane fouling Limited life of membrane Expensive High pressure	Pure effluent
Flocculation	Chemicals required Depend on basin design	Generate very fine particles of precipitates
Flotation	Less selective for heavy metals	Costly
Electrodialysis	Takes time Large electrode surface area used Fouling Expensive	Metal selective

2.5.1 Bioremediation

Bioremediation is the use microorganisms such as bacteria to remediate polluted environmental compartments. For uranium(VI) bioremediation, a possible viable alternative approach is that of reducing the soluble and thus mobile U(VI) to relatively insoluble U(IV) which precipitates in solution (Lovley *et al*., 1991; Finneran *et al*., 2002; Anderson *et al*., 2003) using microorganisms. This can prevent further migration and spread of the uranium contamination (Kelvin *et al*., 2005). Several researchers, like that at Stanford University and Oak Ridge National Laboratory (ORNL) have shown that several common types of bacteria can be used to convert an unstable form of uranium, U(VI), into a more stable form, U(IV). The implication of this is that the environmental and health threat of uranium contamination is reduced (Ginder-Vogel *et al*., 2006).

Numerous common dissimilatory metal reducing bacteria (DMRB) and sulphate reducing bacteria (SRB) are known. These include *Shewanella*, *Geobacteraceae*, and *Desulfovibrio* species. They couple the oxidation of organic matter and H_2 to the reduction of U(VI) resulting in U(IV) and the subsequent precipitation of uraninite (UO_2) (Gorby and Lovley, 1992; Fredrickson *et al*., 2000), a sparingly soluble phase. Figure 2.7 demonstrates how *Geobacteraceae* species can be used to effectively remove uranium from contaminated groundwater by reducing soluble U(VI) to the relatively insoluble U(IV) with organic compounds serving as electron donors.

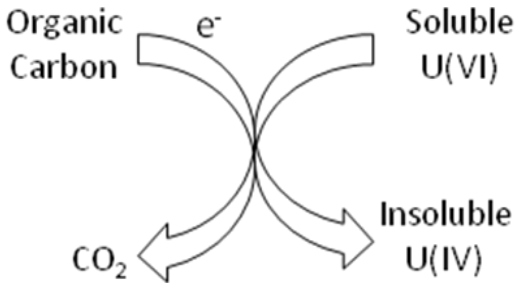


Figure 2.7: Uranium(VI) reduction driven by microbial respiration (modified from Ginder-Vogel *et al*., 2006).

Polti *et al*. (2009) provided quantitative information on the reduction of Cr(VI) in soil samples by an indigenous actinomycete, *Streptomyces sp.* MC1. This species, previously isolated from sugarcane demonstrated its ability to reduce Cr(VI) in liquid minimal medium. Chatterjee *et al*. (2011) studied the Cr(VI) reduction capability of a bacterial strain *Cellulosimicrobium cellulans* in two environments, of nutrient-supplemented and non-supplemented. In the former, the bacterial strain was observed to be reduced by 54.89% Cr(VI) from the wastewater. In their study, Mishra *et al*. (2012) investigated the Cr(VI) resistance in *Lactobacillus* strains and they also evaluated the reduction of Cr(VI) by the same species. A complete bacterial reduction of 32 mg L^{-1} of Cr(VI) was observed within 6 to 8 hours.

2.5.2 Permeable reactive barriers (PRBs)

Permeable Reactive Barriers are trenches or fence-like arrays of non-pumping wells placed in the subsurface at depths of up to 45 m to intercept the flow of contaminated ground water (Freethey *et al.*, 2002). The fill materials contained within the PRBs react by degrading or sequestering the dissolved contaminants. The PRBs act as large *in-situ* filters for cleaning up ground water. Some of the advantages for the use of PRB technologies are that they offer lower operating costs, are highly energy efficient and require no surface facilities or ground water pumping (Freethey *et al.*, 2002; Morrison and Spangler, 1992; Shoemaker *et al.*, 1995). The use of PRBs is a relatively new technology that offers promise to overcome these problems encountered with convectional methods such as pump-and-treat which is ineffective especially when dealing with large contaminated areas. Two commonly used PRBs contaminant-removal mechanisms are: (a) precipitation reactions in which metal contaminants are sequestered within freshly formed mineral phases, and (b) oxidative degradation of contaminants by particulate iron metal. For PRBs to be cost-effective they should be reusable for a longer period of time. They should not be susceptible to clogging or rapid passivation by reaction products (Fuller *et al*., 2003).

2.5.3 Chemical precipitation

Chemical precipitation is a method of wastewater treatment where chemicals are added to form particles which settle and remove contaminants. It is a favourable method especially when dealing with large volume of matter which contains heavy metal ions in low concentration (Eisazadeh, 2008). The solubility of precipitated metal compounds should be known for the successful implementation of the chemical precipitation approach. If a metal can form an insoluble compound, then the compound can be removed *via* clarification and filtration (Amer, 1998). However, this technique has a disadvantage that it produces a large amount of sludge precipitate that requires further treatment (Acheampong *et al*., 2010). Iron mediated reductive precipitation of redox active metal species has been proposed for the removal of soluble metals and radionuclides from contaminated ground water (Cantrell *et al*., 1995). Cantrell *et al*. (1995) and Gu *et al*. (1998), attributed the removal of the soluble uranium to reductive precipitation of U(VI) to less soluble U(IV) species and adsorption of the uranyl to iron corrosion products. Zero valent iron can reduce uranium species adsorbed on its surface (Fiedor *et al*., 1998). Under anaerobic conditions, the thermodynamics of U(VI) reduction by zero valent iron can be described by the following redox couples (Pourbaix, 1966):

$$UO_2^{2+} + 2e = UO_2^{o} \qquad E = 0.221 + 0.0295 \log [UO_2^{2+}] \tag{2.3}$$

$$Fe^{o} = Fe^{2+} + 2e \qquad E = 0.440 - 0.0295 \log [Fe^{2+}] \tag{2.4}$$

Iron can be used to precipitate chromium(VI). However, this is pH dependent as investigations of Olazabal *et al*. (1997) showed. Precipitation equilibria and spectroscopic studies of the Cr(VI)/Fe(III)/H_2O system have been performed and the identified precipitates which existed were $FeOHCrO_4$, $FeOHCrO_4 \cdot 2Fe(OH)_3$ and $Fe(OH)_3$, depending on the pH used. Gheju and Balcu (2011) investigated the total removal of chromium from Cr(VI) aqueous solutions by reduction with scrap iron and subsequent precipitation of the resulted cations with NaOH. Another precipitation reagent is sodium metabisulphite which was used by Ramakrishnaiah and Prathima (2012) as reducing agent for the reduction of

hexavalent chromium to trivalent chromium. Their results showed that total chromium can be removed from synthetic and industrial effluents by chemical precipitation.

2.5.4 Ion exchange

Ion exchange is an exchange of ions between two electrolytes or between an electrolyte solution and a complex using solid polymeric or minerilistic ion exchangers. Synthetic resins have been widely reported to be efficient in removing uranium from contaminated groundwater. Pakalns (1980) stated that Chelex-100 resin (a weakly acidic metal-chelating resin) conditioned at pH 4.6 separated uranium from fresh and saline waters. Diphonix is also a chelating resin that was found to remove uranium from water at near-neutral pH conditions (Chiarizia *et al*., 1997). At low pH conditions, uranium was found to be strongly adsorbed by strong-base anion exchange resins (DowexTM 1-X8 and Purolite A-520E) (Gu *et al*., 2004).

2.5.5 Phytoextraction

Phytotechnologies involving use of plants for pollutant removal have gained importance during the last two decades. The sequestration of heavy metals in plants is achieved mainly by absorption and accumulation mechanisms (Dhir, 2010). Phytoremediation technology involving use of aquatic plants can provide an economical and eco-friendly option for treating wastewaters containing heavy metals (Dhir, 2010). Many plants have been used for the remediation of uranium from soils and aquatic environments and some of them are *Brassica* juncea, *Brassica chinensis* (Huang *et al*., 1998) and *Lemna gibba L.* (duckweed) (Mkandawire *et al*., 2004).

Ipomoea aquatica exhibits uniform absorption characteristics showing over 75% removal of added Cr(VI) and this plant was selected due to its easy establishment, tolerance and growing easiness. Since in its use it showed no toxicity symptoms, it is a potential phytoremediant (Weerasinghe *et al*., 2008). Revathi *et al*. (2011)

successfully used a hyperaccumulator sorghum plant for phytoremediation of chromium metal from polluted soil of Ranipet Tanneries.

Phytoremediation has many limitations which include death of the plants if contaminant concentrations are too high. The toxicity and bioavailability of biodegradation products is not always known. The success of phytoremediation may be seasonal depending on location. Other climatic factors will also influence its effectiveness. If the plants contain high levels of heavy metals, disposal of harvested plants can be a problem.

2.5.6 Electrodialysis

Electrodialysis is a decontamination technique used to transport salt from one solution (the diluate) to another solution (the concentrate), by applying an electric current in an electrodialysis cell. Inside an electrodialysis unit, the solutions can be separated by alternately arranged anion exchange membranes, permeable only for anions and cation exchange membranes permeable only for cations. By this, two kinds of compartments are formed. By applying a current, cations within the diluate move toward the cathode passing the cation exchange membrane and anions move towards the anode passing the anion exchange membrane. A further transport of these ions, now being in a chamber of the concentrate is stopped by the respective next membrane. Zaheri *et al*. (2010) investigated the ability of electrodialysis for continuous removal of uranium from aqueous solutions in a bench scale unit.

2.6 Adsorption techniques

The shortfalls of the conventional methods have prompted the use of adsorbents as an alternative approach. Adsorption techniques are used mainly for metal recovery from dilute solutions. Thus, to find out an effective adsorbent that can be used repeatedly to adsorb metals is particularly important (Wang *et al*., 2011). Some of the common adsorbents that have been used to remove uranium(VI) and chromium from wastewaters are reviewed.

2.6.1 Zeolites

Zeolites are hydrated aluminosilicate materials having cage-like structures with internal and external surface areas of up to several hundred square meters per gram and cation exchange capacities of up to several milliequivalents per kilogram. At least 41 types of natural zeolites are known to exist, and many others have been synthesized. Both natural and synthetic zeolites are used in industry as adsorbents (Baker *et al*., 2009). Camacho *et al*. (2010) used clinoptilolite zeolite to remove uranium from groundwater. Mongolian natural zeolite was applied for adsorptive removal of hexavalent chromium contained in tannery wastewater (Bolortamir and Egashira, 2008).

2.6.2 Activated carbon

Activated carbon with low polar properties is a typical adsorbent commonly used for the removal of polar organic materials in water and wastewater (Ying *et al*., 1990). Commercial activated carbon (CAC) can also remove heavy metals such as Cd, Ni, Cr and Cu from wastewater (Demirbas *et al*., 2004, Ahn *et al*., 2009). Pellet-600 and PVA-300 with high mesoporous volumes and surface area were used by Yue *et al*. (2009) as a low-cost, chemically activated carbon materials. Their findings were that these two showed more effective removal efficiency of Cr(VI) from water than commercially available activated carbons tested. Acharya *et al*. (2009) activated carbon prepared from *Tamarind wood* with zinc chloride. They also studied the uptake of chromium(VI) on this adsorbent and the results indicated effective adsorption of chromium(VI) from aqueous solutions.

2.6.3 Carbon nanotubes

Due to a large surface area, and small, hollow and layered structures, carbon nanotubes (CNTs) have already been investigated as promising adsorbents (Chen *et al*., 2009). Extensive efforts have been put in the utilization of CNTs for removal of metal ions. Unlike many adsorbents, CNTs possess different features that contribute to the superior removal capacities such as fibrous shape with high aspect ratio, large accessible external surface area and well developed mesopores

(Gupta *et al*., 2011). Recently, it was shown that magnetic CNTs are very promising materials for efficient removal of heavy metal ions from aqueous solutions. Magnetic CNTs are composed of metallic cores of the diameter range 5-100 nm, which are completely wrapped in carbon coatings of thickness range 1-5 nm. The carbon coatings isolate the encapsulated nanoparticles. The crystallinity of these coatings is similar to carbon nanotubes. The magnetic CNTs-based sorbents are fully mobile as they can be very easily moved and separated by external permanent magnets.

2.7 Magnetic nanoparticles

One of the most important research and development frontiers in modern science is nanoscience (Faraji *et al*., 2010). Nanoparticle materials have drawn a lot of attention because most of their physical properties differ significantly from those of the corresponding bulk materials (Franco *et al*., 2005; Burke *et al*., 2002; Dimitrov and Wysin, 1994). These properties include electrical, optical, magnetic, and chemical properties (Hyeon, 2002). In literature, there are many nanoparticles that have been used and they include metals such as gold, iron, nickel, platinum, silver, cobalt, semiconductors like cadmium selenide, lead selenide, or hybrids like CdSe/Zn selenide (ZnS) (Burda *et al*., 2005). Among these magnetic particles, metal oxides are often preferred over pure metals (Schmidt, 2007: Ramanujan and Yeow, 2005) because they are more stable to oxidation. An example of these metal oxides is magnetite, Fe_3O_4.

These magnetic nanoparticles, have attracted a lot of attention over the past years and have found wide applications in many biomedical fields such as bioseparation, site-specific drug delivery and magnetic resonance imaging (Pankhurst *et al*., 2003). Good physicochemical properties of magnetic nanoparticles are taken advantage of in order to make full use of them. The ideal magnetic nanoparticles are expected to be of high magnetic properties, small size with narrow size distribution and superparamagnetic characteristics (Yang *et al*., 2004). Magnetic susceptibility is normally used to characterize magnetic materials and these materials can be classified into three main categories namely,

ferromagnetic, paramagnetic and diamagnetic. In antiferromagnetism, which includes certain metals and alloys in addition to some ionic solids, there is a spontaneous alignment of electrons at relatively low temperatures into opposite directions throughout the material. This antiparallel arrangement implies that there is no net spontaneous magnetization. Fe, Co and Ni are materials associated with ferromagnetism, together with their alloys. There are also many other materials which exhibit ferromagnetic behaviour. Typical ferromagnetic substances show permanent spontaneous magnetization even without external applied fields. For a ferromagnetic material, magnetic susceptibility, a material specific constant, is greater than the susceptibility of paramagnetic or diamagnetic materials. In ionic compounds, such as oxides, more complex forms of magnetic ordering can occur as a result of crystal structures. One type of magnetic ordering is called ferrimagnetism where the magnetic structure is composed of two magnetic sublattices separated by oxygen atoms. The exchange interactions are mediated by the oxygen anions. Superexchange interactions result in an antiparallel alignment of spins between the two sublattices. In ferrimagnetism, the magnetic moments of the sublattices are not equal to each other and as a result, there is a net magnetic moment. Figure 2.8 shows the orientation of electrons in different environments.

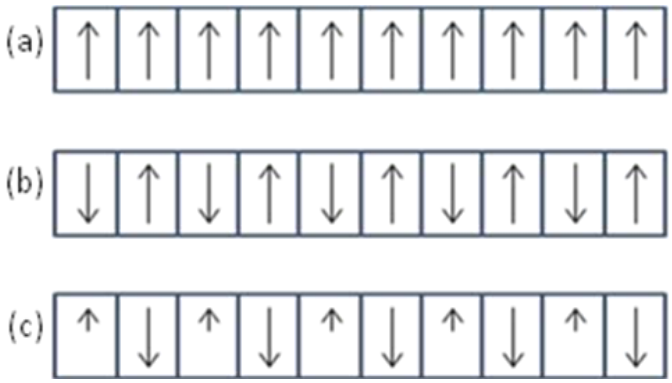


Figure 2.8: Orientation of domains in (a) ferromagnetism (b) aniferrimagnetism and (c) ferrimagnetism (Inorganic Materials Chemistry, Core Module 7).

2.7.1 Superparamagnetism

Lu *et al*. (2007) noted that, in most applications, the nanoparticles perform best when the size of the nanoparticles is below a critical value, which is dependent on the material but is typically around 10-20 nm. Below this critical value, each nanoparticle will become a single magnetic domain and shows superparamagnetic behaviour when the temperature is above the blocking temperature (Lu *et al*., 2007) and this is contrary to bulk materials (Frey *et al*., 2009). Nanoparticles can be easily magnetized and keep no remanent magnetization in the absence of the field.

By definition, superparamagnetism is a name given to a paramagnetic behaviour of small single-domain magnetic particles which are themselves internally coupled ferromagnetically or antiferromagnetically (Shaw and Heasley, 1967). Other new physical behaviours exhibited by nanoparticles apart from superparamagnetism are high field irreversibility, high saturation field, extra anisotropy contributions or shifted loops after field cooling. All these phenomena arise from finite size and surface effects that dominate the magnetic behaviour of individual nanoparticles (Tartaj *et al*., 2003).

2.7.2 Magnetic properties of magnetic particles

Instead of the ferromagnetic behaviour observed in bulk magnetic materials, the nanometer magnetic composition of a magnetic particle can lead to a superparamagnetic behaviour (Ganguly, 2005). The hysteresis loop or magnetization curve can be used to characterize magnetic materials and an illustration of this is shown in Figure 2.9.

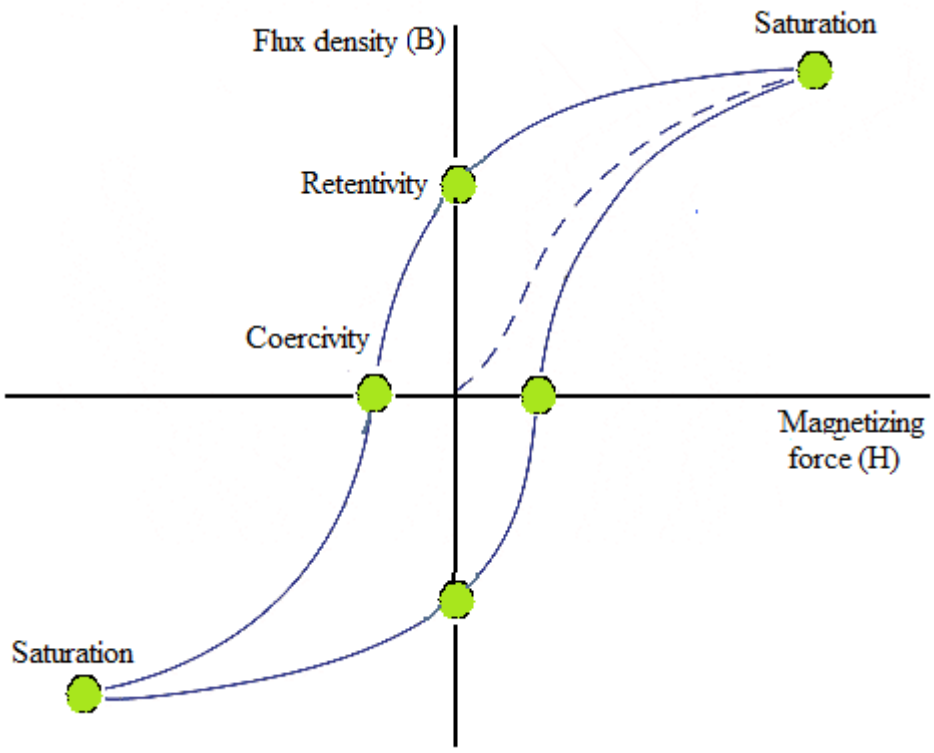


Figure 2.9: The Hysteresis loop of a superparamagnetic material.

From the hysteresis loop, a number of primary magnetic properties of a material can be determined, and these include coercivity and remanence. In superparamagnetism, magnetization does not return to zero and hysteresis behaviour is observed. The intercept of the magnetization curve with the flux density (B) axis gives the remanent magnetization, while the intercept with the magnetizing force (H) axis gives the coercivity. Superparamagnetic materials have high saturation magnetization and zero coercivity and remanence which make them distinguishable from ferromagnetism and paramagnetism (Superparamagnetism).

2.7.3 Magnetite and its magnetic properties

Among all known iron oxides, magnetite, Fe_3O_4, presents the most interesting and unusual behaviour because of the presence of both divalent and trivalent iron states, Fe^{2+} and Fe^{3+}, in the cubic inverse spinel structure (Daou *et al*., 2006; Ravikumar and Bandyopadhyaya, 2011). Its formular can be written as $[Fe^{3+}][Fe^{3+}Fe^{2+}]O_4$. In stoichiometric magnetite, the ratio of Fe^{3+}/Fe^{2+} = 2. Both

Fe^{2+} and Fe^{3+} are present in the final product. The magnetic properties reflect the splitting of the 5d orbitals, as shown in Figure 2.10 for octahedral and tetrahedral coordinations of the Fe atoms by oxygen atoms. The small splitting between the two sets of d orbitals caused by oxide ligands means that all Fe^{3+} ions have five unpaired electrons and all Fe^{2+} ions have four unpaired electrons as shown in Figure 2.10. Fe^{3+} and Fe^{2+} ions that are in octahedral sites are ferromagnetically coupled through a double exchange mechanism. The electron spins of the Fe^{3+} and Fe^{2+} in the octahedral interstices are aligned in a parallel manner.

The hopping of electrons between Fe^{2+} and Fe^{3+} ions in the octahedral sites at room temperature renders magnetic and metallic properties to magnetite. The Fe^{3+} ions in tetrahedral and octahedral sites are antiferromagnetically coupled through the intervening oxygen atom and their spins are anti parallel. Thus, the Fe^{3+} spins in the tetrahedral and octahedral sites cancel and what remains are unpaired spins from the Fe^{2+} ions in octahedral sites.

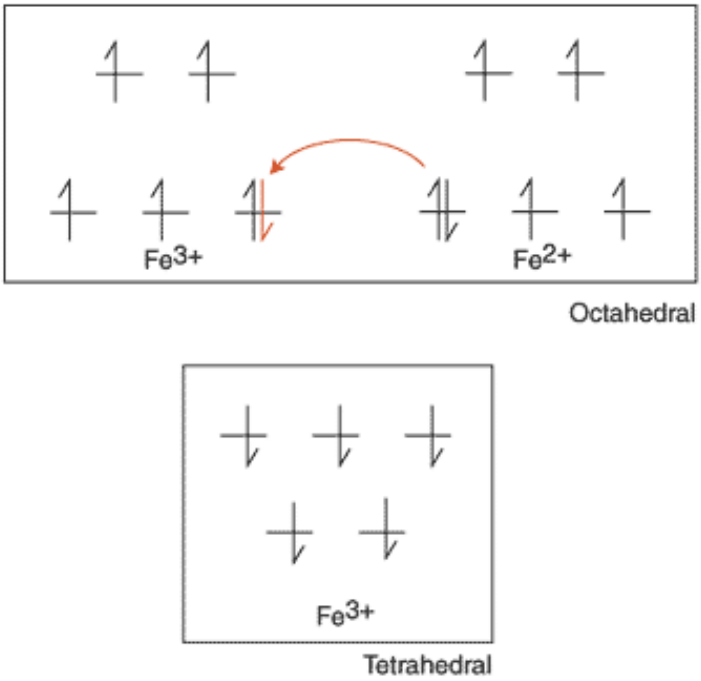


Figure 2.10: Electronic configuration in magnetite (Nanostructured Materials and Interfaces, Lecture notes).

2.7.4 Synthesis of magnetic nanoparticles

Magnetic properties of magnetic nanoparticles can be influenced by their particle sizes and size distributions. The particle sizes and size distributions of magnetic nanoparticles are in turn affected by their synthetic routes (Chin *et al*., 2011). Tartaj *et al*. (2003) further noted that the performance of nanoparticles will be dependent on their chemical and physical characteristics. In order to take maximum advantage of those novel properties, synthetic protocols are needed in which significant control can be exercised over those parameters (Chen *et al*., 2007). For these reasons, numerous physical and chemical synthesis approaches have been developed to produce Fe_3O_4 nanoparticles in order to obtain the desired properties (Chin *et al*., 2011). Some of these synthetic routes are briefly discussed in the following section.

2.7.4.1 Co-Precipitation

Co-precipitation is the simplest chemical pathway to synthesize magnetite (Burda *et al*., 2005; Laurent *et al*., 2008). This method has attracted a lot attention as it is environmental friendly because the synthesis is carried out in aqueous solutions without using any organic solvents under mild reaction conditions at relatively low temperatures (Iwasaki *et al*., 2009). The synthesis involves addition of the ferrous and ferric salts to an aqueous solution followed by the addition of a base, equation 2.5, in an alkaline hydrolysis reaction (Finotelli *et al*., 2008). A black Fe_3O_4 precipitate forms upon addition of a base.

$$Fe^{2+} + 2Fe^{3+} + 8OH^- \rightarrow Fe_3O_4 + 4H_2O \qquad (2.5)$$

Magnetite can be formed over a wide pH range for given concentrations of Fe^{2+} and Fe^{3+}. A complete precipitation of Fe_3O_4 is expected in the pH range of 7.5-14 while maintaining a molar ratio of Fe^{2+}:Fe^{3+} at 1:2 under an inert atmosphere. However, under oxidative environment, Fe_3O_4 may be oxidized to other forms of iron oxide as given by the equations 2.6 and 2.7 (Kim *et al*., 2003).

$$Fe_3O_4 + 0.25\ O_2 + 4.5\ H_2O \quad \rightarrow \quad 3\ Fe(OH)_3 \qquad (2.6)$$

$$Fe_3O_4 + 0.25\ O_2 \rightarrow 1.5\ Fe_2O_3 \quad (2.7)$$

2.7.4.2 Thermal decomposition

Highly crystalline and monodisperse Fe_3O_4 nanoparticles have been synthesized by conducting reactions at high temperature (>200^oC) through thermal decomposition of organometallic precursors in nonpolar organic solvents (Sun *et al.*, 2003; Park *et al.*, 2005). Park *et al.* (2005), performed a thermal decomposition of iron pentacarbonyl, $[Fe(CO)_5]$, for the preparation of monodisperse γ-Fe_2O_3 nanoparticles with average diameters in the nanoscale range. They achieved this by controlling the molar ratio of $[Fe(CO)_5]$ and the surfactant, oleic acid. This synthetic route is however unpopular since $[Fe(CO)_5]$ is very expensive and toxic. Chin *et al*. (2011) used different concentrations of iron (III) acetylacetonate, $Fe(acac)_3$ and varied volumes of polyethylene oxide in a quest to study their effects on the particle size of Fe_3O_4 nanoparticles formed. In their research, Maity *et al*. (2009) proposed a mechanism for solubility of the as-prepared by using surface charges and surface coating of the magnetite nanoparticles in aqueous suspension. They also used thermal decomposition of $Fe(acac)_3$ in tri(ethyleneglycol).

2.7.4.3 Microemulsion

For microemulsion to occur, the mixture system has to consist of an oil phase, a surfactant phase and an aqueous phase (Koutzarova *et al*., 2006). Generally in this method, nano-particles are synthesized in oil-in-water micro-emulsions by suspending a ferrous salt-surfactant to a water solution. The magnetic precipitate will then form as soon as a base is added to the reaction mixture (Thorek *et al*, 2006). In water-in-oil micro-emulsions, the aqueous phase is dispersed as micro-droplets surrounded by a monolayer of surfactant molecules in a continuous non-aqueous (hydrocarbon) phase. The soluble metal salt will reside within the aqueous droplets surrounded by the oil (Ha *et al*., 2008). In this method, co-precipitation occurs in tiny droplets of water embedded with a surfactant, so-called reverse micelles, which are distributed in an oil phase (Makovec *et al*., 2005). Nassar and Husein (2005) subjected $FeCl_3$ bulk solid powder to the action

of microemulsion formed with sodium bis (2-ethylhexyl) sulfosuccinate. Iron chloride was first solubilized in water of the microemulsions and then reacted with sodium hydroxide to eventually form the iron oxide nanoparticles.

2.7.4.4 Hydrothermal synthesis

Hydrothermal synthesis is a method to produce metal oxide crystals from metal salt aqueous solutions by application of heat (Dawson, 1988; Matijevic and Hsu, 1987). For example, hydrothermal treatment of iron salt could generate iron oxides when the applied conditions are appropriate (Mohapatra and Anand, 2010).

Hu *et al*. (2010) developed a hydrothermal method to fabricate sheet-like and pseudo-octahedral magnetite crystals. NaOH was added to $K_4[Fe(CN)_6]$ aqueous solution with constant stirring. Hydrothermal treatment was done at 160^oC after which magnetite precipitate was collected. In another study, Togashi *et al*. (2012) synthesized water dispersible magnetite (Fe_3O_4) nanoparticles in an aqueous environment under high temperature and pressure in the presence of 3, 4-dihydroxyhydrocinnamic acid by using a tubular flow reactor. Haw *et al*. (2010) synthesized Fe_3O_4 nanoparticles by precipitating $FeSO_4{\cdot}7H_2O$ and $FeCl_3$ in NaOH. However, prior to the addition of a base, dilute HCl was used to prevent the formation of other iron oxides. The precipitated black product was immediately added into a Teflon-lined stainless steel autoclave which was then placed in a furnace at 200^oC for 1 h.

2.7.5 Coating of magnetite

Due to the van der Waals' forces and magnetic dipole-dipole interactions resulting from residual magnetic moments, unmodified magnetite nanoparticles have a tendency to agglomerate and flocculate, Kim *et al*. (2003), thereby inhibiting the advantages of the specific properties by single-domain (Sun *et al*., 2005). This is also true for ferrofluids which are stable colloidal suspensions of single domain ferro or ferrimagnetic particles in a liquid carrier (Voit *et al*., 2001). Among other parameters, Häfeli *et al*. (2002) noted that surface coating and aggregation tendencies can influence the overall magnetic responsiveness of magnetic

particles. Coating of the magnetite particle surfaces can effectively prevent agglomeration and this is achieved by covering the magnetite with a surfactant or coating layer. Coating of the ferrofluids enables stabilization of the particles against gravimetrical forces and to avoid strong interaction and also agglomeration of the particles (Voit *et al*., 2001).

Selection of the appropriate core and monolayer material will then become critical as each layer or coating agent dictates a specific function (Lodhia *et al*., 2010). There are several choices of coating agents which include organosilanes, having C_{18} or aminopropyl groups, polymers (Inoue *et al*., 1990), biomass, hemimicelles/admicelles of ionic surfactant, alkyl carboxylates and many others.

As already mentioned these polymeric networks of the coating agents or surfactants encapsulate oxide monodomains and hold them apart against clustering together. Apart from this, the formation of a polymer layer on the surface of the magnetite nano-particles prevents further oxidation (Kim *et al*., 2003). According to Lee *et al*. (2003), if not properly coated, iron oxide can produce secondary contaminants when it comes into contact with water and oxygen. However, as noted by Niu *et al*. (2012), these coating agents cannot totally prevent the agglomeration and oxidation of nanoparticles in certain conditions such as in acidic solutions.

For coating with silicon alkoxide, a well-known Stöber process can be used (Ohmori and Matijevic, 1992), which comprises the hydrolysis and condensation of a sol-gel silicon alkoxide-based precursor (Cui *et al*., 2009), e.g. tetraethyl orthosilicate (TEOS). This method has been used to coat iron oxide nanoparticles by a number of researchers (Lu *et al*., 2002).

2.8 Ion imprinted polymers

Molecular imprinting can be defined as the assembly of a cross-linked polymer matrix around an imprint molecule that is held in place, either covalently or non-covalently or semi-covalently, by judiciously chosen functional monomers. The removal of the imprint molecule yields an imprint cavity of a specific size

(Lofgreen *et al*., 2011) and shape complementary to the imprint molecule. When the interaction between the template and monomers within is due to ionic interaction, this is called ion imprinting producing ion imprinted polymers. The product polymer, after template removal, thus contains the specific chemical "memory" in sites that selectively and discriminately recognize the imprint and are thus capable of its reuptake (Mosha and Mkayula, 2005). This product is the one which is generally called the molecularly imprinted polymer, MIP. In some cases, before polymerization reaction is complete and while it is still in a gel form, it can be used to form various shapes of MIPs like polymer monoliths, membranes, microspheres and nanospheres for different applications (Esfandyari-Manesh *et al*., 2011). The general technique of MIP synthesis is summarized in Figure 2.11.

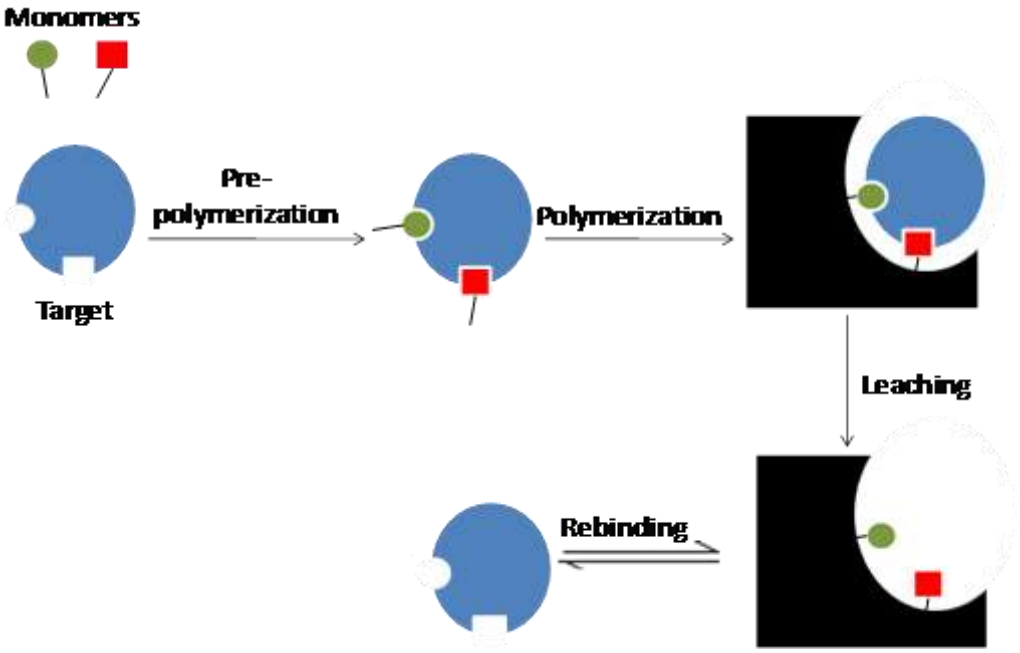


Figure 2.11: Schematic diagram depicting imprinting polymerization (Haupt and Belmont, 2008).

These recognition sites mimic the binding sites of biological receptor molecules such as antibodies and enzymes (Karim *et al*., 2005; Haupt and Belmont, 2008). The concept of molecular imprinting was first introduced in 1931 and has attracted wide interest from the beginning of the 1970s. Organic polymers with

predetermined ligand selectivities were prepared independently in 1972 by Wulff and Sarhan (1972) and Klots and Takagishi (1972) (Park and Seo, 2002). Over decades of research, molecularly imprinted polymers (MIPs) have gained more and more acceptance with respect to their application as polymeric antibodies in analytical chemistry and separation science (Yu and Lai, 2010).

The use of MIP sorbents was firstly directed at extracting of organic chemicals from complex samples. Pichon and Chapuis-Hugon (2008) and Turiel and Martin-Esteban (2010) have reviewed the role of MIPs for selective extraction of various organic compounds. Recently, a lot of publications have also been reported on selective extraction of metal ions using ion imprinted polymers, IIPs. IIPs are similar to MIPs but they can recognize metal ions after imprinting and retain all the advantages of MIPs (Daniel *et al*., 2005). Roa *et al*. (2004; 2006) have reviewed the metal ion imprinted polymers as novel materials for selective recognition of inorganics. Metal ion-imprinted resins which could adsorb the target metal ion from weakly acidic solutions were first reported by Nishide *et al*. (1976). Ion imprinted polymers are currently being increasingly explored in many techniques because of many outstanding advantages such as predetermined selectivity in addition to being simple and convenient to prepare (Metilda *et al*., 2004). The selectivity of these IIPs comes from the specificity of the ligand on the coordination geometry of the ion-template complex, coordination number of the ions, charges on the ions and on their sizes (Zhan *et al*., 2011). The synthesis process of IIPs is easy, low-cost and the resulting polymers are stable, versatile and resistant to a wide range of pHs, solvents and temperatures (Scorrano *et al*., 2011).

2.8.1 Magnetic ion imprinted polymers

Ion-imprinted polymers cannot be separated rapidly and effectively after treatment from polluted water. If the ion-imprinted polymers encapsulating Fe_3O_4 as magnetic cores could be synthesized, the adsorbing polymers would be separated easily by use of external magnetic fields replacing the centrifugation and filtration process in a convenient and economical way (Zhan *et al*., 2011; Philippova *et al*.,

2011; Ansell, 2008; Pan *et al*., 2011). Synthesis and properties of magnetic polymer beads constitute a new topic of research rapidly developing in the last 15 years. The magneto responsive polymeric beads benefit from the combination of features inherent to both their components: magnetic particles and polymers. Magnetic separation method is considered rapid and effective as compared to the traditional centrifugation and filtration techniques. Synthesis of magnetic polymer beads is generally performed in three different ways (Philippova *et al*., 2011):

- Synthesis of magnetic particles inside polymer matrix.
- Synthesis of the polymer in the presence of magnetic particles.
- Preparation of from pre-formed polymer and magnetic particles.

2.8.2 Types of template/monomer interactions

A crucial step in the synthesis of imprinted polymers is the prearrangement stage. At this stage, a complex is formed between the template and a functional monomer or a number of functional monomers. This complex is formed through a pre-polymerization reaction. The quantity and quality of the imprinted polymer recognition sites relates directly to the function of the mechanisms and extent the functional monomer-template interactions present in the pre-polymerization mixture (Karim *et al*., 2005). Depending on the type of interaction between functional monomer(s) and template involved in the imprinting and binding processes, molecular imprinting can be classified into three different categories (Esfandyari-Manesh *et al*., 2011; Turiel and Martín-Esteban, 2010) namely, the covalent, the semicovalent or sacrificial spacer and the non-covalent approaches.

In the covalent approach, reversible covalent bonds are formed between the template and the functional monomer(s). However, this approach is not so popular since it is not easy to come up with an appropriate template-monomer complex in which covalent bond formation and cleavage are readily reversible under mild conditions (Martin-Esteban, 2010). Non-covalent imprinting is based on the formation of relatively weak non-covalent interactions between selected monomer(s) and template molecule before polymerization. The monomer(s) and

template are simply mixed together and allowed to interact *via* self assembly (Cai and Gupta, 2004). Non-covalent imprinting approach uses intermolecular forces such as hydrogen bonding, electrostatic, hydrophobic interactions, ion pairs, dipole-dipole interactions, and van der Waals forces to form template-functional monomer(s) species in solution (Mayes and Whitcombe, 2005). This technique of non-covalent approach is most widely used because of the easiness of removing the template from the MIP resulting in greater number of affinity sites (Jiang *et al*., 2007). The imprinting process in semi-covalent imprinting is approached in the same way as the covalent method (Tulla-Puche and Albericio, 2008). However, this approach differs from covalent imprinting in that the rebinding step is non-covalent in nature (Qi *et al*., 2010). When the template, covalently embedded in the polymer matrix is removed from the MIP, functional groups capable of interacting non-covalently with the template species are left behind in the MIP at the cleavage site (Tulla-Puche and Albericio, 2008).

2.8.3 Polymerization reagents

There are several factors and reagents that influence polymerization, and hence the subsequent performance of the imprinted polymers. These include the nature of monomers, crosslinkers, porogen, template, initiator used, method of initiation, polymerization time and the dielectric constant of the porogens employed. Some of these reagents are reviewed in the following section.

2.8.3.1 Functional monomers

Excess of functional monomers will result in the presence of monomer units that are not complexed to templates. These monomers can undergo dimerization on their own. In their study to establish the effect of dimerization of the monomers, Zhang *et al*. (2010) used excess methacrylic acid (MAA) and realized that the accessible recognition sites were effectively diminished, thereby reducing the efficiency of the imprinting process. This was so because MAA has a strong tendency to form hydrogen-bonded dimers (Malosse, *et al*., 2008; Ansell *et al*., 2008 and Ansell and Wang, 2009).

Methacrylic acid is the most commonly used functional monomer because it can be used to synthesize MIPs of high selectivity for a large number of target molecules. It however fails for some targets, and therefore, other monomer combinations need to be found (Lanza and Sellergren, 2004). Figure 2.12 shows some other common functional monomers that can be used.

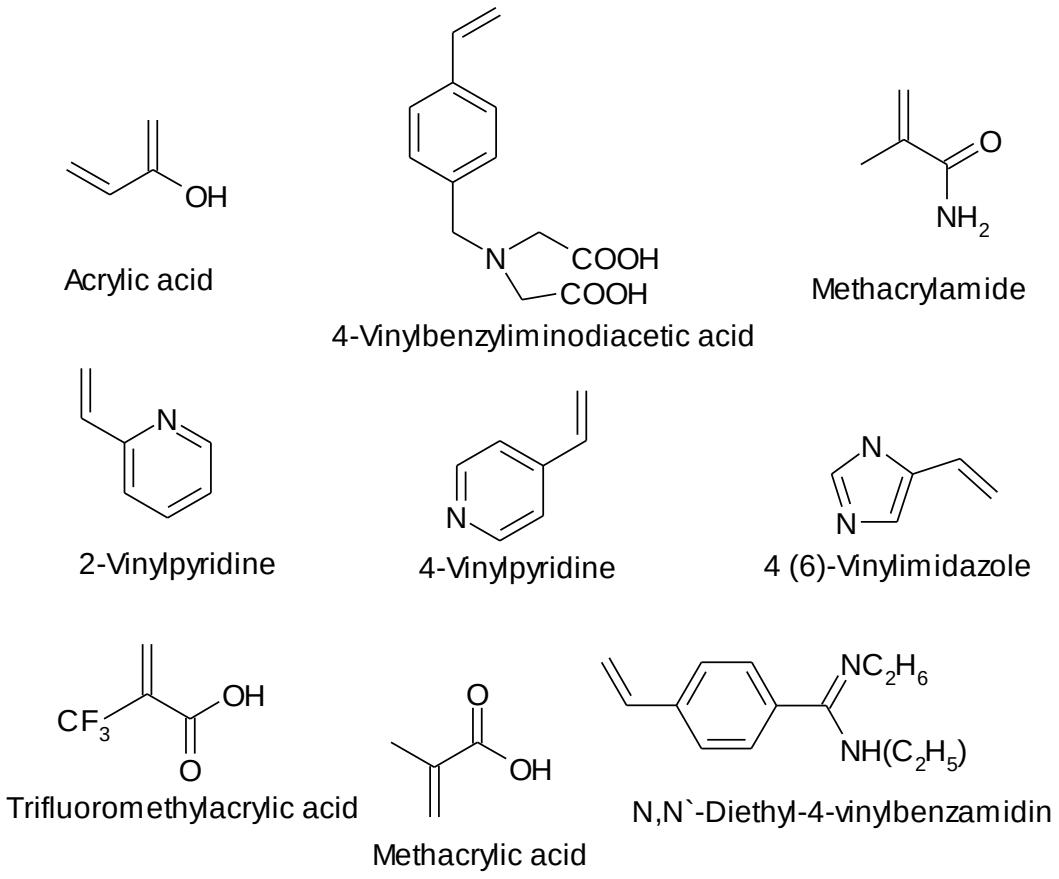


Figure 2.12: Common functional monomers used in imprinted polymerizations.

2.8.3.2 Cross-linkers

In order to have a permanent induced memory, the imprinted polymer needs to be rigid enough and the polymer needs to be macro-porous so as to allow the template molecules to easily diffuse in and out. To satisfy this, 80 mol% of the crosslinking monomer needs to be added as a reagent in the polymerization mixture (Idziak, 2000). Cross-linking monomers have two or more functional groups that are able to bind with the polymer chain to form a rigid three dimensional structure (Arnold *et al.*, 1999; Moreno-Bondi *et al.*, 2008). The

control of the morphology of the polymer matrix by cross-linking monomers is found in all types of polymer forms.

Approximately 80-90% of the imprinted polymers are composed of the cross-linking monomers and the other 10-20% comprises of other polymerization reagents. Having realized this large proportion of the cross-linking monomer in the polymer, Spivak and Sibrian-Vazquez (2002) directed their focus on designing cross-linking monomers for molecular imprinting in order to improve the performance of MIPs.

The most common cross-linking monomers have been EGDMA and DVB, which are commercially available. These cross-linking monomers are inexpensive and readily available in large quantities. In other applications of imprinted polymers, economic prices considerations are of less concern. Instead, cross-linking materials which give the best performance are used. Cross-linkers also control the hydrophobicity of the imprinted polymers. Hydrophobicity of the polymer is important in imprinted polymers because it influences the target analyte mass transfer into the cavity of the polymer. For example, non-polar analytes require a hydrophobic background. Since diffusion of the porogenic solvent is also dependant on the degree of cross-linking, the cross-linking monomers, together with their concentrations, should be carefully selected in order to give maximum performance. Figure 2.13 shows some commonly used cross-linkers.

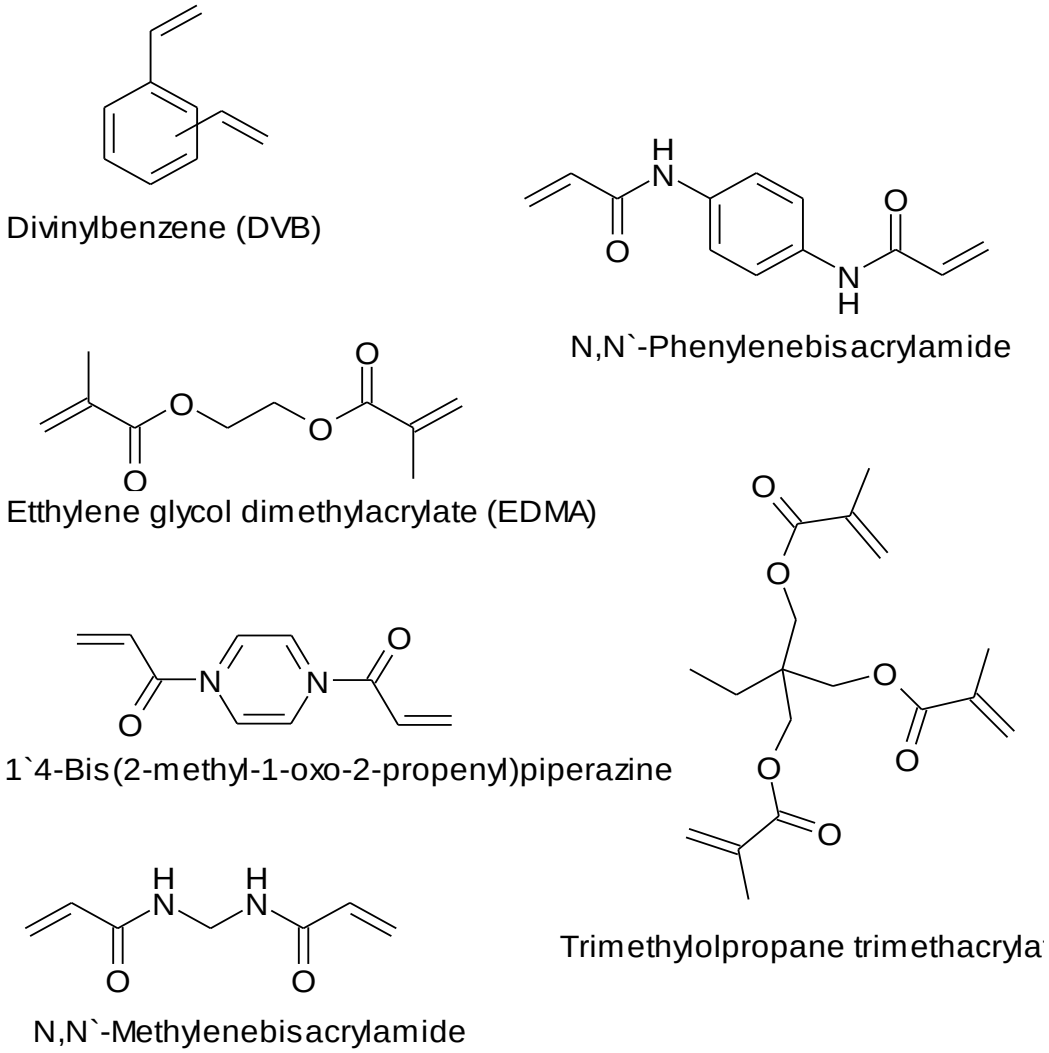


Figure 2.13: Common cross-linkers used in imprinted polymerization.

2.8.3.3 Initiators

The initiation step within the polymerization reaction is a two part process in which the initiator breaks up into free radicals. These radicals will then attach themselves onto monomers, thereby forming monomeric radicals. The cleavage of the radicals is normally as a result of subjecting them to heat, electromagnetic radiation or chemical reaction, which will homolyse them to radicals with higher reactivity than the monomer radicals. However, the reactivity must be low enough to allow the initiator radical to react with the monomer.

Azo and peroxide initiators with bond energies of 105-170 kJ mol^{-1} are particularly useful in this regard and are the mostly used initiators in the synthesis of molecular imprinted polymers (Sellergre, 2003). Azo initiators (R-N=N-R) normally have tertiary R groups that are able to stabilize the incipient radicals (Moad and Solomon, 1995).

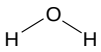
2.8.3.4 Porogen

Most imprinting techniques reported to date have employed relatively apolar and aprotic porogens such as toluene or chloroform (Yoshizako *et al*., 1998). This choice of porogens is clearly useful for obtaining accurate formation of the assembly (Yoshizako *et al*., 1998). In their investigations, Gladis and Rao (2004) found out that the selectivity varies with the polarity of the porogen used during polymerization. Uranyl-IIPs prepared in 2-methoxyethanol porogen gave high retention capacity and selectivity over thorium as compared to other porogens which were methanol, tetrahydrofuran, acetic acid, dichloroethane, N,N-dimethyl formamide and toluene.

Haginaka *et al*. (2008) also investigated the effect and influence of various porogens on the performance of the MIPs on the uptake of *d*-chlorpheniramine. Of the four porogens used, the specific surface areas and pore volumes followed the order toluene > phenylacetonitrile > benzylacetonitrile > chloroform.

In general, a low polarity solvent is normally chosen to preserve the interaction between the functional monomer(s) and the template during the pre-polymerization reaction. This came as an observation that there is a high correlation between the dielectric constant and the hydrogen bond donor/acceptor ability of the porogen (Mirsky and Yatsimirsky, 2011), Table 2.5.

Table 2.5: Examples of porogens used in molecular imprinting preparation and their physical properties.

Name	Chemical structure	Dielectric constant ($20^{o}C$)	H-Bonding
Toluene		2.4	Poor
Chloroform		4.8	Poor
Acetone		21.0	Moderate
Acetonitrile		36.6	Moderate
Dimethyl sulfoxide		47.2	Moderate
Methanol		33.0	Strong
Water		80.1	Strong
*Benzene		2.3	Poor
*Dimethylformamide		36.7	Poor
*1-Propanol		20.1	Strong

*****Mirsky and Yatsimirsky, 2011

2.8.4 Approaches in preparation of IIPs

2.8.4.1 Cross-linking of bifunctional reagents with linear chain polymers

In this approach, a linear polymer is formed with one ligand (with two functional groups) capable of forming metal-ligand complex. The ligand has functional groups that can help to polymerize at the same time. A good example is 4-vinyl pyridine. Polymerization is performed in the presence of a metal ion in a suitable solvent. The ligand therefore acts both as monomer and cross-linker forming a linear polymer. Nishide *et al*. (1976) cross-linked poly(4-vinylpyridine) with 1, 4-dibromobutane in the presence of metal ions such as Cu(II), Zn(II), Co(II), Ni(II), Hg(II) and Cd(II) as templates. The linear polymer can also be made up of two different monomers. Both or one of the monomers can act as a ligand for the metal ion. Kabanov *et al*. (1979) is reported to have cross-linked a copolymer of diethyl vinyl phosphonate and acrylic acid with N,N-methylene diacrylamide in the presence of metals. Figure 2.14 shows a typical linear chain polymer from bifunctional reagent.

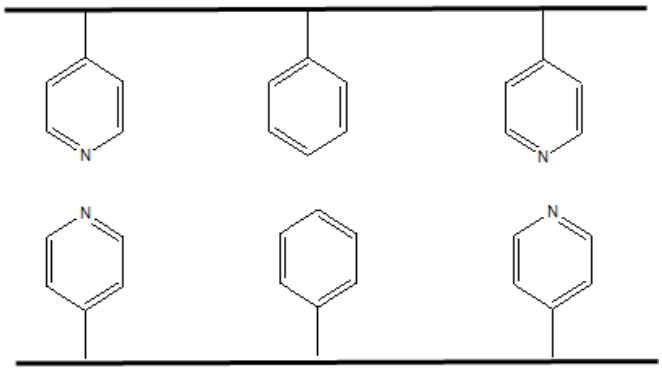


Figure 2.14: An example of a linear polymer with 4-VP enchored in the polymer matrix.

2.8.4.2 Chemical immobilization

In this approach, a vinylated ligand is chemically immobilized in the polymer matrix Figure 2.15. The ligand is chemically anchored to the cross-linked polymer. this is the most common used method for preparing IIPs (Rao *et al*.,

2006). A new IIP based on chemical immobilization has been reported for palladium ions by Rao *et al*. (2006). The IIP was synthesized by bulk polymerization using palladium iodide/thiocyanate-4-vinyl pyridinium ternary ion association complex in the presence of 2-hydroxyethymethacrylate and ethylene glycol diamine methacrylic acid (Daniel *et al*., 2006). Along the same lines, platinum IIP has been reported (Daniel *et al*., 2005). Many other IIPs based on this approach have been prepared for metal ions such as those of copper (Say *et al*., 2003), nickel (Ersoz *et al*., 2004), calcium and magnesium (Rosatzin *et al*., 1991) and zinc (Chen *et al*., 1997).

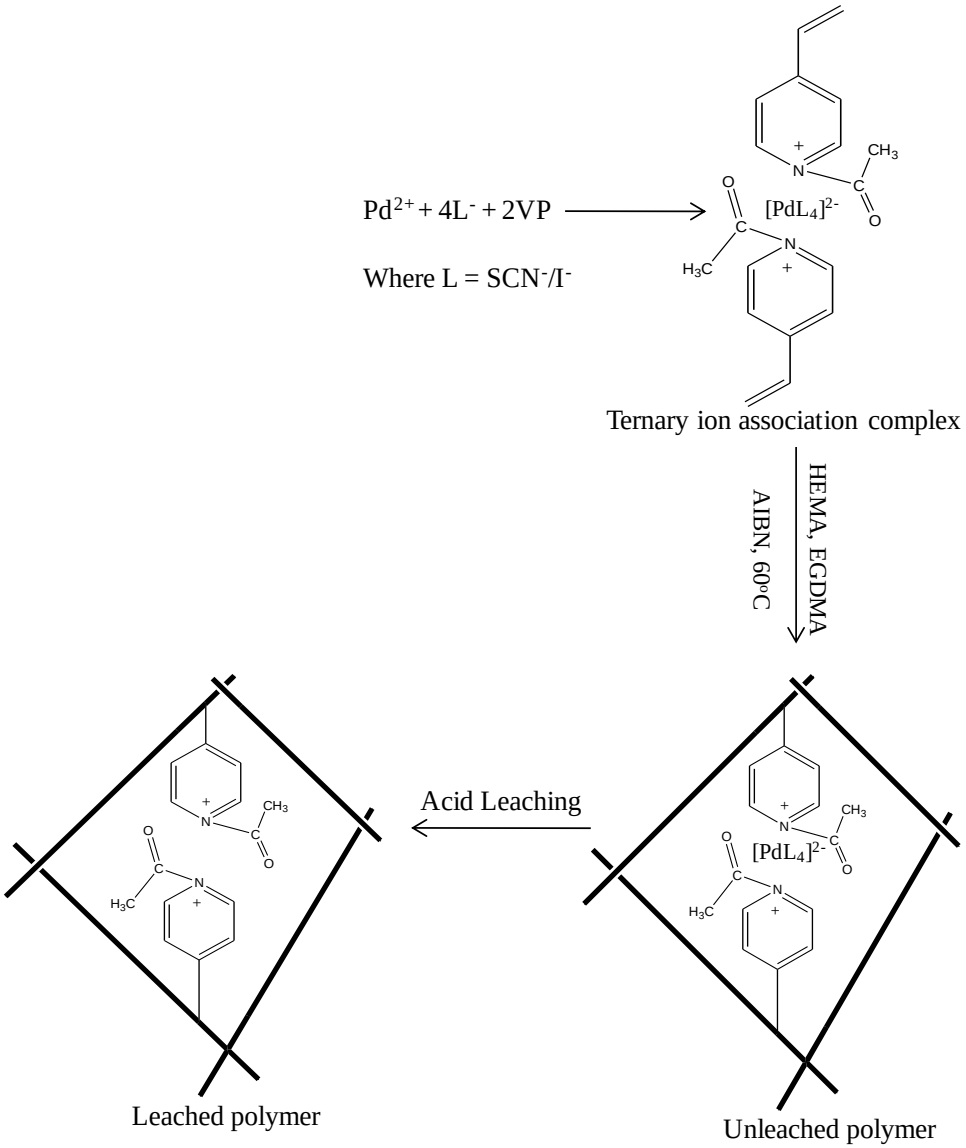


Figure 2.15: An example of the chemical immobilization approach in IIP preparation (Rao *et al*., 2006).

2.8.4.3 Surface imprinting

This approach involves emulsion polymerization using a functional monomer, an emulsion stabilizer, a polymer matrix forming co-monomer and print template. It is thus specific to emulsion polymerization. It is called surface imprinting because the microspheres are allowed first to form but before they are fully swollen, a metal ion is added to achieve complexation with ligand on the surface and then polymerization proceeds at room temperature. After polymerization, the template is removed which results in polymeric resins with functional groups on the surface giving recognition sites with preferential rebinding potential for the template ions. Surface imprinting is also called water-in-oil or oil-in-water emulsion IIPs. A number of IIPs have been reported for various metal ions such as Cu(II), Ni(II) and Co(II) (Tsukaghoshi *et al*., 1993; 1995; Yu *et al*., 1992; Okubo *et al*., 1987; Watanabe and Bunseki, 1977). It is, however, not as popular as chemical immobilization approach. Figure 2.16 shows an example of the preparation using this approach.

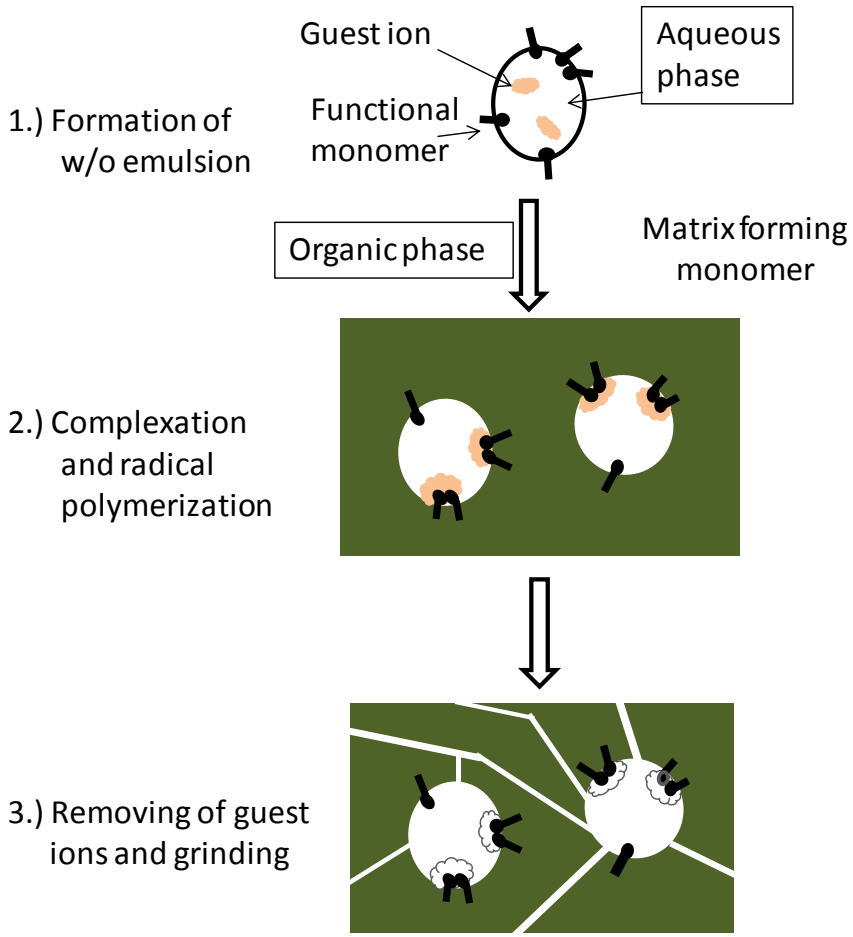


Figure 2.16: An example of surface imprinting approach in IIP preparation (Uezu *et al.*, 1998).

2.8.4.4 Trapping

This is a method that involves a vinylated and non-vinylated chelating agent (Rao *et al.*, 2006). Polymerization results in chemical bonding of the vinylated ligand as in chemical immobilization. However, the non-vinylated ligand does not have any polymerizable groups and is just trapped inside the polymer matrix. This method is also very common and perhaps it is as common as chemical immobilization. Many IIPs have been prepared for various ions such as those of dysprosium (Biju *et al.*, 2003), erbium (Kala *et al.*, 2004), neodymium (Gopikrishna *et al.*, 2005), uranium (Gladis and Rao, 2003; 2004), palladium (Daniel *et al.*, 2003; 2004), mercury (Liu *et al.*, 2005) *etc.* Figure 2.17 shows an example of the preparation using this approach.

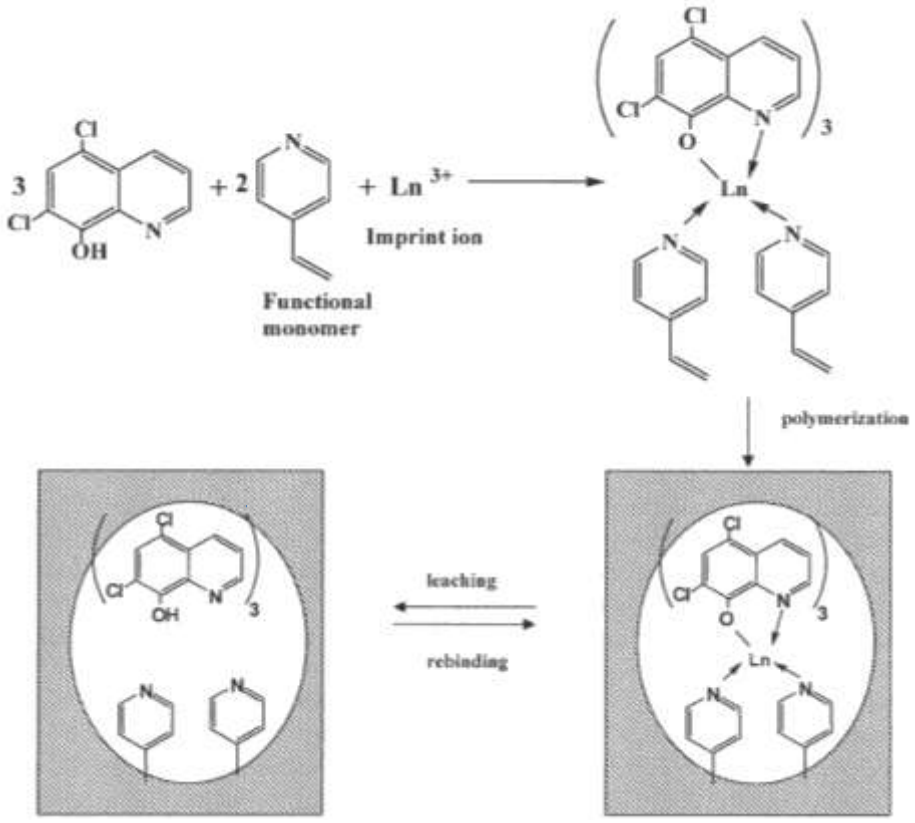


Figure 2.17: An example of trapping approach in IIP preparation (Rao *et al.*, 2006).

2.8.4.5 Metal coordination

In metal coordination, the template ion is a central ion surrounded by an array of ligand where it is bound. These ligands donate at least one pair of electrons to the central ion. This approach has been reported for IIP for zinc ions (Fan and Wang, 2010). The schematic representation is shown in Figure 2.18.

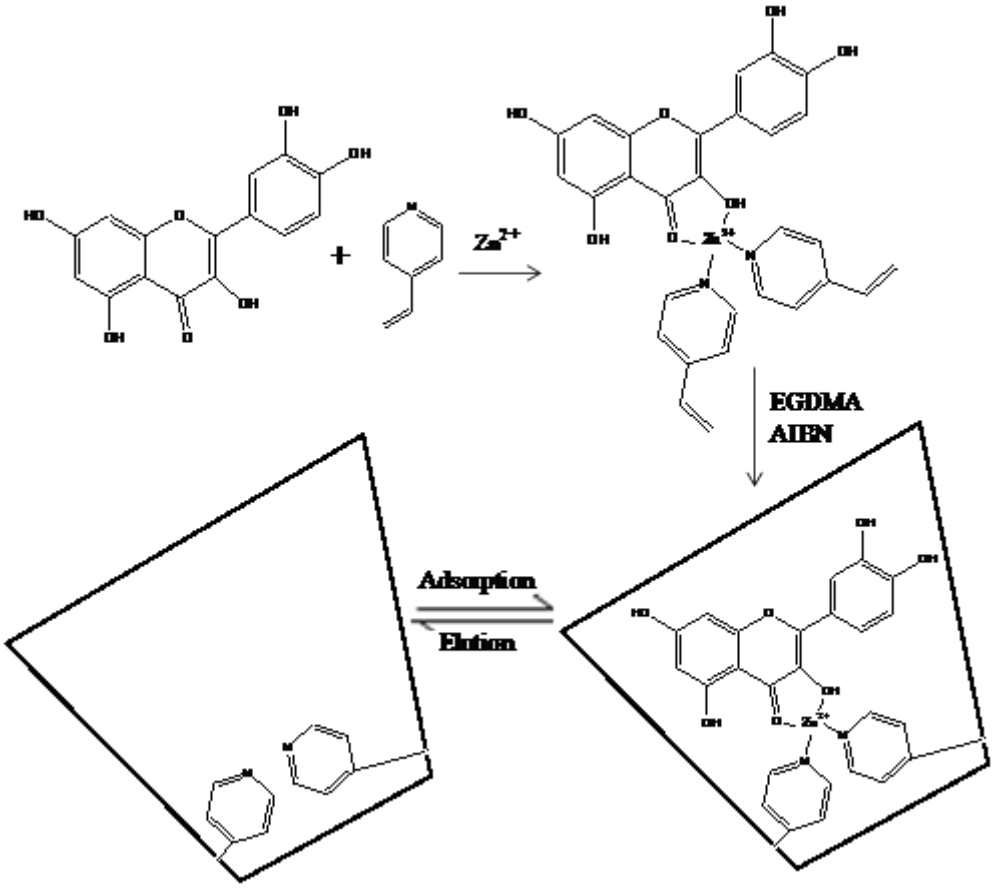


Figure 2.18: A scheme showing the metal coordination approach for zinc ion imprinted polymers (Fan and Wang, 2010).

The strength of the interaction depends on the oxidation state of the metal ion and on the ligand characteristics but it can be as strong as a covalent bond (Moreno-Bondi *et al*., 2008). This approach has also been used by Matsui *et al*. (1996) in their research on the removal of Co^{2+} where they used dibenzoyl methane, cobalt(II) ion, styrene, divinylbenzene and 4-vinyl pyridine as pre-polymerization reagents. Uranyl ions have a unique shape and coordination geometry and can interact strongly with oxygen donating ligands according to hard-hard interaction concept as compared to other actinide ions (Fasihi *et al*., 2011). As such, there have been a lot of investigations and reports on the complexation of uranium with different organic and inorganic ligands in solutions (Guillaumont *et al*., 2006). Oxygen donor organic ligands are present in most of naturally occurring organic compounds, like carboxylic and amino carboxylic acids, lipids, (poly) phenols, acidic (poly) saccharides, humic substances, *etc* (Berto *et al*., 2011). UO_2^{2+} has

also a tendency of reacting with nitrogen and sulfur donor ligands, showing a partial "soft" behaviour (Berto *et al*., 2011).

2.8.5 Types of polymerizations

The polymerization techniques in IIPs are similar for MIPs for organic and ionic compounds. Bulk polymerization has been the most commonly used method though it is seen as time consuming and labour intensive. Other methods such as precipitation and emulsion polymerizations have been used (Rao *et al*., 2004; 2006). Table 2.6 gives a summary of the various polymerization techniques that have been reported. Various types of polymerization are briefly discussed below.

Table 2.6: Summary of some reported IIPs and polymerization techniques used.

Template	Polymerization approach	Polymerization technique	Reference
Cu(II)	Chemical immobilization	Suspension	Qi *et al*., 2008
Cr(III)	Chemical immobilization	Suspension	Birlik *et al*., 2007
Pb(II)	Chemical immobilization	Suspension	Zhu *et al*., 2009
Hg(II)	Chemical immobilization	Suspension	Wu *et al*., 2007
CH_3-Hg	Chemical immobilization	Suspension	Buyuktiryaki *et al.*, 2007
UO_2^{2+}	Chemical immobilization	Bulk	Preetha *et al*., 2006
UO_2^{2+}	Trapping	Suspension	Sadeghi and Mofrad *et al*., 2007
Zn(II)	Surface imprinting	Emulsion	Uezu *et al*., 1998
Cd(II)	Surface imprinting	Emulsion	Fang *et al*., 2005

2.8.5.1 Bulk polymerization

Presently, most MIPs are synthesized by the classical bulk polymerization method (Pérez *et al*., 2000). The formed bulk polymers are then be crushed, ground and sieved to obtain particles mainly in the 25-50 μm size range (Pichon and Chapuis-Hugon, 2008). Grinding of the polymers normally produce particles that are irregularly shaped, polydisperse and usually include a large portion of fine particulate materials which are of no real use. Extensive sieving and sedimentation is done to achieve a narrower size distribution and to remove fine particles (Wang *et al*., 2006). With all the steps involved, it is evident that bulk polymerization is time consuming, labour-intensive and wasteful as well since only 30-40% of the ground polymer is recovered as useable material. A polymer yield of useful particles can even be as low as 20% (Brüggemann *et al*., 2000).

2.8.5.2 Precipitation polymerization

The main difference between bulk polymerization and precipitation polymerization is in the volume of the porogenic solvent used (Mohajeri *et al*., 2011). The key point in precipitation polymerization is the use of a porogen in which the monomers are soluble but the resulting polymers are not (Biffis *et al*., 2012).

2.8.5.3 Suspension polymerization

Suspension polymerization is an important process in industrial polymerization practice (Polacco *et al*., 2000). In aqueous suspension polymerization systems, one or more monomers are dispersed into droplets. This is normally achieved by rapid stirring as well as addition of small amounts of water-soluble dispersing agents (Kalfas *et al*., 1993). The size of the monomer droplets can be controlled by adjusting the stirring speed. Oil soluble initiators are normally used and the polymers are produced inside the drops in the same manner bulk polymers are produced (Brooks, 2010).

The function of the stabilizers in suspension polymerization is to hinder the coalescence of the functional monomer(s) droplets and of the formed polymer particles whose tendency to agglomerate may become critical when the polymerization has advanced (Kalfas *et al*., 1993). Wang *et al*. (2006) used liquid paraffin as a dispersing agent. Water and liquid perfluorocarbon have generally been used as an aqueous continuous phase and an organic phase, respectively (Wang *et al*., 2006).

The temperature that is used for suspension polymerizations is usually in the range of 40-90^{o}C under atmospheric pressure or it can be elevated to around 160^{o}C but at elevated pressure since operation must always be below the boiling point of the continuous phase (Kalfas *et al*., 1993).

2.7.5.4 Emulsion polymerization

Emulsion polymerization is a unique chemical process widely used to produce waterborne resins with various colloidal and physicochemical properties (Büttiker *et al*., 2011). Dvorakova *et al*. (2010) synthesized nanosized MIP particles by non-aqueous emulsion polymerization. Their motivation was that the standard emulsion polymerization for MIP synthesis using water disrupts the functional monomer-template interactions. This is due to the strong polarity and high hydrogen bonding capability of water. Ultimately, the efficiency of the imprinting process is greatly reduced. In Pickering emulsion, dispersed liquid droplets are stabilized by solid particles instead of conventional surfactants. The stabilizing particles are located at the interface between the two immiscible liquids, thereby preventing coalescence. She *et al*. (2011) used SiO_2 as stabilizing particles.

2.8.6 Application of imprinting technology

Synthetic molecularly selective receptors such as MIPs and IIPs find a widespread application in many areas of science as depicted in Figure 2.19. A particularly promising application of IIP is in solid phase extraction, SPE, where it is used to pre-concentrate and/or separate target species from other co-existing ions from complex matrices (Daniel *et al*., 2005). Not much has been reported about the use

of these materials for environmental remediation. MIPs as sorbents with better selectivities than those of traditional SPE adsorbents have recently been introduced as novel adsorbents for the extraction and clean-up of target compounds from various matrices such as wastewater or river water samples (Ersöz *et al*., 2004; She *et al*., 2010).

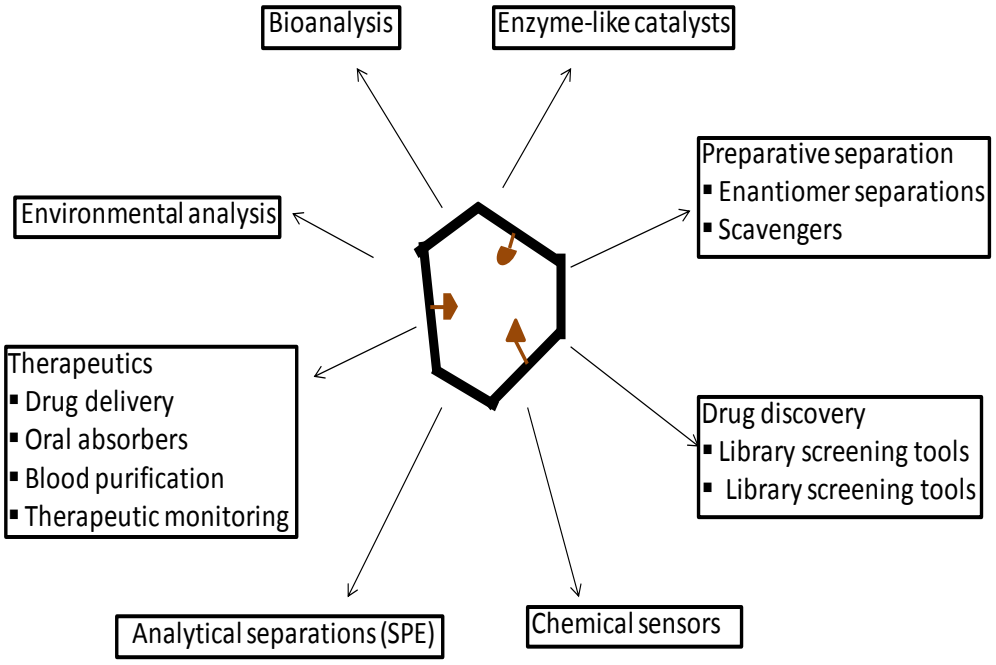


Figure 2.19: Scheme outlining the main applications envisaged for MIPs and IIPs, adapted from Sellergren and Allender, 2005.

In polymeric sorbents, the chelating functionality usually consists of some type of mono-, bi-, or polydentate moieties with donor groups which contain atoms like nitrogen, oxygen and sulphur. A review of some recent synthetically-prepared polymeric sorbents obtained by immobilizing a particular type of chemical moiety on magnetic materials is presented in Tables 2.7. Some polymeric sorbents have high capacity for metals. The high adsorption capacity of the sorbent is very important in applications to real samples. This is because of possible competition for adsorption with other anions such as SO_4^{2-} for Cr(VI) (Pakade *et al*., 2011). High capacity of the polymer allows the Cr(VI) to still being extracted in the presence of such competitors. The situation could be different for selectivity polymers such as ion imprinted polymers where even with low adsorption

capacity it is still capable of binding target metal ion (Pakade *et al*., 2011). However, even in such selective polymers, the cavities might still be large enough to allow co-extraction of other competitors like F^- (Pakade *et al*., 2011).

The synthetic polymeric sorbents or modified natural sorbents in theory should have high selectivity and fast mass transfers kinetics because the final functional groups of the sorbents are tailored to bind target metal ions. However, in many reported publications, selectivity studies are often not done and this makes it difficult to compare performance in this aspect. The equilibration time seem to depend on the actual sorbent and not the type. However, on average, synthetic polymeric sorbents and modified natural sorbents seem to have low equilibration time (20-60 min), thus with fast mass transfer kinetics. Most sorbents, regardless of the type, work best in acidic pH of the sample. This is perhaps expected especially since Cr(VI) is negatively charged so a sorbent with positively charged functional groups is needed for this metal ion. Most of these functional groups are amine based and therefore work best in acidic media that favours the positive charge on the functional group (Zhao *et al*., 2010). Duranoglu *et al*. (2010) observed the reduction of Cr(VI) to Cr(III) during the adsorption of the former onto activated carbon derived from acrylonitrile-divinylbenzene copolymer at sample pH of 2. This might not influence the overall adsorption if the formed Cr(III) is also adsorbed by the sorbent. For sorbents that are selective for Cr(VI), this reduction process could lower the amount adsorbed.

Most sorbents prepared are used to remediate polluted wastewaters such as acid mine drainage water where the pH of such wastewaters is generally acidic (Pakade *et al*., 2011). Most reported polymers are therefore very suitable for application to such polluted wastewaters. The only disadvantage is that at such low pH, samples have also high concentration of Fe^{3+} and SO_4^{2-} which are the major competitors for adsorption with uranium and Cr(VI), repectively (Pakade *et al*., 2011; 2012). Duranoglu *et al*. (2010) studied the various anionic competitors (Cl^-, NO_3^-, SO_4^{2-}, PO_4^{3-}) during the adsorption of Cr(VI) onto activated carbon derived from acrylonitrile-divinylbenzene copolymer at sample pH of 2. Factors that influence adsorption of these competitors include size, charge and hydration

degree. In their study, Duranoglu *et al*. (2010) experienced a maximum fall in adsorption of Cr(VI) by the sorbent owing to PO_4^{3-}. The reason for this is that PO_4^{3-} has more negative charges and is also polyatomic with similar molecular dimensions and consequently same hydration degree (Duranoglu *et al*., 2010). Cl^- has similar charge to Cr(VI) but has higher charge density due to the small molecular dimensions. However, it has higher hydration than $HCrO_4^-$. Cl^- had therefore the least influence on adsorption of Cr(VI) on the sorbent. In the pH range of 1-6, chromium ions coexist in forms of $Cr_2O_7^{2-}$, $HCrO_4^-$, $Cr_3O_{10}^{2-}$ and $Cr_4O_{13}^{2-}$ of which $HCrO_4^-$ is the most dominant while at higher pHs, CrO_4^{2-} and $Cr_2O_7^{2-}$ are the most dominant species (Garg *et al*., 2007).

Table 2.7: Polymeric sorbents for the removal of U(VI) and Cr(VI) from environmental samples.

Sorbent	Target	Binding capacity (mg g^{-1})	Equilibrium time (min)	Initial pH	Reference
Ion-imprinted chitosan composite magnetic microspheres	U(VI)	9	30	3.5	Wang *et al*., 2011
3-Aminopropyl triethoxysilane on silica coated Fe_3O_4	U(VI)	26	30	4.0	Sadeghi and Aboobakri, 2012
Magnetic Fe_3O_4-SiO_2 composite particles	U(VI)	52	16	6.0	Fan *et al*., 2012
Magnetic poly-(MA-DVB) graft dendrimer microspheres	Cr(VI)	232	12	3.0	Wang *et al*., 2012
Biofunctional magnetic beads	Cr(VI)	7	480	1.0	Li *et al*., 2008
Magnetic poly-(GMA-EGDMA)	Cr(VI)	138	120	2.0	Bayramoglu and Arica, 2008
Ethylenediamine on Fe_3O_4 magnetic polymer	Cr(VI)	137	30	2.5	Zhao *et al.*, 2010
Ethylenetriamine on Fe_3O_4 magnetic polymer	Cr(VI)	150	30	2.5	Zhao *et al.*, 2010
Triethylenetetramine on Fe_3O_4 magnetic polymer	Cr(VI)	204	30	2.5	Zhao *et al.*, 2009
Tetraethylenepentamine on Fe_3O_4 magnetic polymer	U(VI)	370	30	2.5	Zhao *et al.*, 2010
Tetraethylenepentamine on Fe_3O_4 magnetic polymer	Cr(VI)	-	60	2.0	Yao *et al*., 2012
N,N`-bis (3-methoxylsalicylidene)-1,2-phenylenediamine on Fe_3O_4	U(VI)	94	360	2.0	Zhang *et al*., 2012

Chapter 3

Research Objectives

This chapter outlines the aims and objectives of the research study. These objectives were used to focus the research so that the desired results would be obtained.

3.1 General objective

The general objective of this study was to synthesize nanomagnetic U(VI) and Cr(VI) imprinted polymers which can be used in the remediation of U(VI) and Cr(VI) in the presence of other competing metal ions. These polymers were made magnetic for easy removal by use of an external magnetic field after they had adsorbed U(VI) and Cr(VI) from solution.

3.2 Specific objectives

- To synthesize superparamagnetic magnetite.
- To functionalize of magnetite using γ-MPS and oleic acid as surfactants.
- To prepare the magnetic nano-composite materials based on ion-imprinted polymers specific for U(VI) and Cr(VI).
- To characterize the prepared magnetite, functionalized magnetite and magnetic nano-composites polymers selective for U(VI) and Cr(VI).
- To study the binding capacity and selectivity of U(VI) and Cr(VI) onto the prepared magnetic nano-composite beads from aqueous solutions.
- To apply the prepared magnetic nano-composites for the removal of U(VI) and Cr(VI) from wastewaters in batch formats.

3.3 Key questions

- Can the synthesized nano-magnetic IIPs be used in the remediation and recovery of U(VI) and Cr(VI) from wastewaters?
- Can the nano-magnetic IIPs be removed from the solutions by use of external magnetic field?
- Is the adsorption of U(VI) and Cr(VI) onto synthesized nano-magnetic IIPs selective?
- Can the polymers be regenerated for reuse?

- Is there a possibility of applying these magnetic polymers practically in real wastewater samples?

3.4 Significance of the research

Most methods of adsorption of metal ions in wastewaters are non-selective. In this study, effective and selective removal of U(VI) and Cr(VI) from acid mine drainage and wastewater using nano-magnetic IIPs was established. The preparation and use of magnetic materials for remediation of polluted wastewaters is a relatively new field. The South African mining sector has huge problems with polluted wastewaters. The potential use of selective sorbents based on magnetic materials is therefore of interest.

3.5 Hypothesis

Nano-magnetic-ion imprinted polymers can be used to selectively remove U(VI) and Cr(VI) from wastewaters and the polymers can be removed from the solutions by application of an external magnetic field. The performance of nano-magnetic IIPs is better than that of nano-magnetic NIPs in the uptake of uranium and chromium from wastewaters.

3.6 Novelty

Although the technology of smart polymers based on molecularly imprinted polymers is now well known, preparation of magnetic ion imprinted polymers for U(VI) and Cr(VI) is still very scarce (Wang *et al.*, 2011).

This study is therefore one of the first ones that has made attempt to prepare smart polymers for (VI) and Cr(VI) that are magnetic. Further, this study carried out a detailed study on the selectivity of the prepared magnetic ion imprinted polymer which has rarely been done in previous studies (Zhao *et al.*, 2010; Wang *et al.*, 2011, Fan *et al.*, 2012; Li *et al.*, 2008; Bayramoglu and Arica, 2008).

Chapter 4
Materials and Methods

The purpose of this chapter is to expound details on chemicals, equipment and procedures used in order to achieve the research objectives outlined in Chapter 3. The major experimental protocol of the research was subdivided into the activities given below:

- Synthesis of the magnetite followed by its coating and then preparation of magnetic polymers for U(VI) and Cr(VI).
- Techniques for characterization of the magnetite and the magnetic polymers were: Raman spectroscopy (RS), Transmission electron microscopy (TEM), Energy dispersive spectrometry (EDS), Powder X-ray diffraction (PXRD) analysis, Brunauer, Emmett and Teller (BET) analysis, Ultraviolet visible (UV-vis) spectroscopy, Fourier-transform infrared (FTIR), Thermo-gravimetric analysis (TGA), Carbon, hydrogen, nitrogen and sulphur (CHNS) analysis, Diffuse reflectance spectroscopy (DRS) and Atomic force microscopy (AFM).
- Optimization of a number of parameters which included sample pH, amount of magnetic sorbent, contact time and initial uranium and chromium concentrations. Kinetic and adsorption modellings were also done on the prepared magnetic polymers. Selectivity studies of these synthesized magnetic polymers were carried out on synthetic waters.
- Finally, applications of the synthesized adsorbents were tested for uranium and chromium selectivity on acid mine drainage and municipal wastewater effluents.

4.1 Chemicals, stock solutions and equipment

4.1.1 Chemicals

For the synthesis of magnetite, $FeCl_2 \cdot 4H_2O$ and $FeCl_3 \cdot 6H_2O$, of analytical grades were supplied by Sigma Aldrich (Steinheim, Germany). NH_4OH and the washing solvent, methanol, were also from Sigma Aldrich (Steinheim, Germany).

For the synthesis of the magnetic polymers, the following chemicals were used: ethylene glycol dimethacrylate (EDGMA), methacrylic acid (MAA), 1,1`-azobis(cyclohexanecarbonitrile), salicylaldoxime (SALO), 4-vinylpyridine (4-VP), 2-methoxyethanol as well as surfactants for coating magnetite, γ-methacryloxypropyltrimethoxysilane (γ-MPS) and oleic acid (OA) all purchased from Sigma Aldrich (Steinheim, Germany). The imprint, uranyl nitrate ($UO_2(NO_3)_2 \cdot 6H_2O$) was bought from BDH Chemical Ltd, (Poole, England). All other salts were of the highest analytical grades and were from Sigma Aldrich (Steinheim, Germany). The leachants used for uranyl removal were HCl and $NaHCO_3$ all from Sigma Aldrich (Steinheim, Germany).

Deionized water was prepared from Millipore instrument (Massachusetts, USA). Analytical grade solutions from Merck (Darmstadt, Germany) were used to prepare different buffers systems for pH optimization and adjustments: for pH 1 and 2, HCl/KCl was used, Na_2HPO_4/citric acid was used for pH 3, CH_3COOH/CH_3COONa was used for ph 4, 5 and 6, borax/H_3BO_3 was used for pH 7, 8 and 9.

4.1.2 Stock solutions

A uranium(VI) stock solution was prepared by dissolving an appropriate amount of uranyl nitrate hexahydrate in one litre of deionized water with 0.05% (*v;v*) HNO_3.

Stock solutions of 1000 mg L^{-1} (for selectivity of Cr(VI)-magnetic ion imprinted polymers) were prepared by dissolving the following appropriate amounts of dried salts in 1 L volumetric flasks: NaF, $NaNO_3$, KH_2PO_4, Na_2SO_4 and $Na_2Cr_2O_7 \cdot 2H_2O$.

A 1000 mg L^{-1} stock solution of chromium(VI) was prepared by dissolving an appropriate amount of sodium dichromate, $Na_2Cr_2O_7$ (analytical reagent grade) in deionized water. Working solutions were prepared daily from the stock solution through serial dilutions. The stock solution was stored at 4°C when not in use.

4.1.3 Equipment

All pH measurements were performed on a 766 Calimatic pH meter equipped with a Shott N61 pH electrode from Knick (Berlin, Germany). In batch adsorption studies, a Laser Photo/Contact Tachometer DT-1236L from Lutron (Taipei, Taiwan) was used to measure the rotational speed of the magnetic stirrer. A Fritsch pulveriser (Idar-Oberstein, Germany) was used to crush the synthesized bulk polymers for homogenization.

4.2 Analytical and characterization equipment

All instruments used in this study for quantification and determination of analytes (U(VI) and Cr(VI)) in solution as well as characterization of U(VI) and Cr(VI) magnetic ion imprinted polymers and other materials are briefly described below.

4.2.1 Ultraviolet visible (UV-vis) spectroscopy

A Varian Cary 50 Conc, UV-Vis spectrophotometer with a Varian Cary 1E double beam spectrophotometer (Palo Alto, CA, USA) scanning from 200 to 750 nm was used for obtaining UV-Vis absorption spectra.

4.2.2 Raman spectroscopy

Raman spectra were acquired using a Jobin-Yvon T64000 Raman spectrograph from Wirsam Scientific (Pty) Ltd (Johannesburg, South Africa) operated in single spectrograph mode and the 514.5 nm of an argon ion laser as the excitation source. An Olympus BX40 microscope attachment was used to focus the incoming light on the sample and the backscattered light was dispersed via a 600 lines mm^{-1} grating onto a liquid nitrogen cooled CCD detector for acquisition via LabSpec v 4.18 software.

4.2.3 Transmission electron microscopy (TEM)

A FEI TECNAI SPIRIT (TEM-EDS) electron microscope (Eindhoven, Netherlands) was used. Approximately 0.2 g of the powdered samples were put in eppendorf tubes where 1 mL of methanol was added. The mixtures were then sonicated for 15 minutes. After this, an aliquot was drawn and applied to a Cu grid coated with carbon film. For the excess liquid to dry, the grids were placed on the Whatman filter paper for about 5 minutes. These were then loaded into the TEM microsope where they were viewed.

4.2.4 Size distribution

Because of their ultra small size, the actual diameter of each particle cannot be measured precisely, hence the use of particle size distribution. To achieve this, the size diameters for both the uncoated magnetite and the γ-MPS coated magnetite were done on the respective TEM micrographs by use of the *image j,* a public domain image processing program.

4.2.5 Energy-dispersive X-ray spectroscopy (EDS)

Energy-dispersive X-ray spectroscopy is an analytical technique used for the elemental analysis or chemical characterization of a sample and was carried out using a FEI TECNAI SPIRIT (TEM-EDS) electron microscope (Oxford, UK). With this technique, elemental composition of the synthesized magnetic polymers was determined. This characterization technique was also used to study the degree of leaching of the uranium as well as the magnetite from the magnetic polymers.

4.2.6 Powder X-ray diffraction (PXRD) analysis

A crystallographic study was performed on a synthesized iron oxide powder by a D2 Bruker Powdered X-ray Diffractometer (Karlsruhe, German), using Cu K_α radiation (= 1.5418 Å). The positions and the intensities of the peaks are used for identifying the underlying structure (or phase) of the material. The particle sizes of the magnetic nanoparticles were deduced from PXRD using Scherrer equation which can be written as in equation 4.1:

$$\overline{D} = \frac{57.3k\lambda}{\beta Cos\theta} \qquad (4.1)$$

where $\overline{D}$ is the mean size of the ordered (crystalline) domain, which may be smaller or equal to the grain size, k is shape factor, λ is the wavelength of the radiation corresponding to the Cu Kα peak, β is the full-width at half maximum (FWHM) and θ is the Bragg`s angle. The factor 57.3 is used for conversion of β from degree to radians. The Scherrer equation is limited to nano-scale particles. It is not applicable to grains larger than about 0.1 μm.

4.2.7 Brunauer, Emmett and Teller (BET) analysis

Surface area, pore volume and pore size were determined for both the uranyl-imprinted magnetic polymers and the control polymers. The effect of 1 mol dm^{-3} HCl and 1 mol dm^{-3} $NaHCO_3$ leachants on surface area formation was also investigated. An amount of 0.2 g of each of the above samples was degassed in N_2 at 150^oC for 4 hours prior to analysis with the Micromeritics Flow Prep 060 instrument (Aachen, Germany). After the degassing stage, surface area, pore volume and pore size were determined at -196^oC. This was achieved through N_2 adsorption and desorption using the Micromeritics Tristar surface area and porosity analyzer. BET is the commonly used gas sorption model which extends the model of gas sorption to multi-layer. It is normally solved graphically by plotting $1/[v(p/p_o)-1]$ versus p/p_o. The BET specific surface areas of the polymeric adsorbents are calculated from the corresponding isothermal adsorption of

nitrogen within the relative pressure (*p/po*) range of 0.05 to 0.35 (*p/po*) by use of the BET equation 4.2:

$$\frac{p/p_o}{v(1-p/p_o)} = \frac{1}{v(p/p_o - 1)} = \frac{1}{v_m c} + \frac{c-1}{v_m}.\frac{p}{p_o} \qquad (4.2)$$

where p is adsorbate pressure, p_o is adsorbate vapour pressure and v is adsorbed volume v_m is monomolecular layer volume and c is a quantity related to heats of adsorption and liquefaction. These two constants can be calculated from the slope, s, and the intercept, i, through use of equations 4.3 and 4.4.

$$v_m = \frac{1}{(s+i)} \qquad (4.3)$$

$$c = \frac{s}{i} + 1 \qquad (4.4)$$

4.2.8 Fourier-transform infrared (FTIR)

Fourier-transform infrared spectra were recorded in the frequency range of 400-4000 cm^{-1} using a Bruker FTIR spectrometer, Model Tensor 27 (Ettlingen, Germany) and the spectra were recorded in the solid state. This technique is useful in the identification of functional groups in a sample.

4.2.9 Thermo-gravimetric analysis (TGA)

Thermogavimetric analysis for the prepared materials was performed with Perkin Elmer Pyris 1 TGA Thermogavimetric Analyser (Massachusetts, USA) using nitrogen as the purge gas, at a flow rate of 20 mL min^{-1} and a heating rate of 5^oC per minute from 0-1000^oC. This technique was used to investigate changes in a sample weight as the heating temperature was changed. These changes are usually associated with weight loss resulting from dehydration or decomposition of the sample as the temperature increases. About 0.05 g of the sample was used for the thermal gravimetric analysis.

4.2.10 Carbon, hydrogen, nitrogen and sulphur (CHNS) analysis

A LECO-932 CHNS analyser from LECO Corporation (Michigan, USA) was used to determine the amount of carbon, hydrogen and nitrogen in the organic moiety which coated the magnetite. The products of combustion in CHNS analysis are CO_2, H_2O, N_2 and SO_x, depending on the elemental composition of the compound analyzed. High temperature combustion was used as the means of removing the elements from material. Samples (2 mg) were weighed into tin boats, compressed and encapsulated into capsules and taken to sample loading and then dropped into the furnace. The sample was combusted in the heated oxygen rich environment. Programmable control of the direct oxygen jet injection during high-temperature combustion guaranteed complete combustion. The gaseous combustion products were purified, separated into their components by special adsorption traps, and sequentially analyzed with universally used thermoconductivity detector (TCD). Calibration was performed with corn gluten for this CHNS test.

4.2.11 Diffuse reflectance spectroscopy (DRS)

Varian Cary 500 UV-Vis-NIR spectrophotometer using a diffuse reflectance attachment from SMM Instruments (Johannesburg, South Africa) was used in the scanning range of 200 to 1000 cm^{-1}. In DRS, different types of iron oxides exhibit different colours. These differences are the basis for distinction to some extent among Fe oxides. The analysis of corresponding DRS can be used to identify and characterize different types of iron oxides.

4.2.12 Atomic force microscopy (AFM)

Atomic force microscopy was applied to study pore formation in the polymer from the study of the images of the samples before and after leaching of the uranyl ions. A Veeco/Digital Instruments Dimension 3100 Scanning Probe Microscope (Santa Barbara, USA) was used in AFM-tapping mode.

4.2.13 Ion chromatography (IC) analysis

Metrohm 762 Compact Ion Chromatograph (Leonberg, Germany) with a Metrosep A Supp 5 (6.1006.520) 150 x 4.0 mm analytical column was used for the determination of fluoride, nitrate, sulphate and phosphate anions. The eluent solution was of the composition of 1.0 mM $NaHCO_3$ and 3.2 mM Na_2CO_3. The eluent was pumped at 0.7 mL min^{-1}. The suppressor solution was 50 mM H_2SO_4 and deionized. All the solutions, including eluents used were degassed by ultrasonication and filtered through a 0.45 μm filter paper before being used in the IC.

4.2.14 Inductively coupled plasma-optical emission spectrometer (ICP-OES)

ICP-OES from Spectro Genesis End-on-plasma Spectro Analytical Instruments (Pty) Ltd, (Johannesburg, South Africa), was used for the determination of the metals' concentration in multi-elemental solutions with parameters shown in Table 4.1.

Table 4.1: Operating conditions of the ICP-OES.

Parameter	Setting
RF Power	1400 W
Coolant Gas Flow	14.00 L min^{-1}
Auxiliary Gas Flow	1.00 L min^{-1}
Nebulizer Gas flow	1.00 L min^{-1}
Sample Pump Flow	2.00 L min^{-1}
Sample Aspiration Rate	2.00 L min^{-1}
Replicates	3
Plasma Torch	Quartz
Spray Chamber	Single pass
Nebulizer	Crossflow
Processing Mode	Area

4.2.15 Atomic absorption spectroscopy (AAS)

AAS measurements were made on a PG-990 AAS model (Leicestershire, UK) pyrolytically coated HGA-76 graphite furnace. A uranium hollow cathode lamp was used at 358.5 nm uranium wavelength with a spectral width of 0.2 nm. Argon was used as a purge gas. A scheme diagram for the grahite furnace atomic absorption spectrophotometer is shown in Figure 4.1.

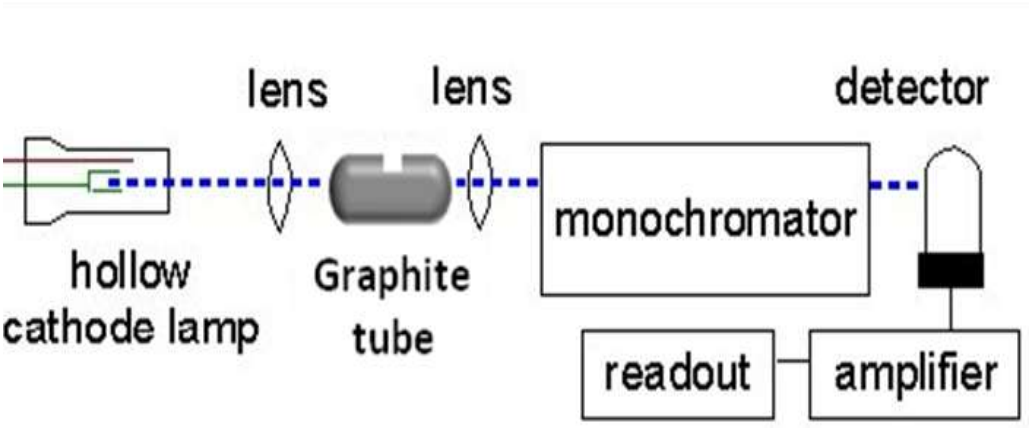


Figure 4.1: Schematic diagram of grahite furnace atomic absorption spectrophotometer.

The graphite furnace is electrically heated and undergoes a heating programme which can consist of many steps. In this work, the heating programme applied consisted of four steps, namely, drying, ashing, atomization and cleaning. The temperatures corresponding to the ramping and holding times are shown graphically in Figure 4.2.

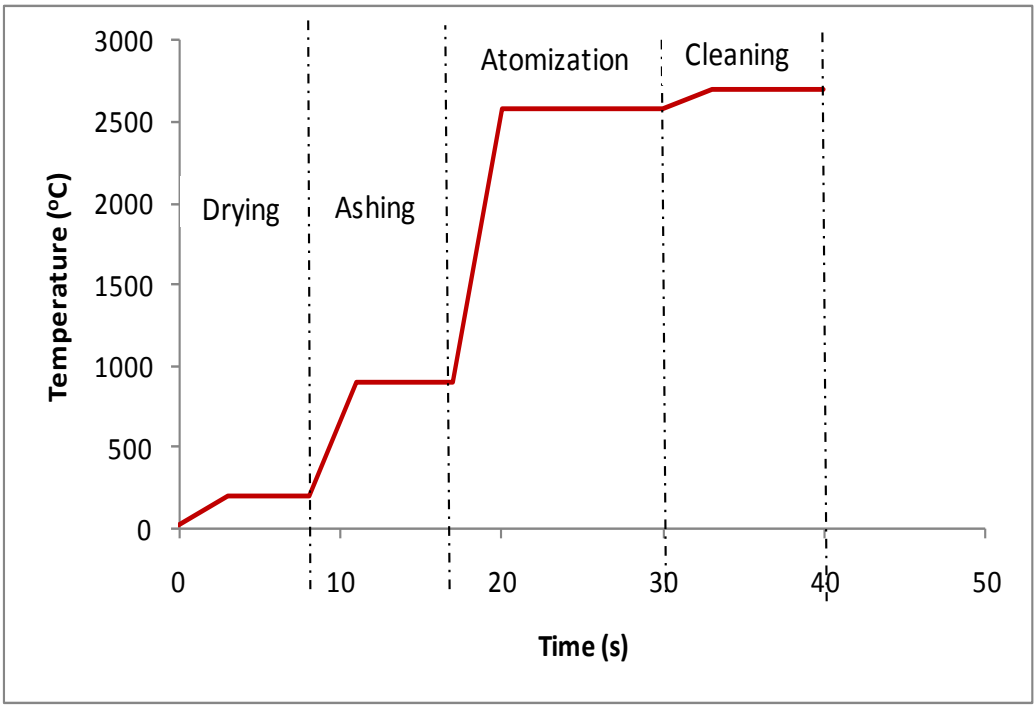


Figure 4.2: The heating programme for uranium in the graphite furnace.

4.3.1 Synthesis of the magnetic IIPs and NIPs

4.3.1.1 Synthesis of the magnetite

Synthesis *via* the co-precipitation of ferrous and ferric salts in an alkaline medium (Thorek *et al.*, 2006) was used. A volume of 180 mL of an aqueous solution containing 11.2 mmol Fe^{3+} and 5.6 mmol Fe^{2+} was heated to 50^{o}C. After heating, 12.5 mL of ammonia was added under vigorous stirring. After 30 min, the reaction was heated and kept at 90^{o}C for 30 min again. An inert atmosphere of N_2 was used for the whole experiment. After completion of the reaction, the black precipitate was collected by an external magnetic field, washed with water and ethanol and dried under vacuum.

4.3.1.2 Coating of magnetite with γ-MPS

In this study γ-methacryloxypropyltrimethoxysilane (γ-MPS) was used as a coating agent. This was chosen because of its physio-chemical properties. γ-MPS have the hydrophobic olefinic end which ushers a platform for polymerization.

Kan *et al.* (2010) approach was used to modify the magnetic nanoparticles with a double bond. In this method, 4 mL γ -MPS was dropwisely added into the mixture of solvents of ethanol and water (1:1, *v/v*) containing dispersed Fe_3O_4 nanoparticles and the reaction was carried out for 12 h at 40^oC under N_2 gas. Then the product was separated and washed by ethanol for several times and dried under vacuum. In these conditions, the methoxyl groups are firstly hydrolyzed to produce the hydrophilic silanol groups which covalently bond with the hydroxyl groups around the magnetite. On the other end of the γ-MPS, there is a hydrophobic olefinic group which ushers a platform for polymerization with the monomers during polymer preparation stage.

4.3.1.3 Coating of magnetite with oleic acid

One gram Fe_3O_4 particles was dispersed in 200 mL ethanol under ultrasonication, and then 5 mL oleic acid was added dropwisely into the above mixture under stirring at 80^oC for 1 h. The oleic acid coated Fe_3O_4 particles were isolated by application of an external magnetic field and washed with water and ethanol to remove redundant oleic acid (Zhao *et al.*, 2010).

4.3.1.4 Bulk polymerization

The polymers were synthesized according to the method of Singh and Mishra (2009) with some modifications. Ion-imprinted polymers were prepared by thermal polymerization. The imprint ion (0.270 g) was complexed with 2 mM salicylaldoxime (SALO) and 2 mM 4-vinylpyridine (4-VP) in 10 mL of 2-methoxyethanol in which 2 g of the functionalized magnetite was suspended. The above ternary complex solutions were then mixed with 12 mmol of methacrylic acid (MAA), 36 mmol of ethylene glycol dimethacrylate (EGDMA) and 50 mg of 1,1`-azobis(cyclohexanecarbonitrile). The polymerization mixture was cooled to 0^oC and purged with N_2 for 10 min, sealed and thermally polymerized in an oil bath at 80^oC while stirring for 3 h. The bulk polymers were dried at 70^oC to remove the solvent (porogen). The polymers were then washed with ethanol, then ethanol and water mixture with increasing amounts of water until only water was used, as shown in Table 4.2. Finally, the resulting polymer was then ground and

sieved to obtain the ion-imprinted polymers in the size range of 27 and 53 μm. Magnetic NIPs were prepared likewise except that the imprint ion was not included.

Table 4.2: Volume composition of the polymer washing solution.

Wash number	1	2	3	4	5
Ethanol (mL)	10	6	5	4	0
Water (mL)	0	4	5	6	10

4.3.1.5 Precipitation polymerization

In precipitation polymerization, the same protocol for the bulk polymerization was followed except that the volume of the porogenic solvent, 2-methoxyethanol, was increased ten-fold to 100 mL.

4.3.1.6 Leaching of γ-MPS and OA based polymers

Three grams of the magnetic polymer (from bulk and precipitate) was transferred to a 250 mL volumetric flask upon which a 100 mL of 2 mol dm^{-3} HCl was added. The mixture was stirred gently for 6 hours, after which filtration was done under vacuum. The filtrate was retained for metals analysis. A freshly prepared HCl leachant, with the same concentration and volume as above, was added to the magnetic polymer. This procedure was repeated for three more times.

A second leachant, 1 mol dm^{-3} $NaHCO_3$ was used in the same way as HCl leachant. Leaching of the oleic acid functionalized magnetite was done in the same way as γ-MPS based polymers but only 1 mol dm^{-3} $NaHCO_3$ was used**.** The magnetic NIPs were subjected to the same treatment.

4.3.2 Optimization of parameters for U(VI) uptake

Sample pH, magnetic polymer amount, contact time and initial U(VI) concentration were optimized. Optimization of was achieved by varying one parameter while keeping the others constant. All experiments were carried out in triplicate. The influence of these parameters was evaluated by calculating the extraction efficiency or recovery as shown in the equation 4.5:

$$\text{Extraction efficiency } (\%) = \frac{(C_0 - C_e)}{C_o} \times 100 \qquad (4.5)$$

where C_o (mg L^{-1}) is the initial concentration and C_e (mg L^{-1}) represents the final equilibrium concentration after adsorption.

The adsorption capacity, q (mg g^{-1}), is defined as mass of substrate bound on a gram of adsorbent. Equation 4.6 shows the mathematical equation for the calculation of the adsorption capacity in which C_o (mg L^{-1}) and C_e (mg L^{-1}) are as described for in equation 4.5 and V (L) is the volume of the sample solution and W the mass (g) of the adsorbent (Zeinali *et al.*, 2010; Kumar and Kirthika, 2009; Maarof and Hameed, 2004).

$$q = \frac{(C_0 - C_e)V}{W} \qquad (4.6)$$

4.3.2.1 Effect of sample pH

In this study, 2 mg L^{-1} of uranium solutions were prepared from a 1000 mg L^{-1} stock solution in 8 volumetric flasks. In order to investigate the effect of sample pH, the uranium solutions were adjusted in the range pH 2-9 and 25 mL of these were then transferred to 30 mL vials where 20 mg of an adsorbent (magnetic IIP and NIP) were added. After this, the uranyl-IIP mixture was allowed to equilibrate with stirring at 1500 rpm for 45 minutes. The loaded magnetic-IIPs were then separated from the mixture by application of an external magnetic field and the filtrate analyzed for uranium content. All adsorption experiments were carried out at room temperature.

4.3.2.2 Effect of the amount of magnetic polymer

Adsorption was carried out in a series of 30 mL vials at room temperature. Each vial was filled with 25 mL of an initial concentration of 2 mg L^{-1} solution of uranium. An optimized sample pH was used. The added magnetic polymer mass was varied between 10 to 100 mg. After stirring the solution for 45 minutes at 1500 rpm, separation of the magnetic polymers was achieved by use of a magnet. The solution was then analysed for uranium content from which the amount adsorbed on the polymer was calculated.

4.3.2.3 Effect of contact time

In order to establish the optimum contact time and adsorption kinetic behaviour of the magnetic polymers, adsorption of uranium onto the magnetic polymers was investigated at various time intervals (10-90 min).

The initial concentration of uranium was kept constant at 2 mg L^{-1}. The optimized amount of the polymer was added into 25 mL uranium solution. This mixture was then mixed at room temperature under a stirring speed of 1500 rpm. After adsorption, the polymers were separated from aqueous phase by use of an external magnetic field and the supernatant analyzed for uranium. Mass balance was then used to calculate the amount of uranium adsorbed onto the polymer. All adsorption experiments were carried out at room temperature.

4.3.2.4 Effect of initial uranium concentration

Adsorption was carried out in a series of 30 mL vials at room temperature. Each vial was filled with 25 mL of uranium solution of five varied initial concentrations ranging from 0.5-10 mg L^{-1}. The pH and amount of the magnetic polymer used were those optimized. After stirring the solution for the optimum period of time at 1500 rpm, separation of the magnetic polymers was achieved by use of a magnet. The solution was then analysed for uranium content from which the amount adsorbed on the magnetic polymers was calculated.

4.3.2.5 Selectivity of the magnetic polymers

Stock solutions (1000 mg L^{-1}) were prepared by weighing out an appropriate amount of the salts, namely: $U(NO_3)_2.6H_2O$, $Ca(NO_3)_2.6H_2O$, $Mg(NO_3)_2.6H_2O$, $Pb(NO_3)_2$, $Ni(NO_3)_2.6H_2O$ and $Fe(NO_3)_3.9H_2O$ by dissolving them in de-ionized water. The pH adjustments were conducted using an appropriate buffer system that gave maximum adsorption capacity in the section above. The working standard solution was obtained by serial dilution of the stock solution. For selectivity studies, a binary metal solution was made from 2 mg L^{-1} of U(VI) and of another metal ion. Aliquots of 25 mL of these binary metal solutions were transferred to 30 mL vials where the optimized weight (50 mg) of the magnetic IIP was added. A batch adsorption experiment was then performed at room temperature for a prescribed time of 45 minutes at 1500 rpm. Separation of the polymers was then carried by application of a magnetic field. The metals remaining in solution were then quantified with ICP-OES but uranium was quantified with GFAAS. The respective magnetic NIP was used for the control experiment.

The distribution coefficients, K_d, of UO_2^{2+}, Mg^{2+}, Fe^{3+}, Ni^{2+} and Pb^{2+} were calculated using equation 4.7:

$$K_d = \frac{(C_o - C_e)}{C_e W} \tag{4.7}$$

where K_d is the distribution coefficient (L g^{-1}) and the other variables are as described for equations 4.5 and 4.6. Equation 4.8 was used to calculate the selectivity coefficients for the binding of a uranyl ion in the presence of the other competing ion in a binary system:

$$K = \frac{K_d(UO_2^{2+})}{K_d(B)} \tag{4.8}$$

where K represents the selectivity coefficient and B represents U(VI) competing ions mentioned above. The value of K gives an indication as to how selective the

polymer is for U(VI) ions in the presence of other competing species in solution. If K = 1, it means competing ions and uranyl ions are bound equally. A large value of K is therefore preferred indicating that the magnetic polymer favours uranyl ions.

Another important parameter is the relative selectivity coefficient, K′, which represents the enhanced effect of imprinting on selectivity and adsorption affinity for the template onto the polymer. The K′ of the magnetic-IIP against the magnetic-NIP was calculated using equation 4.9:

$$K' = \frac{K_{IIP}}{K_{NIP}} \qquad (4.9)$$

where K_{IIP} and K_{NIP} are the selectivity coefficients of the IIP and NIP, respectively.

4.3.2.6 Reusability of the magnetic uranyl IIPs

In order to test the stability and reusability of the magnetic imprinted polymers, a 25 mL uranyl solution with an initial concentration of 2 mg L^{-1} was exposed to 50 mg of the magnetic polymers. After 45 min of extraction and equilibration, the aqueous solution was filtered and the magnetic polymer particles were transferred to another sample vial. After filtering the mixture, the filtrate was analyzed for U(VI) content while the magnetic polymer residues were regenerated by leaching out uranium with 25 mL of 1 M HCl solution at a stirring rate of 1500 rpm at room temperature for 45 min. These magnetic polymers were then used for the next rebinding studies.

4.3.3 Kinetic modelling

Kinetic modelling is important in order to gain insight into the mechanism and rate controlling steps affecting the kinetics of adsorption.

Adsorption data can be modelled using the Elovich equation, Intraparticle diffusion Weber-Morris kinetic model, the film diffusion model according to the Reichenberg equation, the film diffusion model according to Vermeulen's approximation, pseudo-first order or pseudo-second order models. The last two are the most widely used models for the adsorption of a solute from aqueous solution and were the ones used in this research.

4.3.3.1 Pseudo-first-order kinetic model

The pseudo-first-order kinetic model is given by:

$$\frac{dq_t}{dt} = k_1 (q_e - q_t) \qquad (4.10)$$

where q_t (mg g^{-1}) is the amount of adsorbed metal ion on the adsorbent at time t (min), q_e (mg g^{-1}) the amount adsorbed at equilibrium and k_1 (min^{-1}) is the rate constant of first-order adsorption.

After integration between boundary conditions t = 0 to t and q_t = 0 to q_e, equation 4.10 becomes:

$$\log (q_e - q_t) = \log q_e - \frac{k_1}{2.303} t \qquad (4.11)$$

where q_e and k_1 can be determined from the intercept and slope of the plot, respectively. A plot of log (q_e – q_t) against t gives a straight line and the constants q_e and k_1 are obtained from the intercept and gradient, respectively.

4.3.3.2 Pseudo-second-order kinetic model

Pseudo-second order model is applied when the applicability of the first-order kinetics becomes unattainable. It is based on the sorption capacity of the solid phase. The equation of pseudo second-order is given in the equation below.

$$\frac{dq_t}{dt} = k_1(q_e - q_t)^2 \qquad (4.12)$$

where k_2 is the rate constant of second-order model. For boundary conditions t = 0 to t and $q_t = 0$ to q_e, equation 4.12 becomes:

$$\frac{t}{q_t} = \frac{1}{k_2 q_e^2} + \frac{1}{q_e} t \qquad (4.13)$$

The plot of $\frac{t}{q_t}$ versus t should give a straight line if pseudo-second-order kinetic model is applicable and q_e and k_2 can be determined from the slope and intercept of the plot, respectively.

4.3.4 Adsorption isotherm models

Equilibrium relationships of how adsorbates interact with the adsorbent materials are generally described by adsorption isotherms. These adsorption isotherms are important for optimization of the adsorption mechanism pathways, expression of the surface properties and capacities of adsorbents (El-Khaiary, 2008; Thompson, 2001). In literature, there are many adsorption isotherms which include Langmuir, Freundlich, Dubinin-Radushkevich, Temkin and BET but the first two still remain the two most commonly used adsorption isotherm equations (Kinniburgh, 1986). The applicability of the isotherm equations is judged by the value of their correlation coefficients, R^2 and is also used in order to understand the extent and degree of favourability of adsorption (Treybal, 1981).

4.3.4.1 Freundlich isotherm model

The Freundlich model is an empirical equation which assumes that the adsorbent has a heterogeneous surface composed of adsorption sites with different adsorption potentials. The model equation is as follows:

$$q_e = K_f C_e^{\frac{1}{n}} \quad (4.14)$$

where q_e (mg g^{-1}) is amount adsorbed at equilibrium and C_e (mg L^{-1}) is the equilibrium concentration. K_f (L g^{-1}) and n are equilibrium constants and Freundlich coefficients which are temperature dependent and are related to adsorption capacity and intensity, respectively. The linearized form of the Freundlich sorption isotherm is:

$$\ln q_e = \ln K_f + \frac{1}{n}\ln C_e \quad (4.15)$$

A plot of $\ln q_e$ versus $\ln C_e$ gives a linear graph where coefficients K_f and n can be calculated from the intercept and slope, respectively; $\frac{1}{n}$ is an indicator of adsorption effectiveness. The Freundlich coefficient, n, should have values in the range of $0 < n < 1$ for a favourable adsorption reaction.

4.3.4.2 Langmuir isotherm model

The Langmuir equation is based on a kinetic approach and assumes a uniform surface, single layer of adsorbed material and constant temperature. The model is useful when there is a strong specific interaction between the surface and the adsorbate so that a single adsorbed layer forms and no multi-layer adsorption occurs. It also assumes that the surface is homogeneous. The Langmuir isotherm can be expressed by the equation:

$$q_e = \frac{q_m b C_e}{1 + b C_e} \quad (4.16)$$

where q_e (mg g^{-1}) is the substance amount of adsorbate adsorbed per gram of the adsorbent, q_m (mg g^{-1}) is the maximum adsorption of adsorbate per gram, b (mg^{-1} dm^3) is the adsorption constant and C_e (mg dm^{-3}) is the equilibrium concentration of the adsorbate in solution. The linearized form of the Langmuir equation becomes:

$$\frac{1}{q_e} = \frac{1}{q_m b C_e} + \frac{1}{q_m} \qquad (4.17)$$

A plot of $\frac{1}{q_e}$ versus $\frac{1}{C_e}$ gives a straight line and the constants q_m and b are obtained from the intercept and gradient, respectively.

4.3.5 Sampling sites

The performance and potential future application of the magnetic U(VI) IIPs on the removal of hexavalent uranium from wastewater samples in the presence of other competing metal ions was tested on two types of water samples. These were the acid mine drainage from Germiston and the treated wastewater effluent from Goudkoppies Wastewater Treatment Plant in Soweto. The sampling sites from which the real water samples were sampled from are shown encircled in red in Figures 4.3(b) and 4.4(b).

The Germiston area is located in the Central Rand area and is part of the Witwatersrand Basin where some 70 different ore minerals have been identified in the conglomerates. The most abundant ones include pyrite (FeS_2) and uranite (UO_2). This site is near an old gold mining tailings dump that underwent reprocessing.

The other sampling site on Goudkoppies Wastewater Treatment Plant treats domestic and industrial wastewater from the City Centre and South-Eastern areas of Johannesburg before being discharged to a stream that eventually flows into Klip River. Raw water treatment at Goudkoppies involves several stages; among them are degritting, digestion and chlorination.



Figure 4.3: (a) Germiston site (b) Google map of the Germiston area with pointers 26°13`07.10 ``S and 28°08`03.79``E and an elevation height of 1652 m.





Figure 4.4: (a) Goudkoppies Wastewater Treatment Plant site (b) its google map with pointers 25°66`42.12``S and 27°69`17.07``E and an elevation height of 1378 m.

4.3.6 Application of magnetic U(VI) IIPs to real water samples

The samples were collected, treated and stored according to published procedures (Parks *et al*., 2004) and before the application of magnetic IIPs to real water samples, analysis in triplicates of the metal content in these samples was performed using ICP-OES. The pH and conductivity of solutions were measured in the field. The extraction of U(VI) from real water sample was then carried out in batch mode.

Mine decant sample from Germiston was buffered at pH 4 and divided into three 150 mL portions, which were spiked with 0, 5 and 10 mg L^{-1} of uranium solution. In triplicate, 25 mL of each sample was contacted with 20 mg of magnetic IIP particles while stirring at room temperature for 45 min. The uranium adsorbed on magnetic IIP particles was then leached out with 20 mL of 3 M HCl solution at a stirring rate of 1500 rpm at room temperature for 45 min. All solutions were then filtered through a 0.45 μm filter paper and analysed for uranium content using ICP-OES.

Goudkoppies wastewater was buffered at pH 4 and divided into four 25 mL portions which were spiked with 0, 1, 5 and 10 mg L^{-1} uranium. These solutions were then subjected to the same treatment as the AMD water sample from Germiston (described above).

4.4.1 Synthesis of imprinted polymers for Cr(VI) recovery

4.4.1.1 Synthesis of magnetic poly(4-vinylpyridine)

Prior to the synthesis of poly(4-vinylpyridine), the monomer 4-vinylpyridine was distilled at 65^{o}C to remove the inhibitor, hydroquinone (Berkowitz *et al*., 1958).

An amount of 2.5 mg of γ-MPS-coated magnetite was added to a volume of 28 mL of the distilled 4-vinylpyridine. This mixture was then transferred to a 50 mL volumetric flask to which 50 mg benzoyl peroxide was added with magnetic stirring. The flask was then placed into an oil bath at 85^{o}C for 2 hours and then the temperature was elevated to 135^{o}C where it was maintained for an hour. The

whole reaction was performed under an inert atmosphere of nitrogen. The polymerization was then stopped by cooling it to 0^{o}C. The unreacted 4-vinylpyridine monomer was removed by washing the poly(4-vinylpyridine) with 35 mL of methanol. The free bulk poly(4-vinylpyridine) polymer was recovered by heating off the methanol solvent by use of rotary evaporator (Rotavapour II, Buchi, Switzerland).

4.4.1.2 Synthesis of poly(4-vinylpyridine)

The synthesis of non-magnetic poly(4-vinylpyridine) followed exactly the same procedure for the synthesis of magnetic poly(4-vinylpyridine) except that γ-MPS-coated magnetite was not added.

4.4.1.3 Preparation of magnetic and poly(n-propyl-4 vinylpyridinium) bromide

Quaternization of magnetic and non-magnetic poly(4-vinylpyridine) was achieved by refluxing 11.34 g of magnetic and non-magnetic poly(4-vinylpyridine) in 40 mL of DMF with a slight stoichiometric excess of 1-bromopropane (10 mL). These reactions were carried out for 42 hrs at 60^{o}C.

4.4.1.4 Preparation of magnetic and non-magnetic poly(n-propyl-4-vinylpyridinium) dichromate

Magnetic poly(n-propyl-4-vinylpyridinium) bromide was dissolved in 50 mL of DMF containing 0.34 g of dissolved sodium dichromate. This solution was stirred at room temperature for 2 hours. Magnetic poly(n-propyl-4-vinylpyridinium) dichromate was then obtained by driving off the excess solvent by use of a rotary evaporator. The corresponding magnetic NIP was similarly synthesized except that the dichromate imprint was excluded.

4.4.1.5 Leaching of chromium

After polymerization ceased, the synthesized magnetic IIPs and NIPs of chromium were ground and sieved to a particle size range of 27-53 μm range. The particles were then washed repeatedly with de-ionized water to remove all unreacted pre-polymerization reagents. The imprinted chromium was then removed by stirring 5 g of the magnetic polymers in 100 mL of 1 M HCl for 6 hours. Magnetic IIP and NIP particles were filtered through a 0.45 μm filter paper where the filtrate was analyzed for chromium content and the residue was subjected to a fresh HCl leachant for the same period of time. This cycle was repeated several times until the chromium content detected in the filtrate was almost non-detectable.

4.4.2 Optimization of parameters for Cr(VI) uptake

4.4.2.1 Effect of initial pH of Cr(VI) solution

The effect of pH on the adsorption of Cr(VI) onto the magnetic IIP and NIP was investigated in the pH range of 2-8. This was achieved by stirring 25 mg of the polymer particles at a stirring speed of 600 rpm in a 25 mL solution of Cr(VI) with initial concentration of 5 mg L^{-1} for 60 min at room temperature. After 60 min, the solution was equilibrated for 10 min followed by filtration and the chromium content was then determined by FAAS.

4.4.2.2 Effect of the amount of the magnetic polymer

After adjusting the pH of the sample solution to pH 4, a batch adsorption was carried out in a series of 30 mL vials at room temperature. Each vial was filled with 25 mL of an initial concentration of 5 mg L^{-1} chromium solution. The added magnetic polymer mass was varied between 5 to 120 mg. After stirring the solution for 60 minutes at a stirring speed of 600 rpm, separation of the magnetic polymers was achieved by use of a magnet. The solution was then analysed for chromium content from which the amount adsorbed on the magnetic polymer was calculated.

4.4.2.3 Effect of contact time on chromium(VI) adsorption

The effect of contact time on the extraction of Cr(VI) was investigated by stirring 20 mg of magnetic IIP and NIP at room temperature in a solution containing 25 mL of 2 mg L^{-1} of Cr(VI) at a fixed pH. The time intervals investigated were 5, 15, 45, 60 and 90 min. After each stirring time, the Cr(VI) amount was determined as described earlier.

4.4.2.4 Effect of initial concentration of chromium(VI) on its uptake

The effect of 25 mL of various initial Cr(VI) concentrations (2, 5, 8 and 10 mg L^{-1}) on the adsorption removal efficiency by magnetic IIP and NIP was investigated by stirring the 20 mg of the magnetic polymers at room temperature. The initial pH of the solutions was adjusted to that optimized above. After 45 min. the mixture was filtered and the filtrate was analyzed for Cr(VI) content with the FAAS.

4.4.2.5 Selectivity studies on the adsorption of Cr(VI) by magnetic IIP

Four point calibration standards were prepared from a mixture of four anions, namely, F^-, NO_3^-, SO_4^{2-} and PO_4^{3-}. The concentrations used were 1, 5 and 10 and 20 mg L^{-1}. Selective adsorption of Cr(VI) onto magnetic polymers was investigated by means of binary mixtures with other anionic species which were F^-, NO_3^-, SO_4^{2-} and PO_4^{3-}. The initial concentration of Cr(VI) and the other analyte was 2 mg L^{-1}. Twenty five millilitres of these mixtures were then equilibrated with 20 and 65 mg of magnetic IIP and NIP, respectively. After adjusting the pH to 4 with NaOH and HCl, the contact time was set at 45 min and the stirring rate set at 600 rpm. These experiments were performed in a batch mode and the unadsorbed concentration of each anionic species was measured using ion chromatography and AAS for the dichromate. The results obtained were used to calculate the distribution ratios, the selectivity coefficients and the relative selectivity coefficients through application of equations 4.7, 4.8 and 4.9, respectively.

4.4.2.6 Reusability of chromium(VI) IIP

The stability and reusability of the magnetic polymers was investigated by adding to the 50 mg of the polymer 2 mg L^{-1} chromium(VI) solution. The optimum conditions found in previous experiments were used. The contact time was allowed for 45 min after which the mixture was filtered. The magnetic polymer residue was then stripped off the adsorbed chromium(VI) by stirring it in a 20 mL solution of 1 M NaOH for 20 min. This was followed by filtration and analysis of dichromate anions in the filtrate by FAAS. This procedure was repeated for a number of times in order to investigate the stability and reusability of these magnetic polymers.

Chapter 5
Results and Discussion

This chapter presents results and discussion for the experimental procedures outlined in chapter four. These results relate to the synthesis of magnetite, it's coating with organic surfactants as well as preparation of magnetic ion imprinted polymers. Full characterization of the synthesized magnetic polymers is also presented and discussed. The chapter concludes with adsorption studies on real water samples and kinetic and adsorption modelling is also included as part of the discussion.

5.1 Synthesis and characterization of magnetic uranyl-imprinted polymers

5.1.1 Synthesis of the magnetite

The synthesis of magnetite by co-precipitation of the ferrous and ferric salts produced a black precipitate upon increasing of pH by addition of ammonia. The magnetic response of the magnetite towards a magnet is demonstrated in Figure 5.1.

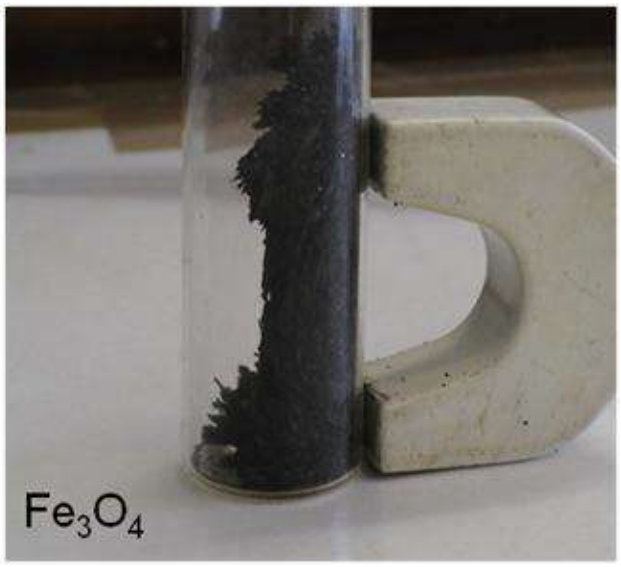


Figure 5.1: Magnetic response of magnetite.

Since this synthesis is carried out in aqueous environment, it means there is likely to be water and hydroxyl ions adsorbed on the surface of the magnetite as schematically depicted in Figure 5.2.

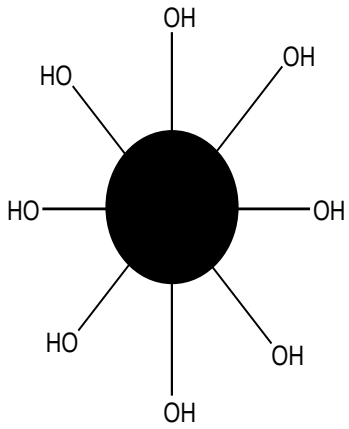


Figure 5.2: Magnetite showing the adsorbed hydroxyl ions.

5.1.1.1 Powder X-ray diffraction (PXRD) analysis

Powder X-ray diffraction was used as a diagnostic tool to check the phase of the iron oxide. In the case of magnetite, the characteristic peaks occur at 2θ = 30.1, 35.5, 43.1, 53.4 and 57.0^o (Aguilar-Artega *et al*., 2010). It is clear that the bulk of the particles consist mainly of Fe_3O_4 phase, Figure 5.3. It is however evident that there are some impurities in the samples as observed from peaks at $2\theta > 60^o$.

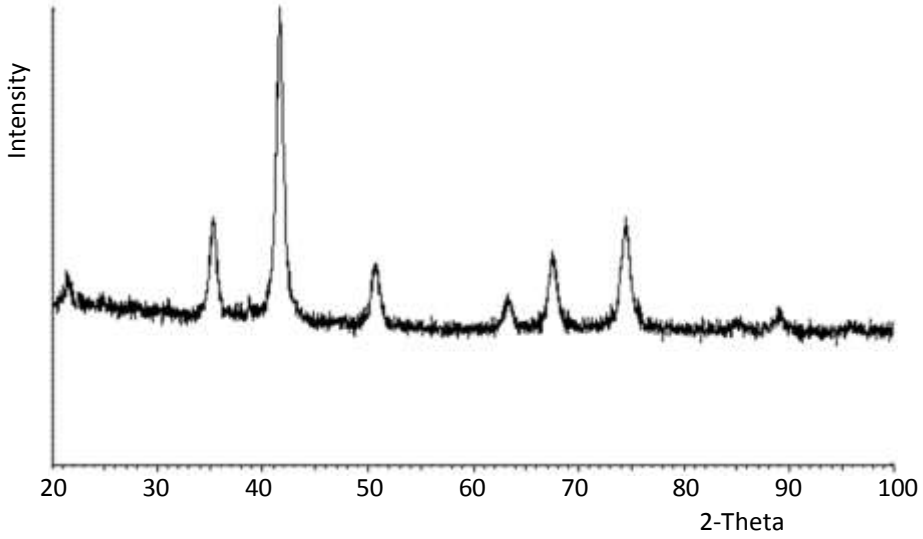


Figure 5.3: PXRD pattern for the synthesized magnetite.

The particle size of the magnetite nanoparticles, as deduced from the Scherrer equation (eqn 4.1) was found to be 11.9 nm. The result is consistent and in perfect agreement with that obtained from TEM analysis (11.39 ± 2.54 nm). The PXRD patterns of the dried sample of Fe_3O_4 from the studies of El Ghandoor *et al*. (2012) gave the crystallite size of 10 nm after application of the Scherrer formula. The other PXRD patterns of the synthesized Fe_3O_4 nanoparticles obtained by Sadeghi and Aboobakri (2012) in the 2θ region of 10-80° displayed diffraction lines at 2θ = 30.3, 35.4, 43.3, 57.3 and 62.8^o which were characteristic of spinel structure of Fe_3O_4. The PXRD spectra of bare Fe_3O_4 and ethylenediamine-modified magnetic chitosan synthesized by Wang *et al*. (2011), showed six peaks at 2θ = 30.1, 35.4, 43.0, 53.5, 57.0 and 65.2^o. After comparing the peaks to that of the database in JCPDS file (PDF No. 65-3107), the researchers concluded that the resultant magnetic iron oxide were pure Fe_3O_4 with a spinel structure.

5.1.2 γ-MPS and OA functionalization of magnetite

5.1.2.1 Functionalization of magnetite with γ-MPS

The Stöber-sol-gel method is the most widely used method for coating nanoparticles with silica. It relies on the use of silicon alkoxides as the source of silica matrix (Kan *et al*., 2010). These silica matrices are formed through hydrolysis of γ-MPS in basic alcohol/water mixtures. The silanol groups (Si-OH) will then be transform to siloxane bonds (Si-O-Si) through condensation (Kan *et al*., 2010). When hydrolyzed, Figure 5.4, the other end of γ-MPS with the methyl groups produce hydrophilic silanol groups that bond covalently with the hydroxyl groups around the magnetite, Figure 5.5. The silica layer formed on the surface of the magnetite could screen the dipolar attraction between the magnetite which favours the dispersion of this magnetite in the liquid media and also protects them from leaching in acidic environments. Coating also prevent oxidation of the magnetite to maghemite in aqueous media. Figure 5.6 shows a pictorial illustration of the central magnetite coated with γ-MPS.

Chen *et al*. (2011) used 3-methacryloxyproyltrimethoxysilane with three alkoxides which was hydrolyzed for 5 h to produce a hydrophilic end. Apart from γ-MPS, there is a wide range of coating agents that have been reported in literature. For instance, Ma *et al*. (2011) successfully encapsulated the magnetite within methacrylic acid. Qian *et al*. (2008) prepared paramagnetic magnetite/polystyrene nanocomposite by firstly modifying the magnetite nanoparticles with a Y-shaped surfactant (12-hexanoyloxy-9-octadecenoic acid).

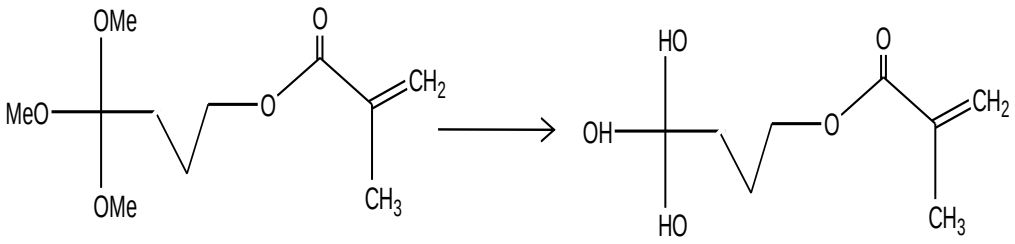


Figure 5.4: The hydrolysis of γ-MPS.

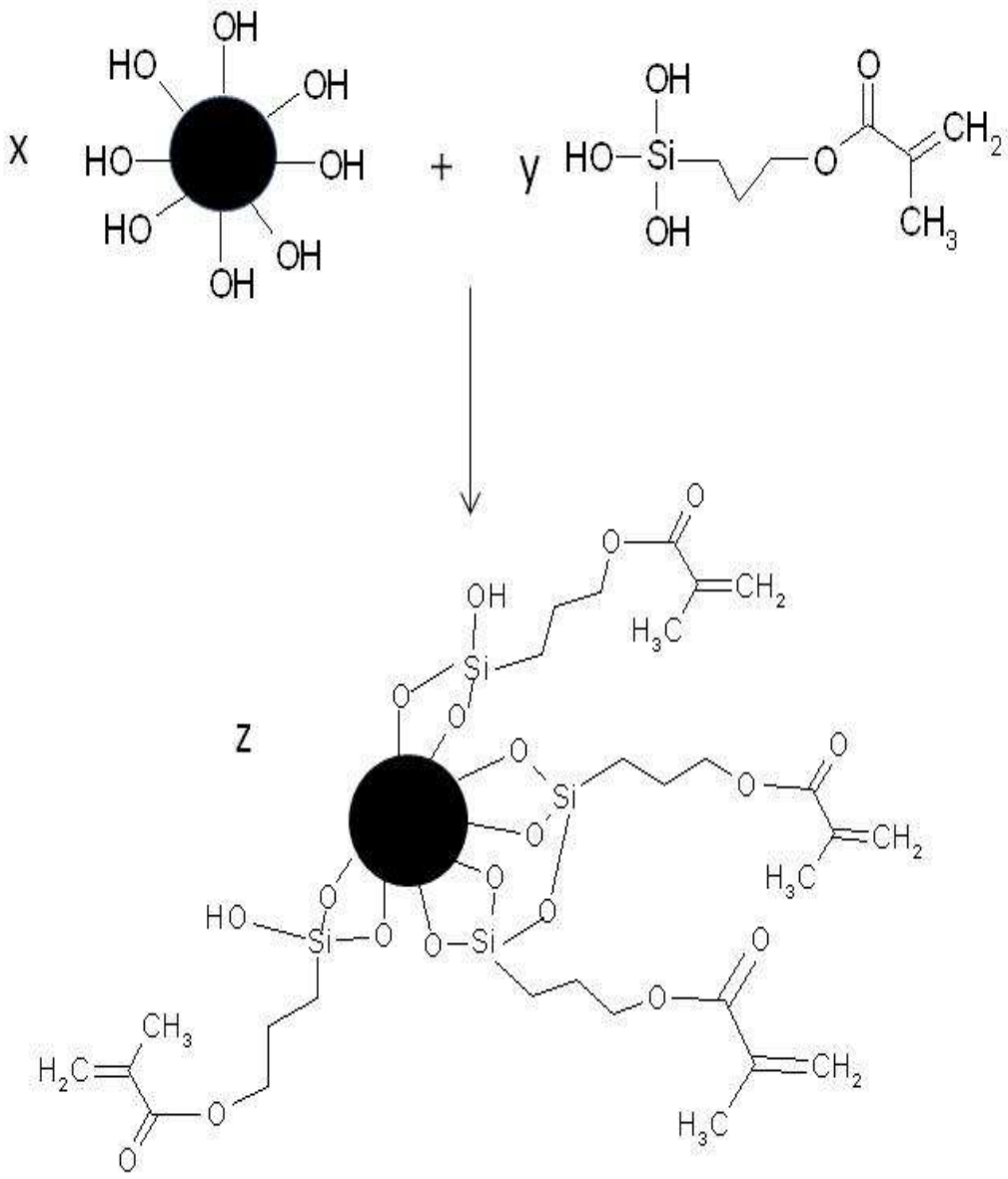


Figure 5.5: Coating of the magnetite with the hydrolysed γ-MPS.

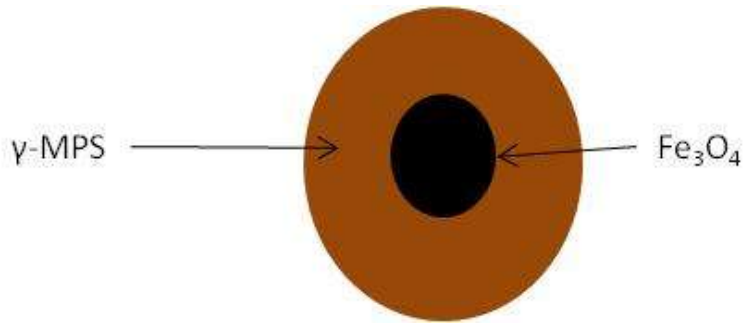


Figure 5.6: An illustration of the arrangement of γ-MPS around the magnetic core.

5.1.2.2 Functionalization of magnetite with oleic acid

Oleic acid (OA) is also another commonly used coating agent used to stabilize the magnetic nanoparticles synthesized by the traditional co-precipitation method. Some studies have proved that there is a strong chemical bond formed between the carboxylic acid and the amorphous iron and amorphous iron oxide nanoparticles (Zhang, 2006).

A structure of OA is shown in Figure 5.7. The hydrophilic carboxylate terminal will undergo charge delocalization first before it forms bidentate ligand. This ligand is shown in Figure 5.8 and its reaction with magnetite is shown in Figure 5.9.

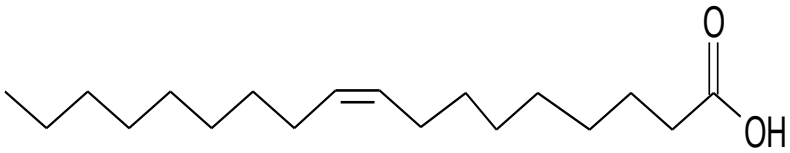


Figure 5.7: The structure of oleic acid.

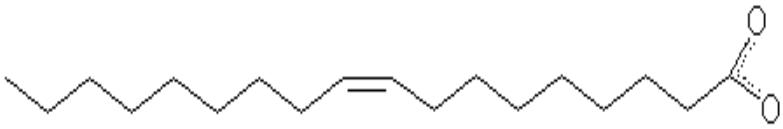


Figure 5.8: Charge delocalization on the carboxylate of the oleic acid.

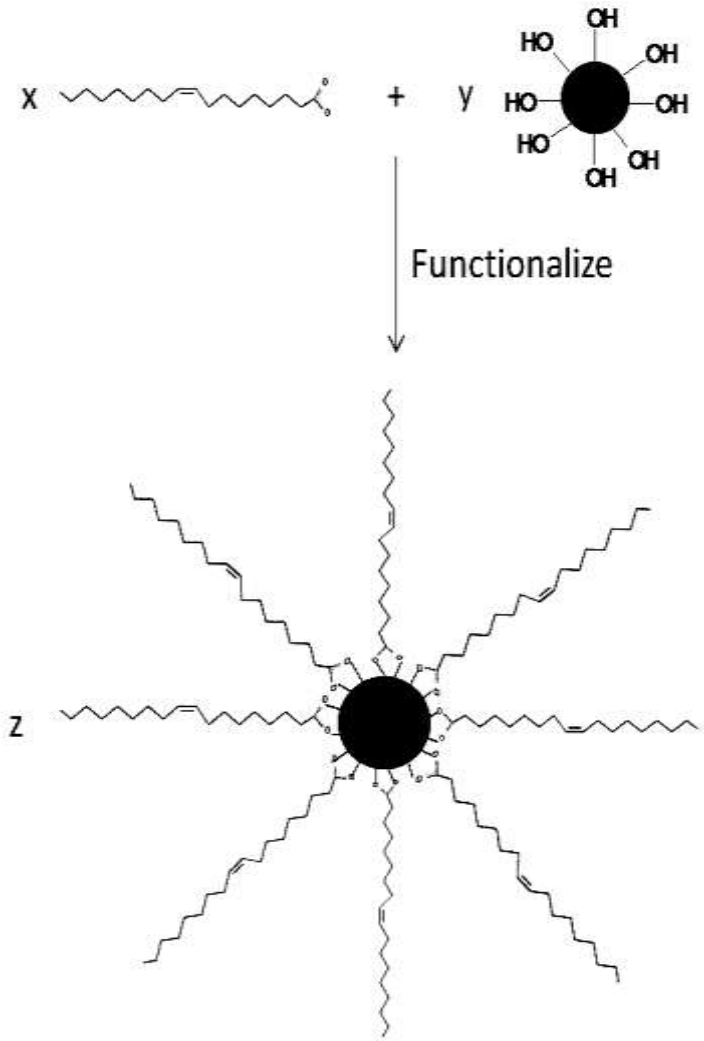


Figure 5.9: Scheme for the functionalization of magnetite with OA.

5.1.2.1 Carbon, hydrogen, nitrogen and sulphur (CHNS) analysis

Elemental analysis (CHNS) was done in order to determine the degree of coating of γ-MPS and OA on magnetite and the results are given in Tables 5.1 and 5.2. This was achieved by measuring the carbon and hydrogen content in the organic moieties.

Table 5.1: Elemental analysis of γ-MPS coated magnetite.

mass (g)	% C	% H	Ligand concentration (mmol g^{-1}) *
2.00	20.16	2.94	16.8
2.00	19.25	2.92	15.8
2.00	18.92	2.84	15.8

*Values for the ligand concentration were all based on the carbon content.

Table 5.2: Elemental analysis of OA coated magnetite.

mass (g)	% C	% H	Ligand concentration (mmol g^{-1}) *
2.05	4.63	1.38	3.86
2.01	4.82	1.46	3.99
2.01	4.48	1.39	3.71

*Values for the ligand concentration were all based on the carbon content.

From values in Tables 5.1 and 5.2, the ligand concentrations on the magnetite was found to be 16.1 and 3.82 mmol g^{-1} for γ-MPS and OA coated magnetite, respectively (The mathematical calculation is shown in the appendix section).

5.1.2.2 Diffuse reflectance spectroscopy (DRS)

Oxidation of synthesized superparamagnetic magnetite converts Fe_3O_4 to γ-Fe_2O_3 and this can be accomplished through exposure to oxygen or other oxidizing agents (Thorek *et al*., 2006). This result in the change of the material appearance from a black-brown to a red-brown as Fe^{2+} in the magnetite lattice is oxidized (Thorek *et al*., 2006).

From Figure 5.10, DRS peaks were observed at 443, 652 and 826 cm^{-1}. However, these peak signals were very weak due to the strong absorption of the dark magnetite samples. The colour of the iron oxide synthesized as shown in Figure

5.1, was observed to be black. This is indicative of the presence of the magnetite phase of the iron oxide.

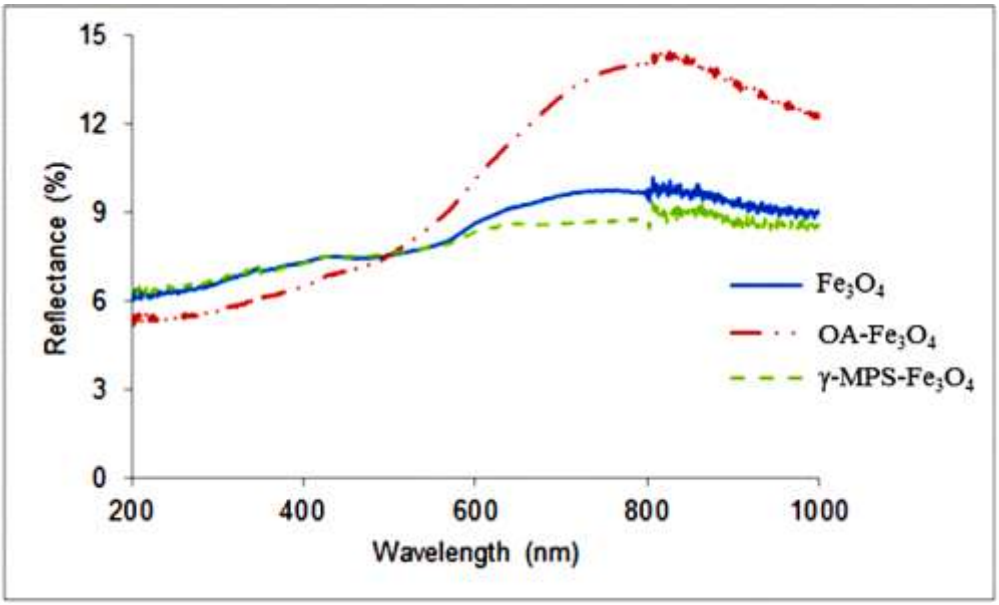


Figure 5.10: DR spectra of magnetite as well as γ-MPS and OA coated magnetite.

A few examples of different colours of iron oxides are shown in Table 5.3. However, particle size, aggregation and the presence of impurities can cause some discrepancies in the colours of the iron oxides (Torrent and Borron).

Table 5.3: Colours of different iron oxides.

Iron oxide	**Colour**
Magnetite	Black
Hematite	Yellowish-red
Maghemite	Dark brown

The absorption bands exhibited by the Fe oxides at UV to near IR wavelengths originate from electronic transitions within the $3d^5$ shell of the Fe^{3+} ion. Magnetite can also be identified by a unique band at 1500 nm due to Fe (II) to Fe(III) intervalence charge transfer (Scheinost *et al.*, 1998) which was however not observable in the wavelength range used in the DRS analysis.

5.1.2.3 Raman spectroscopy

Raman spectroscopy can be used to distinguish minerals like magnetite, hematite and maghemite. Both magnetite and maghemite have been used as naturally occurring magnets. Near room temperature, magnetite very slowly oxidizes to maghemite and then at higher temperatures, to hematite through a process called martitization (de Faria *et al*., 1997). The oxidation of magnetite (Fe_3O_4) to hematite (α-Fe_2O_3) proceeds either directly or *via* maghemite (γ-Fe_2O_3) (Sidhu, 1988), Figure 5.11.

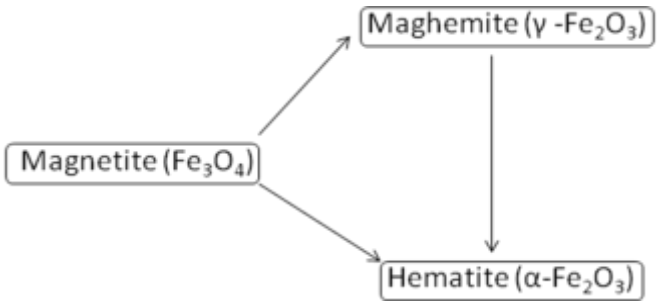


Figure 5.11: Oxidation of magnetite through two different routes.

These three phases of iron oxide (magnetite, hematite and maghemite) have very distinct bulk Raman spectra and this was used to determine the phase of the uncoated and coated iron oxide particles. The nanoparticles showed a diagnostic Raman peak at around 672 cm^{-1} which corresponds to magnetite (Tang *et al*., 2003). Other assignments of the band positions for phase identification were compiled by Slavov *et al*. (2010) and are presented in Table 5.4. Iron oxide and γ-MPS-iron oxide under study are also included in the table together with their corresponding wavelength bands.

Table 5.4: Raman bands for magnetite, maghemite and hematite.

	Iron oxide	Wavelengths (cm^{-1})
Literature	Fe_3O_4 (magnetite)	193, 306, 538, 668
	γ-Fe_2O_3 (maghemite)	350, 500, 700
	α-Fe_2O_3 (hematite)	225, 247, 299, 412, 497, 613
Observed	Iron oxide	667
	γ-MPS-iron oxide	670, 1400, 1600

The presence of the strong peaks around 667 cm^{-1} in Figures 5.12, 5.13 and 5.14 indicated that the phase of the iron oxide present was magnetite (Fe_3O_4).

According to Adar (2009) and Wang *et al*. (1990), all carbon systems show only a few prominent bands, no matter the final structure, and these intense bands occur between 1000-2000 cm^{-1}. In this work, the carbon system used was from γ-MPS, which is an organic moiety, had a lot of carbon atoms. The exact peaks of the carbon peaks in the Raman spectrum for this γ-MPS were identified at 1400 cm^{-1} and 1600 cm^{-1}.

However, the same peaks, but of low intensity, were observed in the unmodified magnetite. This was unexpected and can be attributed to some organic contamination. It can therefore be concluded that the synthesized iron oxide was magnetite and it remained in this phase even in γ-MPS-Fe_3O_4 as evidenced by the presence of the 670 cm^{-1} band. This might have been a due to the use of a nitrogen protective layer purged for 10 minutes during functionalization which prevented oxidation of the magnetite.

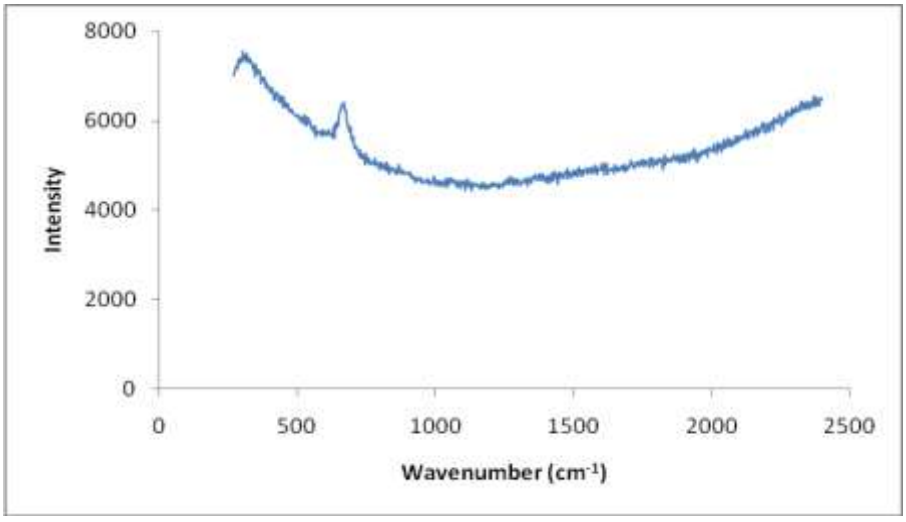


Figure 5.12: Raman spectrum of pure magnetite.

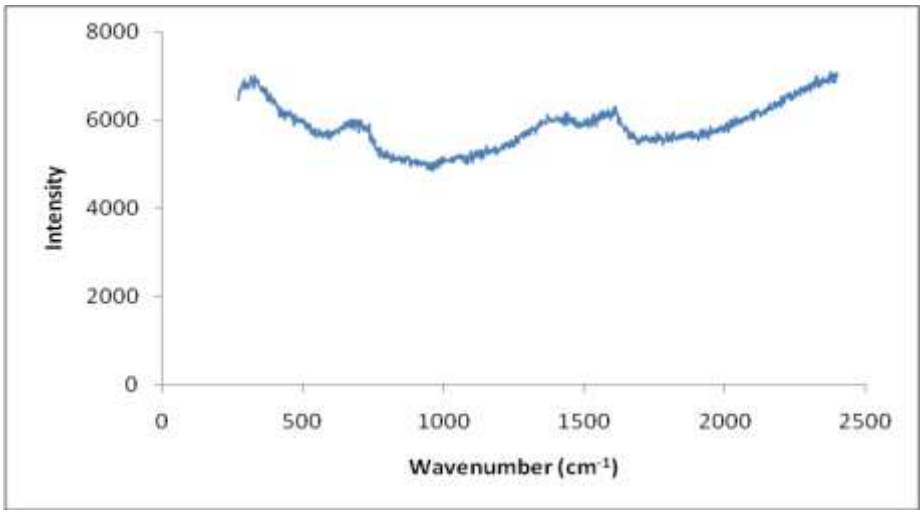


Figure 5.13: Raman spectrum of the unmodified magnetite.

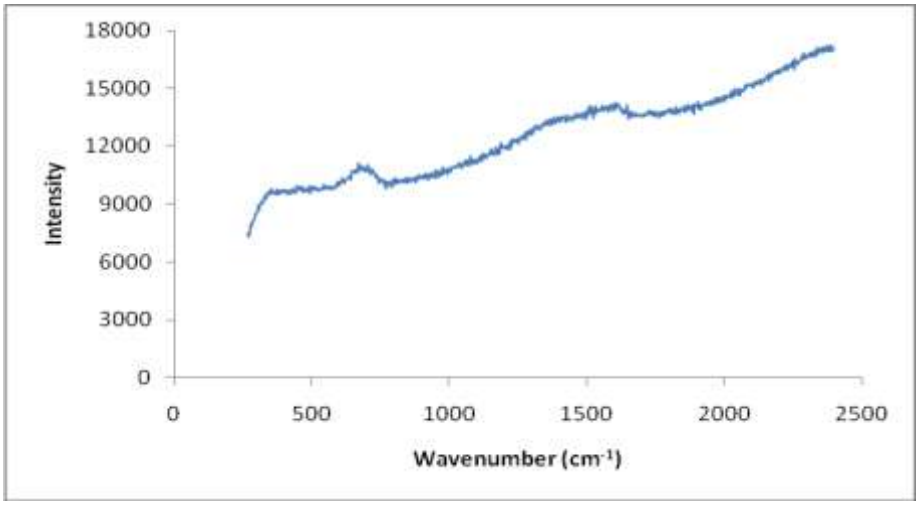


Figure 5.14: Raman spectrum of the γ-MPS modified magnetite.

5.1.2.4 Transmission electron microscopy (TEM) analysis

The prominent large black spots on the TEM image in Figure 5.15(a) indicate that the particles have a tendency of agglomerating. This is especially so when they are synthesized in aqueous medium. One of the ways to stabilize the magnetite is by functionalizing it with coating agents and surfactants. In Figure 5.15(b), the coating agent was γ-MPS whose hydrophilic silanol reacted with the hydroxyl groups around the magnetite. The other end of the γ-MPS, the hydrophobic end, contained a double bond which made it possible for polymerization to occur. The agglomeration of the coated magnetite, after coating, was still evident though to a

lesser degree. It was also observed that the synthesized particles were mostly spherical in shape. When they are coated with silica, the magnetite particles still retained their spherical shapes.

From the micrograph of Fe_3O_4 obtained by El Ghandoor *et al*. (2012), it was seen that spherically shaped particles with a narrow size distribution with mean diameter of 10.59 nm were obtained. In another study by Qian *et al*. (2008), it was revealed that the magnetic particles were dispersed very well, with an average diameter of 10 nm. Nanoparticles prepared by coprecipitation of a mixture of ferric nitrate and ferrous sulphate solutions with added 1M NaOH solution of ethanol and water (1:1, *v/v*) gave a mean particle size of 5.0 nm with a standard deviation of 0.2 (Roca *et al*., 2009).

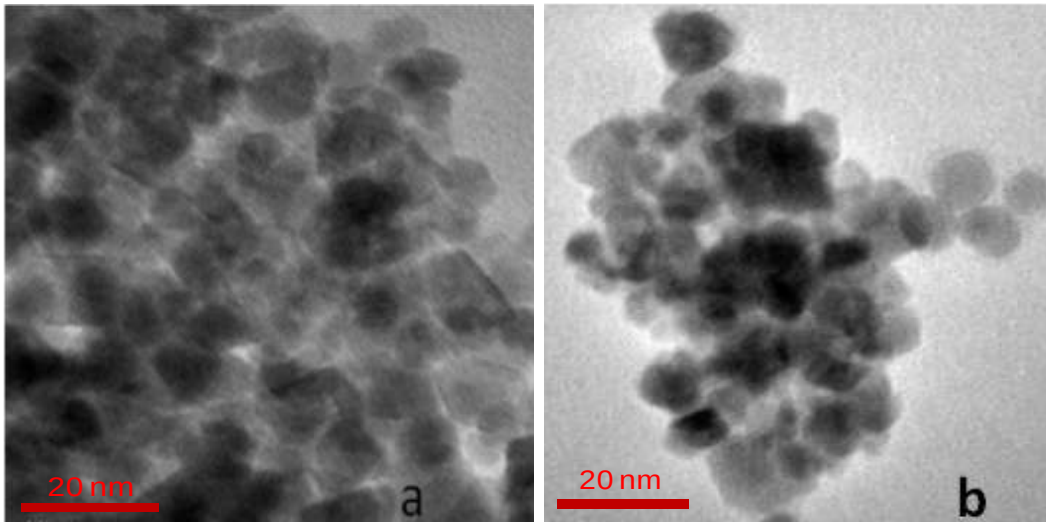


Figure 5.15: Transmisssion Electron Micrographs of (a) uncoated and (b) γ-MPS coated magnetite.

5.1.2.5 Size distributions

For the uncoated magnetite, a total of 237 particles were measured from four different TEM images to get the particle size distribution shown in Figure 5.16. It was found that the mean diameter of the uncoated magnetite was 11.4 ± 2.5 nm. This diameter was consistent with that found by Lu and Forcada (2006) who obtained a mean diameter of 10 nm after synthesizing their magnetite by co-precipitation. Pan *et al*. (2011) also obtained a mean diameter of 10 nm in their

study. The curve in Figure 5.16 is skewed to the right of the mean implying that most of the particles were having a greater diameter than the mean. This can be attributed to the agglomeration of the superparamagnetic particles.

For the γ-MPS coated magnetite, a total of 110 particles were measured from 8 TEM images for particle size distribution is shown in Figure 5.17. The mean size diameter of the γ-MPS coated magnetite was found to be 13.4 ± 1.4 nm. The increase in diameter supports the idea that magnetite was coated with γ-MPS.

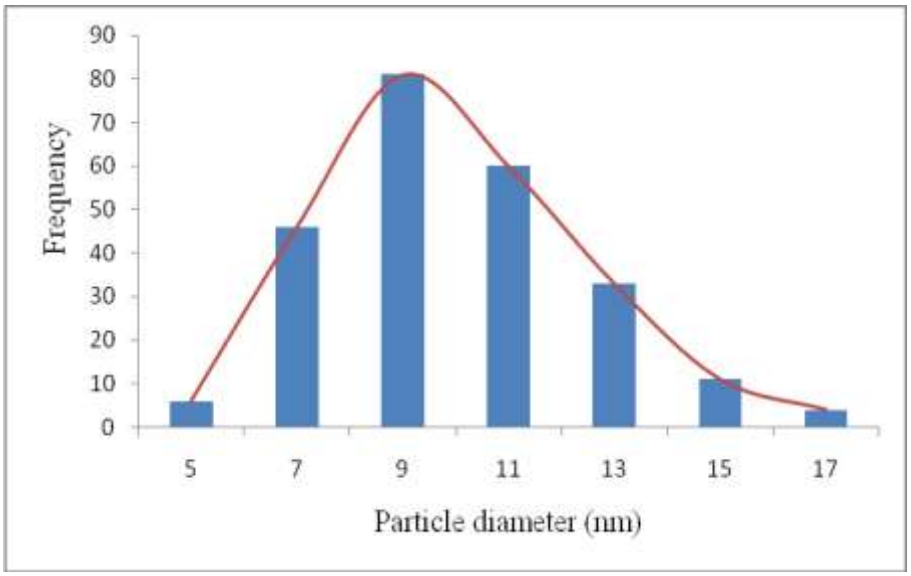


Figure 5.16: Particle size distribution of the uncoated magnetite.

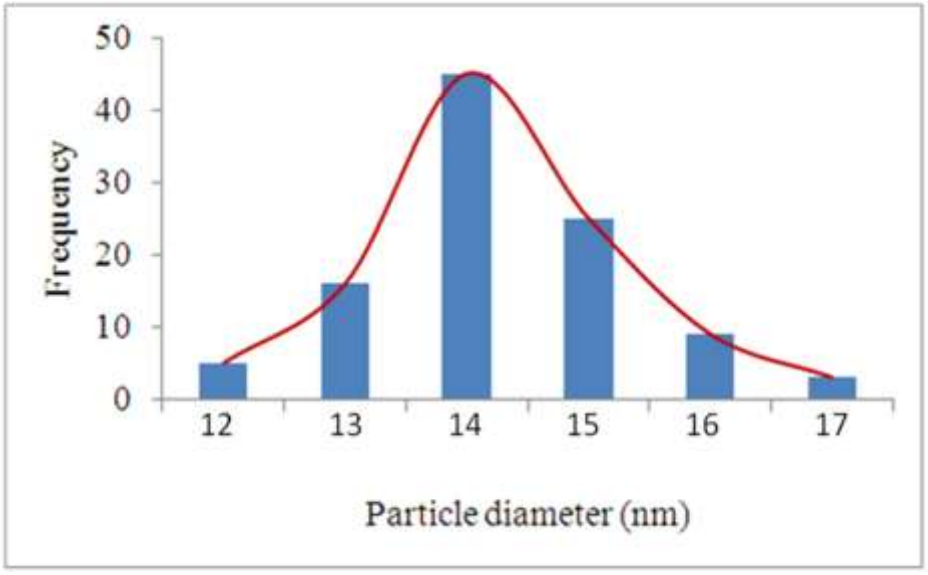


Figure 5.17: Particle size distribution of the coated magnetite.

5.1.2.6 Fourier-transform infrared (FTIR) analysis

Fourier-transform infrared results for both the uncoated and γ-MPS coated magnetite are shown in Figure 5.18. Figure 5.18(a) depicts the IR spectrum of the synthesized magnetite. According to Roonasi (2007), the broad bands around 570 and 360 cm^{-1} correspond to stretching and bending vibrations of Fe-O bonds typical of the crystalline lattice of magnetite. The band at 483 cm^{-1} from Figure 4.27(a) can be assigned to the bending vibrations of the Fe-O bonds. It is associated with the torsional vibration modes of the magnetite Fe-O bonds in octahedral sites. The lower band of 360 cm^{-1} was not able to be assigned because all the spectra obtained in this work were from 400 to 4000 cm^{-1}.

For the γ-MPS coated magnetite spectrum in Figure 5.18(b), the shift at 1104 cm^{-1} can be attributed to the stretch of Si-O-Si, indicating the formation of silica film on the magnetite. The success of functionalization can also be observed by the presence of the C=O band at 1716 cm^{-1}, from the carboxylate of γ-MPS.

Ma *et al*. (2011) used FTIR spectroscopy for the determination of the chemical structure of Fe_3O_4-γ-MPS. They identified that both Fe_3O_4 and Fe_3O_4-γ-MPS had a characteristic peak of Fe-O at a stretching frequency of 586 cm^{-1}. Besides, they observed a strong stretching vibration of Si-O-Si at 1089 cm^{-1} for Fe_3O_4-γ-MPS. Their conclusion from the two observed bands was that γ-MPS was successfully grafted onto the surface of magnetite. In another study, Qian *et al*. (2008) attributed the bands at 582 and 437 cm^{-1} to correspond to the vibration of Fe^{2+}-O^{2-} and Fe^{3+}-O^{2-}, respectively. The same strong absorption bands appearing in all functionalized magnetic polymers were ascribed to Fe_3O_4 by Nan *et al*. (2010). These bands were observed at around 570 cm^{-1}. In the studies conducted by Sadeghi and Aboobakri (2012), the FTIR spectrum of Fe_3O_4 nanoparticles showed, among others, an absorption peak at 577 cm^{-1} which they attributed to the Fe-O vibration frequency. In general, the bands that occur between 560-660 cm^{-1} are associated with the metal-O stretching vibration (Wang *et al*., 2011).

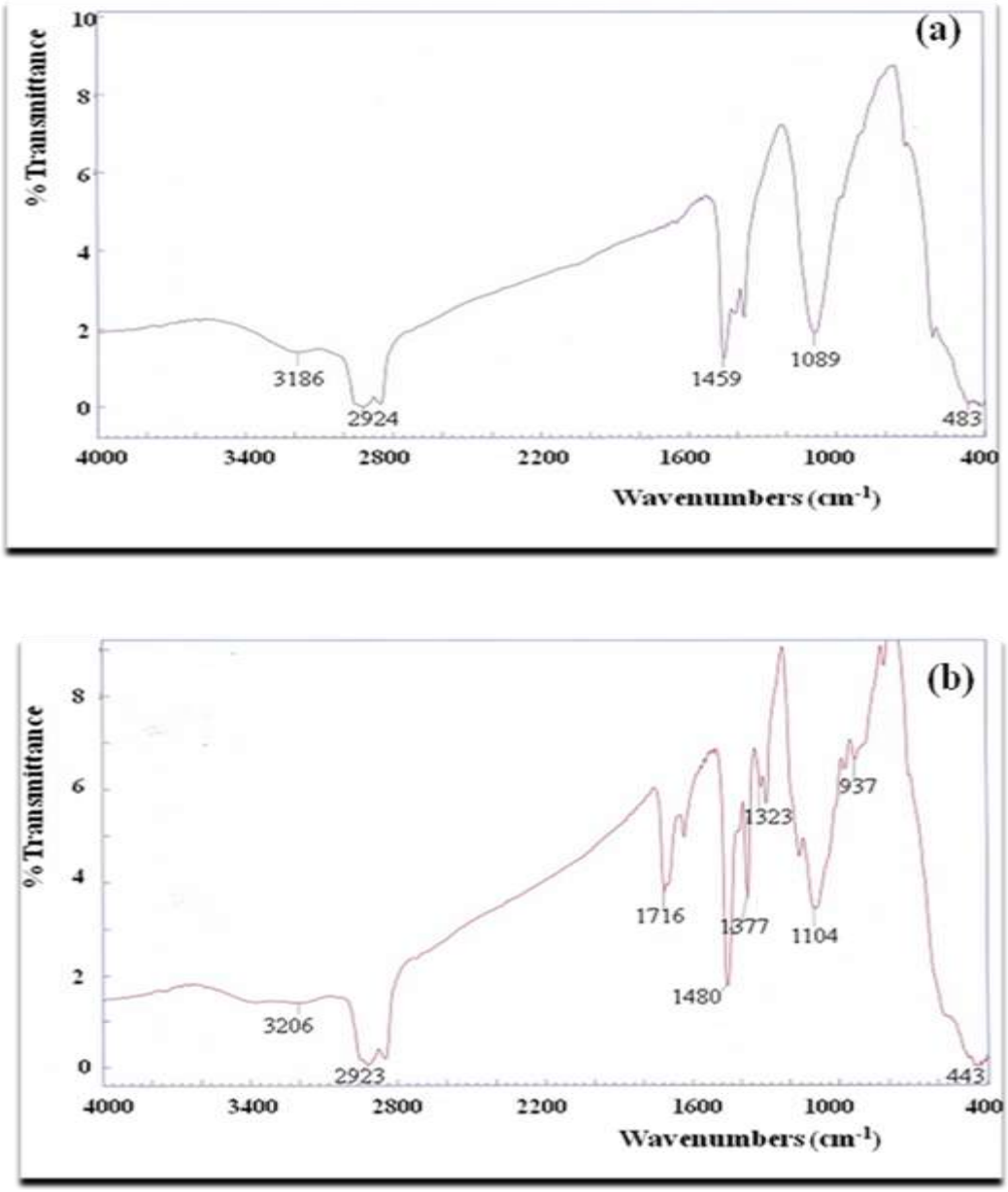


Figure 5.18: FTIR spectra of (a) uncoated magnetite and (b) γ-MPS coated magnetite.

One striking feature of the FTIR spectrum of OA-Fe_3O_4 is the absence of the C=O stretching frequency as shown in Figure 5.19. This was expected to be present since from the structure of oleic acid, Figure 5.7, it can be seen that the carbonyl group is present. This therefore implies that there was a special type of interaction between the magnetite and the oleic acid coating agent. The magnetite, as seen from its structure in Figure 5.2, has hydroxyl groups around it and it was expected that the type of interaction with oleic acid is esterification. But by charge

delocalization of the carboxylate (Figure 5.8), a bidentate ligand was formed and the scheme for the interaction of OA and magnetite is shown in Figure 5.9. The two bands between 2900 and 2800 cm^{-1} are attributed to the asymmetric CH_2 stretch and the symmetric CH_2 stretch of the oleic acid.

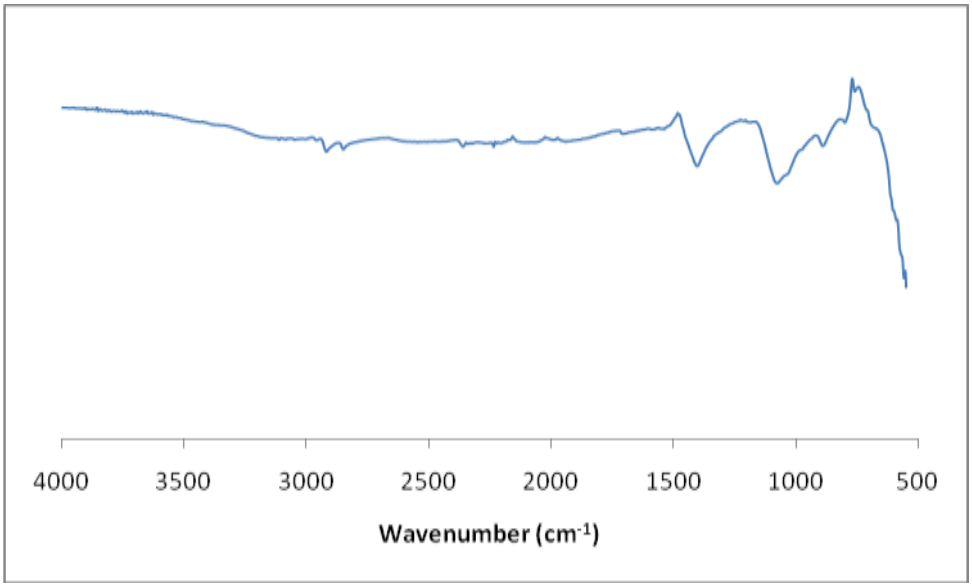


Figure 5.19: FTIR spectrum of OA-Fe_3O_4.

5.1.2.7 Dispersibility and stability of γ-MPS-Fe_3O_4

To examine the dispersibility and stability of γ-MPS-Fe_3O_4 in water, modified magnetite nanoparticles were added to water and dispersed by ultrasonic wave for 10 min. The dispersibility and stability were evaluated by ultraviolet visible (UV-vis) absorption spectroscopy.

Figure 5.20 shows the UV-vis absorption spectra of γ-MP-modified magnetite particles as a function of time. The absorbance (at λ = 350 nm) decreased from 0.90 to 0.19 over time because the magnetite particles coagulated by magnetic interaction and precipitated to the bottom of the UV cell.

The absorbance was almost constant at 0.19 because of steric repulsion of γ-MPS chains on the magnetite surface that hindered coagulation. According to Matsuno *et al.* (2003), the dispersion of the modified particles depends on whether the

solvent is a good or poor. In this case dispersibility and stability of magnetite in water were thus improved by this surface modification using γ-MPS.

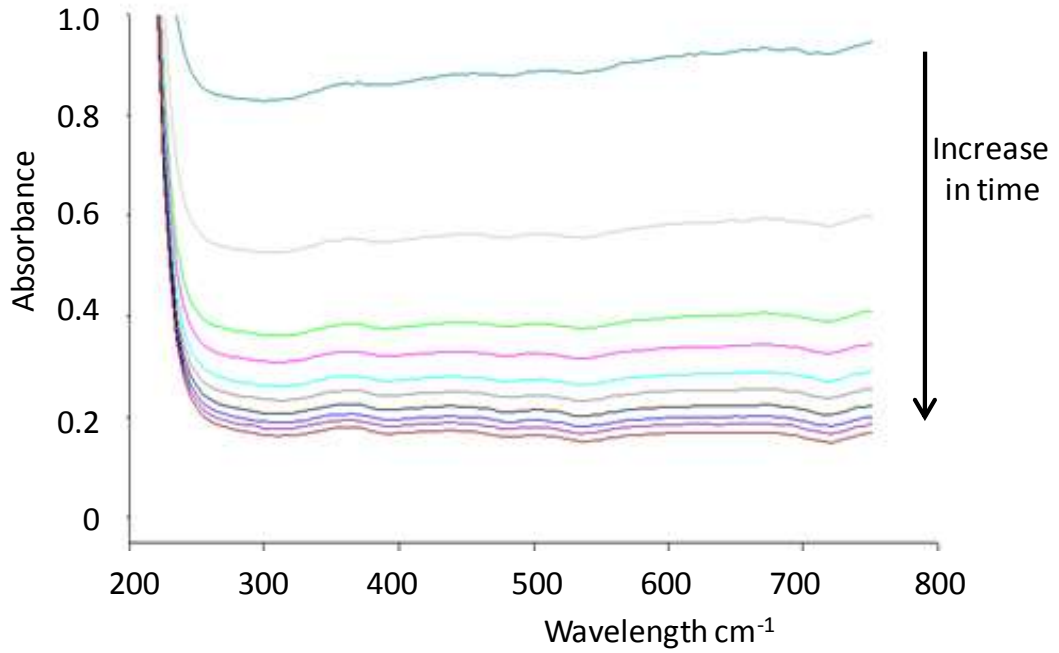


Figure 5.20: UV-Vis spectra of γ-MPS-Fe_3O_4 dispersed in water (Taken every after 10 min).

5.1.3 Magnetic polymer synthesis

Both the bulk and the precipitation polymerization follow the same mechanism shown in Figure 5.21. In this mechanism, 4-vinyl pyridine (4-VP) and salicylaldoxime (SALO) have a direct interaction with the uranyl in the pre-polymerization step. SALO bonds to the uranyl cation through co-ordination with the lone pair of electron on the N and O atoms. 4-VP also bonds co-ordinatively through the lone pair of electrons on its N atom.

γ-MPS-Fe_3O_4 or OA-Fe_3O_4 is added to the pre-polymerization mixture before the actual polymerization is effected. Also added is the cross-linker ethylene glycol methycrylate for structural rigidity.

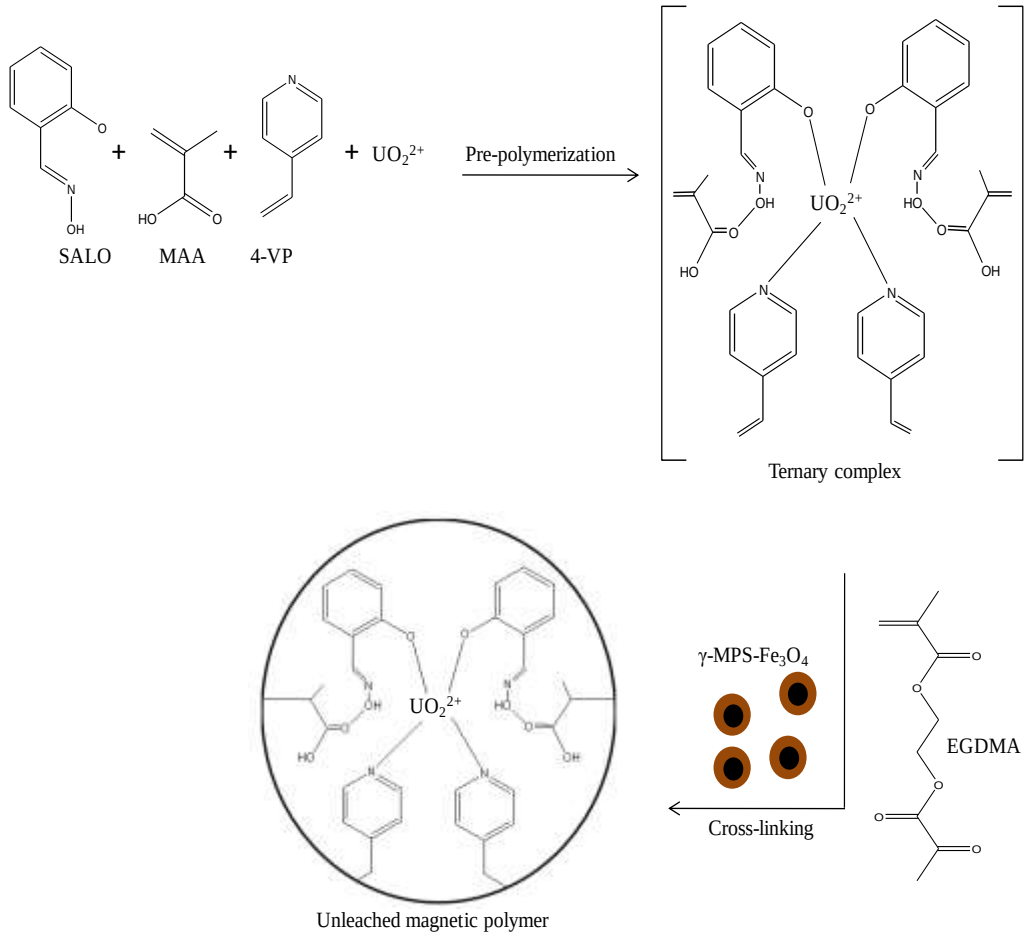


Figure 5.21: Polymerization on the γ-functionalized Fe_3O_4 particles.

The difference between bulk and precipitation polymerization was only in the amount of the porogenic solvent, 2-methoxyethanol. For precipitation polymerization 100 mL, was used whilst 10 mL was used for bulk polymerization, Figure 5.22.

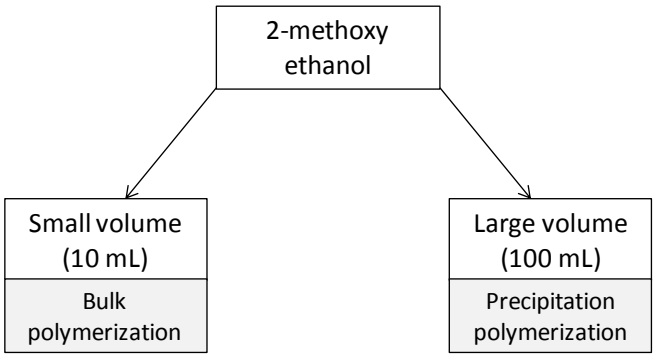


Figure 5.22: Volumes of the porogenic solvent used to effect bulk and precipitation polymerization.

5.1.4 Leaching analysis

Figure 5.23 shows the leaching of the uranyl from the magnetic polymer matrix.

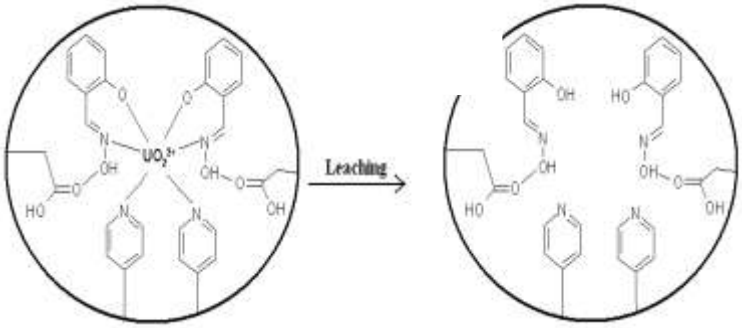


Figure 5.23: The leaching of the uranyl ion from the magnetic polymeric matrix.

The results in Figure 5.24 and 5.25 show the expected decrease of the amount of leached uranyl from some selected magnetic polymers over time. This trend was observed for both the bulk and precipitate polymers. However, there was a parallel unwanted leaching of the embedded magnetic core from the polymers. This was so pronounced for those polymers leached with 1 mol dm^{-3} HCl. In their study, Singh and Mishra (2009) had the same observation that the HCl had a greater percent removal of uranyl ion as compared to the $NaHCO_3$. On the other hand, 1 mol dm^{-3} $NaHCO_3$ showed that it was a weak leachant towards the washing away of the magnetic core and this was desirable. However, it is also observed that the leaching of the uranyl ion was again weak with this leachant. This is undesirable as the uranyl might bleed out when the polymers are being applied to real environmental water samples.

It can also be noted that bulk polymers tended to lose more of both the uranyl as well as the magnetite than those from precipitation polymerization. This could be attributed to the crushing of the polymers in bulk polymers.

Sadeghi and Aboobakri (2012) synthesized aminopropyl triethoxysilane on functionalized silica coated Fe_3O_4 nanoparticles. This was done in the presence of a uranyl ion as a template. Finally, the uranyl was washed with 0.1 M EDTA solution for its complete removal to form an imprinted polymer selective of uranyl. Singh and Mishra, (2009) used the same ternary monomers as those used

in this work. After crosslinking, they went further to even optimize the leachants where they used HCl, HNO_3, $NaHCO_3$, Na_2CO_3 and H_2SO_4 at various concentration.

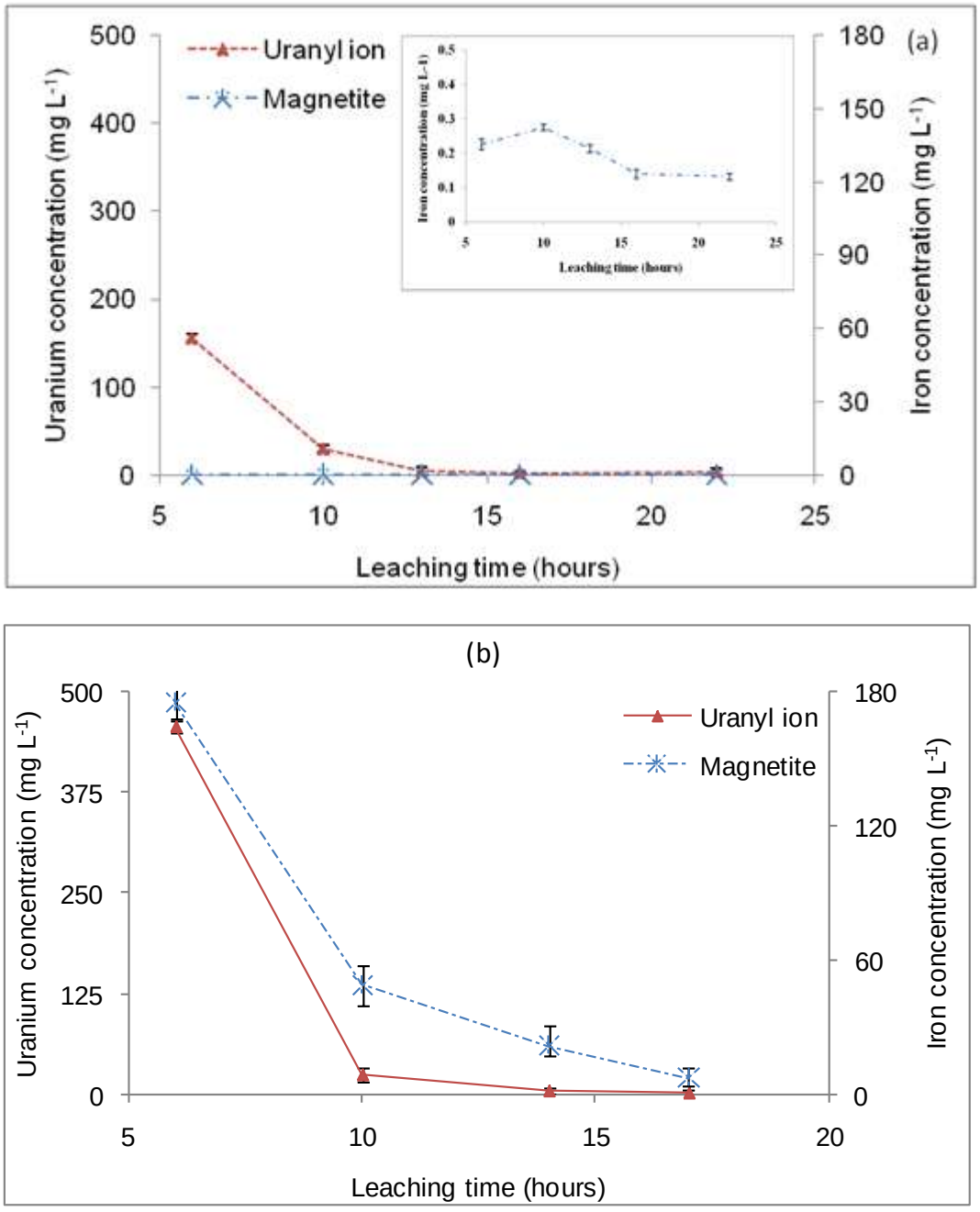


Figure 5.24: Polymers leached with 1 mol dm^{-1} $NaHCO_3$: (a) bulk magnetic IIP (b) precipitate magnetic IIP.

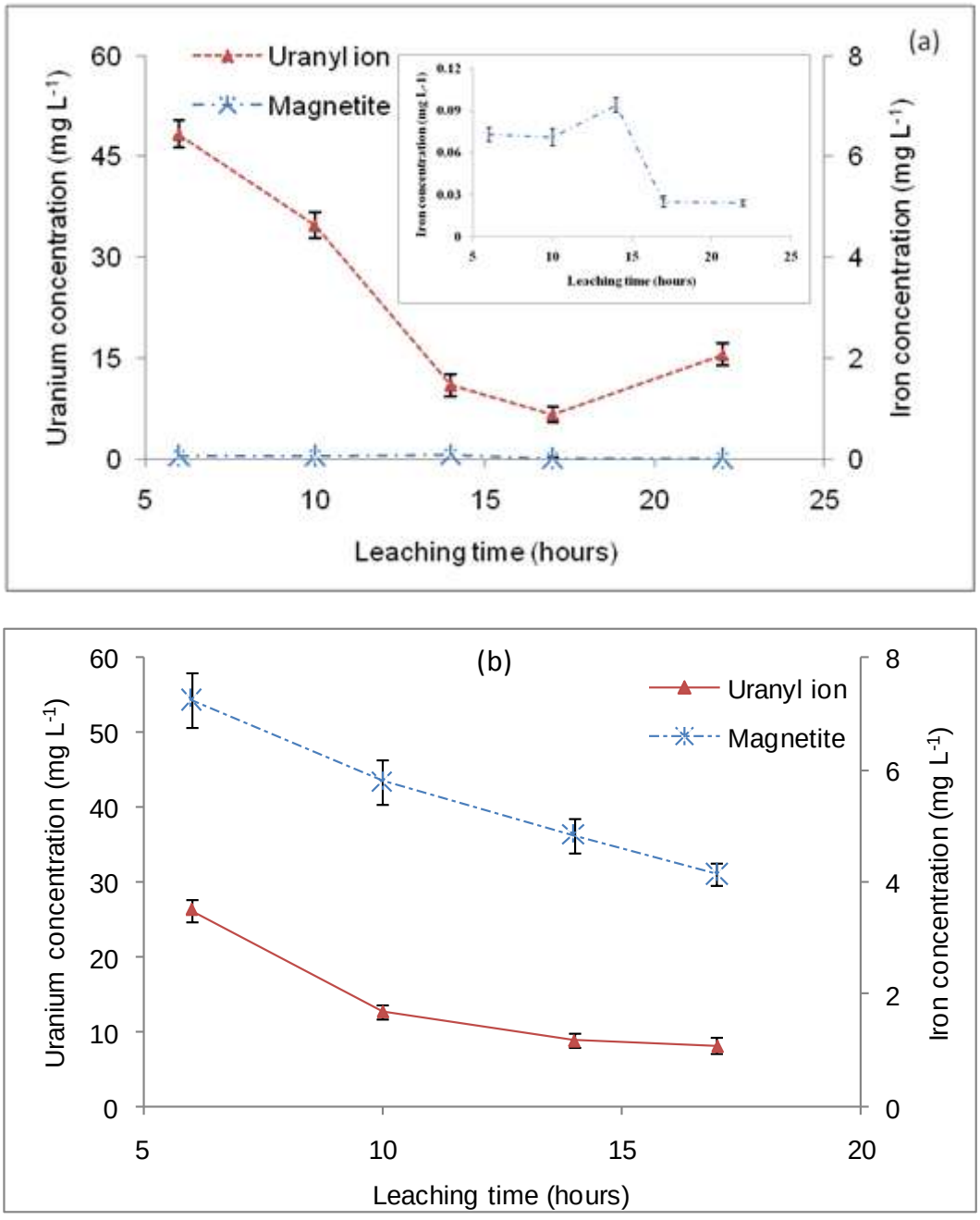


Figure 5.25: Polymers leached with 1 mol dm^{-1} HCl: (a) bulk magnetic IIP (b) precipitate magnetic IIP.

Another concern was the possible problem of swelling and shrinkage of the magnetic polymers. This had a potential of causing slow bleeding of the residual templates embedded deep in the polymer matrix.

According to Sellergre (2003), the unextracted template may act as a nucleation site for template cluster formation. Also, since the solvating properties of the

media are changing during polymerization, the template may again form clusters which would then be the actual species imprinted. It is therefore important to carefully determine the recovered template and to verify its identity.

5.1.4.1 Atomic force microscopy (AFM)

Imaging of unleached magnetic IIPs using tapping mode AFM proved difficult, as the tip was repelled from the surface it was supposed to image. The encircled black spots highlighted in the optical view of the magnetic IIP in Figure 5.26 are the magnetic particles responsible for this repulsion. However, imaging of the leached magnetic polymers was successful. This was made possible by the fact that some magnetite was lost during leaching hence the residual magnetite did not have sufficient power to repel the AFM probing tip.

Figures 5.27 and 5.28 are the AFM images of 20 μm^2 magnetic IIPs leached with 1M $NaHCO_3$ and 1M HCl solutions, respectively. From the two Figures and the surface roughness data in Figure 5.29, it can be concluded that HCl was stronger leachant than $NaHCO_3$. Figure 5.30 shows a three dimensional AFM image of $NaHCO_3$ leached polymer and it clearly shows the pores formed by the leaching of the uranyl ions from the polymer surface.

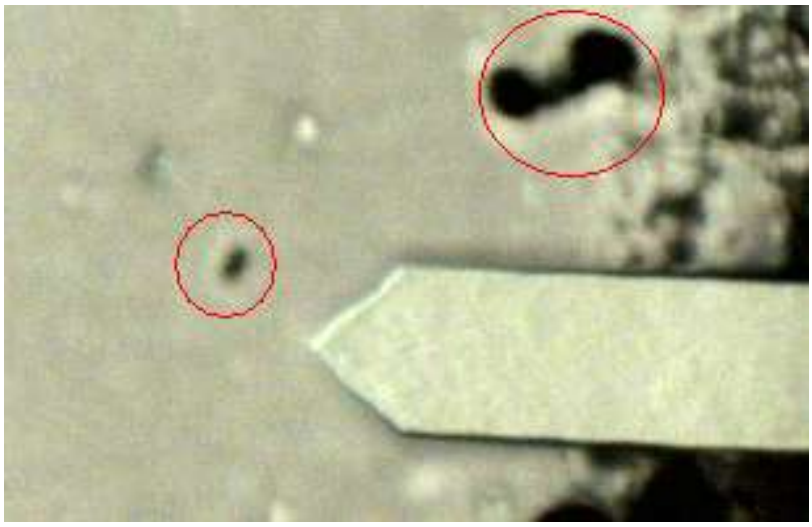


Figure 5.26: Optical view of magnetic IIP with an AFM tip of width ~25 micro metres.

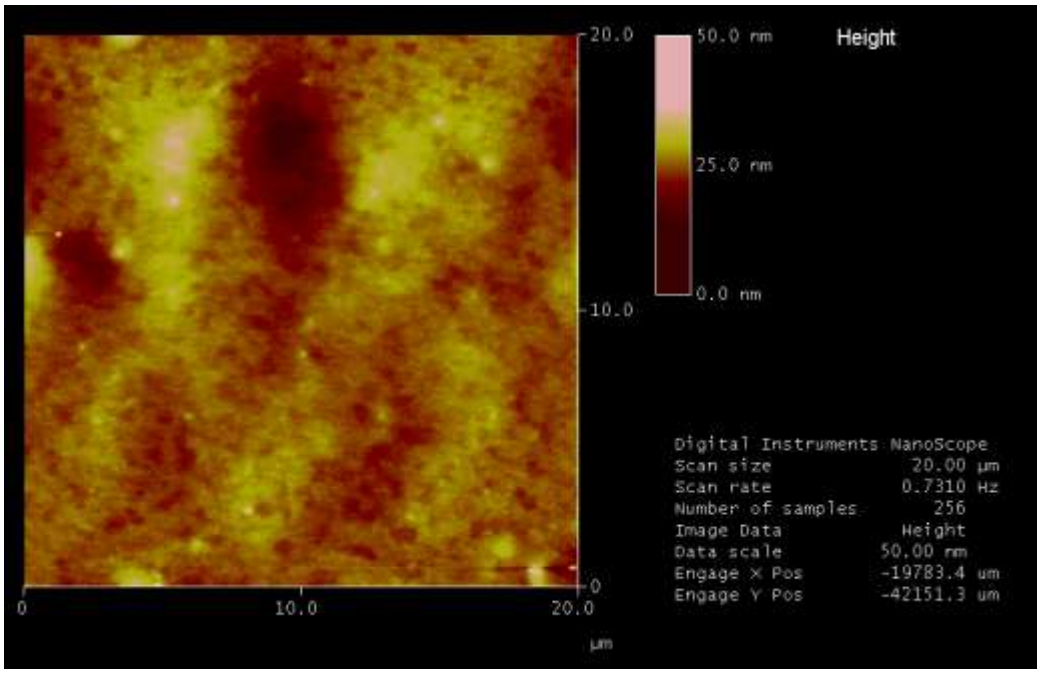


Figure 5.27: AFM image of $NaHCO_3$ leached magnetic IIP.

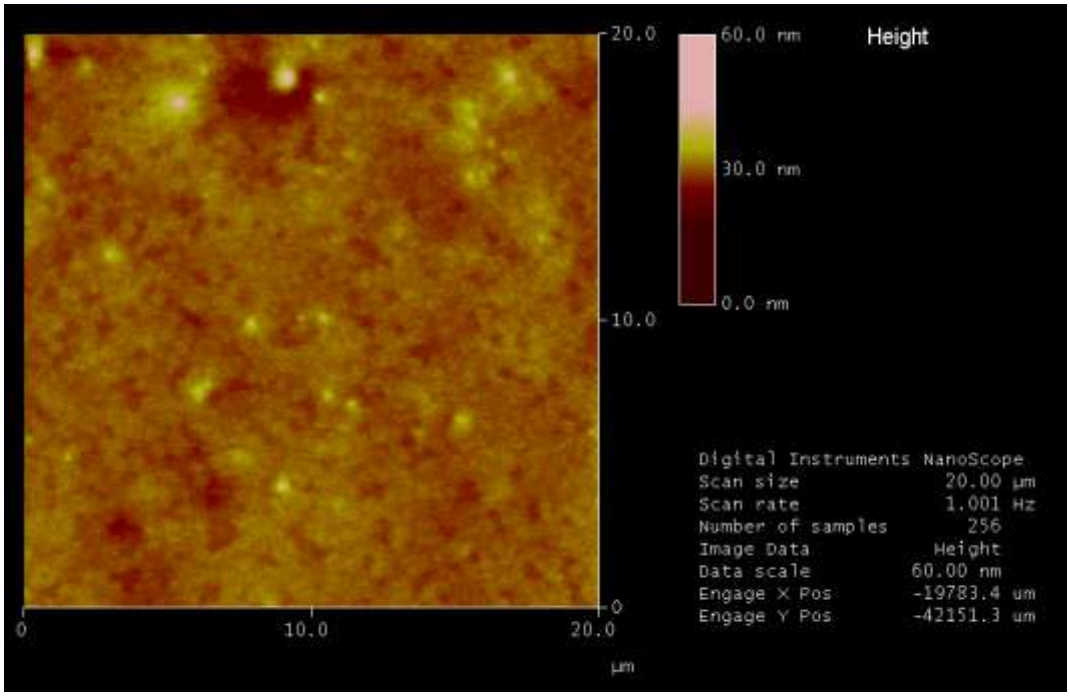


Figure 5.28: AFM image of HCl leached magnetic IIP.

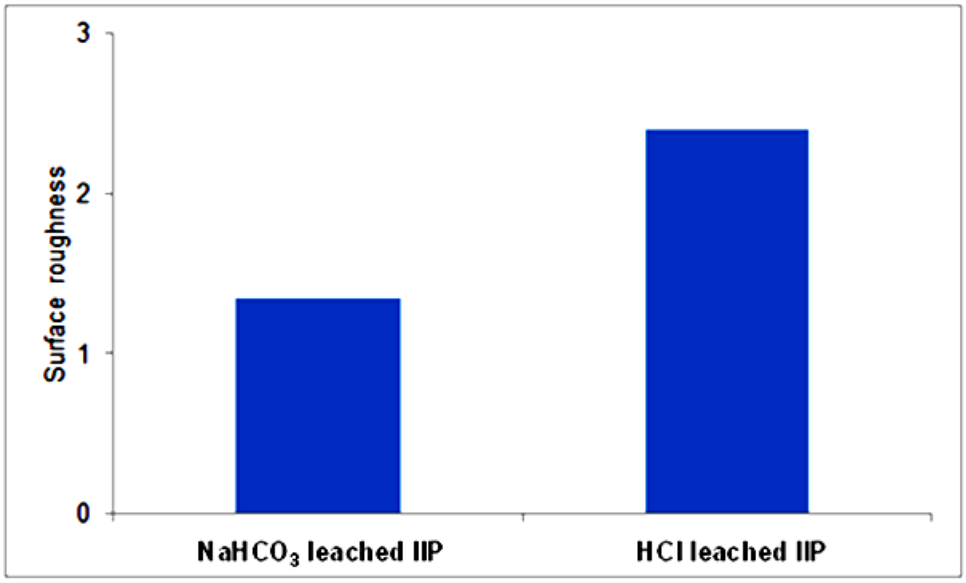


Figure 5.29: Image Roughness of the $NaHCO_3$ and HCl leached magnetic IIPs.

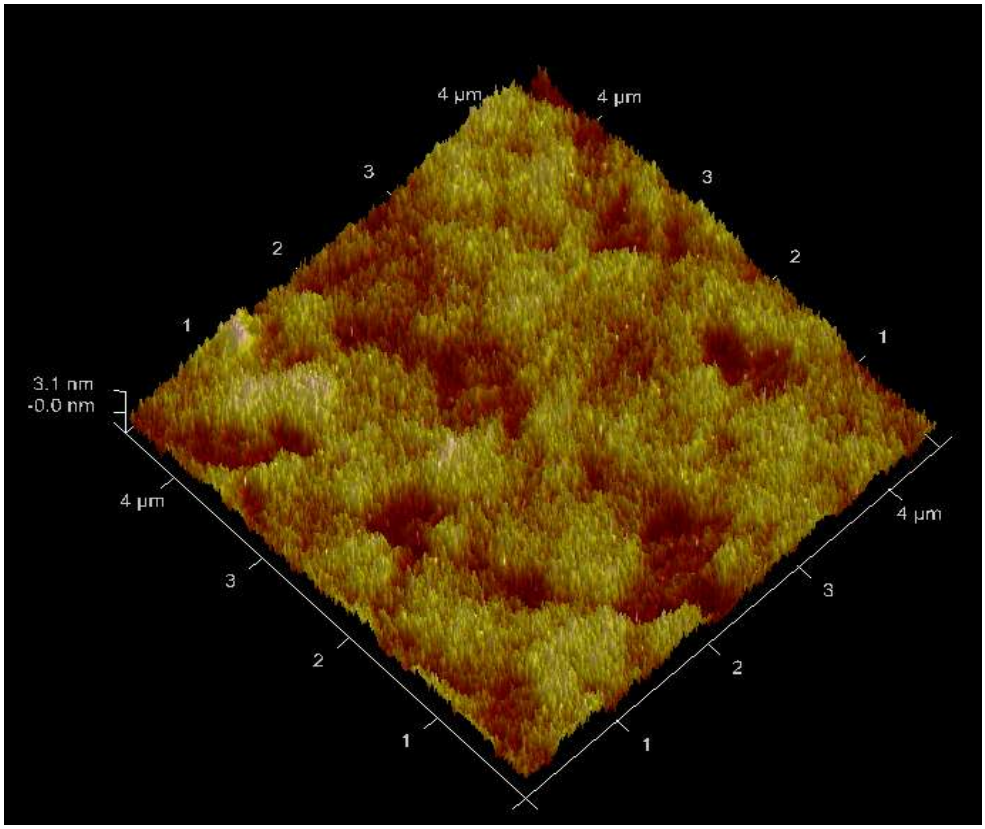


Figure 5.30: A three dimensional AFM image of $NaHCO_3$ leached polymer.

5.1.4.2 Energy-dispersive X-ray spectroscopy (EDS) analysis

Figures 5.31 and 5.32 show the results of EDS spectra of two polymers leached with 1 mol dm^{-3} $NaHCO_3$ and 1 mol dm^{-3} HCl. Figures 5.31(a) and 5.32(a) confirm the incorporation of the magnetic core within the polymer matrix of the bulk and the precipitate polymers, respectively, by virtue of the presence of the Fe band. The main elements present were Fe, Si, O and U in the case of unleached magnetic polymers (both in precipitation and bulk polymers). Ideally, after leaching it is expected that the peaks due to U disappear. This was the case with the washed bulk magnetic polymers and not for the precipitated polymers. Total uranium leaching was expected as the uranium, deeply embedded in the polymeric matrix of the bulk polymer become exposed to the surface at the grinding stage of the magnetic polymer. The template exposure implies that the uranyl will be easily leached out with the $NaHCO_3$ and HCl leachants. On the other hand, precipitation polymers showed some residual uranium even though they were in contact with the leachant for the same amount of time as that of the bulk polymers. This could be attributed to the fact that the technique of precipitation does not involve grinding. The uraniun remains deeply encapsulated. The leaching agent does not penetrate into the polymer matrix with the same ease it does in crushed and ground polymers. The presence of the Si implies the presence of the coating agent γ-MPS on magnetite.

The strong permanent peaks of Be and Cu present in all the spectra originated from the instrument. The instrument, FEI Tecnai 120V TEM, uses a Be window where beams of X-rays are passed through. This implies that the Be peaks are present in all samples analyzed with this instrument. The strong Cu peaks are as a result of the use of the sample grids which are coated with Cu.

In the process of leaching out uranyl ions, there was a parallel unwanted leaching of the magnetite in both the bulk and precipitation magnetic IIPs. This was the case for the IIPs leached with either 1 mol dm^{-3} $NaHCO_3$ or 1 mol dm^{-3} HCl as evidenced by the reduction or disappearance of the iron bands in all leached polymers. The extent of the iron leaching was greater in those polymers leached with 1 mol dm^{-3} HCl. It was also noted that the bulk polymers lost much

magnetite as compared to the precipitated polymers. These results were consistent with those obtained from the ICP-OES analysis.

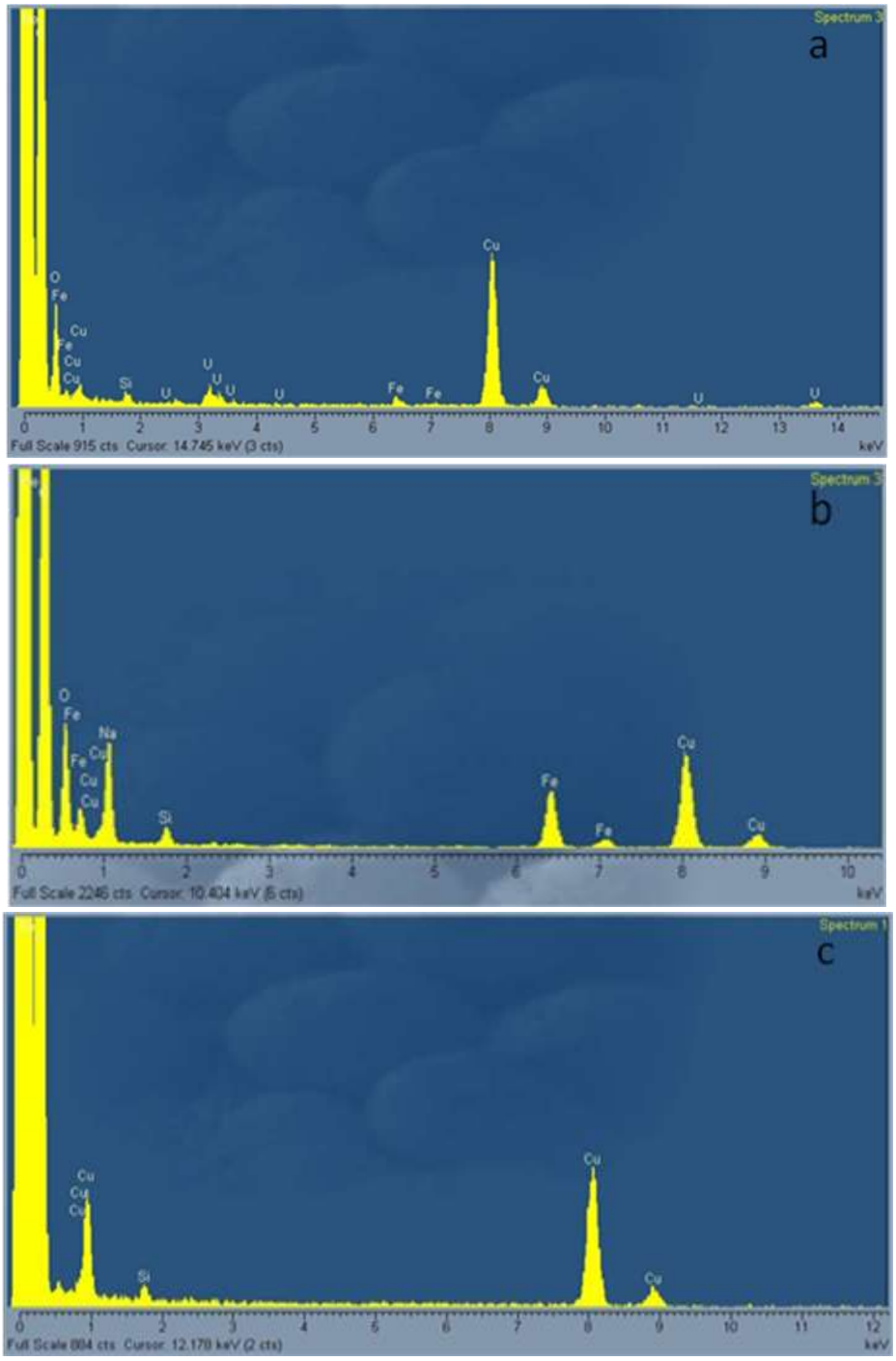


Figure 5.31: Energy dispersive spectra of (a) unleached bulk magnetic IIP (b) washed with 1 mol dm^{-3} $NaHCO_3$ (b) and (c) 1 mol dm^{-3} HCl.

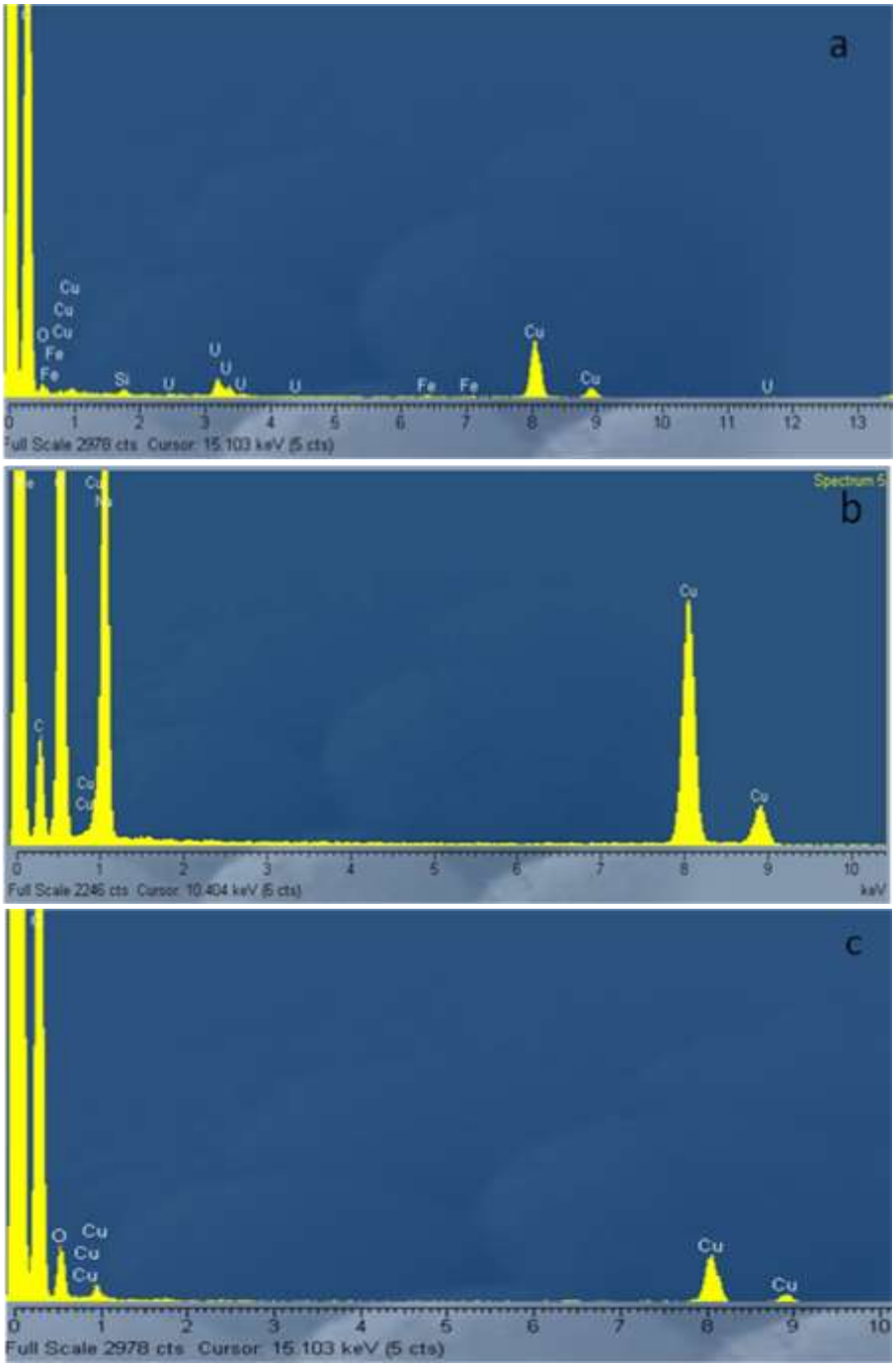


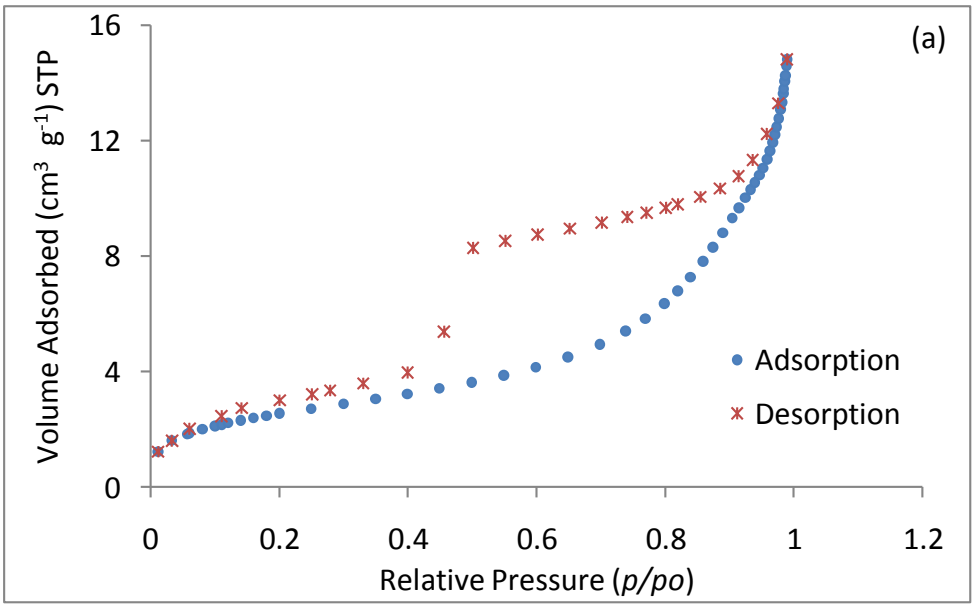
Figure 5.32: Energy dispersive spectra of (a) unleached precipitation magnetic IIP (b) washed with 1 mol dm^{-3} $NaHCO_3$ (c) and 1 mol dm^{-3} HCl.

5.1.4.3 Brunauer, Emmett and Teller (BET) surface area analysis

The BET surface area measurements are summarized in Figures 5.33, 5.34 and 5.35. The results demonstrated that there was an increase in the surface area of the magnetic polymers as a result of leaching action. The bulk unleached IIP had a measured surface area of 8.8 m^2 g^{-1} whilst that of the corresponding HCl and $NaHCO_3$ leached were increased to 88.1 and 65.2 m^2 g^{-1}, respectively. These values are single point surface area measured at p/p_o = 0.2998. The results show consistence with the other characterization techniques, like the AFM results. These results show that the leaching with HCl resulted in magnetic polymers with a greater surface area. This is because there was a greater leaching of the uranyl from the polymer as well as the magnetic core as supported by the EDS results. The removal of these two ions left some voids which enhanced the surface area, because these pores became available for the nitrogen adsorption in the BET analysis. On the other hand, leaching with $NaHCO_3$ did not remove the uranyl as well as the magnetite completely. The implication of this is that the BET surface area was kept low because some of these two ions were still much present and embedded in the polymer matrix of the magnetic IIPs. The monomolecular layer volume, v_m and BET constant, c, for the bulk polymers were calculated from the slopes and intercepts of Figures 5.33(b), 5.34(b) and 5.35(b) and are shown in Table 5.5.

The imprinted polymer nanospheres for uranium prepared by complexing uranyl ion onto quinoline-8-ol functionalized 3-aminopropyltrimethoxysilane modified silica nanoparticles by Milja *et al*. (2011), had BET surface areas of 134.69 and 188.87 m^2 g^{-1} for the IIP and NIP, respectively. This was evidently higher than the surface areas obtained in this research and was probably due to the strength of the monomer-template interaction and/or the strength and type of the leachants used. However, Ahmadi *et al*. (2010) found a BET surface area of 18.5 m^2 g^{-1} for the unleached polymer particles. As expected, the porosity changed after the removal of uranyl ions from the IIP particle to 33.2 m^2 g^{-1} which was far less than what was obtained in this study. Ahmadi *et al*. (2010) prepared their adsorbent by

copolymerizing of a ternary complex of uranyl ions with styrene and divinylbenzene.



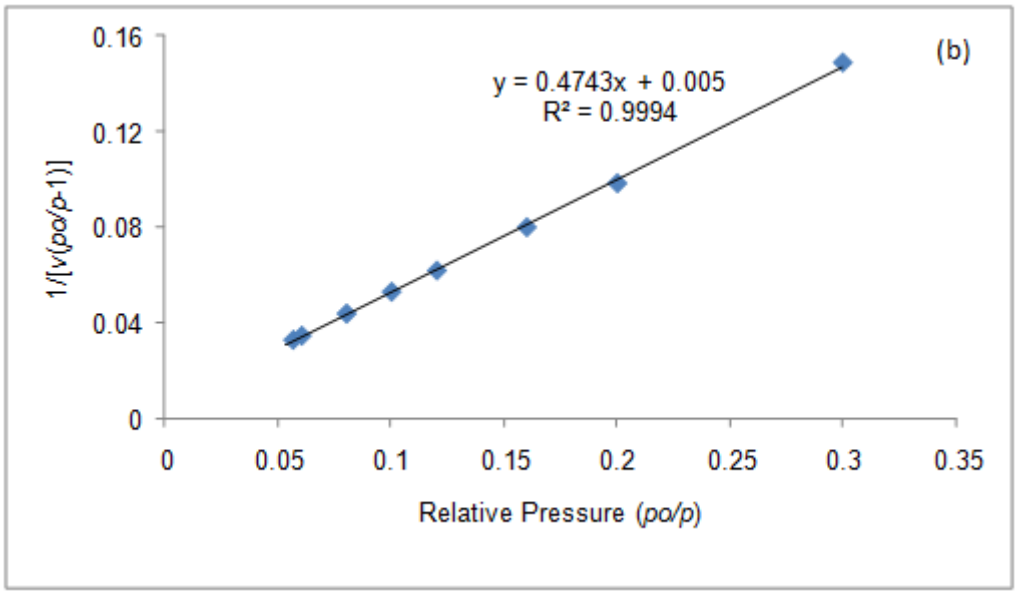


Figure 5.33: (a) The nitrogen adsorption-desorption isotherms for the unleached bulk magnetic IIP and (b) its corresponding BET plot.

Table 5.5: BET suface areas and constants for the bulk magnetic IIPs.

	BET surface area ($m^2\ g^{-1}$)	v_m	c
Unleached magnetic IIP	8.8	2.09	94.86
HCl leached magnetic IIP	88.1	2.10	95.20
$NaHCO_3$ leached magnetic IIP	65.2	15.43	129.6

5.1.4.4 Fourier-transform infrared (FTIR) analysis

Figure 5.34 shows three spectra of the unleached IIP, leached IIP as well as the NIP of magnetic bulk polymers. The close similarities in these three sprectra point to the fact that these three magnetic polymers have the same structural backbone. In all these magnetic polymers, it should be noted that EGDMA was used in excess for structural rigidity. Again, all these magnetic polymers were prepared using 2-methoxyethanol, which indicates they have similar polymeric matrices.

The absorption peaks at 1455-1470 cm^{-1} and 1350-1493 cm^{-1} may be assigned to C=N groups of salicylaldoxime in magnetic IIP and NIP. There was an observable change in C=N stretching frequency to higher region in the leached magnetic polymer and this proved the successful removal of uranyl ion from the magnetic polymer. Singh and Mishra (2009) synthesized similar polymers selective of uranyl though they were not magnetic. They also found similar frequency bands at 1456-1460 and 1359-1391 cm^{-1} for the IIP (leached and unleached) and the NIP.

Salicylaldoxime (SALO) was used as one of the functional monomers but it should be borne in mind that it was not chemically bound in the magnetic polymer matrix as it did not have a polymerizable double bond. It is instead trapped inside the magnetic polymer during the polymerization reaction. This is the case for both the bulk and the precipitation routes. Since SALO plays a role of binding the uranyl template directly, there was need to establish whether it will be still anchored even after leaching. The N=O stretching frequency observed at 1155-950 cm^{-1} showed that SALO was still trapped in the magnetic polymer matrix after even after leaching.

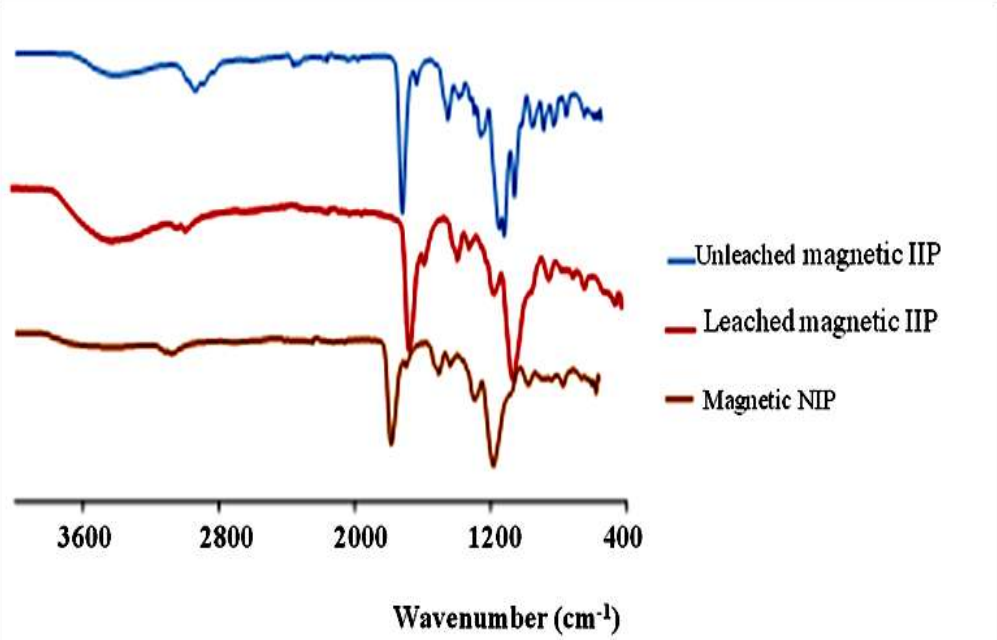


Figure 5.34: Fourier-transform infrared spectra for γ-MPS based polymers.

5.1.4.5 Thermo-gravimetric analysis (TGA)

Thermo-gravimetric analysis was employed to quantify the amount of Fe_3O_4 encapsulated in the magnetic particles (Zhan *et al.*, 2011). The analysis was carried out in an oxygen free environment to prevent the oxidation of the Fe_3O_4. Thermo-gravimetric analysis was also used for further structural elucidation of the γ-MPS-Fe_3O_4.

The TGA spectra in Figures 5.35, 5.36 and 5.37 showed that the magnetite was stable under heating throughout the temperature range of 0-1000^{o}C. From the first derivative in Figure 5.38, it was noted that the decomposition temperature at 305^{o}C was the temperature considered to be the decomposition of the coating agent γ-MPS. The temperature of maximal decomposition was 393°C.

From Figure 5.35, it was also observed that after the analysis, at 1000^{o}C, the residual weight of the γ-MPS-Fe_3O_4 was 69.17%. This meant that the other 30.83% was from the decomposed organic surface coating agent, γ-MPS. It was also noted that the leaching of the bulk and precipitate magnetic polymers reduced the residual weight significantly. This can be explained by the fact that the

leaching of the uranyl resulted in the washing of away of the magnetic core as well, Figures 5.36 and 5.37.

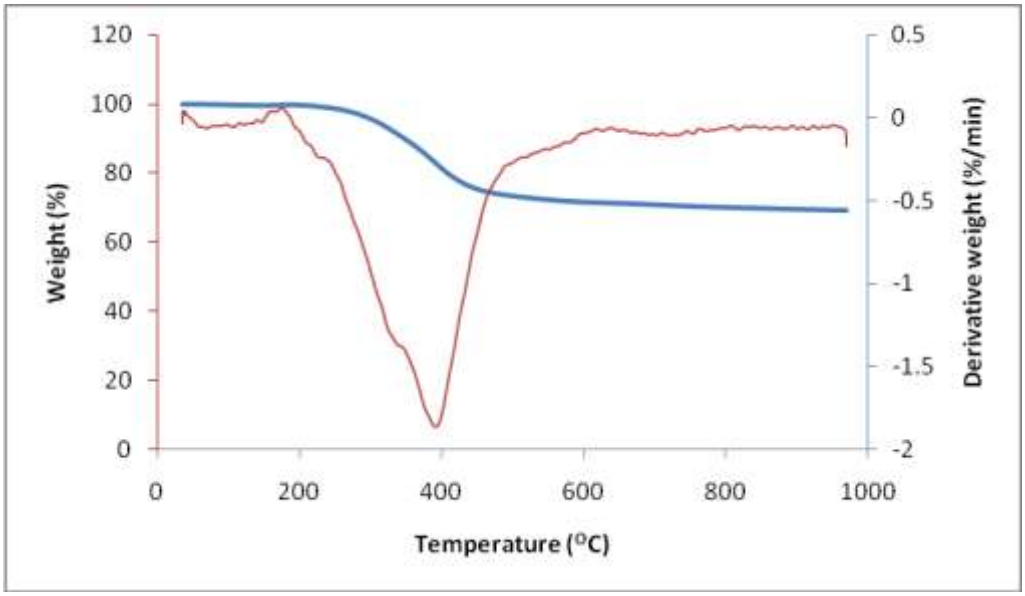


Figure 5.35: Thermo-gravimetric analysis results for γ-MPS-Fe_3O_4.

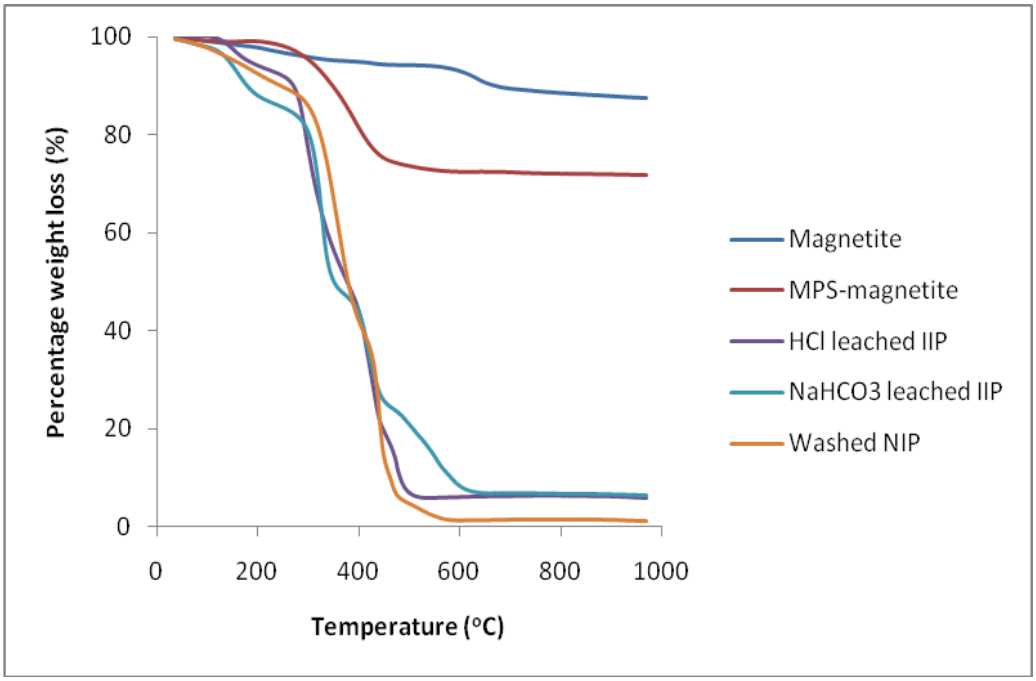


Figure 5.36: Thermo-gravimetric analysis of precipitation magnetic polymers.

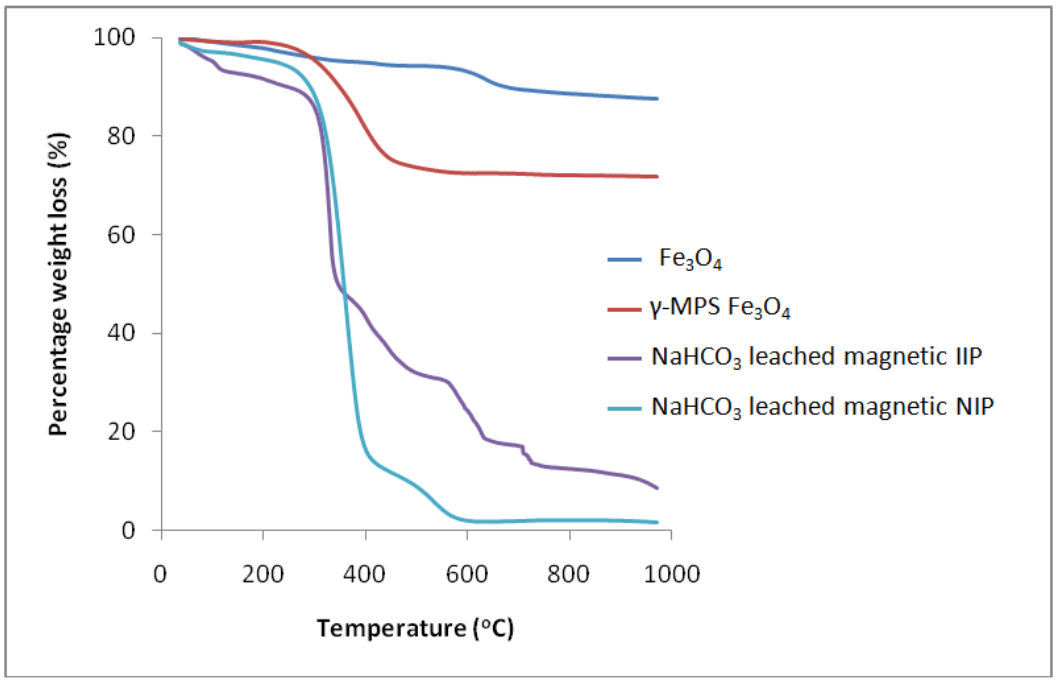


Figure 5.37: Thermo-gravimetric analysis of bulk magnetic polymers.

At temperatures above 600°C, there was a complete decomposition of γ-MPS from the metallic oxide core, Fe_3O_4. The small initial weight loss of magnetite around 100°C was likely due to the loss of physically adsorbed water on the magnetite as well as dehydroxylation of the internal hydroxyl groups.

5.1.4. Magnetic response

The magnetic response of the Fe_3O_4, functionalized Fe_3O_4, unleached and leached magnetic polymer showed an expected decreasing trend with the bare magnetite (Fe_3O_4) exhibiting the strongest response and the leached magnetic polymers the least. This is because the magnetic core is embedded inside the polymer matrix of the magnetic IIPs and NIPs. They are far inside the polymer implying that the magnetic force between it and the external magnet is diminished (magnetic force (F) is inversely proportional to the square of the distance (r^2)).

5.1.5 Optimization of parameters for U(VI) uptake

5.1.5.1 Effect of sample pH

The adsorption efficiencies of uranyl ions by magnetic polymers at various pH values are presented in Figures 5.39-5.42.

The general trend for all magnetic polymers was as expected, i.e., the magnetic IIPs had superior extraction efficiencies compared to their corresponding magnetic NIPs. Bearing in mind that the magnetic polymers are to be used in AMD there was a need to investigate the efficiency of these magnetic IIPs and NIPs in acidic conditions as well. The variation of the adsorption percentages with the pH is clearly noticeable as they are lower in acidic medium whereas at pH > 4, the adsorption of uranium reached the maximum.

This result is important as it indicates that the pH plays an influential role in the adsorption of uranium. Complex formation between 4-VP, SALO, MAA and uranyl ions present in a sample is pH dependent. The low uptake of uranium at low pH values may be due to the fact that there is a higher concentration of H^+ ions which are preferentially adsorbed ahead of uranium.

Another point about the low uptake of uranium at low pH is that the amine and the hydroxyl chelating groups in the polymer matrix are protonated. This protonation means that the lone pairs for coordination with the cationic uranyl will not be present for coordination. There will rather be electrostatic repulsion of the cationic uranyl from the adsorption sites in the magnetic polymer matrix. The optimum pH was taken to be 4 and was used in subsequent experiments.

In another study involving uranyl uptake, Wang *et al*. (2011) obtained an optimum pH of 3. However, they used a different adsorbent in the form of ethylenediamine-modified magnetic chitosan which also performed poorly at lower pH and this was also as a result of protonation of some functional groups within the adsorbent. Zhou *et al*. (2012) obtained an almost optimum pH (= 5) as that obtained in this work (= 4). However, they experienced a decrease in the

uranyl uptake after the optimum value and they attributed this to the formation of various oligomeric and monomeric hydrolyzed species of uranyl.

Figure 5.38 shows that the atoms responsible for the coordination with the uranyl cation are the nitrogens on 4-vinyl pyridine and salicylaldoxime as well as the oxygen on salicylaldoxime. Both these atoms have lone pairs of electrons which are responsible for the coordinate bonding.

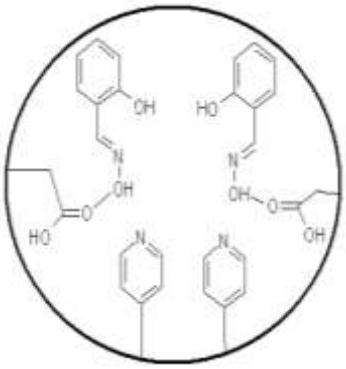


Figure 5.38: Uranium imprinted polymer showing heteroatoms responsible for the uptake of uranyl ions.

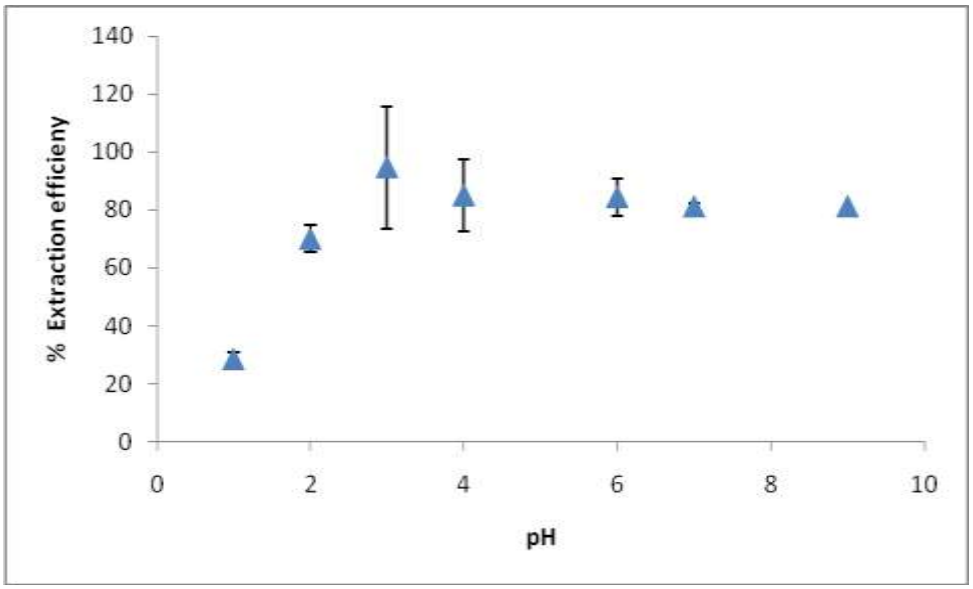


Figure 5.39: Effect of sample pH for OA IIP bulk $NaHCO_3$ leached. Experimental conditions: Amount of magnetic polymer, 20 mg; sample volume, 25 mL; uranium concentration, 2 mg L^{-1}; contact time, 45 minutes; stirring speed, 1500 rpm; temperature, room temperature.

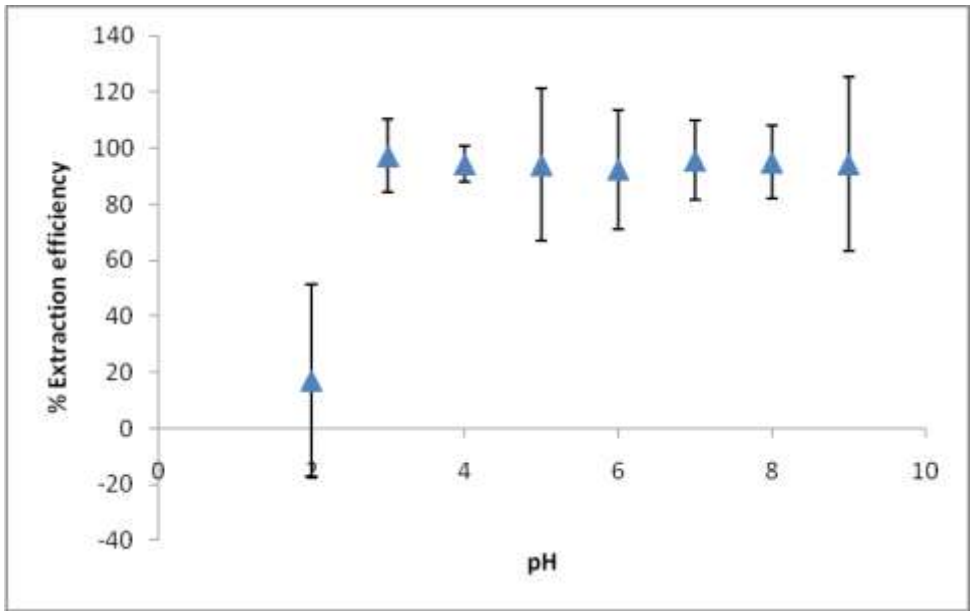


Figure 5.40: Effect of sample pH for OA NIP bulk $NaHCO_3$ leached (Experimental conditions: Same as those in Figure 5.39).

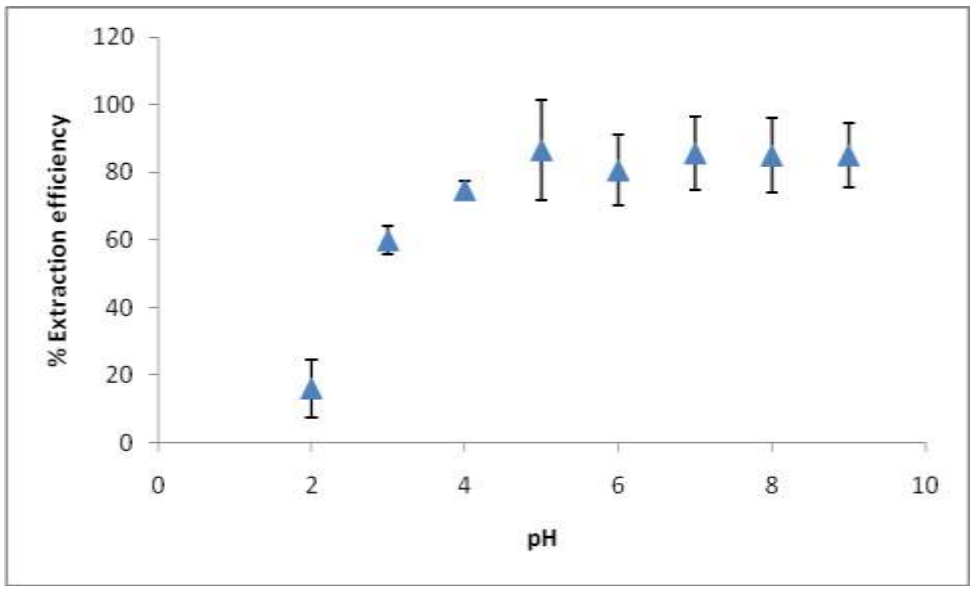


Figure 5.41: Effect of sample pH for γ-MPS IIP precipitate $NaHCO_3$ leached (Experimental conditions: Same as those in Figure 5.39).

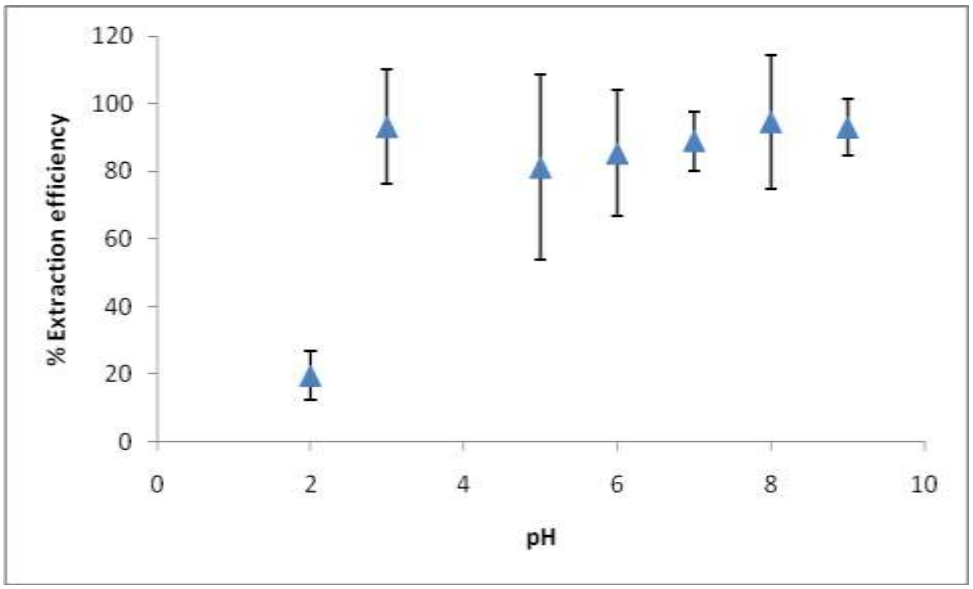


Figure 5.42: Effect of sample pH for γ-MPS IIP precipitate HCl leached (Experimental conditions: Same as those in Figure 5.39).

5.1.5.2 Effect of the amount of magnetic polymer

Figures 5.43-4.47, illustrate dependency of the amount of uranium adsorbed on the quantity of the adsorbent used. It was found that with the increasing dosage of the magnetic adsorbent, the amount of removal of uranium increased steadly to an almost constant value. For most magnetic polymers, the maximum uranium uptake was found when the mass of the magnetic polymer was about 50 mg which was then taken as the optimum doseage.

In the work of Ahmadi *et al*. (2010), a ternary complex of UO_2^{2+} with N,N-ethylenebis (pyridoxylideneiminato) and 4-vinylpyridine was synthesized and polymerized with styrene and divinylbenzene. They found that the changes in the extraction percentage in the range of 0.05-0.5 g were very small and they took 100 mg of polymer particles to be effective for enrichment. For imprinted polymer nanospheres for uranium which were prepared by complexing uranyl ion on to quinoline-8-ol functionalized 3-aminopropyltrimethoxysilane modified silica nanoparticles, the optimum amount of material required for the abstraction of uranium was found to be 20 mg (Milja *et al*., 2011). In another study, N,N`-bis (3-methoxylsalicylidene)-1,2-phenylenediamine on Fe_3O_4 by Zhang *et al*. (2012) showed that the adsorption capacity of uranium(VI) increased with the increase of

adsorbent dosage at m < 20 mg and then remains almost constant at m > 20 mg. Therefore, 20 mg was taken as the optimum mass of the adsorbent.

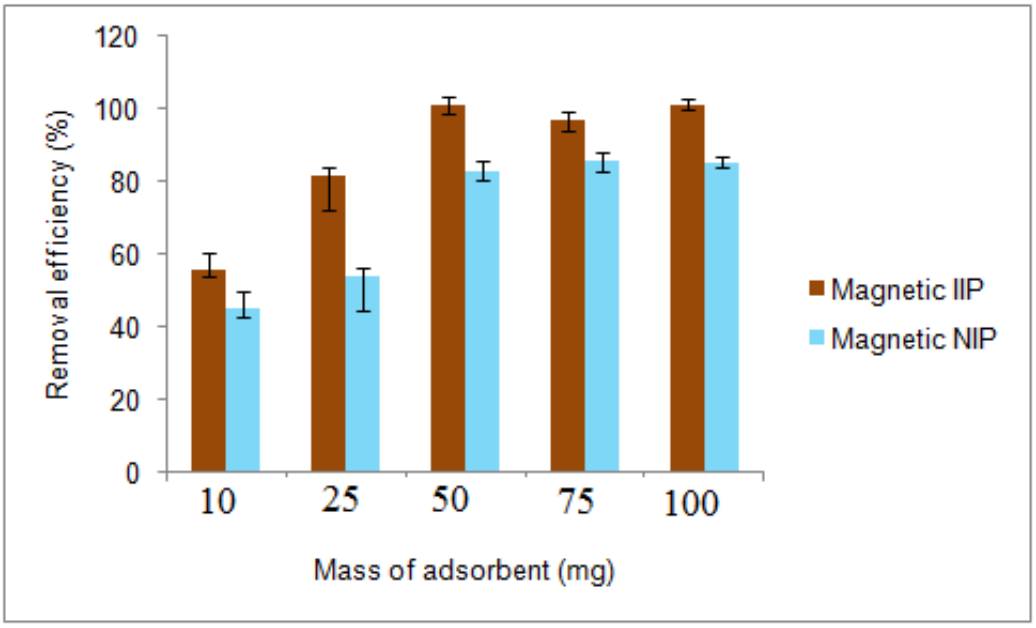


Figure 5.43: Adsorption efficiency obtained by varying the mass of (a) γ-MPS IIP ppt-HCl leached and (b) γ-MPS NIP ppt-HCl leached. Experimental conditions: Sample pH, 4; sample volume, 25 mL; uranium concentration, 2 mg L^{-1}; Contact time, 45 minutes; stirring speed, 1500 rpm; temperature, room temperature.

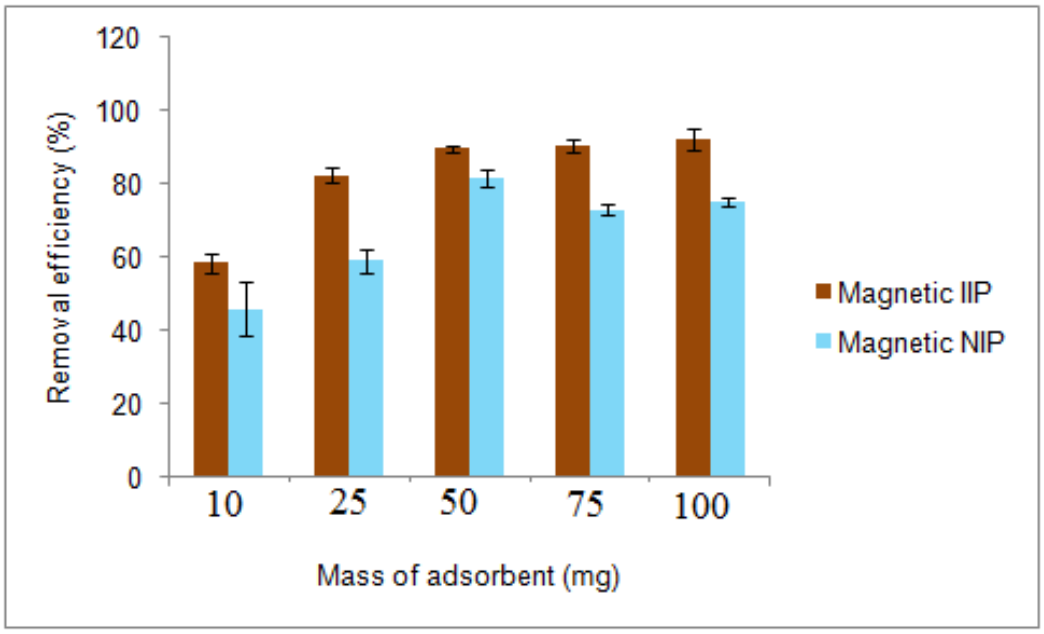


Figure 5.44: Adsorption efficiency obtained by varying the mass of (a) γ-MPS IIP bulk-$NaHCO_3$ leached and (b) γ-MPS NIP bulk-$NaHCO_3$ leached (Experimental conditions: Same as those in Figure 5.43).

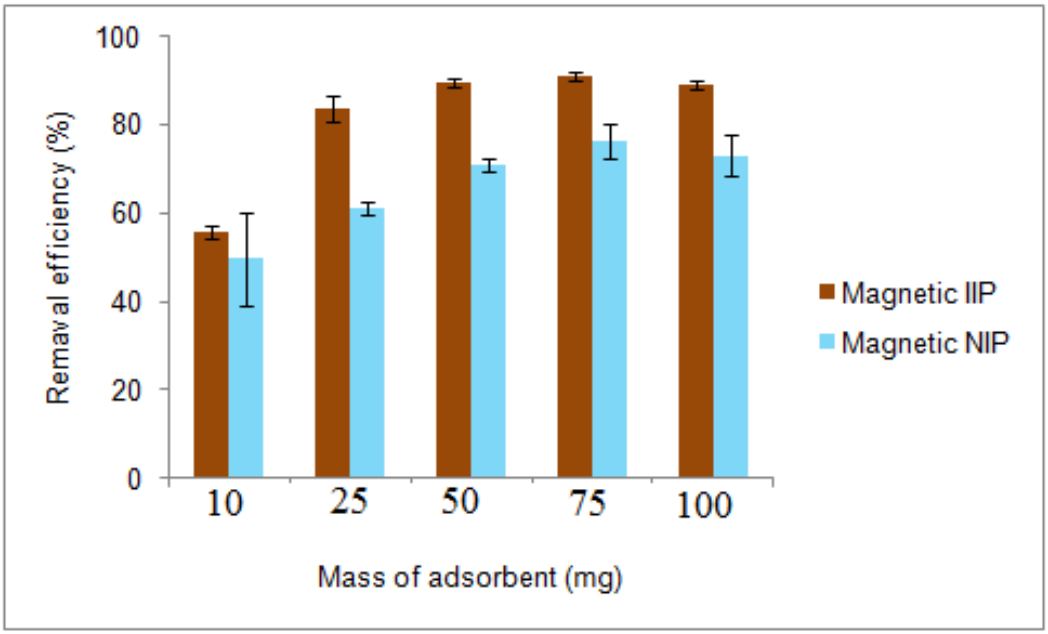


Figure 5.45: Adsorption efficiency obtained by varying the mass of (a) OA IIP bulk-$NaHCO_3$ leached and (b) OA NIP bulk-$NaHCO_3$ leached (Experimental conditions: Same as those in Figure 5.43).

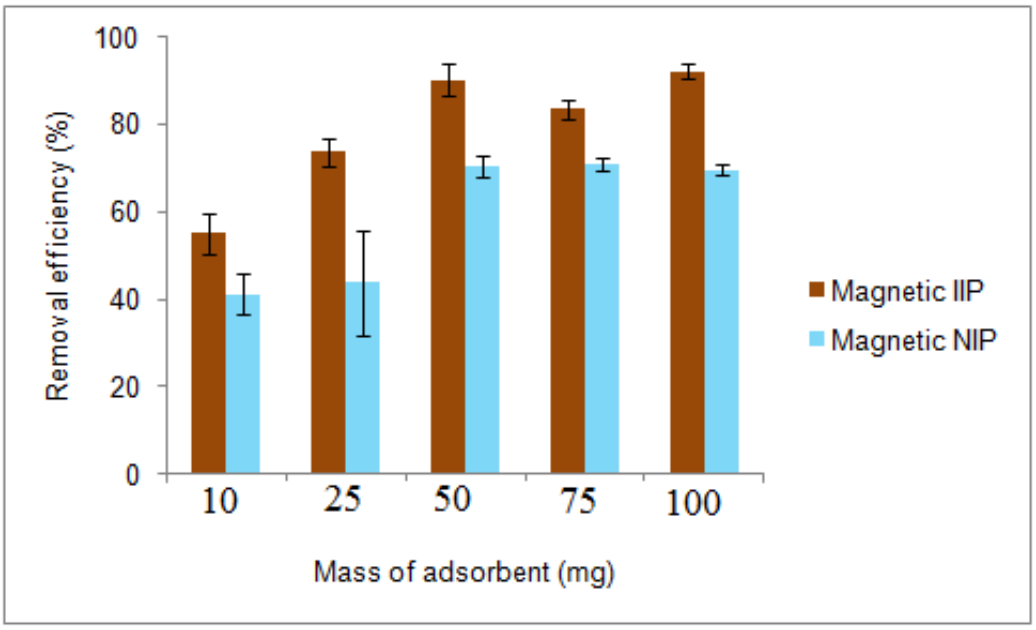


Figure 5.46: Adsorption efficiency obtained by varying the mass of (a) γ-MPS IIP ppt-$NaHCO_3$ leached and (b) γ-MPS NIP ppt-$NaHCO_3$ leached (Experimental conditions: Same as those in Figure 5.43).

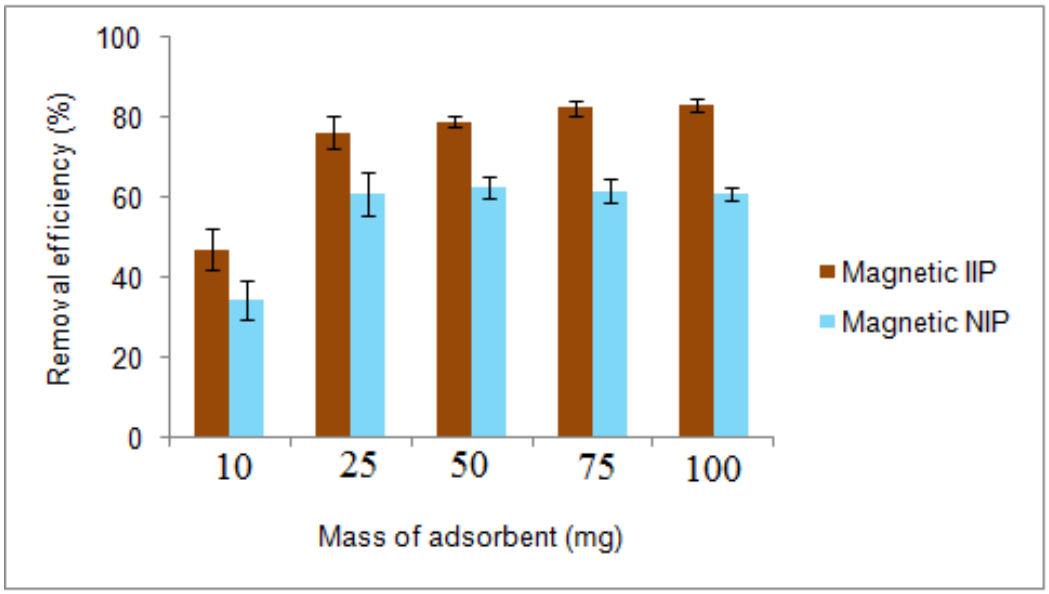


Figure 5.47: Adsorption efficiency obtained by varying the mass of (a) OA IIP ppt-$NaHCO_3$ leached and (b) OA NIP ppt-$NaHCO_3$ leached (Experimental conditions: Same as those in Figure 5.43).

5.1.5.3 Effect of contact time

The relationships between the amounts of uranium adsorbed and contact time for different magnetic polymers are shown in Figures 5.48-5.52. Under the used experimental conditions, it was observed that there was an increase in the amount of uranium adsorbed by all magnetic polymers from 0 to 45 minutes, after which equilibrium was reached. A contact time of 45 minutes was therefore selected as the optimum time as it was sufficient for the attainment of equilibrium. A further increase in time had no effect on the adsorption of uranium onto the magnetic polymers. As expected, the adsorption performances of the magnetic IIPs were all higher than of the corresponding magnetic NIPs.

Other studies for the selective uranyl uptake have demonstrated long abstraction times. For instance, from the prepared magnetic Schiff of N,N`-bis(3-methoxylsalicylidene)-1,2-phenylenediamine synthesized by Zhang *et al*. (2012), it was observed that the adsorption rate increased rapidly during the initial stages of the adsorption process. After that, uptake rate slowly declined with lapse of time and tends to reach equilibrium after 6 h. This was extremely slower than the prepared magnetic IIP in this study. On the other hand, some polymeric adsorbents which were faster in the uptake of uranium(VI) were prepared by Wang *et al*. (2011); Sadeghi and Aboobakri (2012); Fan *et al*. (2012) with the first two at 30 min and the last 16 min.

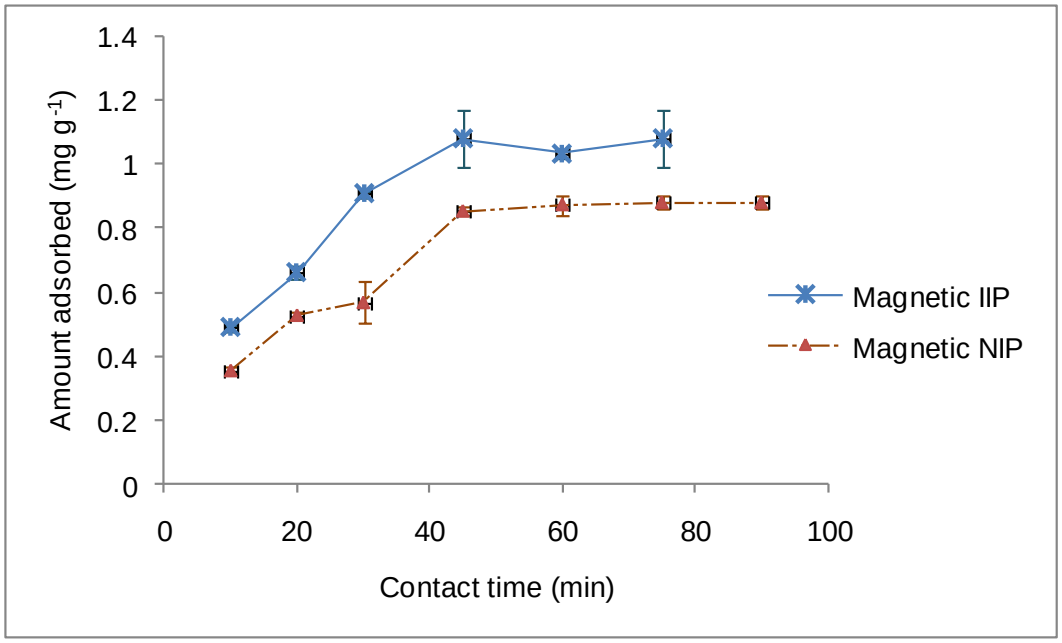


Figure 5.48: Effect of contact time on the uptake of uranium by (a) γ-MPS IIP ppt-HCl leached and (b) γ-MPS NIP ppt-HCl leached. Experimental conditions: Sample pH, 4; sample volume, 25 mL; uranium concentration, 2 mg L^{-1}; polymer weight, 50 mg; stirring speed, 1500 rpm; temperature, room temperature.

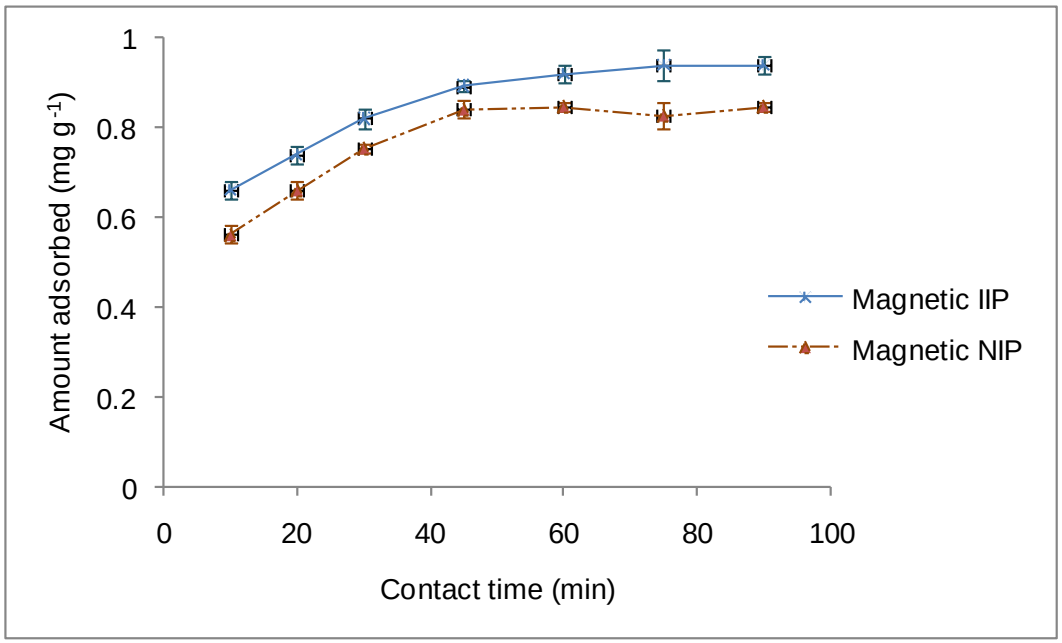


Figure 5.49: Effect of contact time on the uptake of uranium by (a) γ-MPS IIP bulk-$NaHCO_3$ leached and (b) γ-MPS NIP bulk-$NaHCO_3$ leached (Experimental conditions: Same as those in Figure 5.48).

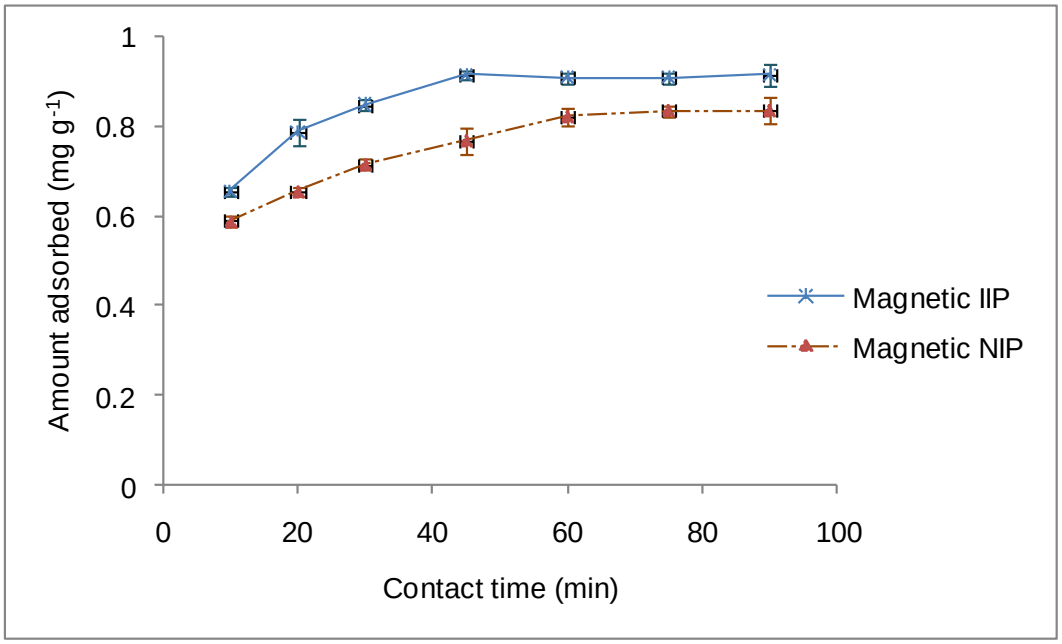


Figure 5.50: Effect of contact time on the uptake of uranium by (a) OA IIP bulk-$NaHCO_3$ leached and (b) OA NIP bulk-$NaHCO_3$ leached (Experimental conditions: Same as those in Figure 5.48).

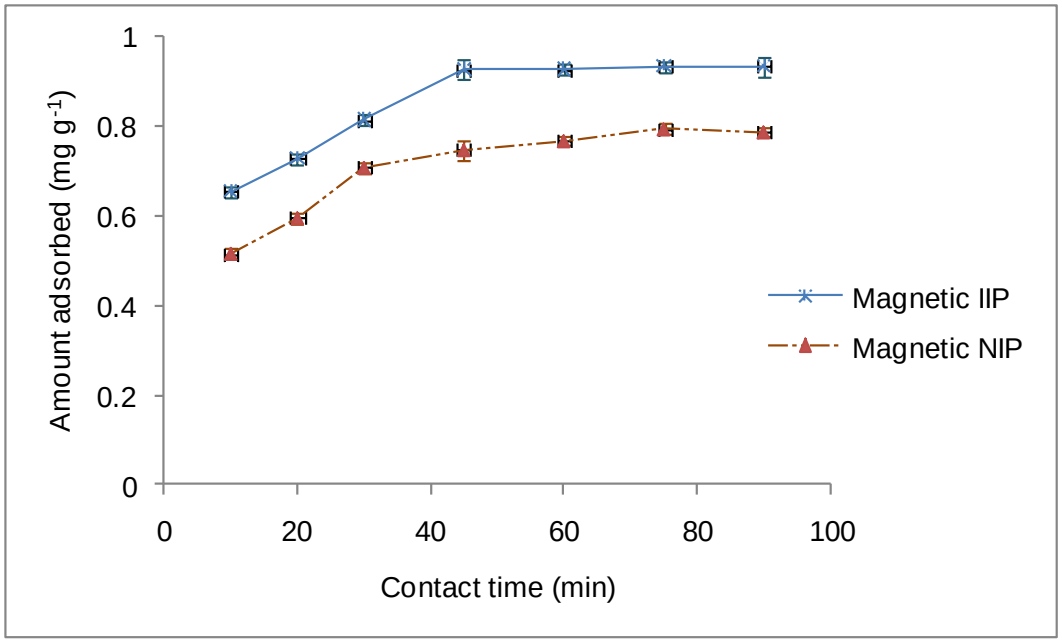


Figure 5.51: Effect of contact time on the uptake of uranium by (a) γ-MPS IIP ppt-$NaHCO_3$ leached and (b) γ-MPS NIP ppt-$NaHCO_3$ leached (Experimental conditions: Same as those in Figure 5.48).

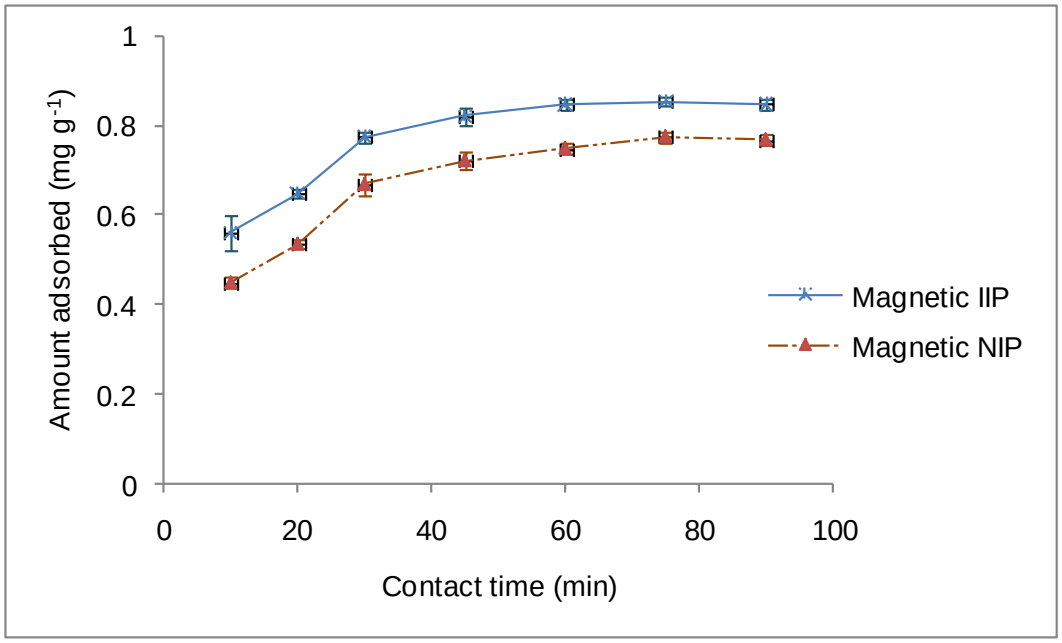


Figure 5.52: Effect of contact time on the uptake of uranium by (a) OA IIP ppt-$NaHCO_3$ leached and (b) OA NIP ppt-$NaHCO_3$ leached (Experimental conditions: Same as those in Figure 5.48).

5.1.5.4 Effect of initial uranium concentration

Figures 5.53-5.56 present the dependence of adsorption capacities of various initial uranium ion concentrations onto different magnetic polymers for fixed magnetic polymer dose, contact time and sample pH. A point to note is that all magnetic polymers showed similar trends. As the amount of uranium ions concentration increased so was the amount adsorbed. This can be attributed to the increasing number of U(VI) ions in solution that competed for a finite number of binding sites on the magnetic polymer surface. This equilibrium loading of uranyl ions per unit mass of the magnetic polymer increased almost linearly upon increasing the initial concentration of U(VI) ions in solution up to an adsorption capacity of between 0.8 and 1.2 mg g^{-1} for all polymers investigated. After reaching maximum adsorption, any further increase in the U(VI) concentration only saturated the binding sites, therefore there wasn`t any further increase in the amount of adsorbed U(VI) ions. In all cases, adsorption performance of magnetic IIPs was always higher than their corresponding magnetic NIPs.

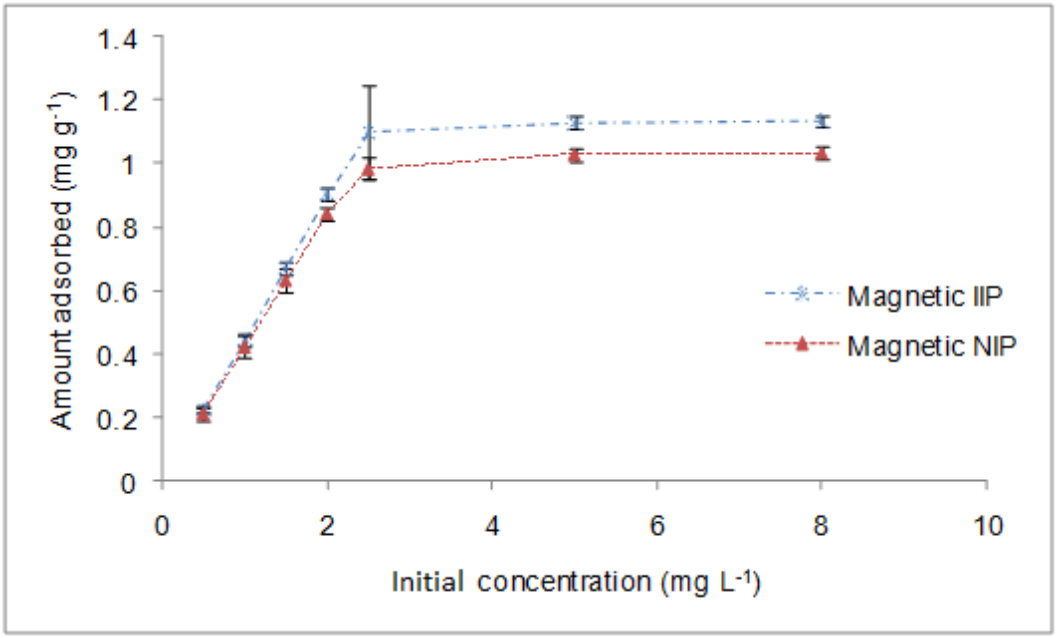


Figure 5.53: Effect of initial concentration on the uptake of uranium by (a) γ-MPS IIP bulk-$NaHCO_3$ leached and (b) γ-MPS NIP bulk-$NaHCO_3$ leached. Experimental conditions: Sample pH, 4; sample volume, 25 mL; polymer weight, 50 mg; stirring speed, 1500 rpm; temperature, room temperature.

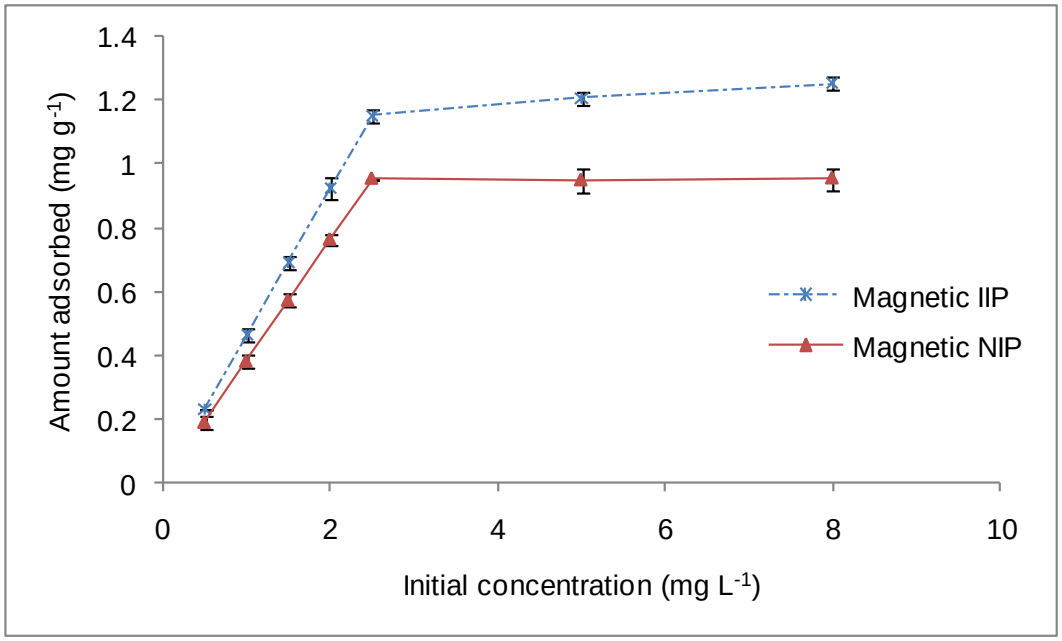


Figure 5.54: Effect of initial concentration on the uptake of uranium by (a) OA IIP bulk-$NaHCO_3$ leached and (b) OA NIP bulk-$NaHCO_3$ leached (Experimental conditions: Same as those in Figure 5.53).

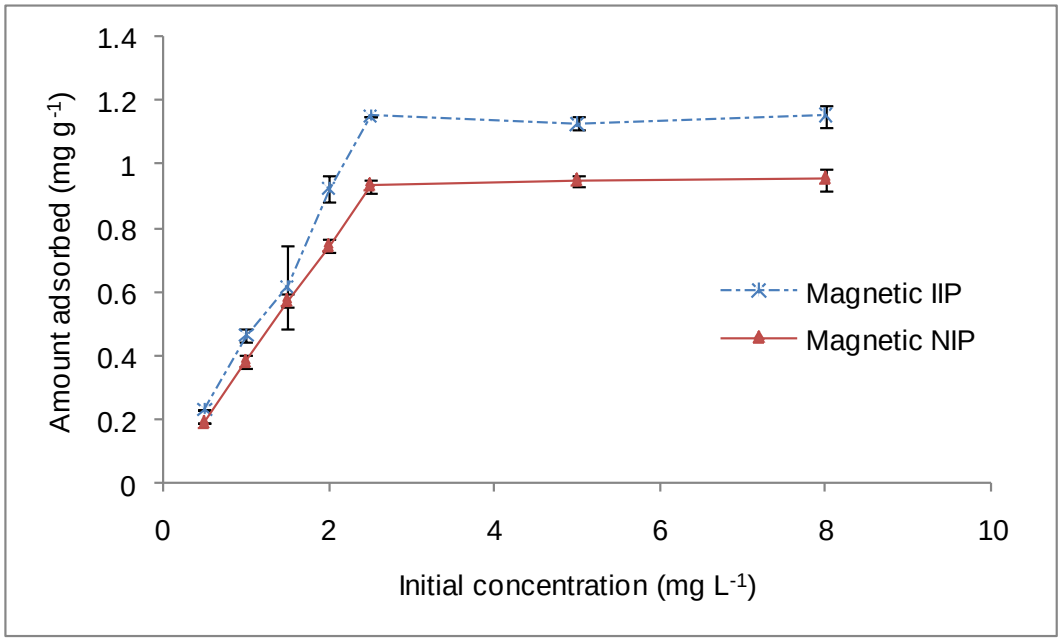


Figure 5.55: Effect of initial concentration on the uptake of uranium by (a) γ-MPS IIP ppt-$NaHCO_3$ leached and (b) γ-MPS NIP ppt-$NaHCO_3$ leached (Experimental conditions: Same as those in Figure 5.53).

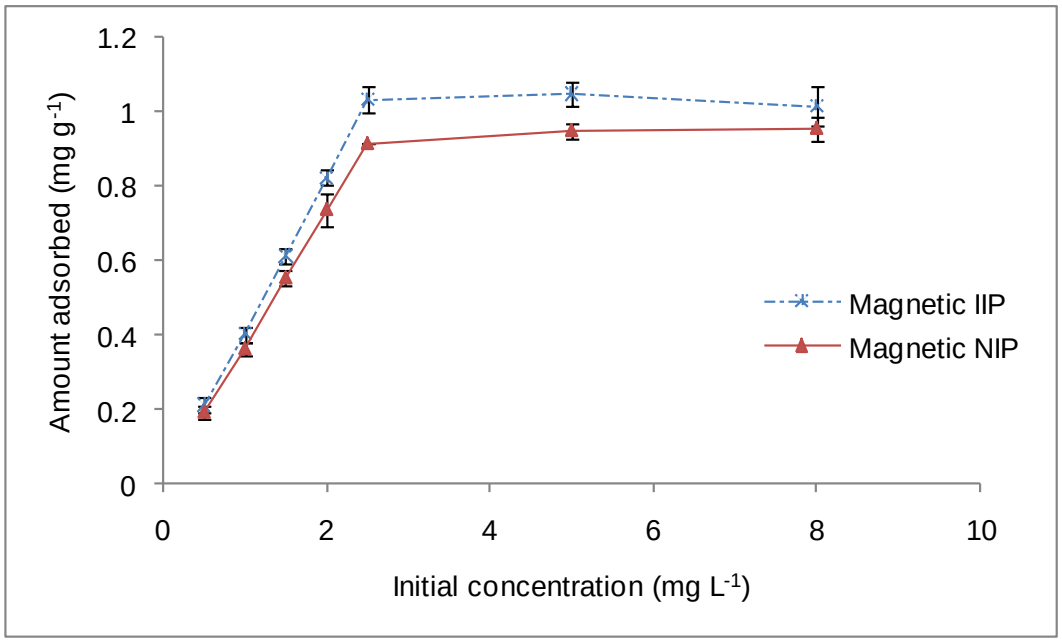


Figure 5.56: Effect of initial concentration on the uptake of uranium by (a) OA IIP ppt-$NaHCO_3$ leached and (b) OA NIP ppt-$NaHCO_3$ leached (Experimental conditions: Same as those in Figure 5.53).

5.1.5.5 Selectivity studies

Competing ions which have similar size to the uranyl ion and which are likely to coexist with uranium in environmental samples were chosen for selectivity studies and are shown in Table 5.6. Additionally, all but Fe(III) of the competing ions have the same charge as the uranyl ion.

Table 5.6: Physical properties of the uranyl ion together with those of its competitors.

Metal ion	Crystal radius (pm)	Hydrated radius (pm)	Hydration energy (kJ mol^{-1})
UO_2^{2+}	95	-	-
Pb^{2+}	132	401	1480
Mg^{2+}	72	300	1828
Ni^{2+}	69	600	2106
Fe^{3+}	63	-	-

Competitive adsorption of the binary mixtures UO_2^{2+}/Ni^{2+}, UO_2^{2+}/Fe^{3+}, UO_2^{2+}/Pb^{2+} and UO_2^{2+}/Mg^{2+} were investigated in an equilibrium-adsorption batch systems and the results are summarized in Figures 5.57-5.61. In these experiments, the concentration of the unadsorbed ions was determined by AAS. In these Figures, it is shown that the recovery of U(VI) was much higher than that of the competing ions (Ni^{2+}, Fe^{3+}, Pb^{2+} and Mg^{2+}), demonstrating that the cavities in the magnetic uranyl IIP had higher affinity for U(VI) because of imprinting.

Tables 5.7-5.11 summarize the distribution coefficient (K_d), the selectivity coefficient (K) and the relative selectivity coefficient (K`) values of the competing ions with respect to the target UO_2^{2+} ions.

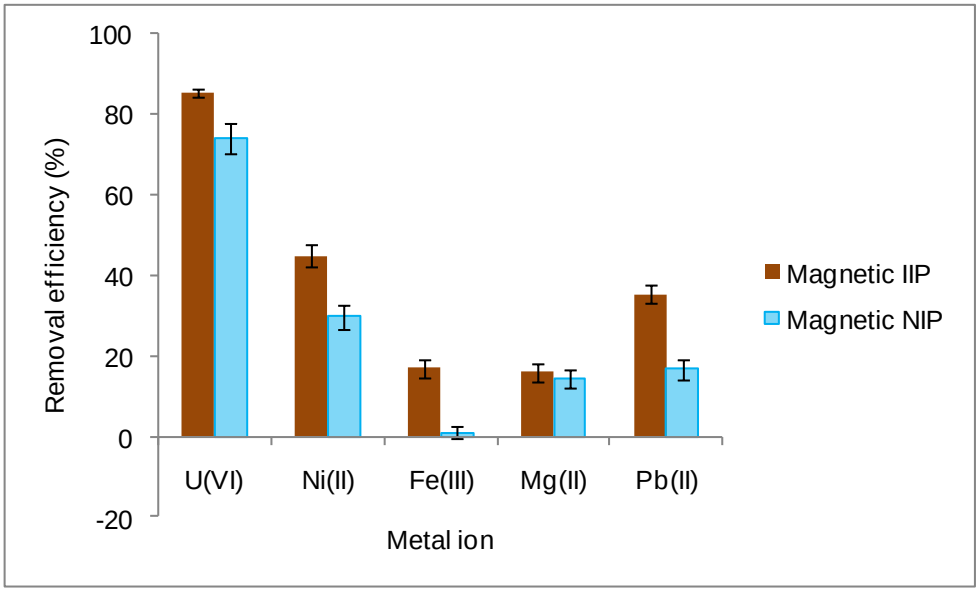


Figure 5.57: Extraction efficiencies of ions extracted by the magnetic IIP and NIP of γ-MPS bulk-$NaHCO_3$ leached from the spiked 2 mg L^{-1} binary mixtures of solutions.

Table 5.7: K_d, K and K` values for the magnetic IIP and NIP of γ-MPS bulk-$NaHCO_3$ in binary mixtures.

UO_2^{2+} cationic competitor	K_d (L g^{-1})				K		K`
	UO_2^{2+} IIP	UO_2^{2+} NIP	Magnetic IIP	Magnetic NIP	Magnetic IIP	Magnetic NIP	
Ni^{2+}	3.07	2.83	0.18	1.33	17.06	2.13	8.01
Fe^{3+}	2.85	2.78	5.95	0.41	0.48	6.78	0.07
Mg^{2+}	3.12	3.18	0.10	0.13	31.20	24.46	1.28
Pb^{2+}	2.93	3.03	0.33	1.17	8.88	2.59	3.43

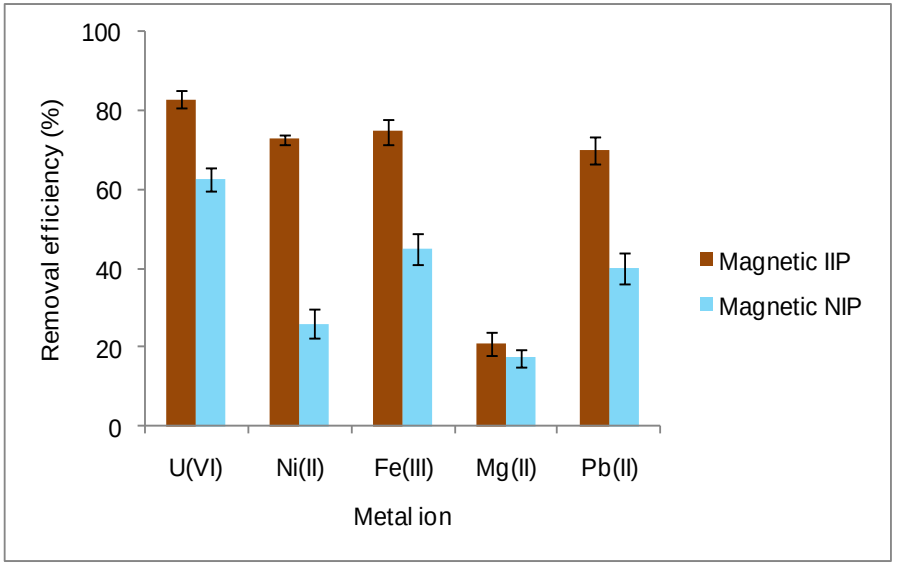


Figure 5.58: Extraction efficiencies of the ions extracted by the magnetic IIP and NIP of γ-MPS ppt-$NaHCO_3$ leached from the spiked 2 mg L^{-1} binary mixtures of solutions.

Table 5.8: K_d, K and K` values for the magnetic IIP and NIP of γ-MPS ppt- $NaHCO_3$ leached in binary mixtures.

UO_2^{2+} cationic competitor	K_d (L g^{-1})				K		K`
	UO_2^{2+} IIP	UO_2^{2+} NIP	Magnetic IIP	Magnetic NIP	Magnetic IIP	Magnetic NIP	
Ni^{2+}	2.03	0.85	0.12	0.61	16.92	1.39	12.17
Fe^{3+}	1.88	0.81	0.53	1.17	3.55	0.69	5.14
Mg^{2+}	1.79	0.89	0.19	0.50	9.42	1.78	5.29
Pb^{2+}	1.93	0.86	0.23	0.95	8.39	0.91	9.22

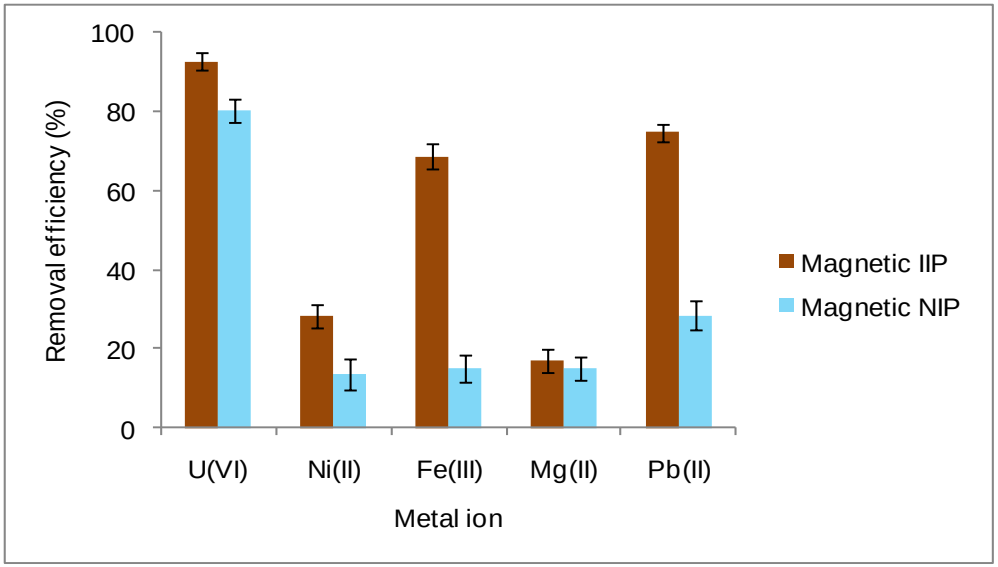


Figure 5.59: Extraction efficiencies of the ions extracted by the magnetic IIP and NIP of γ-MPS ppt-HCl leached from the spiked 2 mg L^{-1} binary mixtures of solutions.

Table 5.9: K_d, K and K` values for the magnetic IIP and NIP of γ-MPS ppt-HCl leached in binary mixtures.

UO_2^{2+} cationic competitor	K_d (L g^{-1})				K		K`
	UO_2^{2+} IIP	UO_2^{2+} NIP	Magnetic IIP	Magnetic NIP	Magnetic IIP	Magnetic NIP	
Ni^{2+}	6.64	1.42	0.21	0.41	31.62	6.76	4.68
Fe^{3+}	6.76	1.41	0.01	0.10	676.00	14.10	47.94
Mg^{2+}	6.19	1.53	0.08	0.09	77.38	17.00	4.55
Pb^{2+}	6.85	1.49	0.10	0.27	68.50	5.52	12.41

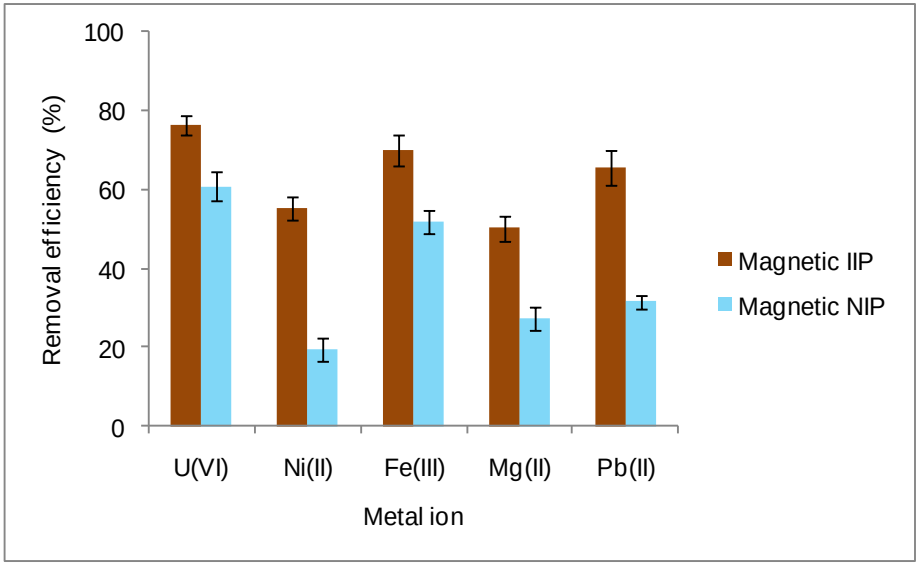


Figure 5.60: Extraction efficiencies of the ions extracted by the magnetic IIP and NIP of OA ppt-NaHCO3 leached from the spiked 2 mg L^{-1} binary mixtures of solutions.

Table 5.10: K_d, K and K` values for the magnetic IIP and NIP of OA ppt-$NaHCO_3$ leached in binary mixtures.

UO_2^{2+} cationic competitor	K_d (L g^{-1})				K		K`
	UO_2^{2+} IIP	UO_2^{2+} NIP	Magnetic IIP	Magnetic NIP	Magnetic IIP	Magnetic NIP	
Ni^{2+}	1.58	0.81	0.10	0.61	15.80	1.33	11.88
Fe^{3+}	1.63	0.75	0.58	1.08	2.81	0.69	4.07
Mg^{2+}	1.19	0.82	0.09	0.49	13.22	1.67	7.92
Pb^{2+}	1.84	0.63	0.41	0.84	4.49	0.75	5.99

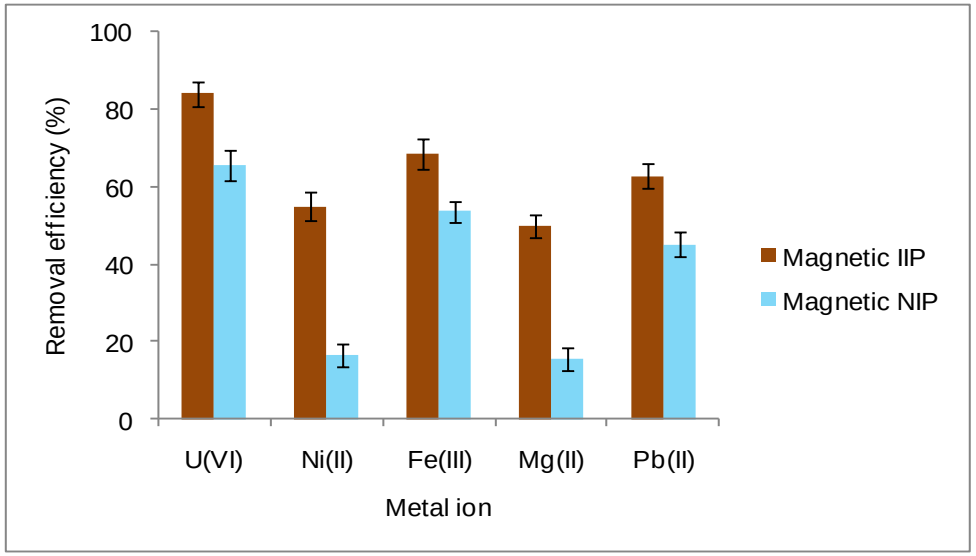


Figure 5.61: Extraction efficiencies of ions extracted by the magnetic IIP and NIP of OA bulk-$NaHCO_3$ leached from the spiked 2 mg L^{-1} binary mixtures of solutions.

Table 5.11: K_d, K and K` values for the magnetic IIP and NIP of OA bulk-$NaHCO_3$ leached in binary mixtures.

UO_2^{2+} cationic competitor	K_d (L g^{-1})				K		K`
	UO_2^{2+} IIP	UO_2^{2+} NIP	Magnetic IIP	Magnetic NIP	Magnetic IIP	Magnetic NIP	
Ni^{2+}	0.97	2.31	0.20	0.08	4.85	28.88	0.16
Fe^{3+}	1.01	2.28	1.09	0.09	0.93	25.33	0.04
Mg^{2+}	0.96	2.25	0.10	0.09	9.60	25.00	0.38
Pb^{2+}	0.96	2.24	1.48	0.20	0.65	11.20	0.06

Because Fe(III) has a smaller ionic radius of 63 pm, it had an ability to enter into the imprinting sites of the magnetic polymers freely, hence it showed highest K_d, K and K` values than its competing counterparts. It was interesting to note that although Mg(II) has a similar ionic charge and ionic radius, its adsorption performance in the imprint sites of the magnetic polymers was poor. This could probably arise from its arrangement in coordination geometry. K_d values are the ratios of how the concentration of a particular ion equilibrates between the imprinted polymer and the aqueous environment. It gives the extraction ability of a unit mass of the polymer for a particular ion in a unit volume of solution. As shown in Tables 5.7-5.11, the K_d values for all magnetic IIPs are higher for UO_2^{2+}, as compared to those of competing ions. Among the competing ions, Fe(III) had the highest K_d because it occupies sizeable fractions of the imprinting sites. It perfectly fitted the fabricated recognition sites to a far greater extent than other competing ions. Another observation from Tables 5.7-5.11 is that the selectivity coefficients of magnetic IIP were higher than those of magnetic NIPs. The functional monomers immobilized within the polymer matrix of the host magnetic IIPs had strict configurations suitable for the guest uranyl ions. Furthermore, the ionic recognition was also influenced by the nature of metal ion, its ionic radius and charge. In conclusion, for all synthesized magnetic polymers, it could generally be deduced that the relative order of magnitude of metal sorption followed the order: $UO_2^{2+} > Fe^{3+} > Pb^{2+} > Ni^{2+} > Mg^{2+}$. These results were in agreement from those of Pakade *et al*. (2012) who found the selectivity order $UO_2^{2+} > Fe^{3+} > Cu^{2+} > Co^{2+} > Mn^{2+} > Zn^{2+} > Ni^{2+}$. Their IIP was not magnetic though, but was just a ternary complex of a uranyl imprint with 1-(prop-2-en-1-yl)-4-(pyrid-2-yl) piperazine and methacrylic acid which they cross-linked. Closer to this work, Singh and Mishra (2009) observed an almost similar trend of selectivity with the order of $Th^{4+} > UO_2^{2+} > Fe^{3+} > Zn^{2+} > Co^{2+} > Cu^{2+} > Ni^{2+} > CrO_4^{2-} > Mn^{2+}$ as deduced from the distribution ratios reported.

5.1.5.6 Reusability of the magnetic uranyl imprinted polymers

The repeated use of the magnetic U(VI)-imprinted polymers is a key factor that determines the applicability of these adsorbents in decontamination of wastewaters. In order to show the reusability and regeneration of the magnetic U(VI)-imprinted polymers, sorption-desorption cycles were repeated 6 times by using the same adsorbents repeatedly. These sorption-desorption cycles of the five magnetic U(VI)-imprinted polymeric sorbents with their corresponding controls are shown in Figures 5.62-5.66. The results clearly demonstrated that the magnetic U(VI) imprinted beads can be used repeatedly without significant decrease in their adsorption capacities. Similar polymers, though not magnetic, showed good reusability and stability towards uranyl ion up to the tenth cycles of repeated experiments (Singh and Mishra, 2009). For Pakade *et al*. (2012), the stability of the polymers were observed up to the eigth cycle of reuse, maintaining a 99% recovery of the uranyl from aqueous solution.

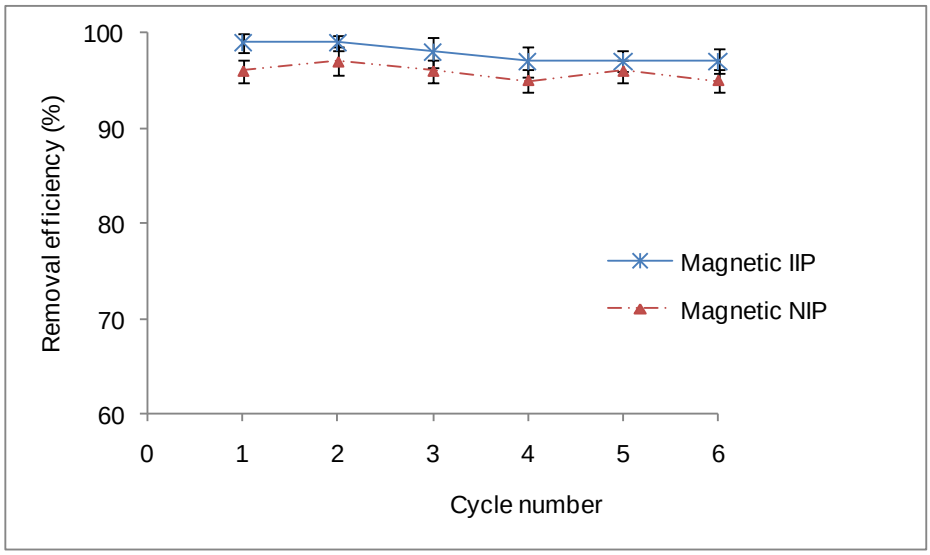


Figure 5.62: Reusability and stability of magnetic IIP and NIP of γ-MPS ppt-HCl leached. Adsorption conditions: Amount of materials, 50 mg; solution pH 4; solution volume, 25 mL; contact time, 45 min, U(VI) concentration, 2 mg L^{-1}, Desorption conditions: Solution volume, 25 mL; contact time, 45 min, [HCl] leachant, 1 M.

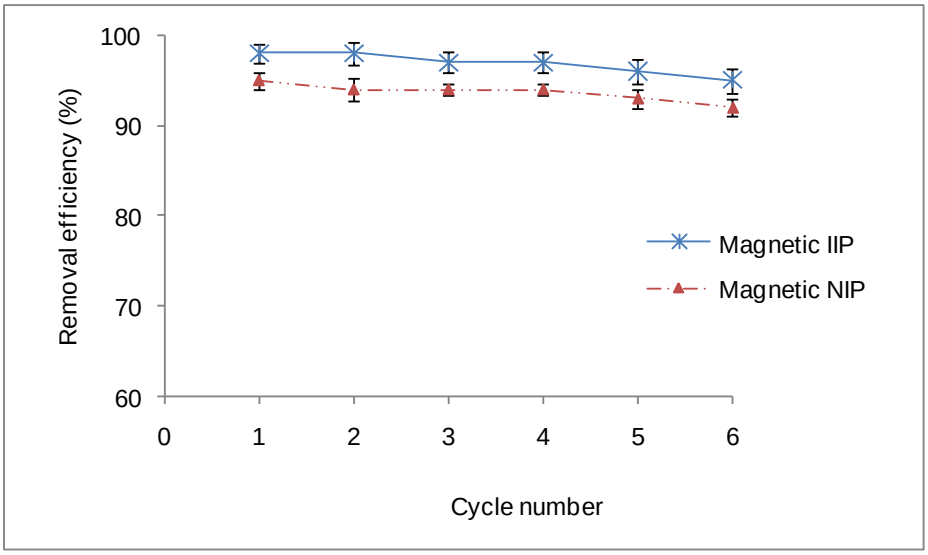


Figure 5.63: Reusability and stability of magnetic IIP and NIP of γ-MPS bulk-$NaHCO_3$ leached. Adsorption conditions: Amount of materials, 50 mg; solution pH 4; solution volume, 25 mL; contact time, 45 min, U(VI) concentration, 2 mg L^{-1}, Desorption conditions: Solution volume, 25 mL; contact time, 45 min, [HCl] leachant, 1 M.

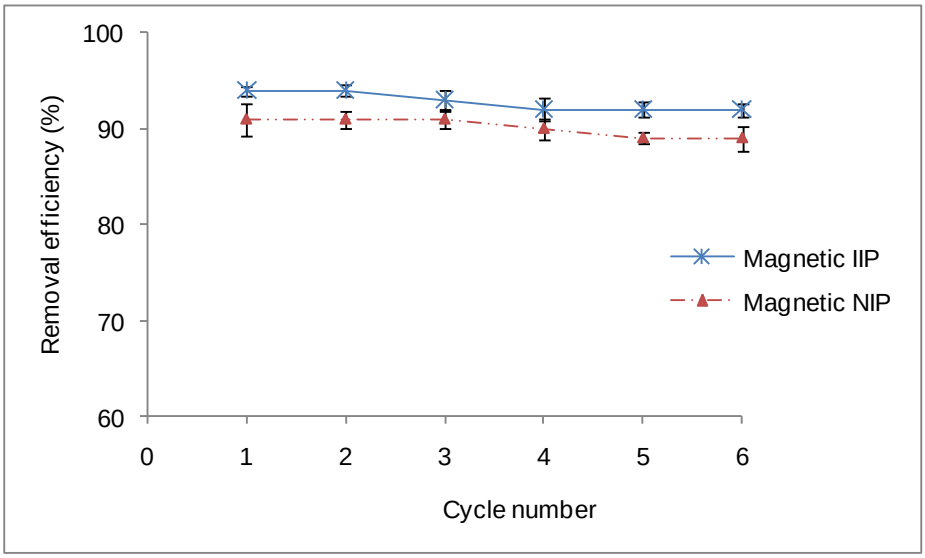


Figure 5.64: Reusability and stability magnetic IIP and NIP of OA bulk-$NaHCO_3$ leached. Adsorption conditions: Amount of materials, 50 mg; solution pH 4; solution volume, 25 mL; contact time, 45 min, U(VI) concentration, 2 mg L^{-1}, Desorption conditions: Solution volume, 25 mL; contact time, 45 min, [HCl] leachant, 1 M.

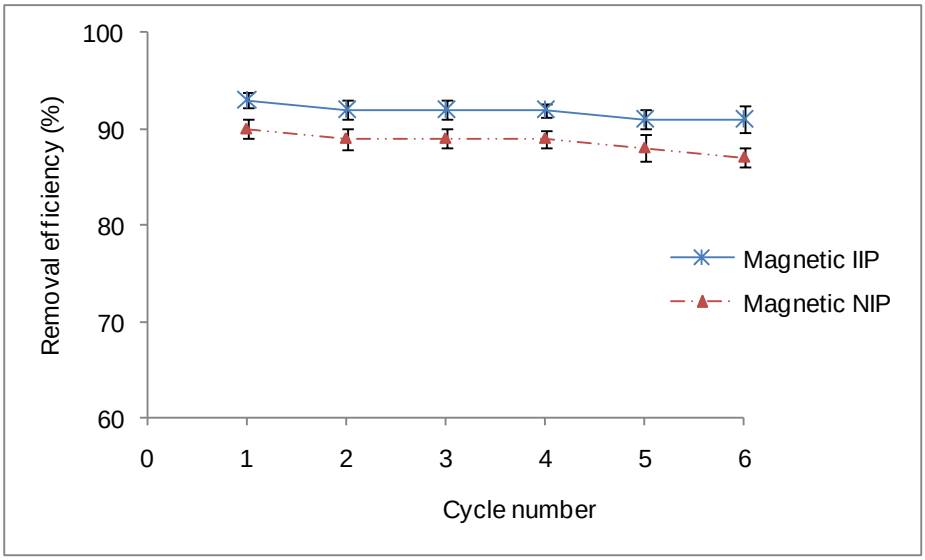


Figure 5.65: Reusability and stability magnetic IIP and NIP of γ-MPS ppt-$NaHCO_3$ leached. Adsorption conditions: Amount of materials, 50 mg; solution pH 4; solution volume, 25 mL; contact time, 45 min, U(VI) concentration, 2 mg L^{-1}, Desorption conditions: Solution volume, 25 mL; contact time, 45 min, [HCl] leachant, 1 M.

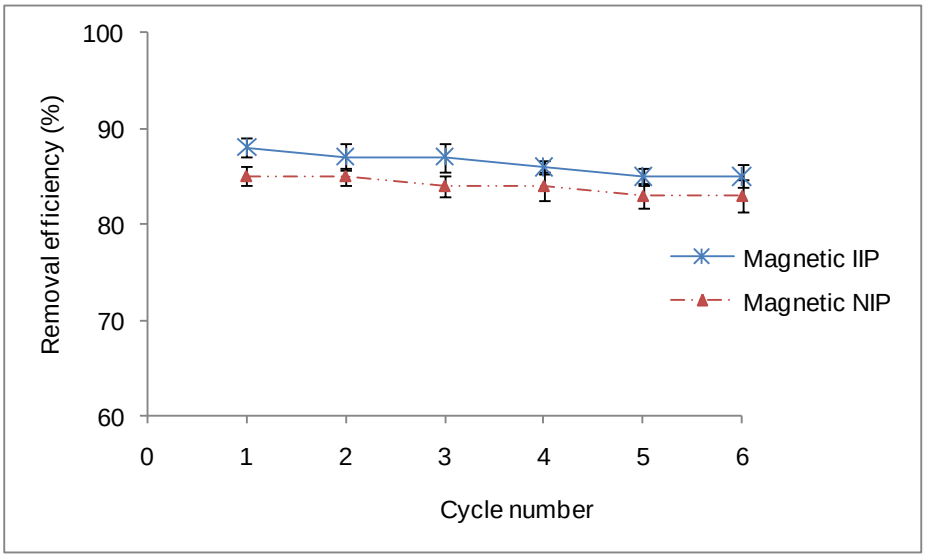


Figure 5.66: Reusability and stability magnetic IIP and NIP of OA ppt-$NaHCO_3$ leached. Adsorption conditions: Amount of materials, 50 mg; solution pH 4; solution volume, 25 mL; contact time, 45 min, U(VI) concentration, 2 mg L^{-1}, Desorption conditions: Solution volume, 25 mL; contact time, 45 min, [HCl] leachant, 1 M.

5.1.6 Kinetic modelling

Table 5.12 gives the calculated results of the pseudo first and second-order rate equations. When the two modelling approaches are compared, the pseudo-second-order model showed better correlation because of the high values of correlation coefficients ($R^2 > 0.97$) based on the linear regression.

Table 5.12: Summary of results of calculated kinetic parameters of pseudo-first order and pseudo-second order for U(VI) adsorption with an initial concentration of 5 mg L^{-1}.

	Pseudo first-order			Pseudo second-order		
Polymer*	R^2	k_1 (min^{-1})	q_e (mg g^{-1})	R^2	k_2 (g mg^{-1} min^{-1})	q_e (mg g^{-1})
1	0.982	0.052	1.005	0.9811	0.042	1.354
2	0.928	0.093	2.163	0.9721	0.039	1.142
3	0.915	-0.026	11.32	0.9940	0.157	1.012
4	0.602	0.048	3,035	0.9976	0.183	0.910
5	0.962	0.061	0.419	0.9992	0.261	0.961
6	0.928	0.056	0.542	0.9988	0.163	0.901
7	0.885	0.088	1.100	0.9979	0.163	1.008
8	0.986	0.054	0.478	0.9988	0.163	0.859
9	0.979	0.071	0.659	0.9982	0.163	0.923
10	0.991	0.057	0.612	0.9977	0.163	0.864

Polymer*: 1. γ-MPS IIP ppt-HCl leached, 2. γ-MPS NIP ppt-HCl leached, 3. γ-MPS IIP bulk-$NaHCO_3$ leached, 4. γ-MPS NIP bulk-$NaHCO_3$ leached, 5. OA IIP bulk-$NaHCO_3$ leached, 6. OA NIP bulk-$NaHCO_3$ leached, 7. γ-MPS IIP ppt- $NaHCO_3$ leached, 8. γ-MPS NIP ppt- $NaHCO_3$ leached, 9. OA IIP ppt- $NaHCO_3$ leached, 10. OA NIP ppt-$NaHCO_3$ leached.

The correlation coefficients values of all pseudo first orders were generally lower than those of the pseudo second orders` thereby showing bad quality of linearization. Again, the q_e values obtained (0.478-11.32 mg g^{-1}) from pseudo first orders differed greatly with the experimental values which means reaction cannot be safely be considered as pseudo first-order.

Generally, the pseudo second-order gave the best fits and it could therefore be used to predict the kinetics of adsorption of uranium onto the magnetic polymers. Riva *et al*. (2008) attached different functional groups to the backbone of synthetic polymers in order to improve the effectiveness of uranyl-binding properties. The polymers obtained after modifications were poly(N-(3-dimethyla mino) propylmethacrylamide), poly((3-dimethylamino) propylacrylate), poly(4-acryloylmorpholine-co-acrylic acid), poly(N-(3-dimethylamino) propylmethacryl amide-co-4-vinyl pyridine), poly((3-dimethylamino,) propylacrylate-co-acrylic acid) and poly(N-(3-dimethylamino) propylmethacrylamide-co-acrylic acid)which gave the adsorption capacities of 2.80, 2.85, 2.40, 3.25, 2.95 and 3.25 mg g^{-1}, respectively. As can be noted, these polymers are endowed with multi ligands and have expectedly higher adsorption capacities as compared to the polymer synthesized in this work.

5.1.7 Adsorption isotherm modelling

The profiles obtained from the study of the effect of initial uranium concentration, Figures 5.53-5.56, were used to obtain Langmuir and Freundlich adsorption isotherms.

5.1.7.1 Langmuir model

The Langmuir constant, *b*, can be used to determine the type of interaction between the adsorbate and adsorbent using the dimensionless separation factor, R_L. This factor is defined quantitatively by equation 5.1, (Hall *et al*., 1966):

$$R_L = \frac{1}{(1 + bC_0)} \qquad 5.1$$

where C_o is the initial metal concentration (mg L^{-1}) and *b* is the Langmuir constant (L g^{-1}). Based on the quantity of R_L values, the affinity of adsorption of the analyte of interest unto the adsorbent can be classified into categories shown in Table 5.13. The Langmuir constant, *b*, as well as q_m, can be deduced from the slopes and intercepts of the Langmuir plots.

Table 5.13: Types of adsorption with respect to Langmuir isotherms.

R_L	Adsorption type
$R_L = 0$	Irreversible
$0 < R_L < 1$	Favourable
$R_L = 1$	Linear
$R_L > 1$	Unfavourable

All R_L values obtained for U(VI) adsorption onto magnetic polymers (IIPs and NIPs) were in the range of 0.13-0.93 and are summarized in Table 5.14. These values showed that favourable adsorption occurred in all magnetic polymers used.

Table 5.14: The Langmuir constants and the R_L values for adsorption of U(VI) on magnetic polymers.

Magnetic polymer	b (L g^{-1})	q_m (mg g^{-1})	R_L	R^2
γ-MPS IIP bulk-$NaHCO_3$ leached	3.34	1.94	0.13	0.965
γ-MPS NIP bulk-$NaHCO_3$ leached	0.16	16.6	0.76	0.999
OA IIP bulk-$NaHCO_3$ leached	0.09	67.1	0.85	1.000
OA NIP bulk-$NaHCO_3$ leached	0.04	45.5	0.93	1.000
γ-MPS IIP ppt-$NaHCO_3$ leached	0.09	67.1	0.85	1.000
γ-MPS NIP ppt-$NaHCO_3$ leached	0.22	7.4	0.69	0.999
OA IIP ppt-$NaHCO_3$ leached	0.95	2.9	0.34	0.982
OA NIP ppt-$NaHCO_3$ leached	0.66	2.6	0.43	0.992

5.1.7.2 Freundlich model

The constants K_f and n are calculated from the intercept and slope of the Freundlich plots and are presented in Table 5.25. These values of K_f and n were found to be in the range of 1.0-6.0 and 1.0-1.3, respectively. According to Treyball (1980), the values of n between 1 and 10 are considered as good adsorbent and this implies that all magnetic polymers synthesized were effective in the uptake of uranium adsorption.

Table 5.15: Freundlich constants of different uranium magnetic polymers.

Magnetic polymer	n	K_f (L g^{-1})	R^2
γ-MPS IIP bulk-$NaHCO_3$ leached	1.21	3.09	0.966
γ-MPS NIP bulk-$NaHCO_3$ leached	1.05	2.39	0.996
OA IIP bulk-$NaHCO_3$ leached	1.00	5.77	1.000
OA NIP bulk-$NaHCO_3$ leached	1.00	1.59	1.000
γ-MPS IIP ppt-$NaHCO_3$ leached	1.00	5.77	1.000
γ-MPS NIP ppt-$NaHCO_3$ leached	1.07	1.43	0.997
OA IIP ppt-$NaHCO_3$ leached	1.07	2.07	0.980
OA NIP ppt-$NaHCO_3$ leached	1.11	1.24	0.993

5.1.8 Application of magnetic U(VI) IIPs to real water samples

Germiston water had a pH, oxidation reduction potential and conductivity of 2.6, 436 mV and 680 μScm^{-1}, respectively. The pH of the water sample which is very acidic and this was expected because of the effect of AMD. In the vicinity of the water source, there are disused mines (as can be seen in the background of Figure 4.3(a)), which were previously engaged in open cast and deep mining. These activities led to the exposure of the pyrite rock, FeS_2, to air and water which further led to the formation of H_2SO_4 which decanted into the water body where the samples were collected. A reduction oxidation potential of 436 mV shows oxidative conditions implying that most metals in the AMD water are subjected to oxidative environments. A high conductivity value of 680 $\mu S\ cm^{-1}$ indicates that most metals which constituted the sample, some of which are shown in Table 5.16, were in their ionic form. This resulted from the action of the highly acidic water which leached out metallic ions as it flowed down to water bodies. When the method was applied to real water samples, extraction efficiencies of over 81% and 64% were obtained for the magnetic IIP and NIP, respectively, Table 5.17-5.21. This was a demonstration of the suitability of the magnetic sorbent to selectively remove uranium from complex aqueous matrix. The method proved to be suitable for quantitative removal of uranium in wastewaters.

Table 5.16: Metal composition in real water samples.

Metal	Al	As	Au	Ca	Cd	Co	Cr	Cu	Fe	Hg	Mg	Mn	Ni	Pb	U	Zn
AMD (mg L^{-1})	648	0.030	0.273	0.123	0.097	22.95	0.836	11.25	1.800	0.675	541	72.05	48.30	0.428	8.500	54.75
SD	0.014	0.004	0.005	0.054	0.003	0.003	0.027	0.002	0.001	0.032	0.016	0.005	0.004	0.049	0.015	0.004
WWTP (mg L^{-1})	0.104	0.011	0.007	23.88	-	0.044	-	0.029	-	0.030	11.85	0.165	0.108	-	-	0.023
SD	0.012	0.001	0.001	0.003	-	0.001	-	0.001	-	0.005	0.001	0.001	0.001	-	-	0.002

Table 5.17: Application of magnetic γ-MPS IIP bulk-$NaHCO_3$ leached and the corresponding NIP on unspiked and spiked real water samples. Sample pH = 4; solution volume = 25 mL; sorbent mass = 20 and 65 mg for the magnetic IIP and NIP, respectively.

Sample	Uranium concentration (mg L^{-1})			% Recovery	
	Spiked	Determined		Magnetic IIP	Magnetic NIP
		Magnetic IIP	Magnetic NIP		
AMD	-	8.50 (0.02)	8.50 (0.02)	-	-
	5.00	13.23 (0.01)	11.34 (0.03)	78	67
	10.0	17.58 (0.05)	15.17 (0.04)	76	66
WWTP	-	< DL	< DL	-	-
	1.00	0.97 0.08)	0.81 (0.02)	78	65
	5.00	4.75 (0.05)	4.20 (0.01)	76	67
	10.0	9.80 (0.03)	8.30 (0.07)	78	66

< DL : Below detection limit and SD values in parenthesis.

Table 5.18: Application of magnetic OA IIP bulk-$NaHCO_3$ leached and the corresponding NIP on unspiked and spiked real water samples. Sample pH = 4; solution volume = 25 mL; sorbent mass = 20 and 65 mg for the magnetic IIP and NIP, respectively.

Sample	Uranium concentration (mg L^{-1})			% Recovery	
	Spiked	Determined		Magnetic IIP	Magnetic NIP
		Magnetic IIP	Magnetic NIP		
AMD	-	8.50 (0.02)	8.50 (0.02)	-	-
	5.00	12.29 (0.03)	10.87 (0.06)	73	63
	10.0	17.21 (0.07)	14.99 (0.08)	74	65
WWTP	-	< DL	< DL	-	-
	1.00	0.92 (0.03)	0.77 (0.02)	74	62
	5.00	4.50 0.06)	3.80 (0.07)	72	61
	10.0	9.30 (0.02)	7.80 (0.01)	74	64

< DL: Below detection limit and SD values in parenthesis.

Table 5.19: Application of magnetic γ-MPS IIP ppt-$NaHCO_3$ leached and the corresponding NIP on unspiked and spiked real water samples. Sample pH = 4; solution volume = 25 mL; sorbent mass = 20 and 65 mg for the magnetic IIP and NIP, respectively.

Sample	Uranium concentration (mg L^{-1})			% Recovery	
	Spiked	Determined		Magnetic IIP	Magnetic NIP
		Magnetic IIP	Magnetic NIP		
AMD	-	8.50 (0.02)	8.50 (0.02)	-	-
	5.00	12.15 (0.08)	9.59 (0.07)	72	57
	10.0	16.47 (0.06)	13.32 (0.03)	71	57
WWTP	-	< DL	< DL	-	-
	1.00	0.88 (0.04)	0.72 (0.02)	70	56
	5.00	4.45 (0.06)	3.75 (0.02)	71	60
	10.0	9.10 (0.02)	7.60 (0.02)	73	61

< DL: Below detection limit and SD values in parenthesis.

Table 5.20: Application of magnetic OA IIP bulk-$NaHCO_3$ leached and the corresponding NIP on unspiked and spiked real water samples. Sample pH = 4; solution volume = 25 mL; sorbent mass = 20 and 65 mg for the magnetic IIP and NIP, respectively.

Sample	Uranium concentration (mg L^{-1})			% Recovery	
	Spiked	Determined		Magnetic IIP	Magnetic NIP
		Magnetic IIP	Magnetic NIP		
AMD	-	8.50 (0.02)	8.50 (0.02)	-	-
	5.00	11.75 (0.04)	9.18 (0.05)	70	54
	10.0	15.73 (0.04)	12.40 (0.03)	68	54
WWTP	-	< DL	< DL	-	-
	1.00	0.87 (0.05)	0.66 (0.04)	70	53
	5.00	4.30 (0.07)	3.40 (0.06)	69	54
	10.0	8.70 (0.03)	6.80 (0.02)	70	54

< DL: Below detection limit and SD values in parenthesis.

Table 5.21: Application of magnetic γ-MPS IIP ppt-$NaHCO_3$ leached and the corresponding NIP on unspiked and spiked real water samples. Sample pH = 4; solution volume = 25 mL; sorbent mass = 20 and 65 mg for the magnetic IIP and NIP, respectively.

Sample	Uranium concentration (mg L^{-1})			% Recovery	
	Spiked	Determined		Magnetic IIP	Magnetic NIP
		Magnetic IIP	Magnetic NIP		
AMD	-	8.50 (0.02)	8.50 (0.02)	-	-
	5.00	10.94 (0.03)	8.75 (0.07)	65	52
	10.0	15.36 (0.06)	11.47 (0.01)	66	50
WWTP	-	< DL	< DL	-	-
	1.00	0.82 (0.06)	0.63 (0.04)	66	50
	5.00	4.15 (0.01)	3.25 (0.02)	66	52
	10.0	8.10 (0.08)	6.40 (0.09)	65	51

< DL: Below detection limit and SD values in parenthesis.

5.2 Synthesis and characterization of magnetic Cr(VI) polymers

5.2.1 Synthesis of magnetic poly(4-vinylpyridine)

4-vinylpyridine was homopolymerized and copolymerized with functionalized magnetite as shown in the schemes in Figure 5.67. The expanded structure of the magnetic poly(4-vinylpyridine) is shown in Figure 5.68.

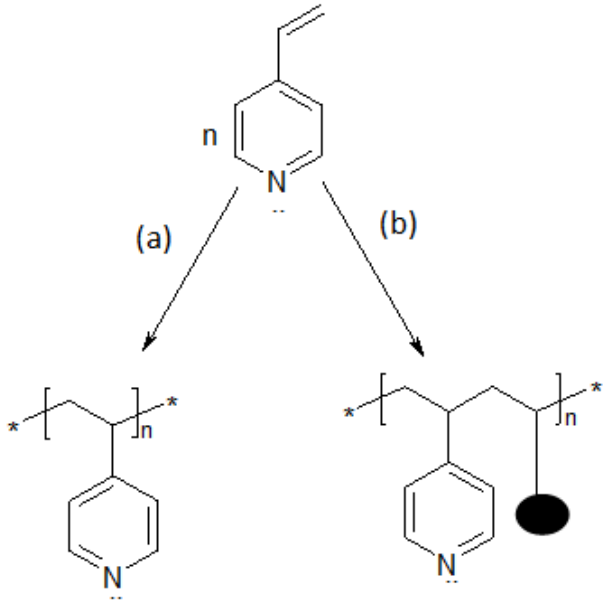


Figure 5.67: Synthetic routes of (a) homopolymer and (b) magnetic polymer of poly(4-vinylpyridine) where the blach dot indicates γ-MPS coated magnetite.

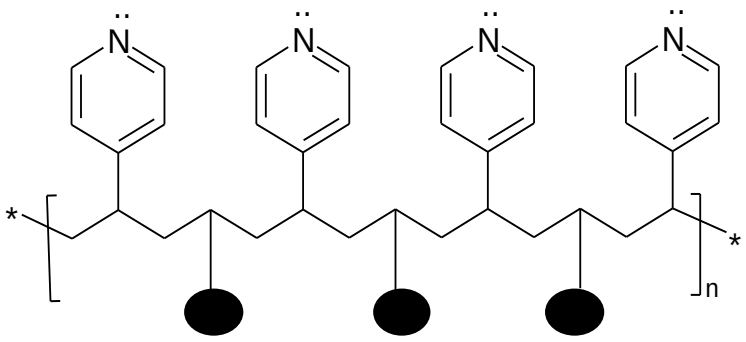


Figure 5.68: Structure of magnetic poly(4-vinylpyridine).

5.2.2 Quartenization of magnetic poly(4-vinylpyridine)

In order to remove metallic oxy-anions in aqueous environments, a positive charge has to be introduced by contacting poly(4-vinylpyridine) particles with acids such as hydrochloric acid (Barakat and Sahiner, 2008). However, in order to introduce a permanent positive charge in the polyelectrolyte, an alkyl group was chosen in this study. N-propyl reacted with the pyridine nitrogen to give quaternized magnetic poly(4-vinylpyridine). In order to have a high positive charge building up in the polymer, a solvent of high dielectric constant should be used (Masamoto *et al*., 1960). In this work, DMF was used as a solvent and the bromide ions formed diffused away from the pyridinium ions of the cationic polyelectrolyte. The proposed reaction of the n-propyl bromide with magnetic poly(4-vinylpyridine) is shown in Figure 5.69.

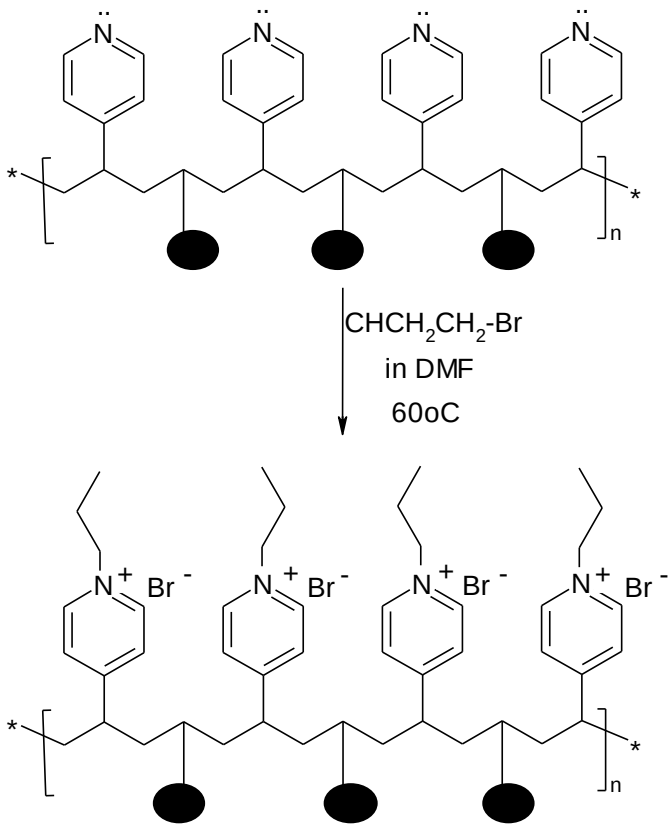


Figure 5.69: Reaction for the quartenization of magnetic poly(4-vinylpyridinium) bromide.

Due to the neighbouring group effect, quarternization of the poly(4-vinylpyridine) does not occur with quantitative conversions and typically, 65-70% quarternization are most common with most alkyl halides (Dautzenberg *et al*., 1994). However, in their research, Bicak and Gazi (2003) found out that methyl iodide is likely to give high quarternization yields of up to 95%.

Another reason of not achieving 100% quartenization was discussed by Sonmez and Bicak (2002). They pointed out that some small percentages of pyridine groups remain embedded deep in the polymer matrix and may remain unreacted. Hence the reaction to introduce a charge on the polyelectrolyte only represents quantitative quaternization of the pyridine rings in accessible positions of the cross-linked matrix.

5.2.2.1 Quartenization study using Fourier-transform infrared

Fourier-transform infrared analysis was carried out to estimate the degree of quarternization. During alkylation of magnetic and non-magnetic poly(4-vinylpyridine) with N-propyl bromide, aliquots of the solutions were withdrawn at 14 hrs intervals and purged with nitrogen to form a viscous solution. This was then FTIR analyzed to check the shift of the band at 1600 cm^{-1}.

In quartenization of magnetic and non-magnetic poly(4-vinylpyridine), a C=N band in pyridine, usually at 600 cm^{-1}, was displaced to higher wavenumbers to 1636 cm^{-1} and 1636 cm^{-1}, respectively, Figures 5.79 and 5.80. These results were consistent with those obtained by Li *et al*. (2005) who obtained a shifted value of 1 636 cm^{-1}.

This was also in agreement with reports of the quaternization reaction by the introduction of a positive charge to form a pyridinyl ring in the polymer structure (Landfester, 2001; Caruso *et al*., 2002). Additionally, the intensity of the band at about 1560 cm^{-1}, as shown in Figure 5.70 and 5.71, corresponds to positively charged nitrogen atoms.

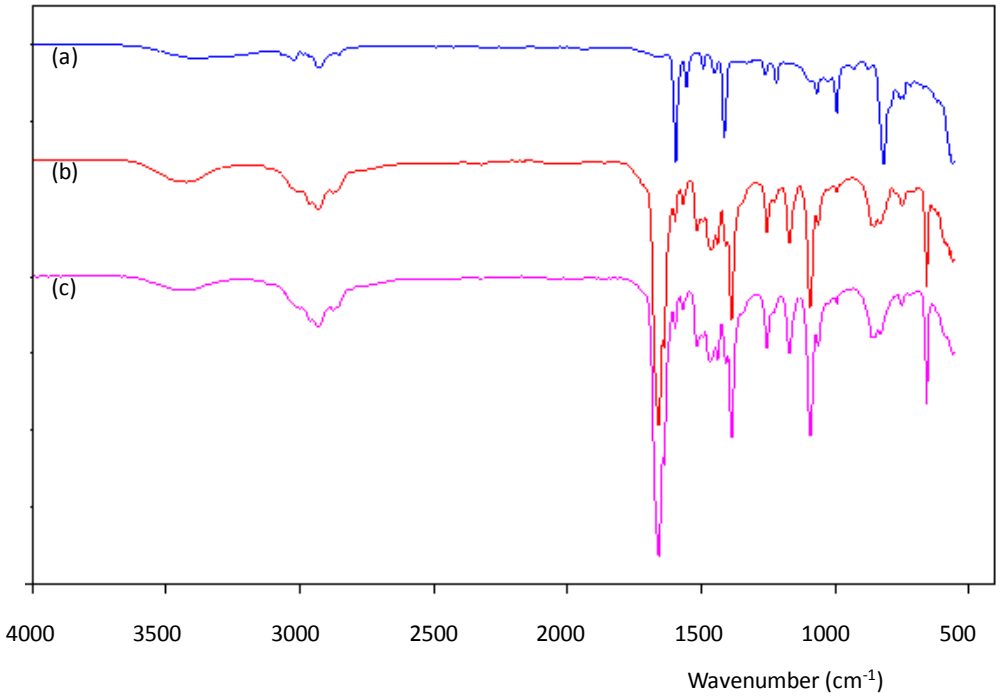


Figure 5.70: FTIR spectra of quartenized poly(4-vinylpyridine) after (a) 0 hrs, (b) 14 hrs and (c) 42 hrs.

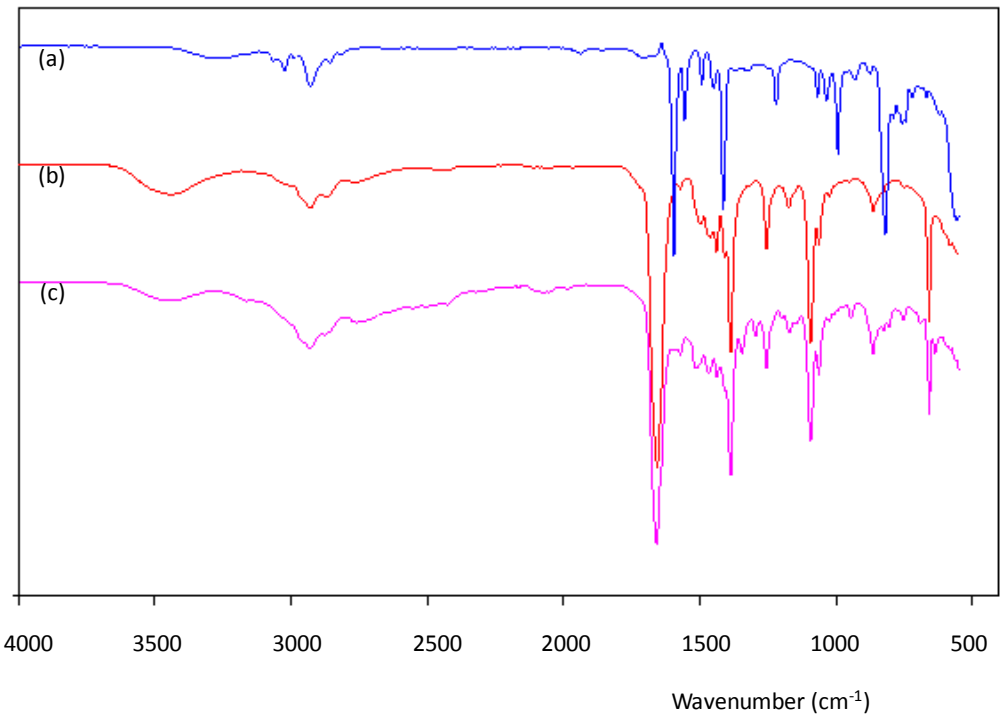


Figure 5.71: FTIR spectra of quartenized magnetic poly(4-vinylpyridine) after (a) 0 hrs, (b) 14 hrs and (c) 42 hrs.

5.2.3 Addition of the dichromate imprint to the magnetic poly(4 vinylpyridine)

The dichromate displaced the smaller bromide anion from the magnetic polymer backbone and that was the start of the formation of micro cavities that were specific for the dichromate ion. The addition of sodium dichromate to magnetic poly(4-vinylpyridinium) bromide is demonstrated in Figure 5.72.

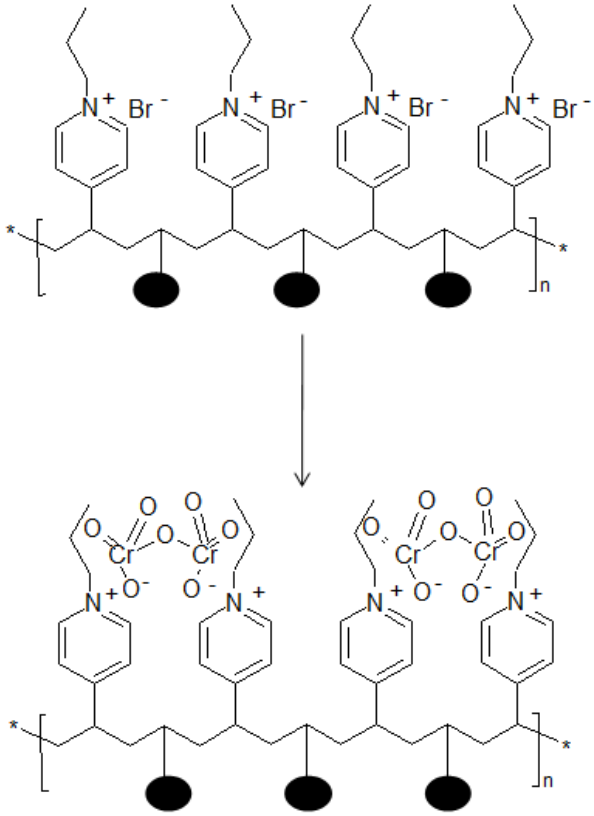


Figure 5.72: Substitution reaction of the bromide ions from magnetic poly(4-vinylpyridinium) bromide by dichromate ions.

5.2.3.1 Fourier-transform infrared (FTIR) analysis

Evidence of the embedment of dichromate into the magnetic polymer is shown by the resonance peak of the Cr-O and Cr=O bonds at 943 cm^{-1} in the spectra in Figures 5.73 and 5.74. In two separate studies by Arslan *et al*. (2006) and Ortiz-Palacios (2008), these resonance peaks were assigned to 943 and 934 cm^{-1}, respectively.

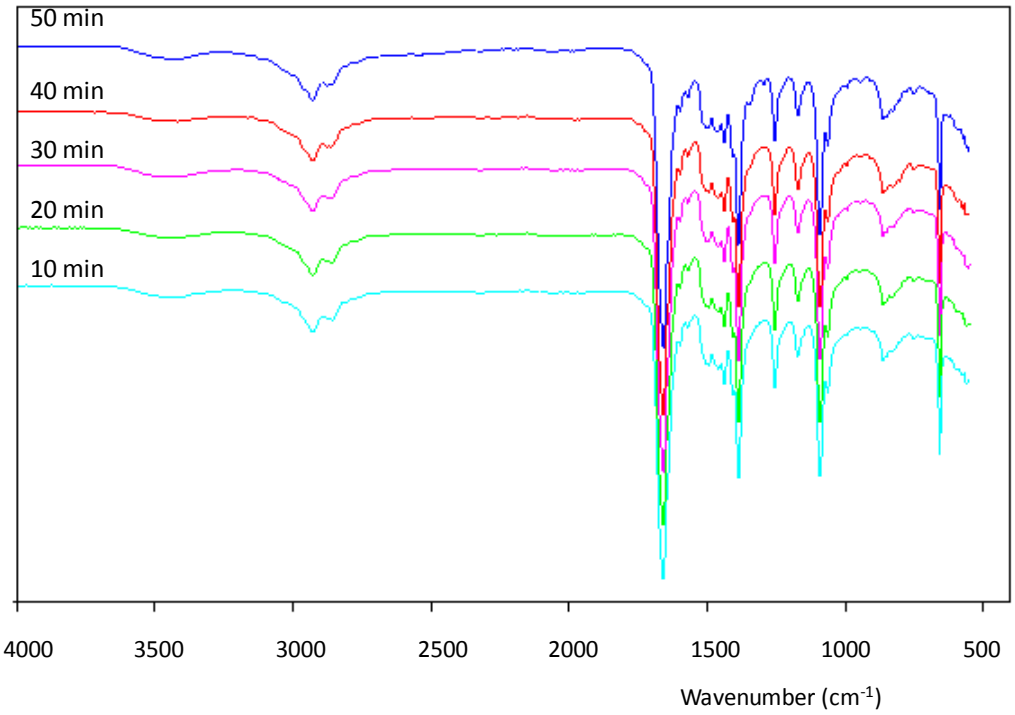


Figure 5.73: FTIR spectra of quartenized poly(4-vinylpyridine) after addition of $Na_2Cr_2O_7$.

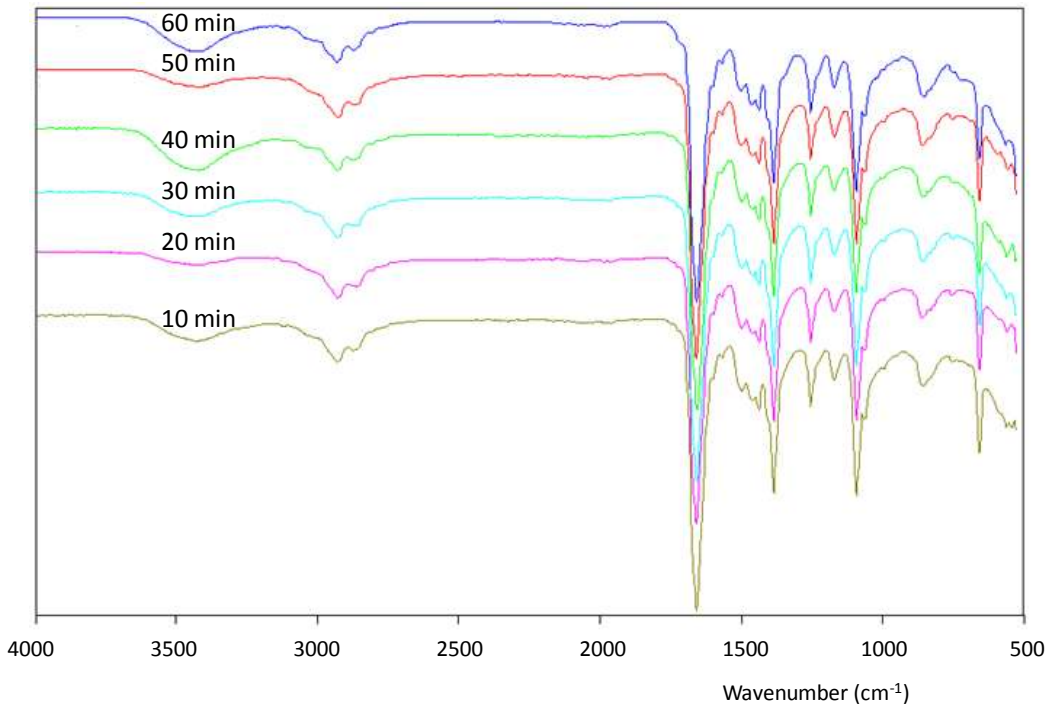


Figure 5.74: FTIR spectra of quartenized magnetic poly(4-vinylpyridine) after addition of $Na_2Cr_2O_7$.

5.2.4 Cross-linking and leaching of dichromate from the magnetic polymers

Cross-linking

For structural rigidity, EGDMA cross-linking monomer was used, Figure 5.75. This ensured that the magnetic polymers could not dissolve in solution during their applications in adsorption studies.

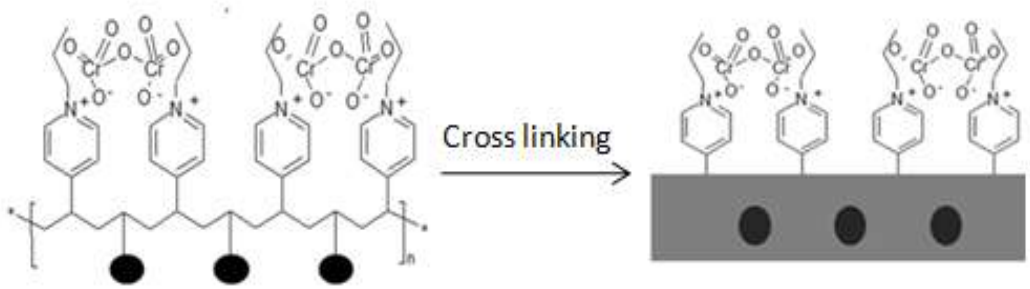


Figure 5.75: Cross-linking of the magnetic polymer.

Leaching of dichromate from the magnetic polymers

After crosslinking, the magnetic polymers were leached for many cycles as illustrated in Figure 5.76. Figure 5.77 shows the first seven solutions collected after washing the magnetic polymers with 1M HCl. These solutions were analyzed for chromium content with the FAAS. Leaching was only stopped after the chromium content was zero or close to zero. The magnetic polymers were then conditioned with deionized water in order to remove all the excess chloride ions from HCl leachant and dried in the oven at 50°C for 12 hours.

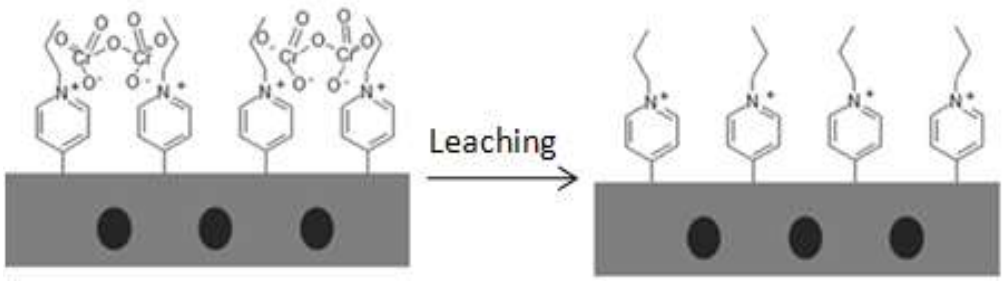


Figure 5.76: Leaching of the dichromate with 1 M HCl.

Leaching studies

The magnetite was washed away from the polymeric matrix and this was in parallel with the leaching of the chromium to form pores within the magnetic polymer matrix. However, it is important to note that the magnetite was not totally washed away otherwise it would have defeated the whole purpose of the project (i.e. making the polymers magnetic). The last washing of the magnetic IIP detected 0.3 mg L^{-1} and 8.6 mg L^{-1} for the chromium and iron, respectively, Figure 5.78. Figure 5.79 shows the decrease of the magnetite when the magnetic NIP was washed and the last washing had an iron content of 11.7 mg L^{-1}.

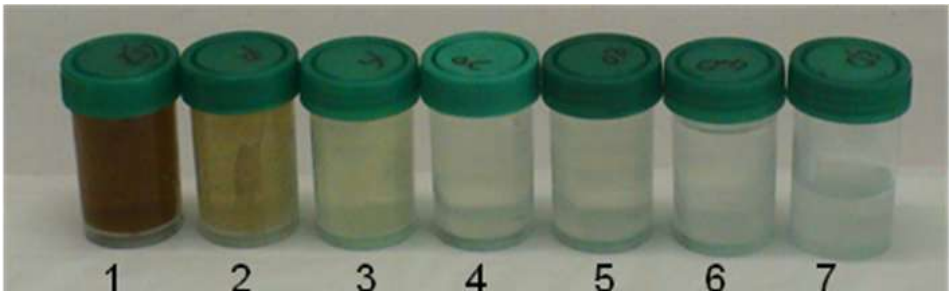


Figure 5.77: Aliquots collected after different leaching times.

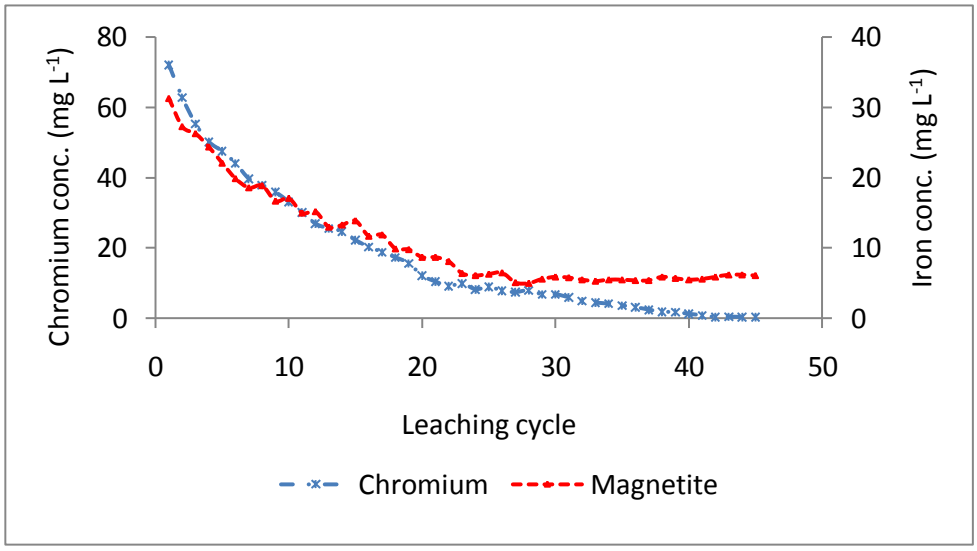


Figure 5.78: Leaching of chromium and iron from the magnetic IIP.

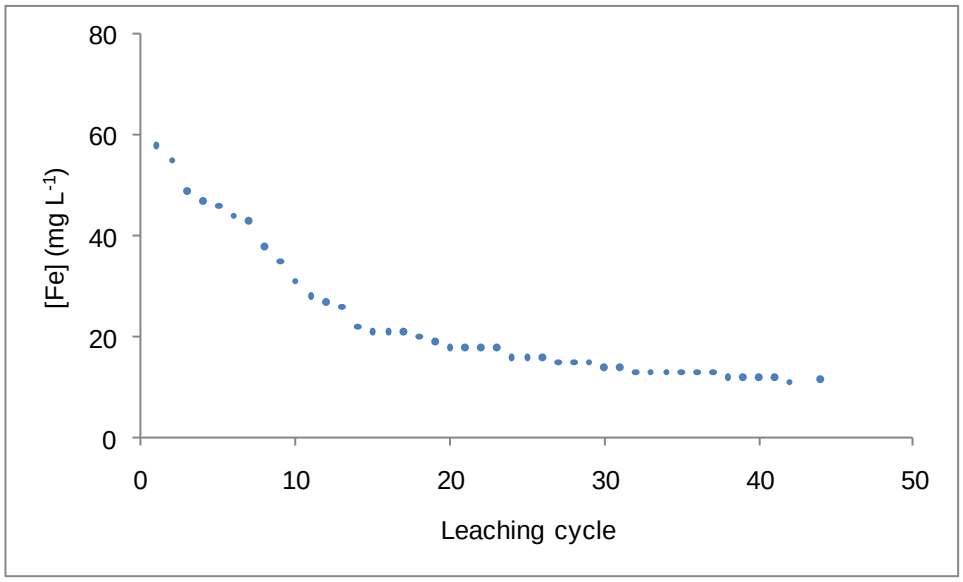


Figure 5.79: Washing of magnetite from magnetic NIP.

5.2.4.1 Brunauer, Emmett and Teller surface analysis

The adsorption data in the relative pressure (p/p_o) range 0.05-0.35 was fitted to the BET model and gave good linear plots as shown in Figure 5,80(b). Similar plots were obtained for other polymers shown in Table 5.22. By application of BET equations, the BET constant, *c*, was found to be 64.81 and the monomolecular layer volume, v_m, was 5.54 for the unleached non-magnetic poly(n-propyl-4-vinylpyridinium) dichromate polymer. As for the unleached magnetic poly(n-propyl-4-vinylpyridinium) dichromate polymer, *c* was 8.71 and v_m was 0.23. The surface areas for the unleached magnetic and unleached non-magnetic poly(n-propyl-4-vinylpyridinium) dichromate polymer were found to be 1.00 ± 0.02 $m^2\ g^{-1}$ and 25.4 ± 0.3 $m^2\ g^{-1}$, respectively.

After leaching of the chromium from the magnetic IIP, there was an increase in the surface area to 132 ± 1 $m^2\ g^{-1}$ which corresponded to 132% increase. However, even though there was an increase in the surface area of the magnetic NIP (16.8%), it was not as significant as that obtained from the magnetic IIP. The BET constants, *c*, for the leached magnetic IIP and NIP were found to be 163 and 124, respectively. The monomolecular layer volumes, v_m, were 30.5 and 6.7, respectively. All the BET suface areas and constants for the magnetic polymers

are summarized in Table 5.22. Bayramoglu and Arica (2008), found that the specific surface area of the IIP and the corresponding NIP particles to be 34.5 m^2 g^{-1} and 21.7 m^2 g^{-1}, respectively, which indicated the presence of microporous on the surface of the Cr(VI)-imprinted particles.

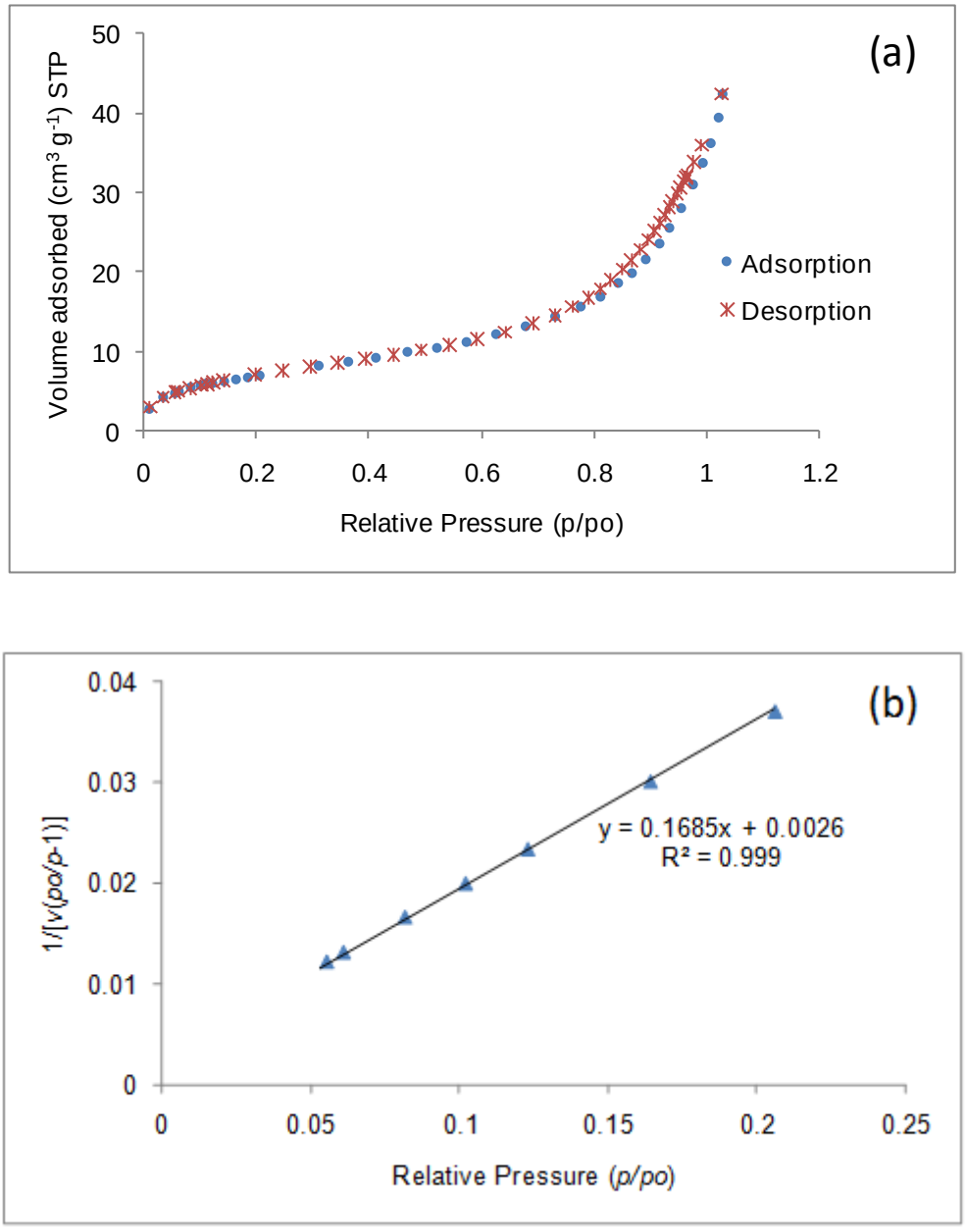


Figure 5.80: (a) The nitrogen adsorption-desorption isotherms for the unleached non-magnetic poly(n-propyl-4-vinylpyridinium) dichromate polymer and (b) its corresponding BET plot.

Table 5.22: BET suface areas and constants for the polymers.

	BET surface area ($m^2\ g^{-1}$)	v_m	c
Unleached non-magnetic	25.4	5.54	64.81
Unleached magnetic	1.0	0.23	8.71
Leached non-magnetic	132	30.5	163
Leached magnetic	16.8	7.7	124

5.2.4.2 Thermo-gravimetric analysis (TGA) analysis

In order to gain insight into the thermal changes in the magnetic polymers, the thermal stability was probed with TGA. Thermal degradation profiles of leached and unleached Cr(VI) magnetic polymers are shown in Figure 5.81. The maximum weight loss occurred at 425°C, corresponding to degradation of the polymer backbone, and a small peak that occurred at around 220°C can be attributed to the loss of moisture from the magnetic polymers. It can also be observed from the TGA spectrum of the Cr(VI) loaded magnetic polymer that the maximum weight loss due to the decomposition of the backbone occurred at a slightly lower temperature. This indicated that the unleached magnetic polymer was slightly more stable than the leached one. It was also observed that the leached and unleached Cr(VI) magnetic polymers had total weight losses of 82.5 and 59.2%, respectively. The remaining mass corresponds to the presence of Cr(VI) and magnetite in the unleached magnetic polymer and magnetite in the leached magnetic polymer.

In almost similar studies by Toral *et al*. (2009), where they quartenized the polymer with an octyl moiety, the stability of the Cr(VI) loaded polymer was also stable as compared to the leached one. The decomposition of the two polymers occurred at around 500 and 400^{o}C, respectively. However, in terms of the residual weight of the leached polymer, they found it to be close to 100%. In this work it was observed to be 59.2% because of the embedded magnetite in the polymer matrix.

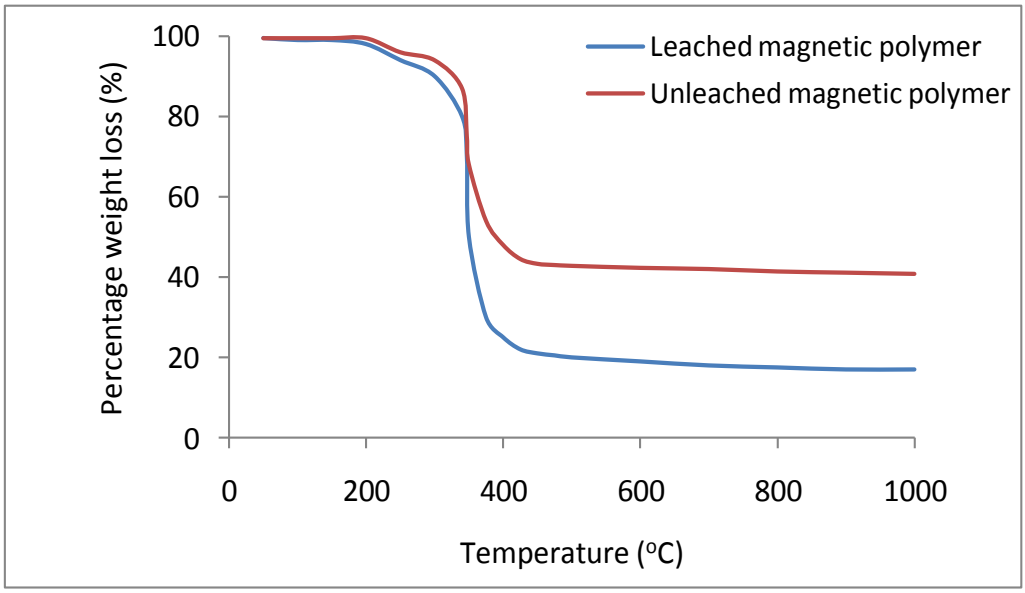


Figure 5.81: Thermogravimetric analysis of chromium magnetic polymer.

5.2.5 Optimization of parameters for Cr(VI) uptake

5.2.5.1 Effect of sample pH

Sample pH dictates the speciation of metals in solution and also the form of protonation on the active sites within the adsorbent. The positive charge on the quartenized nitrogen is responsible for the $Cr_2O_7^{2-}$ uptake and other anions. Since the hydroxyl ions are possible competitors for dichromate sorption, it therefore becomes apparent that sample pH affects the adsorption. This effect is demonstrated in Figure 5.82.

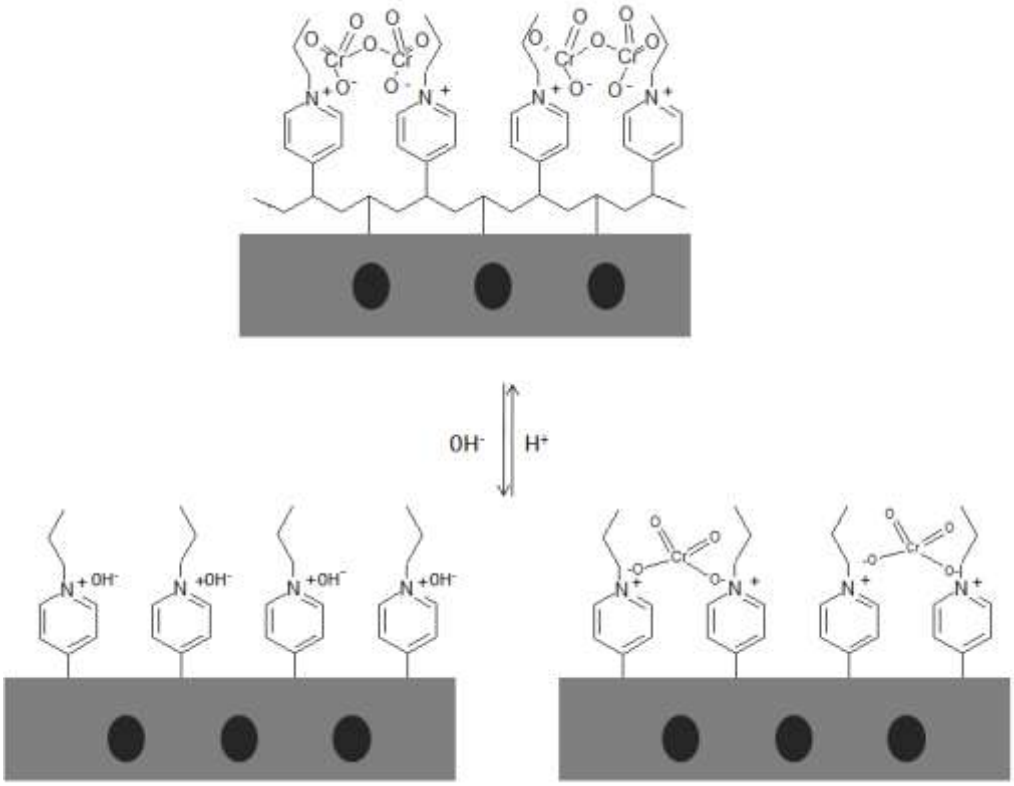


Figure 5.82: The effect of pH and also the demonstration of the chromate/ hydroxyl competition.

The effect of pH on the removal of Cr(VI) was investigated in the pH range of 2-10 at room temperature. The experimental results are presented in Figure 5.83 where it was observed that the maximum adsorption occurred in the pH range 2-6. The optimum pH for the uptake of Cr(VI) was then chosen to be 4 which corresponded to 90 and 73% Cr(VI) removal for the magnetic IIP and NIP, respectively. The Cr(VI) removal efficiency decreased at pH values greater than 6 for both the magnetic IIP and its control polymer. Beyond this pH, there is an anticipated strong competition between hydroxyl ions and the dichromate ions in solution. These two anions compete for the fabricated active adsorption sites on the magnetic polymers. Similar results were obtained by Bayramoglu and Arica (2008) who showed that at high acidic pH of 2-4, adsorption was very high and decreased rapidly after pH 5. However, they did not quartenize their polymers but rather they used 4-VP as a functional monomer. Their Cr(VI)-ion imprinted poly(4-vinyl pyridine-co-2-hydroxyethyl methacrylate) particles were prepared by

bulk polymerization. On poly(4-vinylpyridine) coating onto a granular activated carbon Fang *et al*. (2007) observed a 90% Cr(VI) removal at a pH of 2 which was almost maintained but decreased sharply at pH 6 to 8 and no apparent sorption was observed when pH was above 9. After firstly forming a linear copolymer from 4-VP and styrene, Pakade *et al*. (2011) prepared an IIP selective of Cr(VI) by quartenizing the linear copolymer with 1,4 dichlorobutane. The pH trend they got did not show a drop in Cr(VI) absorption after pH 4-5 may bebecause the pH used only ranged from 1 to 4.

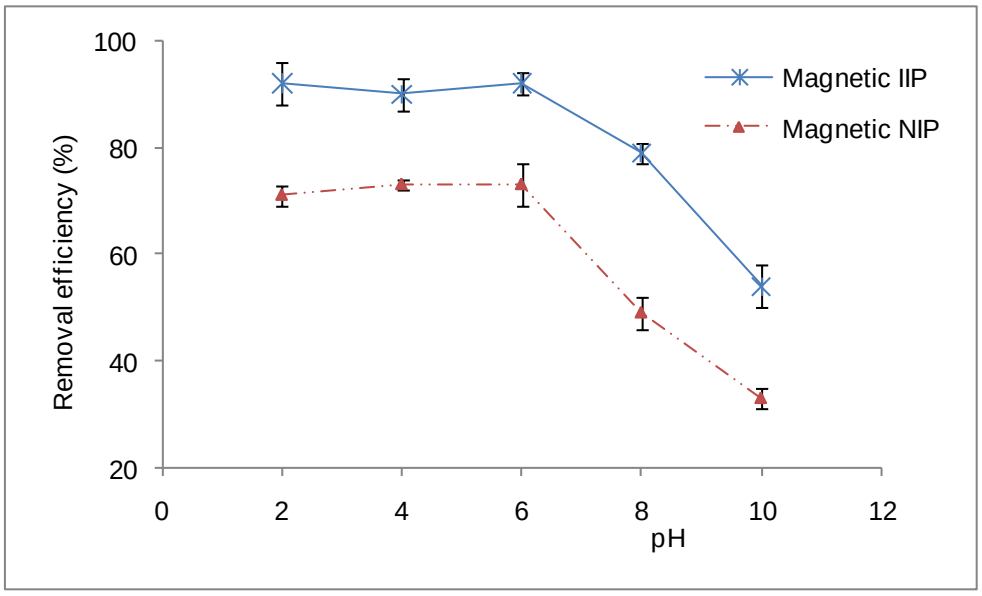


Figure 5.83: Effect of sample pH. Experimental conditions: Polymer amount, 20 mg; sample volume, 25 mL; chromium concentration, 5 mg L^{-1}; contact time, 45 minutes; stirring speed, 600 rpm; temperature, room temperature.

5.2.5.2 Effect of the amount of the adsorbent

The removal of chromium by magnetic polymers at different adsorbent doses (5-120 mg) from a Cr(VI) concentration of 5 mg L^{-1} was investigated. The results (Figure 5.84) showed that, initially, the percent removal of Cr(VI) increased with the increase in the dose of magnetic polymers due to the greater availability of the adsorption sites within the adsorbent. For the magnetic IIP, the increase in adsorbent dosage from 5 to 20 mg resulted in an increase from 83 to 97% in adsorption efficiency of Cr(VI) ions whilst an increase from 47 to around 95% was observed for the dose from 5 to 65 mg for the magnetic NIP. The optimum

amounts of magnetic polymer were then chosen to be 20 and 65 mg for the magnetic IIP and NIP, respectively. Considering an initial volume of 25 mL for both the magnetic IIP and NIP, the normalized volume became 0.8 g L^{-1} and 2.6 g L^{-1}, respectively.

Investigating the effect of polypyrrole/Fe_3O_4 nanocomposite dosage on adsorption of Cr(VI) from aqueous solution showed that Cr(VI) removal efficiency increased with an increase in polypyrrole/Fe_3O_4 dose (Bhaumik *et al*., 2011). The extent of Cr(VI) removal from 50 mL of 200 mg L^{-1} Cr(VI) solution changed from 16.3% at a dose of 25 mg to 100% at a dose of 100 mg which is equivalent to an optimum of 2 g L^{-1} of polypyrrole/Fe_3O_4. In the study by Hadjmohammadi *et al*. (2011), who used pine needles powder as a biosorbent, the uptake of Cr(VI) from 50 mL of 50 mg L^{-1} solutions, the adsorbent dose reached a plateau at 0.5 g of sorbent. This translated to 10 mg L^{-1}. Using tetraethylenepentamine on Fe_3O_4 magnetic polymer adsorbent, Yao *et al*. (2012) found a proportion of 20 mg per 250 mL (0.8 mg L^{-1}) water sample would ensure efficient preconcentration of Cr(VI).

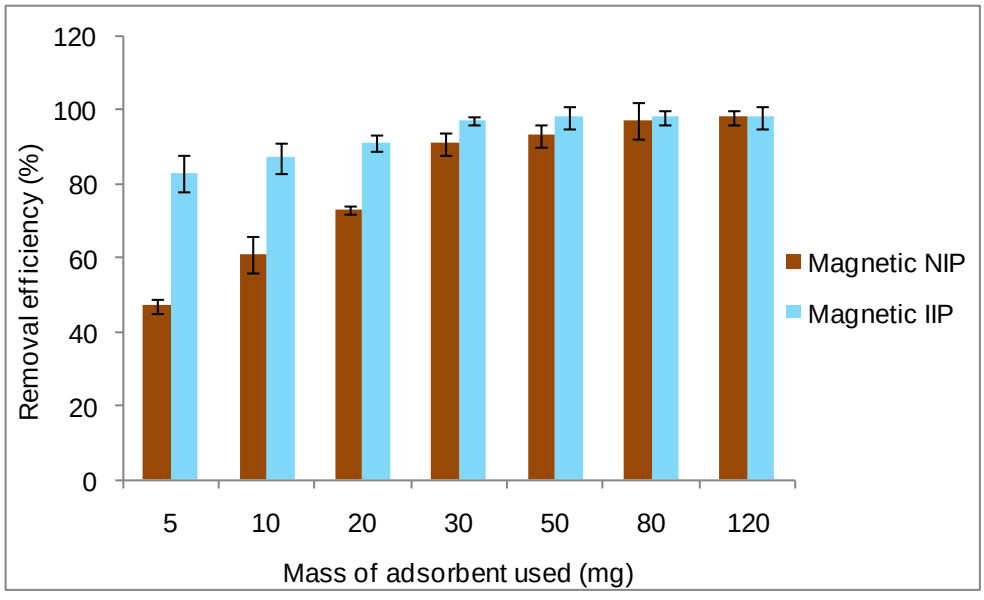


Figure 5.84: Adsorption percentages obtained by varying the mass of magnetic polymers for chromium adsorption. Experimental conditions: Sample pH, 4; sample volume, 25 mL; chromium concentration, 5 mg L^{-1}; contact time, 45 minutes; stirring speed, 600 rpm; temperature, room temperature.

5.2.5.3 Effect of contact time

Cr(VI) removal by magnetic polymers as a function of contact time is shown in Figure 5.85. $Cr_2O_7^{2-}$ uptake was not fast and the maximum uptake was observed within 30-35 min for both the magnetic IIP and NIP. Before this time, there was a high rate of accumulation of the analyte in the adsorption sites within the magnetic polymer matrix. After reaching equilibrium, there was no further increase of adsorption of Cr(VI) as all the adsorption sites were saturated. A similar trend was observed by Yao *et al*. (2012) who used tetraethylenepentamine on Fe_3O_4 magnetic polymer as an adsorbent. Their results showed that the rate of Cr(VI) uptake was initially high, followed by a much slower subsequent adsorption quantity leading gradually to an equilibrium condition. A contact time of 60 min of stirring was considered enough to reach maximum values of separation and preconcentration of C r (VI) ions (Yao *et al*., 2012).

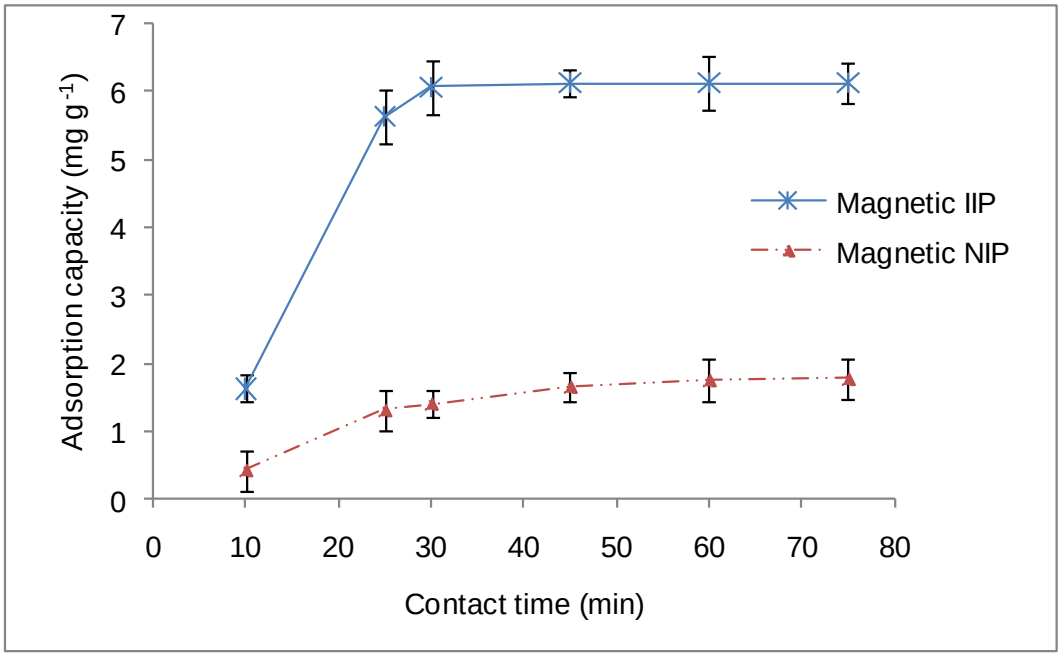


Figure 5.85: Effect of contact time on the uptake of chromium by magnetic polymers. Experimental conditions: Sample pH, 4; sample volume, 25 mL; chromium concentration, 5 mg L^{-1}; polymer weight (20 mg for magnetic IIP and 65 mg for magnetic NIP); stirring speed, 600 rpm; temperature, room temperature.

5.2.5.4 Effect of initial Cr(VI) concentration

The results obtained for the effect of initial concentration on the uptake of chromium by magnetic IIP and NIP are presented in Figure 5.86. An initial chromium concentration of 1-20 mg L^{-1} was investigated. In this experiment, the magnetic polymer dose was fixed as well as the contact time and solution pH of which the values are indicated in the caption of Figure 5.96. It was observed that the magnetic polymers` Cr(VI) removal increased significantly from 1-2.5 mg L^{-1} and 1-1.5 mg L^{-1} for the magnetic IIP and NIP, respectively. An initial Cr(VI) concentration of 5 mg L^{-1} was taken to be the optimum. After this value, equilibrium was attained as there was no appreciable increase in the amount of the analytes adsorbed on the magnetic polymers. The maximum adsorption capacities for the magnetic polymers corresponding to the considered optimum Cr(VI) concentration of 5 mg L^{-1} were 6.20 and 1.87 mg g^{-1} for the magnetic IIP and NIP, respectively.

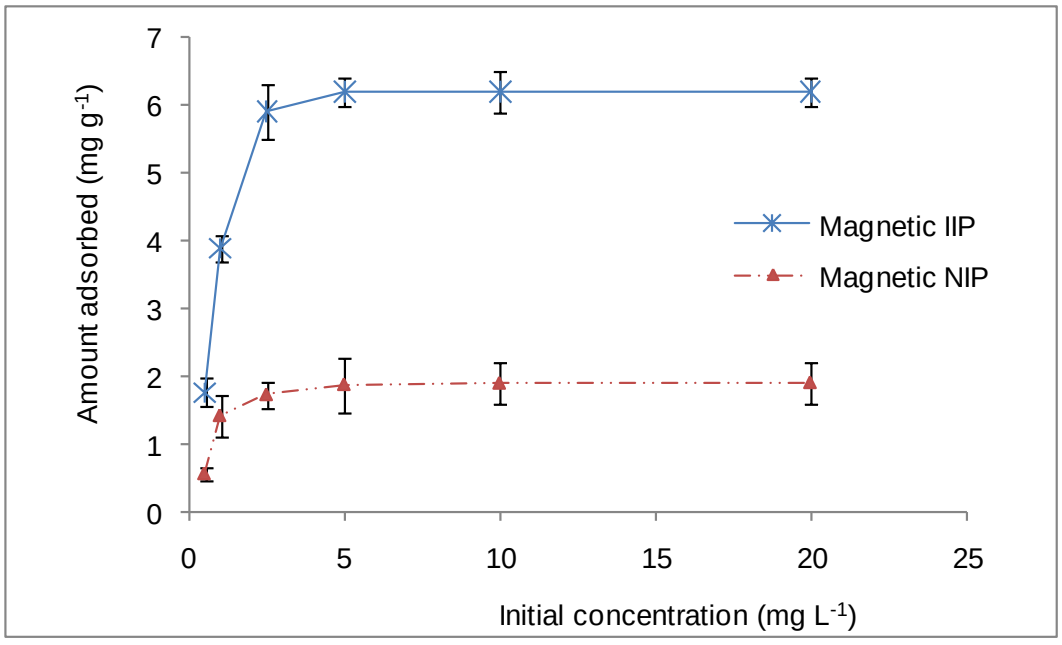


Figure 5.86: Effect of initial concentration on the uptake of chromium by magnetic IIP and NIP. Experimental conditions: Sample pH, 4; sample volume, 25 mL; polymer weight, (20 mg for magnetic IIP and 65 mg for magnetic NIP); contact time 35 min; stirring speed, 600 rpm; temperature, room temperature.

5.2.5.5 Selectivity of Cr(VI)

Competing anions are known to influence Cr(VI) uptake. However, because HCl was used as a leachant, it was likely that the chloride ion would have interfered with the selectivity studies, hence it was not used. The other ions selected, such as the sulphate and phosphate ions were selected as potential competitors because of their chemical similarities to the dichromate ion with respect to charge and oxy-ionic nature. Figure 5.87 is an example of the IC chromatogram of a 5 mg L^{-1} anionic mixture standard. Similar chromatograms of 1, 10 and 20 mg L^{-1} were obtained and were used to construct calibration curves for the respective anions, Figure 5.88. For the binary mixture, $Cr_2O_7^{2-}$/anionic competitor, the anion was also determined by IC and an example is illustrated for the fluoride ion in Figure 5.89. However, the equilibrium dichromate concentrations for all binary systems were determined by use of FAAS after the construction of a calibration curve, Figure 5.90. The selectivity performances of the magnetic polymers are summarized in Figure 5.91 and Table 5.23. The order of selectivity of the investigated anions followed the sequence: $Cr_2O_7^{2-} > SO_4^{2-} > F^- > NO_3^-$.

Pakade *et al*. (2011) investigated the influence of coexisting ions on the uptake of Cr(VI) onto 1,4-dichlorobutane quartenized linear copolymer. Their findings were that the selectivity order was $Cr_2O_7^{2-} > SO_4^{2-} > F^- > PO_4^{3-} > NO_3^- > Cl^-$. After considering two Cr(VI) competitors, Neagu and Mikhalovsky (2010) found that there was also a rather remarkable selectivity towards hexavalent chromium over the sulfate anion. The full order of selectivity was $Cr_2O_7^{2-} > SO_4^{2-} > Cl^-$ which was almost what was obtained in these studies. However, the same authors reported that the adsorption selectivity for the common anions onto commercial styrene anion exchangers and it followed the order: $SO_4^{2-} > I^- > CrO_4^{2-} > Br^- > Cl^-$. Fang *et al*. (2007) also performed some selectivity studies on three competitor ions for Cr(VI) and found the selectivity order of $PO_4^{2-} > SO_4^{2-} > NO_3^-$. For the two Cr(VI) competitors investigated by Bayramoglu and Arica (2011), it was demonstrated that (4-vinyl pyridine-co-hydroxyethyl methacrylate) particles showed excellent selectivity for Cr(VI) and the adsorption capacity of IIP

particles for Cr(VI) anions was 13.8 and 11.7 fold greater than those of the Cr(III) and Ni(II) ions, respectively.

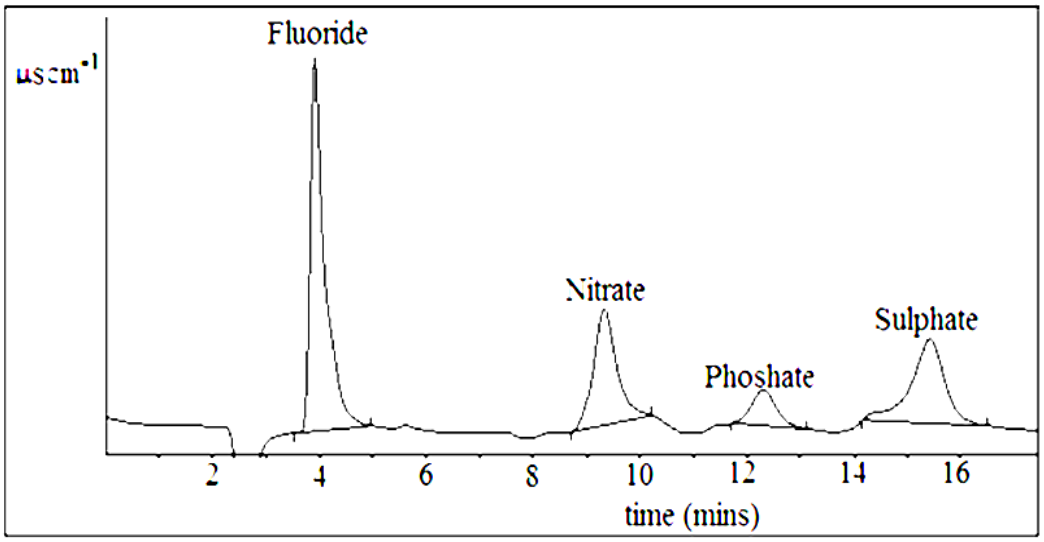


Figure 5.87: A 5 mg L^{-1} anionic mixture standard.

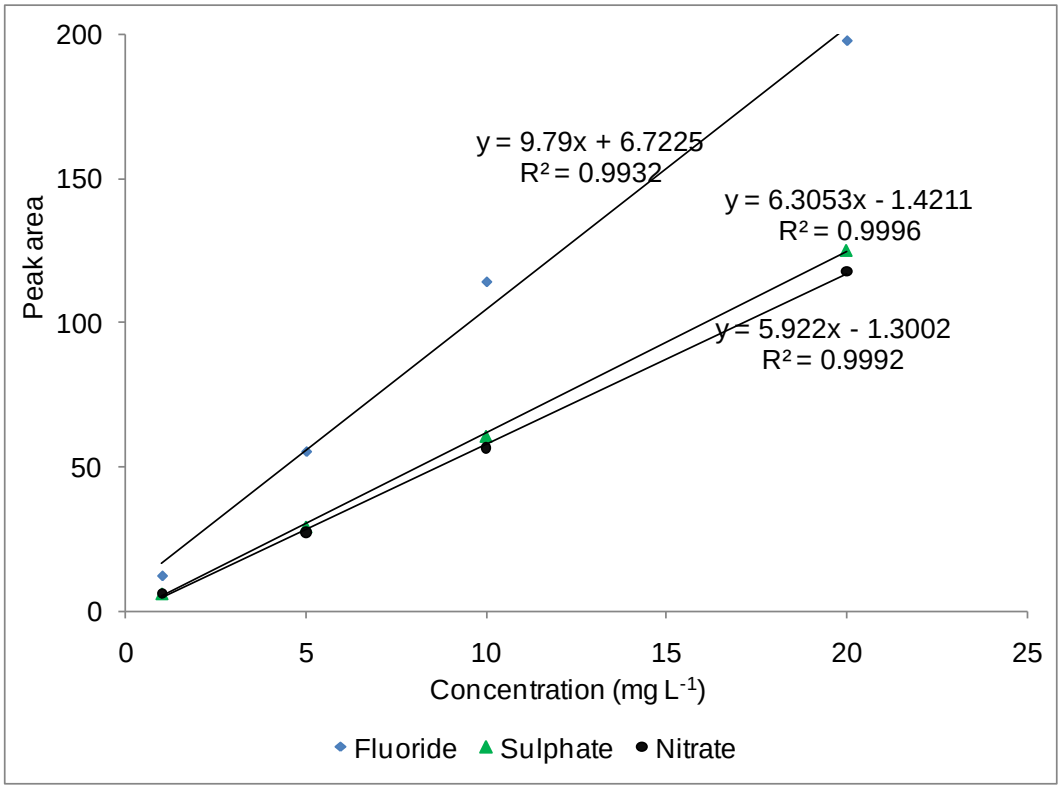


Figure 5.88: Calibration curve for four dichromate anionic competitors.

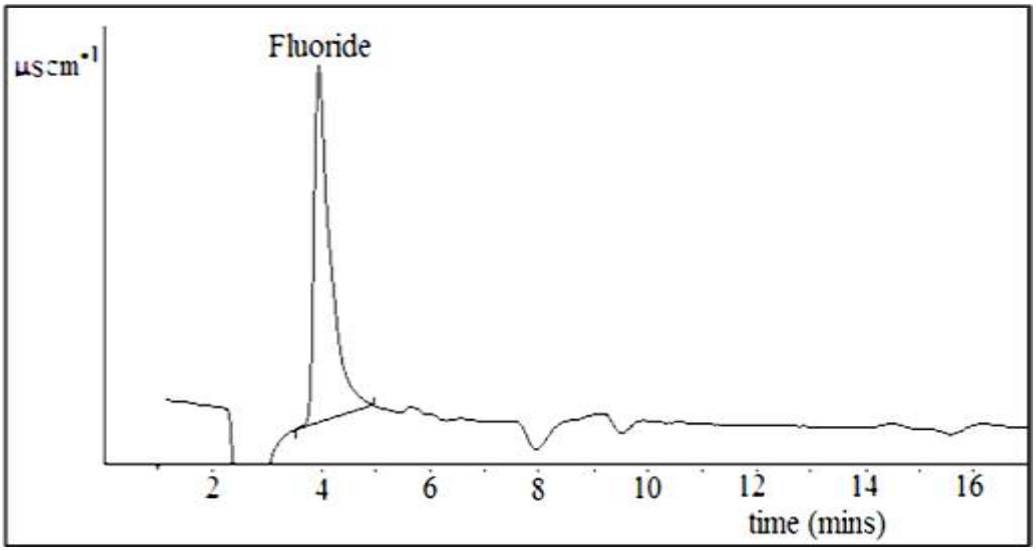


Figure 5.89: An example of a fluoride ion dichromate competitor.

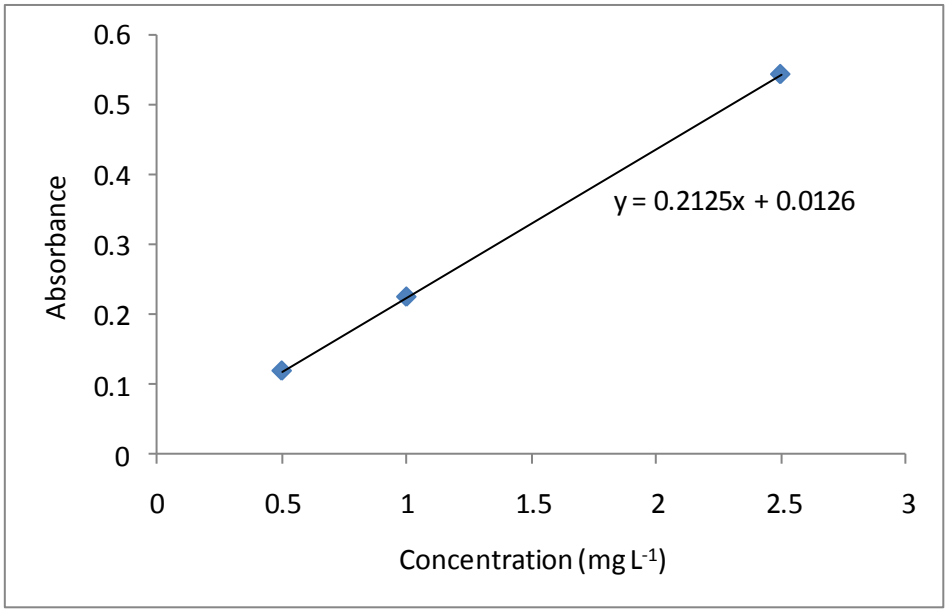


Figure 5.90: Calibration curve for the dichromate anionic standards.

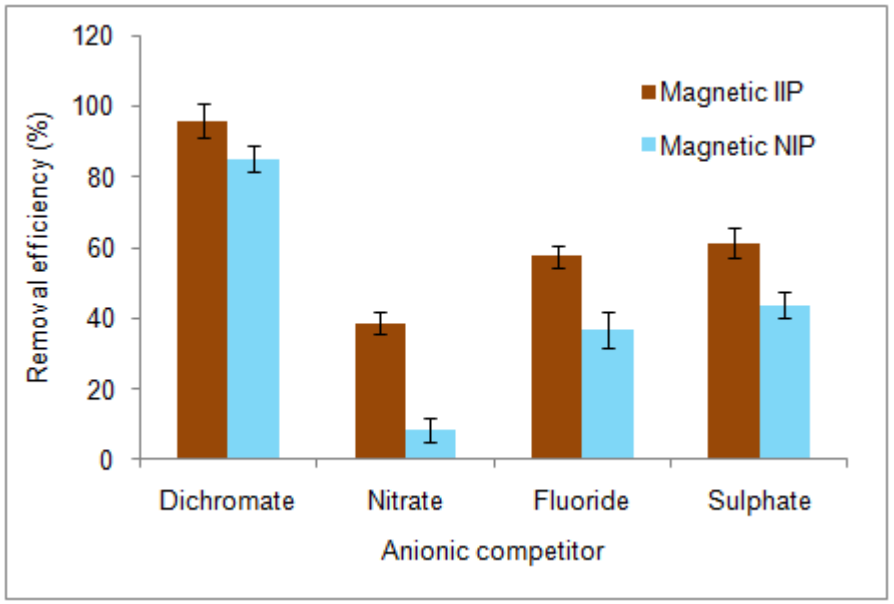


Figure 5.91: Extraction efficiencies of anions extracted by the magnetic Cr(VI) IIP and NIP from 2 mg L^{-1} spiked binary mixtures of solutions.

Table 5.23: K_d, K and K` values for the magnetic Cr(VI) IIP and NIP in binary mixtures.

$Cr_2O_7^{2-}$ ion Competitor	K_d (L g^{-1})				K		K`
	$Cr_2O_7^{2-}$ IIP	$Cr_2O_7^{2-}$ NIP	Magnetic IIP	Magnetic NIP	Magnetic IIP	Magnetic NIP	Magnetic NIP
SO_4^{2-}	11.70	3.06	1.98	0.30	5.91	10.20	0.58
F^-	23.50	1.90	1.69	0.22	13.91	8.64	1.61
NO^{3-}	33.00	5.53	0.79	0.035	41.77	158	0.26

5.2.5.6 Reusability of Cr-magnetic polymers

Since the reusability of the magnetic polymers is an important factor, six adsorption-desorption cycles were performed (Figure 5.92). What was observed is that the magnetic polymers maintained their stability as well as their chromium abstraction capacity of 98.5% and 89% for the magnetic IIP and NIP, respectively. This high robustness of the imprinted polymers has the significance that they can be cleaned, thereby regenerating their adsorption capabilities. For up to 5 cycles, the IIP synthesized by Pakade *et al*. (2011) was still stable as it showed 96% extraction efficiency.

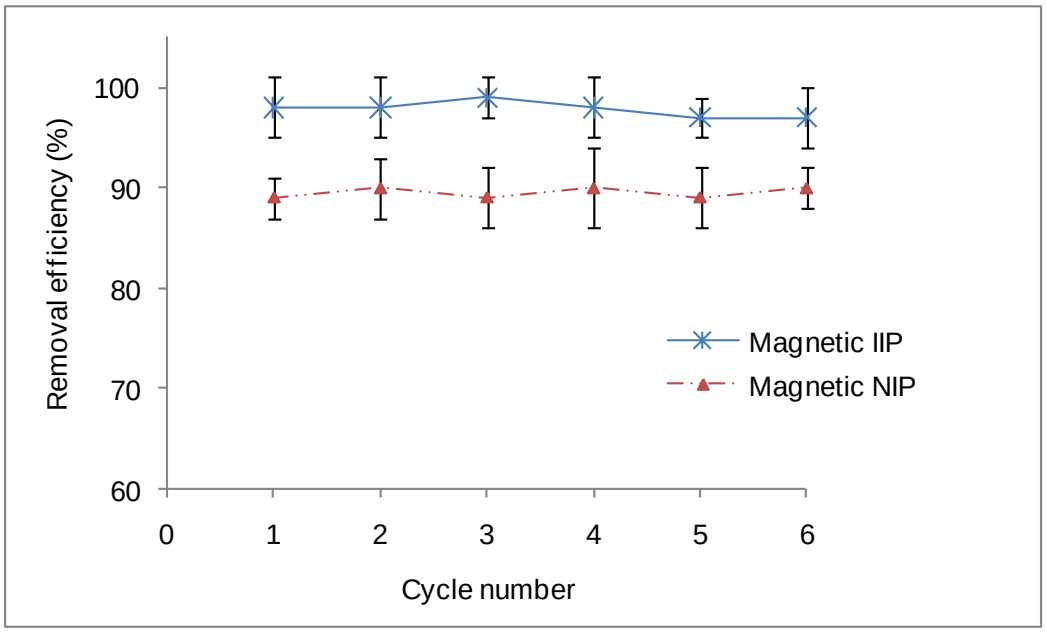


Figure 5.92: Reusability and stability magnetic IIP and NIP selective to chromium. Adsorption conditions: Sample pH, 4; sample volume, 25 mL; polymer weight, (20 mg for magnetic IIP and 65 mg for magnetic NIP); contact time 35 min; initial dichromate concentration, 5 mg L^{-1}; stirring speed, 600 rpm; temperature, room temperature, Desorption conditions: Solution volume, 20 mL; contact time, 20 min, [NaOH] leachant, 1 M.

5.2.6 Kinetic modelling

5.2.6.1 Pseudo-first order kinetics

The correlation coefficients values for the pseudo-first and second order kinetics were calculated from the plots of Figures 5.93 and 5.94, respectively and the kinetic constants deduced from them are shown in Table 5.24.

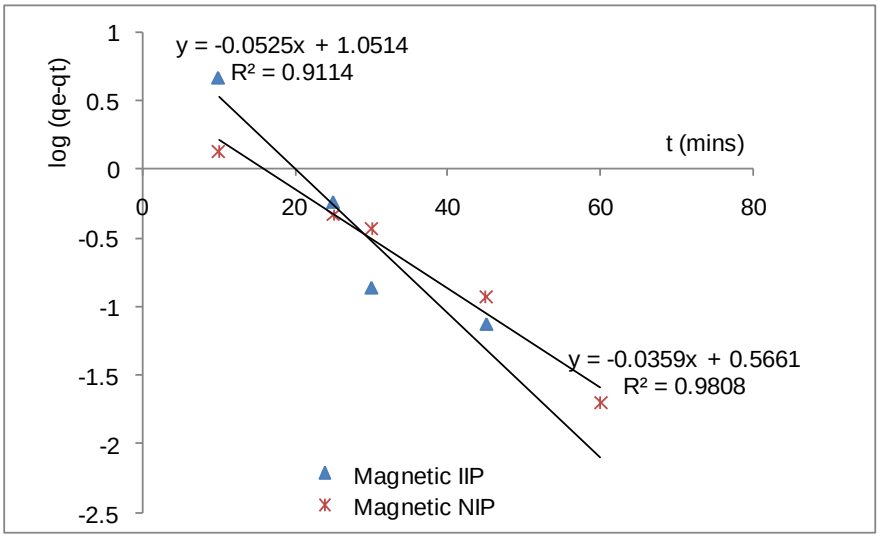


Figure 5.93: Pseudo first-order plots for the adsorption of chromium onto magnetic polymers.

5.2.6.2 Pseudo-second order kinetics

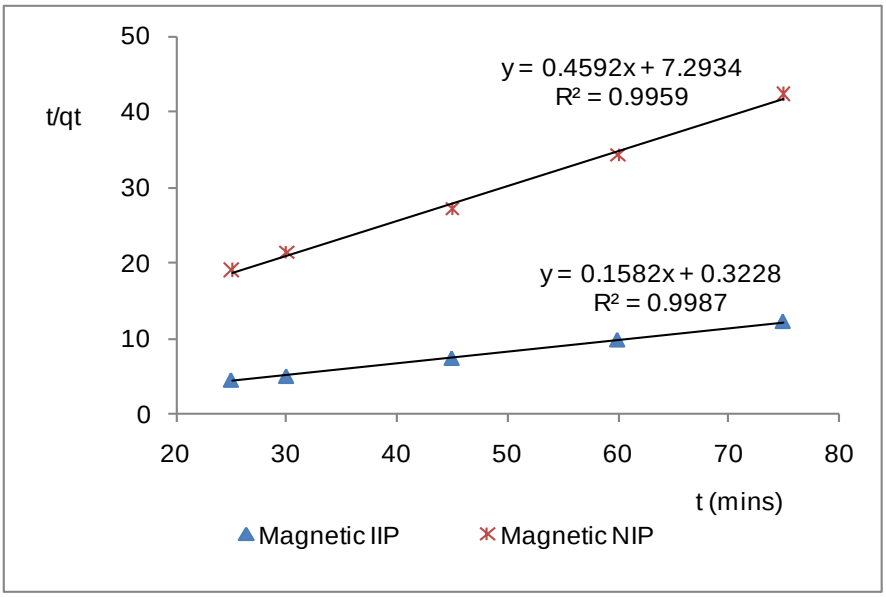


Figure 5.94: Pseudo second-order plots for the adsorption of chromium onto magnetic polymers.

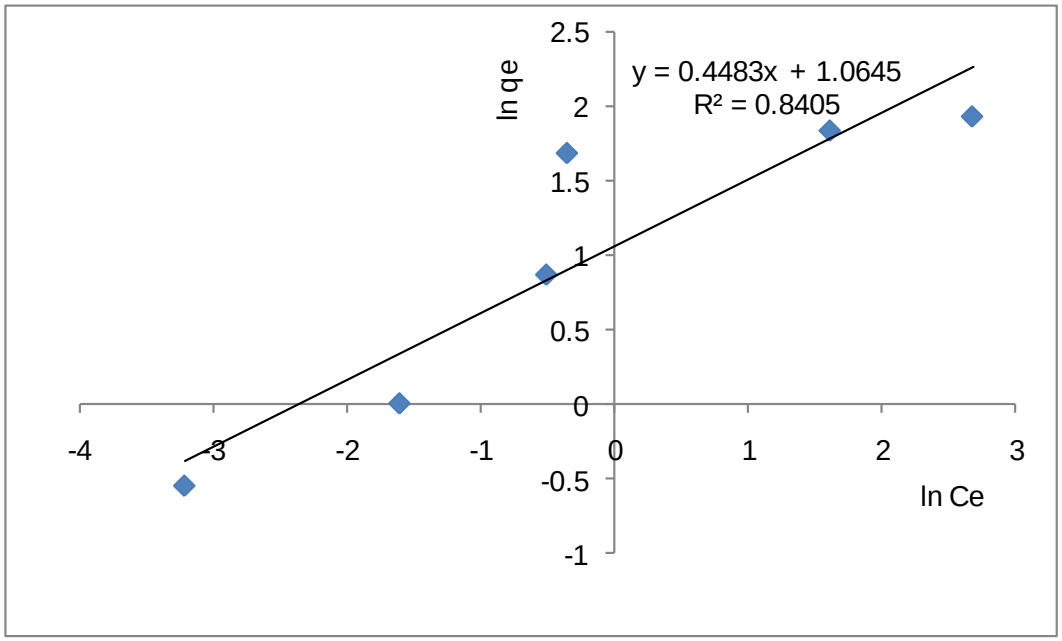
Table 5.24: Calculated kinetic parameters of pseudo-first and pseudo-second orders for initial Cr(VI) concentration of 5 mg L^{-1}.

	Pseudo first-order			Pseudo second-order		
Polymer	R^2	k_1 (min^{-1})	q_e (mg g^{-1})	R^2	k_2 (g mg^{-1} min^{-1})	q_e (mg g^{-1})
IIP	0.9114	0.121	11.256	0.9987	0.078	3.098
NIP	0.9808	0.083	3.682	0.9959	0.029	2.178

It was observed that correlation coefficients values of the pseudo-second order kinetics produced better quality of linearization compared to the pseudo-first order kinetics. Moreso, the adsorption capacity values obtained by this method were much closer to those reported before in this work (6.20 and 1.87 mg g^{-1} for the magnetic IIP and NIP, respectively). A pseudo-second order further suggests that the type of interaction between the target template and the adsorbent surface was chemisorption as a rate controlling step (Wang *et al*. 2011). This interaction was probably due to the exchange of electrons on the dichromate and the quartenized nitrogens.

5.2.7 Freundlich and Langmuir isotherm modelling

Figure 5.95 and 5.96 present the Freundlich and the Langmuir isotherm model for magnetic IIP and NIP, respectively. The Langmuir adsorption constants deduced from Fig 5.96 summarized in Table 5.25.



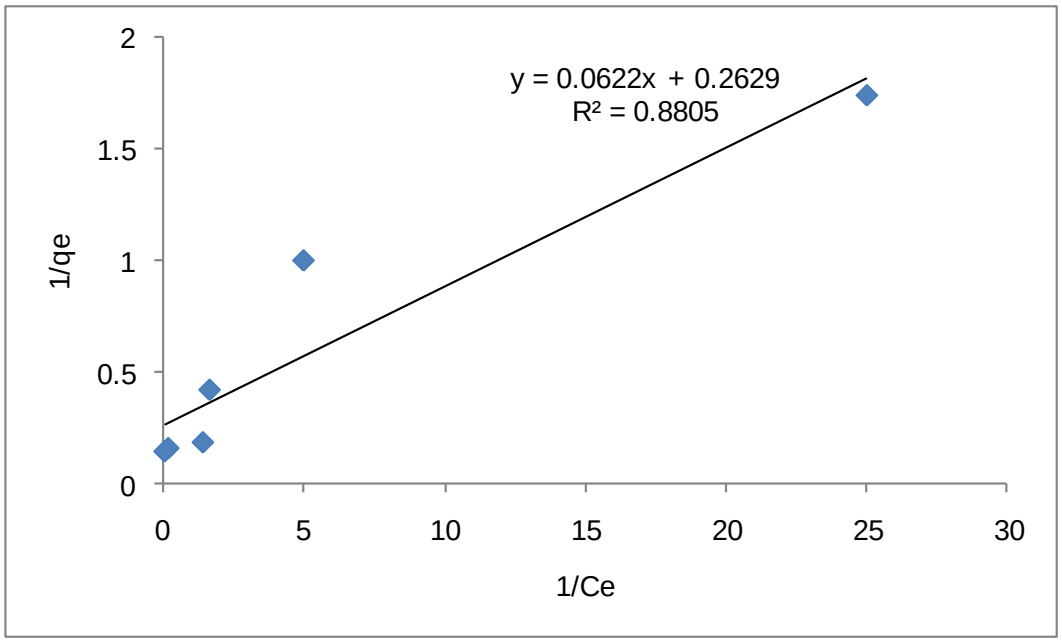


Figure 5.95: (a) Freundlich and (b) Langmuir isotherm model for magnetic IIP.

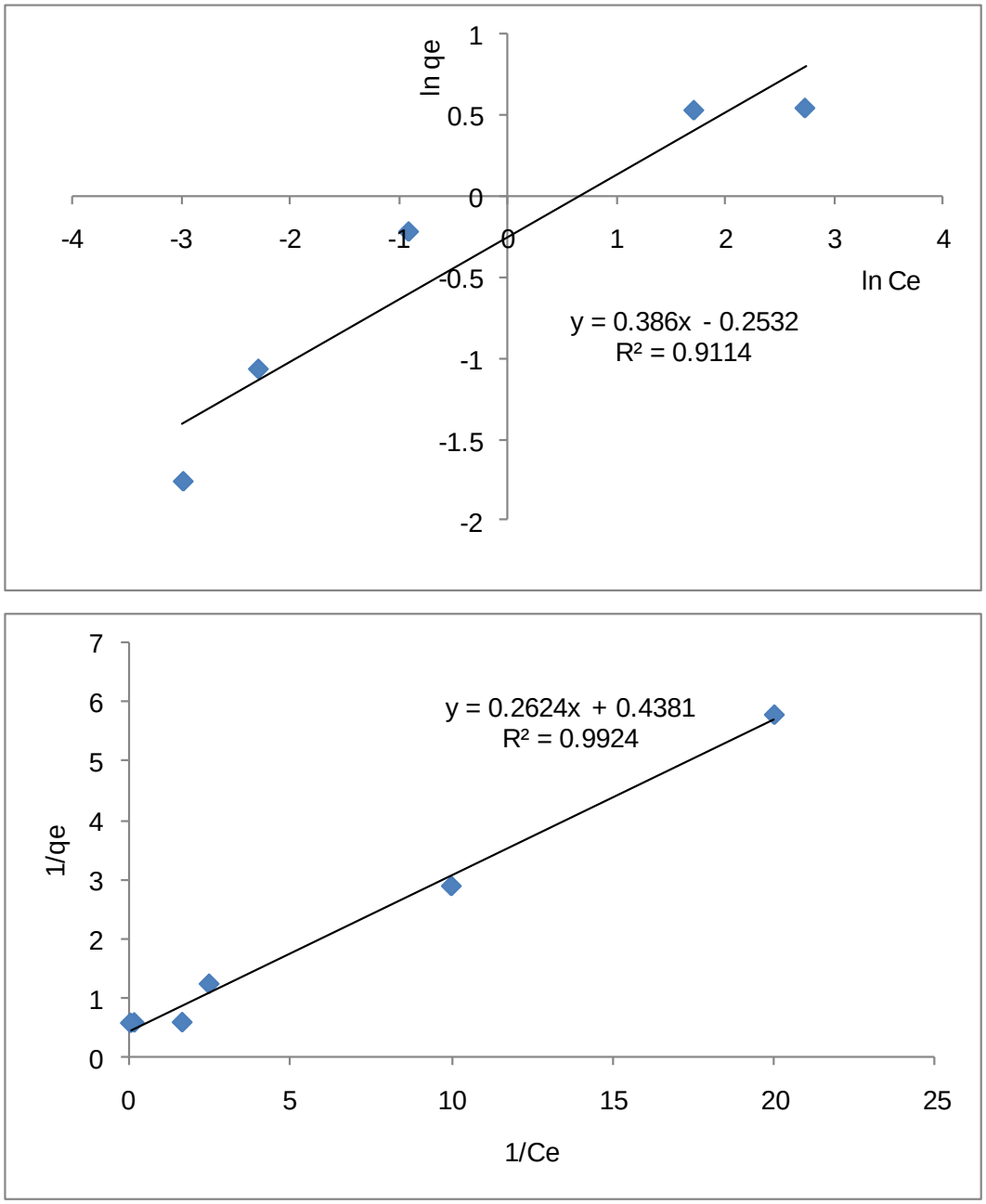


Figure 5.96: (a) Freundlich and (b) Langmuir isotherm model for magnetic NIP.

Table 5.25: The Langmuir constants and the R_L values for adsorption of Cr(VI) on magnetic polymers.

Magnetic polymer	*b* (L g^{-1})	q_m (mg g^{-1})	R_L	R^2
Cr- IIP	4.23	3.8	0.05	0.881
Cr -NIP	1.67	2.3	0.11	0.992

Since the separation factors for both the magnetic IIP and NIP are within the range of zero and unity, Cr(VI) adsorption onto magnetic polymers was deemed favourable. This indicates the suitability of the adsorbent to extract the targert from aqueous solution (Zhou *et al.*, 2012).

Table 5.26: Freundlich constants for chromium magnetic polymers.

Magnetic polymer	n	K_f (L g^{-1})	R^2
Cr- IIP	2.23	2.90	0.841
Cr -NIP	2.59	0.78	0.911

Chapter 6
Conclusions and Recommendations for future work

This chapter summarizes the outputs of the study on the abstraction capacity of the synthesized magnetic polymers towards uranyl and dichromate ions from wastewaters. It compares their potential, efficiency, affinity, selectivity as well as potential research areas identified from this work.

6.1 Conclusions

The imprinting technique proved that a memory of the targets (U(VI) and Cr(VI)) can be induced in the magnetic polymer such that in subsequent use, even in the presence of other competing ions in aqueous media, selectivity was enhanced. After adsorption the adsorbents were traditionally removed from the solutions *via* centrifugation and filtration. The technique of endowering magnetic particles into the polymer matrix, as demonstrated in this research, makes the whole polymer particles magnetic and this necessitated their easy removal from solutions. The successful incorporation of the magnetite into the polymer was evident from the FTIR where a band at was observed implying that the general objective of this to synthesize magnetic polymers selective to U(VI) and Cr(VI) was realized.

Both magnetic IIPs and NIPs showed potential in the uptake of uranium and chromium from contaminated solutions as these imprinted magnetic polymers were successfully applied for the selective extraction of the respective analytes from various complex samples which were AMD and treated wastewater effluent. Adsorption capacities for the U(VI) and Cr(VI) magnetic IIP were 6.20 and 1.87 mg g^{-1} for the magnetic IIP and NIP, respectively and the order of selectivity for the U(VI) magnetic IIP was $UO_2^{2+} > Fe^{3+} > Pb^{2+} > Ni^{2+} > Mg^{2+}$ and that for the Cr(VI) magnetic IIP was: $Cr_2O_7^{2-} > SO_4^{2-} > F^- > NO_3^-$. Magnetic IIPs always expectedly showed a higher uranyl and dichromate uptake as compared to their corresponding magnetic NIPs.

The uptake of the uranyl was made possible by the presence organic ligands (functional groups) with oxygen and nitrogen atoms that provided lone pairs of electrons to the cationic uranyl ion through coordinate bonding. For the adsorption of the Cr(VI), quartenization enabled the extraction of anionic dichromate target.

6.2 Recommendations for future work

- There is need to carry out the polymerization reaction in aqueous media rather than the organic solvents in order to avoid the swelling and shrinkage of magnetic polymers. This however means changing of the initiator to those compatible with water.

- The application of the synthesized magnetic polymers can be applied to a pilot plant scale and ultimately to real environmental systems. It is therefore important to carry out the same adsorption studies in a continuous flow system that mimick a river system. In this approach, the magnetic polymers need to be contained in cartridges such as those used in SPE.

- To use natural adsorbents like chitosan, cellulose that can be compatible with magnetic materials. This is because synthetic polymeric reagents becomes expensive especially when large quantities are required to decontaminate large volumes of wastewaters in real environmental situations. Most natural adsorbents are are cheap and readily available.

- To try other synthetic routes those give the smallest particle sizes of the magnetic particles. This is to ensure that the surface area is increased or alternatively to use other superparamagnetic particles.

- To carry out studies of adsorption dependency on the mass transfer not only at room temperature as industrial wastewaters are discharged at various temperatures.

- There is need to fully identify the leached species as there is a possibility of nucleation of the imprint in the polymer matrix. This will convert the target ion into something that will imprint a `false` memory to the polymer and a direct consequence of this will be poor adsorption and selectivity of the uranyl ions. Possible uranium polymeric species include such species as $(UO_2)_2(OH_2)_2^{2+}$, $(UO_2)_3(OH)_4^{2+}$ and $(UO_2)_3(OH)_5^{+}$.

- To try other methods for coating the magnetite wholly as this is important so that no part of the exposed magnetic core takes part in the adsorption of the uranyl and dichromate ions from solution. Adsorption studies of the uranyl and dichromate ion by a bare magnetite should also be carried out to show its contribution in the case of partial coating.

- In this study, only oxygen and nitrogen bearing functional monomers were used (for uranium magnetic IIP). It is, however, important that monomers with electron lone pair donating atoms like sulpfur be investigated in order to see if there can be an improvement in the adsorption capacity.

PRESENTATIONS ARISING FROM THIS DISSERTATION

1) Tavengwa, N.T., Chimuka, L. and Cukrowska, E.M. Preparation and characterization of magnetic ion imprinted polymers for the removal of uranyl ions from mine wastewaters, University of Witwatersrand 4th Cross Faculty Postgraduate Symposium 2012, 19-22 October 2012, University of the Witwatersrand, Johannesburg, South Africa, *Poster presentation*.

2) Tavengwa, N.T. Preparation, characterization and optimization of magnetic ion imprinted polymers used in the removal of uranium from acid mine drainage and mine wastewaters, Water Research Showcase 2012, 22 June, School of Civil and Environmental, University of the Witwatersrand, Johannesburg, South Africa, *Oral presentation*.

3) Tavengwa, N.T., Chimuka, L. and Cukrowska, E.M. Preparation, characterization and optimization of magnetic ion imprinted polymers used in the removal of uranium from acid mine drainage, 2nd South Africa Young Water Profesionals Regional Conference 2011, 3-5 July, CSIR International Convention Centre, Pretoria, South Africa, *Poster presentation*.

4) Tavengwa, N.T. Preparation, characterization and optimization of magnetic ion imprinted polymers for the removal of uranium from mining wastewaters, Witwatersrand Chemsoc 2011, 27 May, University of the Witwatersrand, Johannesburg, South Africa, *Oral presentation*.

REPORTS ARISING FROM THIS DISSERTATION

1) Tavengwa, N.T., Chimuka, L. and Cukrowska, E.M. (2010), Preparation of magnetic nano composite beads and their application to remediation of mine wastewaters, *WRC Report No 2014*, pp. 1-220 (Accepted).

References

REFERENCES

Acharya, J., Sahu, J.N., Sahoo, B.K., Mohanty, C.R. and Meikap, B.C. (2009), Removal of chromium(VI) from wastewater by activated carbon developed from *Tamarind wood* activated with zinc chloride, *Chemical Engineering Journal*, **150**, pp. 25-39.

Acheampong, M.A., Meulepas, R.J.W. and Lens, P.N.L. (2010), Removal of heavy metals and cyanide from gold mine wastewater, *Journal of Chemical Technology and Biotechnology*, **85**, pp. 590-613.

Adar, F. (2009), Raman Spectroscopy of Carbon - More information than you would, Available from: thinkhttp://www.modernmedicine.com/modernmedicine/article/articleDetail.jsp?id=583774, Accessed on: 28/01/2012.

Agbontalor, A. (2007), Phytoremediation: an environmentally sound technology for pollution prevention, control and remediation in developing countries Erakhrumen, *Educational Research and Review,* **2**, pp. 151-156.

Ahmad, A.L., Kusumastuti, A., Derek, C.J.C. and Ooi, B.S. (2011), Emulsion liquid membrane for heavy metal removal: An overview on emulsion stabilization and destabilization, *Chemical Engineering Journal*, **171**, pp. 870-882.

Ahmadi, S.J., Noori-Kalkhoran, O. and Shirvani-Arani, S. (2010), Synthesis and characterization of new ion-imprinted polymer for separation and preconcentration of uranyl (UO_2^{2+}) ions, *Journal of Hazardous Materials*, **175**, pp. 193-197.

Ahn, C.K., Park, D., Woo, S.H. and Park, J.M. (2009), Removal of cationic heavy metal from aqueous solution by activated carbon impregnated with anionic surfactants, *Journal of Hazardous Materials*, **164**, pp. 1130-1136.

Aksu, Z., Gönen, F. and Demircan, Z. (2002), Biosorption of chromium(VI) ions by Mowital B30H resin immobilized activated sludge in a packed bed: comparison with granular activated carbon, *Process Biochemistry*, **38**, pp. 175-186.

Al-Omair, M.A. and El-Sharkawy, E.A. (2007), Removal of heavy metals *via* adsorption on activated carbon synthesized from solid wastes, *Environmental Technology*, **28**, pp. 443-451.

Amer, S.I. (1998), Treating Metal Finishing Wastewater, *Environmental Technology*, **832**, pp. 539-1020.

Anderson, R.T., Vrionis, H.A., Ortiz-Bernad, I., Resch, C.T., Long, P.E., Dayvault, R., Karp, K., Marutzky, S., Metzler, D.R., Peacock, A and White, D.C. (2003), Stimulating the *in situ* activity of Geobacter species to remove uranium from the groundwater of a uranium-contaminated aquifer, *Applied and Environmental Microbiology*, **69**, pp. 5884-91.

Ansell, R.J., Wang, D.Y. and Kuah, J.K.L. (2008), Imprinted polymers for chiral resolution of (±)-ephedrine. Part 2: probing pre-polymerization equilibria in different solvents by NMR, *Analyst*, **133**, pp. 1673-1683.

Ansell, R.J. and Wang, D.Y. (2009), Imprinted polymers for chiral resolution of (±)-ephedrine. Part 3: NMR predictions and HPLC results with alternative functional monomers, *Analyst*, **134**, pp. 564-576.

Arnold, B.R., Euler, A.C., Jenkins, A.L., Uy, O.M. and Murray, G.M. (1999), Progress in the Development of Molecularly Imprinted Polymer Sensors, Johns *Hopkins Apl Technical Digest*, **20**, pp. 190-198.

Arslan, M., Yigitoglu, M. and Soysal, A. (2006), Removal of Chromium(VI) from Aqueous Solutions Using Poly(4-vinyl pyridine) Beads, *Journal of Applied Polymer Science*, **101**, pp. 2865-2870.

Atia, A.A. (2005), Studies on the interaction of mercury(II) and uranyl(II) with modified chitosan resins, *Hydrometallurgy*, **80**, pp. 13-22.

Australia's Uranium Mines, Available on: www.world-nuclear.org/info/ Australia_mines /emines.html, Accessed on 13/12/2012.

Bai, Y. and Bartkiewicz, B. (2009), Removal of Cadmium from Wastewater Using Ion Exchange Resin Amberjet 1200H Columns, *Polish Journal of Environmental Studies*, **18**, pp. 1191-1195.

Baes, C.F.J. and Mesmer, R.E. (1976), The hydrolysis of cations, Wiley-Interscience, *John Wiley & Sons, New York*, pp. 197-240.

Baker, H.M., Massadeh, A.M. and Younes, H.A. (2009), Natural Jordanian zeolite: removal of heavy metal ions from water samples using column and batch methods, *Environmental Monitoring and Assessment*, **157**, pp. 319-330.

Ball, J.W. and Nordstrom, D.K. (1998), Critical evaluation and selection of standard state thermodynamic properties for chromium metal and its aqueous ions, hydrolysis species, oxides, and hydroxides, *Journal of Chemical and Engineering Data*, **43**, pp. 895-918.

Bamgbose, J.T., Adewuyi, S., Bamgbose, O. and Adetoye, A.A. (2010), Adsorption kinetics of cadmium and lead by chitosan, *African Journal of Biotechnology*, **9**, pp. 2560-2565.

Barakat, M.A. and Sahiner, N. (2008), Cationic hydrogels for toxic arsenate removal from aqueous environment, *Journal of Environmental Management*, **88**, pp. 955-961.

Barkhordar, B. and Ghiasseddin, M. (2004), Comparison of Langmuir and Freundlich Equilibriums in Cr, Cu and Ni Adsorption by *Sargassum*, *Iranian Journal of Environmental Health, Science and Engineering*, **1**, pp. 58-64.

Bayramoglu, G. and Arica Y.M. (2008), Adsorption of Cr(VI) onto PEI immobilized acrylate-based magnetic beads: Isotherms, kinetics and thermodynamics study, *Chemical Engineering Journal*, **139**, pp. 20-28.

Bayramoglu, G. and Arica, M.Y. (2011), Synthesis of Cr(VI)-imprinted poly(4-vinyl pyridine-co-hydroxyethyl methacrylate) particles: Its adsorption propensity to Cr(VI), *Journal of Hazardous Materials*, **187**, pp. 213-221.

Berkowitz, J.B., Yamin, M. and Fuoss, R.M. (1958), The Flory Constants for Poly-4-vinylpyridine in Ethanol, *Journal of Polymer Science*, **XXVIII**, pp. 69-82.

Berto, S., Crea, F., Daniele, P.G., Gianguzza, A., Pettignano, A. and Sammartano, S. (2011), Advances in the investigation of dioxouranium(VI) complexes of interest for natural fluids, *Coordination Chemistry Reviews*, **256**, pp. 63-81.

Bicak, N. and Gazi, G. (2003), Quantitative Quaternization of Poly(4-Vinyl Pyridine), Journal of macromolecular science, *Part A-Pure and Applied Chemistry*, **40 A**, pp. 585-591.

Biffis, A., Dvorakova, G. and Falcimaigne-Cordin, A. (2012), Physical Forms of MIPs, *Topics in Current Chemistry*, **325**, pp. 29-82.

Biju, V.M., Gladis, J.M. and Rao, T.P. (2003), Effect of γ-irradiation of ion imprinted polymer (IIP) particles for the preconcentrative separation of dysprosium from other selected lanthanides, *Talanta*, **60**, pp. 747-754.

Birlik, E., Ersoz, A., Aqikkalp, E., Denizli, A. and Say, R. (2007), Cr(III)-imprinted polymeric beads: Sorption and preconcentration studies, *Journal of Hazardous Materials*, **B140**, pp. 110-116.

Bleise, A., Danesi, P.R. and Burkart, W. (2003), Properties, use and health effects of depleted uranium (DU): a general overview, *Journal of Environmental Radioactivity*, **64**, pp. 93-112.

Bolortamir, T. and Egashira, R. (2008), Removal of Hexavalent Chromium from Model Tannery Wastewater by Adsorption Using Mongolian Natural Zeolite, *Journal of Chemical Engineering of Japan*, **41**, pp. 1003-1009.

Bram, V., Chantal, B., Dries, H., Patrick, L., Miroslava, V., Katarina, S., Georgios, G. and Carlo, V. (2012), Removal of Molybdate Anions from Water by Adsorption on Zeolite-Supported Magnetite, *Water Environment Research*, **84**, pp. 753-760.

Brookins, D.G. (1988), The indoor radon problem: Studies in the Albuquerque, New Mexico area, *Environmental Geology and Water Sciences*, **12**, pp. 187-196.

Brooks, B.W. (2010), Suspension Polymerization Processes, *Chemical Engineering Technology*, **33**, pp. 1737-1744.

Brown, L.M. (1996), Removal of heavy metals from water with microalgal resins: Process development, *Water Treatment Technology Program Report*, **74**, pp. 1.

Brűggemann, O., Haupt, K., Ye, L., Yilmaz, E. and Mosbach, K. (2000), New configurations and applications of molecularly imprinted polymers, *Journal of Chromatography A*, **889**, pp. 15-24.

Brynda, M., Wesolowski, T.A. and Wojcichowski, K. (2004), Theoretical Investigation of the Anion Binding Affinities of the Uranyl Salophene Complexes, *Journal of Physical Chemistry A*, **108**, pp. 5091-5099.

Burda, C., Chen, X., Narayanan, R. and El-Sayed, M.A. (2005), Chemistry and properties of nanocrystals of different shapes, *Chemical Reviews*, **105**, pp. 1025-102.

Burke, N.A.D., Stöver, H.D.H. and Dawson, F.P. (2002), Magnetic Nanocomposites: Preparation and Characterization of Polymer-Coated Iron Nanoparticles, *Chemistry of Materials*, **14**, pp. 4752-4761.

Büttiker, R., Ebert, J., Hinderling, C. and Adlhart, C. (2011), Membranes for Specific Adsorption: Immobilizing Molecularly Imprinted Polymer Microspheres using Electrospun Nanofibers, *CHIMIA*: *International Journal for Chemistry*, **65**, pp. 182-186.

Büyüktiryaki, S., Say, R., Denizli, A. and Ersöz, A. (2007), Mimicking receptor for methylmercury preconcentration based on ion-imprinting, *Talanta*, **71**, pp. 699-705.

Cai, W. and Gupta, R.B. (2004), Molecularly-imprinted polymers selective for tetracycline binding, *Separation and Purification Technology*, **35**, pp. 215-221.

Camacho, L.M., Deng, S. and Parra, R.R. (2010), Uranium removal from groundwater by natural clinoptilolite zeolite: Effects of pH and initial feed concentration, *Journal of Hazardous Materials*, **175**, pp. 393-398.

Cammarota, V.A (1992), Commodity review in SME Mining Engineering Handbook, second edition (edited by Hartman, H.L.), pp. 70.

Campbell, S.E., Collins, M., Xie, L. and BelBruno, J.J. (2009), Surface morphology of spin-coated molecularly imprinted polymer films, *Surface and Interface Analysis*, **41**, pp. 347-356.

Cantrell, K.J., Kaplan, D.I. and Weitma, T.W. (1995), Zero-valent iron for the *in situ* remediation of selected metals in ground water, *Journal of Hazardous Materials*, **42**, pp. 201-212.

Caruso, U., Maria, D.A., Panunzi, B. and Roviello, A.J. (2002), Poly(4-vinylpyridine) as the host ligand of metal-containing chromophores for second-order nonlinear optical active materials, *Journal of Polymer Science Part A: Polymer Chemistry*, **40**, pp. 2987-2993.

Chanda, M. and Rempel, G.L. (1993), Selective chromate recovery with quaternized poly(4-vinylpyridine), *Reactive Polymers*, **21**, pp. 77-88.

Chatterjee, S. Sau, G.B. and Mukherjee, S.K. (2011), Bioremediation of Cr(VI) from Chromium-Contaminated Wastewater by Free and Immobilized Cells of *Cellulosimicrobium cellulans* KUCr3, *Bioremediation Journal*, **15**, pp. 173-180.

Chen, C.L., Wang, X.K. and Nagatsu, M. (2009), Europium Adsorption on Multiwall Carbon Nanotube/Iron Oxide Magnetic Composite in the Presence of Polyacrylic Acid, *Environmental Science and Technology*, **43**, pp. 2362-2367.

Chen, F., Wang, R. and Shi, Y. (2012), Molecularly imprinted polymer for the specific solid-phase extraction of kirenol from *Siegesbeckia pubescens* herbal extract, *Talanta*, **89**, pp. 505-512.

Chen, Y., Peng, D., Lin, D. and Luo, X. (2007), Preparation and magnetic properties of nickel nanoparticles *via* the thermal decomposition of nickel organometallic precursor in alkylamines, *Nanotechnology*, **18**, pp. 1-6.

Chen-Jen, L. (2002), The chemical transformation of chromium in natural waters-A model study, *Water, Air and Soil Pollution*, **139**, pp. 137-158.

Chen, Z., Yang, Q., Peng, K. and Guo, Y. (2011), Surface-Initiated Nitroxide Mediated Radical Polymerization of 4-Vinylpyridine on Magnetite Nanoparticles, *Journal of Applied Polymer Science*, **119**, pp. 3582-3590.

Chiarizia, R., Horwitz, E.P., Alexandratos, S.D. and Gula, M.J. (1997), Diphonixs resin: a review of its properties and applications, *Separation Science and Technology*, **32**, pp. 1-35.

Chin, S.F., Pang, S.C. and Tan, C.H. (2011), Green Synthesis of Magnetite Nanoparticles (*via* Thermal Decomposition Method) with Controllable Size and Shape, *Journal of Materials and Environmental Science*, **2**, pp. 299-302.

Choppin, G.R. (2006), Actinide speciation in aquatic systems, *Marine Chemistry*, **99**, pp. 83-92.

Chromite Mining in South Africa-Overview, Available from: http://www.mbendi.com/indy/ming/chrm/af/sa/p0005.htm, Accessed on 12/01/2013.

Clarke, J.H. and Parker, F.L. (2009), Uranium Recovery and Remediation of Uranium Mill Tailings: Russian and U.S. Experience. Cleaning Up Sites Contaminated with Radioactive Materials: International Workshop Proceedings.

Cui, H., Feng, Y., Ren, W., Zeng, T., Lv, H. and Pan, Y. (2009), Strategies of Large Scale Synthesis of Monodisperse Nanoparticles, *Recent Patents on Nanotechnology*, **3**, pp. 32-41.

Dang, F., Enomoto, N., Hojo, J. and Enpuku, K. (2008), A Novel Method to Synthesize Monodispersed Magnetite Nanoparticles, *Chemistry Letters*, **37**, pp. 530.

Daniel, S., Babu, P.E.J. and Rao, T.P. (2005), Preconcentrative separation of palladium(II) using palladium(II) ion-imprinted polymer particles formed with different quinoline derivatives and evaluation of binding parameters based on adsorption isotherm models, *Talanta*, **65**, pp. 441-452.

Daniel, S., Gladis, J.M. and Rao, T.P. (2003), Synthesis of imprinted polymer material with palladium ion nanopores and its analytical application, *Analytica Chimica Acta*, **488**, pp. 173-182.

Daniel, S., Rao, P.P. and Rao, T.P. (2005), Investigation of different polymerization methods on the analytical performance of palladium(II) ion imprinted polymer materials, *Analytica Chimica Acta*, **536**, pp. 197-206.

Daou, T.J., Pourroy, G., Bégin-Colin, S., Grenéche, J.M., Ulhaq-Bouillet, C., Legare, P., Bernhardt, P., Leuvrey, C. and Rogez, G. (2006), Hydrothermal Synthesis of Monodisperse Magnetite Nanoparticles, *Chemistry of Materials*, **18**, pp. 4399-4404.

Dautzenberg, H., Jaeger, W., Kötz, J., Philipp, B., Seidel, C.H. and Stscherbina, D. (1994), Synthesis of polyelectrolytes. Polyelectroytes: *Hanser/Gardner Publications Inc. Cincinnati*, pp. 9-86.

Dawson, W.J. (1988), Hydrothermal Synthesis of Advanced Ceramic Powders. *American Ceramic Society Bulletin*, **67**, pp. 1673.

de Faria, D.L.A., Silva, S.V. and de Oliveira, M.T. (1997), Raman microspectroscopy of some iron oxides and oxyhydroxides, *Journal of Raman Spectroscopy*, **28**, pp. 873-878.

De Flora, S., Camoirano, A., Bagnasco, M., Bennicelli, C., Corbett, G. E. and Kerger, B.D. (1997), Estimates of the chromium(VI) reducing capacity in human body compartments as a mechanism for attenuating its potential toxicity and carcinogenicity, *Carcinogenesis*, **18**, pp. 531-537.

De la Guardia, M. and Morales-Rubio, A. (2003), Sample Preparation of Trace Element Analysis, *Elsevier*, Chapter **35**, pp. 1115.

Demirbas, E., Kobya, M., Senturk, E. and Ozkan, T. (2004), Adsorption kinetics for the removal of chromium(VI) from aqueous solutions on the activated carbons prepared from agricultural wastes, *Water SA*, **30**, pp. 533-540.

Dhir, B. (2010), Use of aquatic plants in removing heavy metals from Wastewater, *International Journal of Environmental Engineering*, **2**, pp. 185-200.

Diehl, P. (2011), Uranium Mining and Milling Wastes: An Introduction, Available from: http://www.wise-uranium.org/uwai.html, Accessed on 11/11/2011.

Dimitrov, D. and Wysin, G. (1994), Effects of surface anisotropy on hysteresis in fine magnetic particles, *Physical review B Condensed matter*, **50**, pp. 3077-3084.

Duranoglu, D., Trochimczuk, A.W. and Beker, U. (2010), A comparison study of peach stone and acrylonitrile-divinylbenzene copolymer based activated carbons as chromium(VI) sorbents, *Chemical Engineering Journal*, **165**, pp. 56-63.

Dvorakova, G., Haschick, R., Chiad, K., Klapper, M., Müllen, K. and Biffis, A. (2010), Molecularly Imprinted Nanospheres by Nonaqueous Emulsion Polymerization, *Macromolecular Rapid Communications*, **31**, pp. 2035-2040.

DWA (Department of Water Affairs), 1999, Available from: http://www://dwaf.gov.za, Accessed: 3/02/2012.

Eisazadeh, H. (2008), Removal of Arsenic in Water Using Polypyrrole and its Composites, *World Applied Sciences Journal*, **3**, pp. 10-13.

El Ghandoor, H., Zidan, H.M., Khalil, M.M.H. and Ismail, M.I.M. (2012), Synthesis and Some Physical Properties of Magnetite (Fe_3O_4) Nanoparticles, *International Journal of Electrochemical Science*, **7**, pp. 5734-5745.

El-Khaiary, M.I. (2008), Least-squares regression of adsorption equilibrium data: comparing the options, *Journal of Hazardous Materials*, **158**, pp. 73-87.

El-Sayed, A.A. (2008), Kinetics and thermodynamics of adsorption of trace amount of uranium on activated carbon, *Radiochimica Acta*, **96**, pp. 481-486.

Erdem, E., Karapinar, N. and Donat, R. (2004), The removal of heavy metal cations by natural zeolites, *Journal of Colloid and Interface Science*, **280**, pp. 309-314.

Ersöz, A., Say, R. and Denizli, A. (2004), Ni(II) ion-imprinted solid-phase extraction and preconcentration in aqueous solutions by packed-bed columns, *Analytica Chimica Acta*, **502**, pp. 91-97.

Esfandyari-Manesh, M., Javanbakht, M., Atyabi, F., Badiei, A. and Dinarvand, R. (2011), Effect of porogenic solvent on the morphology, recognition and release properties of carbamazepine-molecularly imprinted polymer nanospheres, *Journal of Applied Polymer Science*, **121**, pp. 1118-1126.

Fan, P. and Wang, B. (2010), Regulatory Effects of Zn(II) on the Recognition Properties of Metal Coordination Imprinted Polymers, *Journal of Applied Polymer Science*, **116**, pp. 258-266.

Faraji, M., Yamini, Y. and Rezaee, M. (2010), Magnetic Nanoparticles: Synthesis, Stabilization, Functionalization, Characterization and Applications, *Journal of the Iranian Chemical Society*, **7**, pp. 1-37.

Farrel, J., Bostick, W.D., Jarabek, R.J. and Fiedor, J.N. (1999), Uranium removal from ground water using zero valent iron media, *Ground Water*, **37**, pp. 618-624.

Fasihi, J., Alahyari, S.A., Shamsipur, M., Sharghi, H. and Charkhi, A. (2011), Adsorption of uranyl ion onto an anthraquinone based ion-imprinted copolymer, *Reactive and Functional Polymers*, **71**, pp. 803-808.

Fendorf, S.E. (1995), Surface reactions of chromium in soils and water, *Geoderma*, **67**, pp. 55-71.

Fang, G.Z., Tan, J. and Yan, X.P. (2005), An ion-imprinted functionalized silica gel sorbent prepared by a surface imprinting technique combined with a sol-gel process for selective solid-phase extraction of cadmium(II), *Analytical Chemistry*, **77**, pp. 1734-1739.

Fang, J., Gu, Z., Gang, D., Liu, C., Ilton, E.S. and Deng, B. (2007), Cr(VI) Removal from Aqueous Solution by Activated Carbon Coated with Quaternized Poly(4-vinylpyridine), *Environmental Science and Technology*, **41**, pp. 4748-4753.

Fiedor, J.N., Bostick, W.D., Jarabek, R.J. and Farrel, J. (1998), Understanding the mechanism of uranium removal from ground water by zero valent iron using X-ray photoelectron spectroscopy, *Environmental Science and Technology*, **32**, pp. 1466-1473.

Finneran, K.T., Anderson, R.T., Nevin, K.P. and Lovley, D.R. (2002), Potential for bioremediation of uranium-contaminated aquifers with microbial U(VI) reduction, *Soil and Sediment Contamination*, **11**, pp. 339-357.

Finneran, K.T., Housewright, M.E. and Lovley, D.R. (2002), Multiple influences of nitrate on uranium solubility during bioremediation of uranium-contaminated subsurface sediments, *Environmental Microbiology*, **4**, pp. 510-516.

Finotelli, P.V., Sampaio, D.A., Morales, M.A., Rossi, A.M. and Rocha-Leão, M.H. (2008), Ca alginate as scaffold for iron oxide nanoparticles synthesis, *Brazilian Journal of Chemical Engineering*, **25**, pp. 759-764.

Florence, T.M. and Batley, G.E. (1980), Chemical speciation in natural waters, *Critical Review in Analytical Chemistry*, **9**, pp. 219-296.

Franco, V., Conde, C.F., Conde, A. and Kiss, L.F. (2005), Relationship between coercivity and magnetic moment of superparamagnetic particles with dipolar interaction, *Physical Review*, **72**, pp. 1-10.

Franzreb, M., Siemann-Herzberg, M., Hobley, T.J. and Thomas, O.R.T. (2006), Protein purification using magnetic adsorbent particles, *Applied Microbiology and Biotechnology*, **70**, pp. 505-516.

Fredrickson, J.K., Zachara, J.M., Kennedy, D.W., Duff, M.C., Gorby, Y.A., Li, S.M.W. and Krupka, K.M. (2000), Reduction of U(VI) in goethite (a-FeOOH) suspensions by a dissimilatory metal-reducing bacterium, *Geochimica et Cosmochimica Acta*, **64**, pp. 3085-3098.

Freethey, G.F., Naftz, D.L., Rowland, R.C. and Davis, J.A. (2002), Deep Aquifer Remediation Tools: Theory, Design, and Performance Modeling. In Handbook of Groundwater Remediation Using Permeable Reactive Barriers (ed. Naftz, D.L. Morrison, S.J. Davis, J.A. and Fuller, C.C.), *Academic Press*, pp. 133-163.

Frey, N.A., Peng, S., Cheng, K. and Sun, S. (2009), Magnetic nanoparticles: synthesis, functionalization, and applications in bioimaging and magnetic energy storage, *Chemical Society Reviews*, **38**, pp. 2532-2542.

Fu, F. and Wang, Q. (2011), Removal of heavy metal ions from wastewaters: A review, *Journal of Environmental Management*, **92**, pp. 407-418.

Fuller, C.C., Bargar, J.R. and Davis, J.A. (2003), Remediation of Uranium-contaminated Water at Fry Canyon, Utah, SSRL Science Highlight, Available from: http://www.ssrl.slac.stanford.edu/research/highlights_archive/u_haprb.html, Accessed on 23/03/2012.

Ganguly, R. (2005). Ferrofluid transport analysis for thermal, biomedical and mems applications. In Mechanical Engineering. University of Illinois at Chicago, Chicago.

Garg, U.K., Kaur, M.P., Garg, V.K. and Sud, D. (2007), Removal of hexavalent chromium from aqueous solution by agricultural waste biomass, *Journal of Hazardous Materials*, **140**, pp. 60-68.

Gascoyne, M. (1992), Geochemistry of the actinides and their daughters. In Uranium-series Disequilibrium: Applications to Earth, Marine, and Environmental Sciences, second edition (editors, Ivanovich, M. and Harmon, R.S.), *Clarendon Press*, pp. 34-61.

Gheju, M. and Balcu, I. (2011), Removal of chromium from Cr(VI) polluted wastewaters by reduction with scrap iron and subsequent precipitation of resulted cations, *Journal of Hazardous Materials*, **196**, pp. 131-138.

Ginder-Vogel, M., Wu, W., Carley, J., Jardine, P., Fendorf, S. and Criddle, C. (2006), *In Situ* Biological Uranium Remediation within a Highly Contaminated Aquifer, Available from: http://www-ssrl.slac.stanford.edu/research/highlights archive/u_remed.pdf, Accessed on 17/04/2012.

Gladis, J.M. and Rao, T.P. (2004), Effect of Porogen Type on the Synthesis of Uranium Ion Imprinted Polymer Materials for the Preconcentration/Separation of Traces of Uranium, *Microchimica Acta*, **146**, pp. 251-258.

Gladis, J.M. and Rao, T.P. (2003), Synthesis and Analytical Applications of Uranyl Ion Imprinted Polymer Particles, *Analytical Letters*, **36**, pp. 2107-2121.

Gómez, V. and Callao, M.P. (2006), Chromium determination and speciation since 2000, *Trends in Analytical Chemistry*, **25**, pp. 1006.

Gorby, Y.A. and Lovley, D.R. (1992), Enzymatic uranium precipitation, *Environmental Science and Technology*, **26**, pp. 205-207.

Grenthe, I., Fuger, J., Konings, R.J.M., Lemire, R.J., Muller, A.B., Nguyen-Trung, C. and Wanner, H. (1992), Chemical thermodynamics of uranium; North-Holland Elsevier Science Publishers B.V. Amsterdam.

Gu, B., Ku, Y.K. and Jardine, P.M. (2004), Sorption and binary exchange of nitrate, sulfate, and uranium on an anion-exchange resin, *Environmental Science and Technology*, **38**, pp. 3184-3188.

Gu, B., Liang, L., Dickey, M.J., Yin, X. and Dai, S. (1998), Reductive precipitation of uranium(VI) by zero-valent iron, *Environmental Science and Technology*, **32**, pp. 3366-3373.

Guillaumont, R., Fanghänel, T., Fuger, I., Grenthe, I., Neck, V., Palmer, D.A. and Rand, M.H. (2003), Update on the Chemical Thermodynamics of Uranium, Neptunium, Plutonium, Americium and Technetium, Elsevier Science.

Gupta, V.K., Agarwal, S. and Saleh, T.A. (2011), Chromium removal by combining the magnetic properties of iron oxide with adsorption properties of carbon nanotubes, *Water Research*, **45**, pp. 2207-2212.

Ha, N.T., Hai, N.H., Luong, N.H., Chau, N. and Chinh, H.D. (2008), Effects of the conditions of the microemulsion preparation on the properties of Fe_3O_4 nanoparticles, *VNU Journal of Science, Natural Sciences and Technology*, **24**, pp. 9-15.

Häfeli, U.O., Ciocan, R. and Dailey, J.P. (2002), Characterization of magnetic particles and microspheres and their magnetophoretic mobility using a digital microscopy method, *European Cells and Materials*, **3**, pp. 24-27.

Haginaka, J., Tabo, H. and Kagawa, C. (2008), Uniformly sized molecularly imprinted polymers for *d*-chlorpheniramine: Influence of a porogen on their morphology and enantioselectivity, *Journal of Pharmaceutical and Biomedical Analysis*, **46**, pp. 877-881.

Hagendorfer, H. and Goessler, W. (2008), Separation of chromium(III) and chromium(VI) by ion chromatography and an inductively coupled plasma mass spectrometer as element-selective detector, *Talanta*, **76**, pp. 656-661.

Halimoon, N. and Yin, R.G.S. (2010), Removal of Heavy Metals from Textile Wastewater using Zeolite, *Environment Asia*, **3**, pp. 124-130.

Hall, K.R., Eagleton, L.C., Acrivos, A. and Vermeulen, T. (1966), Pore and solid diffusion Kinetics in fixed bed adsorption under constant pattern conditions, *Industrial and Engineering Chemistry, Fundamentals*, pp. 212-223.

Haupt, K. Molecular imprinting technology and biomimetic polymers, Availalabe from: http://karstenolaf.free.fr/Imprinting.html, Accessed on 12/12/2012.

Haupt, K. and Belmont, A.S. (2008), Molecularly Imprinted Polymers as Recognition Elements in Sensors, Handbook of Biosensors and Biochips, Wiley-Interscience, Hoboken, NJ.

Haw, C.Y., Mohamed, F., Chia, C.H., Radiman , S., Zakaria, S., Huang, N.M. and Lim, H.N. (2010), Hydrothermal synthesis of magnetite nanoparticles as MRI contrast agents, *Ceramics International*, **36**, pp. 1417-1422.

Health Canada, (1999), "Uranium in Drinking Water," Document for Public Comment Prepared by Federal Provincial Subcommittee on Drinking Water.

Health Effects of Uranium Mining. Fact Sheet Uranium Mining 4. Available from: http://www.ippnw.org/pdf/uranium-factsheet4.pdf, Accessed on 02/11/2012.

Hu, M., Ji, R. and Jiang, J. (2010), Hydrothermal synthesis of magnetite crystals: From sheet to pseudo-octahedron, *Materials Research Bulletin*, **45**, pp. 1811-1815.

Huang, J.W., Blaylock, M.J., Pulnik, Y. and Ensley, B.D. (1998), Phytoremediation of Uranium-Contaminated Soils: Role of Organic Acids in Triggering Uranium Hyperaccumulation in Plants, *Environmental Science and Technology*, **32**, pp. 2004-2008.

Hyeon, T. (2002), Chemical synthesis of magnetic nanoparticles, *Chemical Communications*, pp. 927-934.

Idziak, I. (2010), Molecular imprinting-a way to make "Smart Polymers", Canadian Chemcial NewsJarvis, K.E., Gray, A.L. and Houk, R.S. (1992), Handbook of Inductively Coupled Plasma Mass Spectrometry. Chapman and Hall: New York.

Igwe, J.C. and Abia, A.A. (2006), A bioseparation process for removing heavy metals from waste water using biosorbents, *African Journal of Biotechnology*, **5**, pp. 1167-1179.

Ilhan, S., Nourbakhsh, M.N., Kilicarslan, S. and Ozdag, H. (2004), Removal of Chromium, Lead and Copper ions from industrial wastewaters by *Staphylococcus saprophyticus*, *Turkish Electronic Journal of Biotechnology*, **2**, pp. 50-57.

Inorganic Materials Chemistry, Core Module 7, Available from: http://www.york.ac.uk/media/chemistry/research/douthwaite/inorganic%20materials.pdf, Accessed on 23/01/1013.

Inoue, H., Fukke, H. and Katsumoto, M. (1990), Effect of polymer adsorbed layer on magnetic particle dispersion, *IEEE Transaction on magnetic*, **26**, pp. 75-77.

In Situ Leach (ISL) Mining of Uranium, World Nuclear Association, Available from: http://www.world-nuclear.org/info/inf27.htmlIn, Accessed on 13/04/2012.

Iwasaki, T., Kosaka, K., Yabuuchi, T., Watano, S., Yanagida, T. and Kawai, T. (2009), Novel mechanochemical process for synthesis of magnetite nanoparticles using co-precipitation method, *Advanced Powder Technology*, **20**, pp. 521-528.

Jerden, J.L. and Sinha, A.K. (2003), Phosphate based immobilization of uranium in an oxidizing bedrock aquifer, *Applied Geochemistry*, **18**, pp. 823-843.

Jiang, X., Jiang, N., Zhang, H. and Liu, M. (2007), Small organic molecular imprinted materials: their preparation and application, *Analytical and Bioanalytical Chemistry*, **389**, pp. 355-368.

Johnson, B.B. (1990), Effect of pH, Temperature, and Concentration on the Adsorption of Cadmium on Goethite, *Environmental Science and Technology*, **24**, pp. 112-118.

Junghans, M. and Helling, C. (1998), Historical Mining, uranium tailings and waste disposal at one site: Can it be managed? A hydrogeological analysis, in Tailings and Mine Waste '98, *Balkema, Rotterdam*, pp. 117-126.

Kabanov, V.A., Efendiev, A.A. and Orujev, D.D. (1979), Complex-forming polymeric sorbents with macromolecular arrangement favourable for ion sorption, *Journal of Applied Polymer Science*, **24**, pp. 259-267.

Kadirvelu, K., Thamaraiselvi, K. and Namasivayam, C. (2001), Removal of heavy metals from industrial wastewaters by adsorption onto activated carbon prepared from an agricultural solid waste, *Bioresource Technology*, **76**, pp. 63-65.

Kala, R., Biju, V.M. and Rao, T.P. (2005), Synthesis, characterization, and analytical applications of erbium (III) ion imprinted polymer particles prepared via γ-irradiation with different functional and crosslinking monomers, *Analytica Chimica Acta*, **549**, pp. 51-58.

Kala, R., Gladis, J.M and Rao, T.P. (2004), Preconcentrative separation of erbium from Y, Dy, Ho, Tb and Tm by using ion imprinted polymer particles via solid phase extraction, *Analytica Chimica Acta*, **518**, pp. 143-150.

Kalfas, G., Yuan, H. and Ray, W.H. (1993), Modeling and Experimental Studies of Aqueous Suspension Polymerization Processes. Experiments in Batch Reactors, *Industrial & Engineering Chemistry Research*, **32**, pp. 1831-1838.

Kan, X.W., Zhao, Q., Shao, D.L., Geng, Z.R., Wang, Z.L. and Zhu, J. (2010), Preparation and Recognition Properties of Bovine Hemoglobin Magnetic Molecularly Imprinted Polymers, *Journal of Physical Chemistry B*, **114**, pp. 3999-4004.

Kannan, K. (1995), In Fundamentals of Environmental Pollution, S. Chand & Co., New Delhi, 1995.

Karim, K., Breton, F., Rouillon, R., Piletska, E.V., Guerreiro, A., Chianella, I. and Piletsky, S.A. (2005), How to find effective functional monomers for effective molecularly imprinted polymers? *Advanced Drug Delivery Reviews*, **57**, pp. 1795-1808.

Katz, S.A. and Salem, H. (1992), The toxicology of chromium with respect to its chemical speciation: A review, *Journal of Applied Toxicology*, **13**, pp. 217-224.

Kelvin, B., Gregor, Y. and Lovely, D.R. (2005), Remediation and Recovery of Uranium from Contaminated Subsurface Environments with Electrodes, *Environmental Science and Technology*, **39**, pp. 8943-8947.

Kilislioglu, A. and Bilgin, B. (2003), Thermodynamic and kinetic investigations of uranium adsorption on amberlite IR-118H resin, *Applied Radiation and Isotopes*, **58**, pp. 155-160.

Kim, D., Mikhaylova, M., Zhang, Y. and Muhammed, M. (2003), Protective Coating of Superparamagnetic Iron Oxide Nanoparticles, *Chemistry of Materials*, **15**, pp. 1617-1627.

Kinniburgh, D.G. (1986), General Purpose Adsorption Isotherms, *Environmental Science and Technology*, **20**, pp. 895-904.

Khan, N.A., Ibrahim, S. and Subramaniam, P. (2004), Elimination of Heavy Metals from Wastewater Using Agricultural Wastes as Adsorbents, *Malaysian Journal of Science*, **23**, pp. 43-51.

Konstantinou, M., Demetriou, A. and Pashalidis, I. (2007), Adsorption of hexavalent uranium on Dunite, *Global NEST Journal*, **9**, pp. 229-236.

Kosa, S.A., Al-Zhrani, G. and Salam, M.A. (2012), Removal of heavy metals from aqueous solutions by multi-walled carbon nanotubes modified with 8-hydroxyquinoline, *Chemical Engineering Journal*, **181-182**, pp. 159-168.

Kot, A. and Namiesnèik, J. (2000), The role of speciation in analytical chemistry *Trends in analytical chemistry*, **19**, pp. 69-79.

Kotas, J. and Stasicka Z. (2000), Chromium occurrence in the environment and methods of its speciation, *Environmental Pollution*, **107**, **pp.** 263-283.

Kotrba, P., Mackova, M. and Macek, T. (2011), Microbial Biosorption of metals, *Springer*, pp. 26-27.

Koutzarova, T., Kolev, S., Ghelev, C., Paneva, D. and Nedkov, I. (2006), Microstructural study and size control of iron oxide nanoparticles produced by microemulsion technique, *Physica Status Solidi*, **5**, pp. 1302-1307.

Krachler, M. and Carbol, P. (2011), Validation of isotopic analysis of depleted, natural and enriched uranium using high resolution ICP-OES, *Journal of Analytical Atomic Spectrometry*, **26**, pp. 293-299.

Krishna, P., Gladis, J.M., Rao, T.P. and Naidu, G.R.K. (2005), Selective recognition of neodymium (III) using ion imprinted polymer particles, *Journal of Molecular Recognition*, **18**, pp. 109-116.

Kugimiya, A., Kuwada, Y. and Takeuchi, T. (2001), Preparation of sterol-imprinted polymers with the use of 2-(methacryloyloxy)ethyl phosphate, *Journal of Chromatography A*, **938**, pp. 131-135.

Kumar, P.S. and Kirthika, K. (2009), Equilibrium and kinetic study of adsorption of Nickel from aqueous solution onto Bael leaf powder, *Journal of Engineering Science and Technology*, **4**, pp. 351-363.

Kuntakapun, J., Chungsiriporn, J., Hussai+.H. and Intamanee, J. (2010), Adsorption of Zn(II) Metal Ion from an Aqueous Solution Using Tea Waste Char, The Eighth PSU Engineering Conference.

Landfester, K. (2001), The Generation of Nanoparticles in Miniemulsions, *Advanced Materials*, **13**, pp. 765-768.

Langard, S. and Norseth, T. in Friberg, L., Nordberg, G.F. and Vouk, V.B. (Editors), (1990), Handbook on the Toxicology of Metals, Vol. II, Specific Metals, Elsevier, Amsterdam, 2nd ed., pp. 185-210.

Langmuir, D. (1978), Uranium solution-mineral equilibria at low temperature with applications to sedimentary ore deposits, *Geochimica et Cosmochimica Acta*, **42**, pp. 547-569.

Laurent, S., Forge, D., Port, M., Roch, A., Robic, C., Vander Elst, L. and Muller, R.N. (2008), Magnetic iron oxide nanoparticles: synthesis, stabilization, vectorization, physicochemical characterizations, and biological applications, *Chemical Reviews*, **108**, pp. 2064-2110.

Lanza, F. and Sellergren, B. (2004), Molecularly Imprinted Polymers *via* High-Throughput and Combinatorial Techniques, *Macromolecular Rapid Communications*, **25**, pp. 59-68.

Lewinsky, A.A. (2007), Hazardous Materials and Wastewater, Treatment, Removal and Analysis, Nova Science Publishers, Inc. New York.

Li, H., Li, Z., Liu, T., Xiao, X., Peng, Z. and Deng, L. (2008), A novel technology for biosorption and recovery hexavalent chromium in wastewater by biofunctional magnetic beads, *Bioresource Technology*, **99**, pp. 6271-6279.

Li, F.T., Li, X., Zhang B.R. and Ouyang, Q.H. (2004), Removal of Heavy Metals in Effluent by Adsorption and Coagulation, *Chinese Chemical Letters*, **15**, pp. 83-86.

Li, Y., Yang, M.J. and She, Y. (2005), Humidity sensitive properties of cross-linked and quaternized poly(4-vinylpyridine-co-butyl methacrylate), *Sensor and Actuators B: Chemical*, **107**, pp. 252-257.

Liao, S. and Chang, A.W. (2004), Heavy Metal Phytoremediation by Water Hyacinth at Constructed Wetlands in Taiwan, *Journal of Aquatic Plant Management*, **42**, pp. 60-68.

Lin, T.W. and Huang, S.D. (2001), Direct and simultaneous determination of copper, chromium, aluminum, and manganese in urine with a multielement graphite furnace atomic absorption spectrometer, *Analytical Chemistry*, **73**, pp. 4319-4325.

Liu, Y., Cao, X., Le, Z., Luo, M., Xu, W. and Huang, G. (2010), Pre-concentration and determination of trace uranium(VI) in environments using ion-imprinted chitosan resin *via* solid phase extraction, *Journal of the Brazilian Chemical Society*, **21**, pp. 533-540.

Liu. Y., Chang, X., Yang, D., Guo, Y. and Meng, S. (2005), Highly selective determination of inorganic mercury(II) after preconcentration with Hg(II)-imprinted diazoaminobenzene-vinylpyridine copolymers, *Analytica Chimica Acta*, **538**, pp. 85-91.

Lodhia, J., Mandarano, G., Ferris, N.J. and Cowell, S.F. (2010), Development and use of iron oxide nanoparticles (Part 1): Synthesis of iron oxide nanoparticles for MRI, *Biomedical Imaging and Intervention Journal*, **6**, pp. 1-10.

Lofgreen, J.E., Moudrakovski, I.L. and Ozin, G.A. (2011), Molecularly Imprinted Mesoporous Organosilica, *American Chemical Society Nano*, **5**, pp. 2277-2287.

Lone, M.I., He, Z., Stoffella, P.J. and Yang, X. (2008), Phytoremediation of heavy metal polluted soils and water: Progresses and perspectives, *Journal of Zhejiang University science B*, **9**, pp. 210-220.

Lovley, D.R., Phillips, E.J.P., Gorby, Y.A. and Landa, E.R. (1991), Microbial reduction of uranium, *Nature*, **350**, pp. 413-416.

Lowry, J.D. and Lowry, S.B. (1988), Radionuclides in drinking water, *Journal of the American Water Works Association*, **80**, pp. 51-64.

Lu, Y., Yin, Y., Mayers, B.T. and Xia, Y. (2002), Modifying the Surface Properties of Superparamagnetic Iron Oxide Nanoparticles through A Sol-Gel Approach, *Nano letters*, **2**, pp. 183-186.

Lu, S. and Forcada, J. (2006), Preparation and Characterization of Magnetic Polymeric Composite Particles by Miniemulsion Polymerization, *Journal of Polymer Science*, **44**, pp. 4187-4203.

Luo, X., Luo, S., Zhan, Y., Shu, H., Huang, Y. and Tu, X. (2011), Novel Cu (II) magnetic ion imprinted materials prepared by surface imprinted technique combined with a sol-gel process, *Journal of Hazardous Materials*, **192**, pp. 949-955.

Ma, W., Xu, S., Li, J., Lin., Y. and Wang, C. (2011), Hydrophilic Dual-Responsive Magnetite/PMAA Core/Shell Microspheres with High Magnetic Susceptibility and pH Sensitivity via Distillation-Precipitation Polymerization, *Journal of Polymer Science Part A: Polymer Chemistry*, **49**, pp. 2725-2733.

Maarof, H.I. and Hameed, B.H. (2004), Adsorption Isotherms for Phenol Onto Activated Carbon, *Asean Journal of Chemical Engineering*, **4**, pp. 70-76.

Maity, D., Kale, S.N., Kaul-Ghanekar, R., Xue, J. and Ding, J. (2009), Studies of magnetite nanoparticles synthesized by thermal decomposition of iron (III) acetylacetonate in tri (ethyleneglycol), *Journal of Magnetism and Magnetic Materials*, **321**, pp. 3093-3098.

Makovec, D., Košaka, A., Žnidaršič, Z. and Drofenik, M. (2005), The synthesis of spinel-ferrite nanoparticles using precipitation in microemulsions for ferrofluid applications, *Journal of Magnetism and Magnetic Materials*, **289**, pp. 32-35

Manual of Acid ISL Uranium mining technology, International Atomic Energy Agency, 2001

Martin-Esteban, A. (2010), Molecular Imprinting. *SciTopics*, Available from: http://www.scitopics.com/Molecular_Imprinting.html, Accessed on 05/04/2012.

Masamoto, R.M., Wataxabe, M. and Colemax, B.D. (1960), Quaternization Kinetics of Poly-4-Vinylpyridine, *Journal of Polymer Science*, **XVLIII**, pp. 5-15.

Matijevic, E. and Hsu, W.P. (1987), Preparation and Properties Monodispersed Colloidal Particles of Lanthanide Compounds 1. Gadolinium, Europium, Terbium, Samarium, and Cerium (III), *Journal of Colloid and Interface Science*, **118**, pp. 506.

Matsuno, R., Yamamoto, K., Otsuka, H. and Takahara, A. (2003), Polystyrene-Grafted Magnetite Nanoparticles Prepared through Surface-Initiated Nitroxyl-Mediated Radical Polymerization, *Chemistry of Materials*, **15**, pp. 3-5.

Matsui, J., Nicholls, I.A., Takeuchi, T., Mosbach, K. and Karubea, I. (1996), Metal ion mediated recognition in molecularly imprinted polymers, *Analytica Chimica Acta*, **335**, pp. 71-77.

Maximizing South Africa's chrome ore endowment to create jobs and drive sustainable, GROWTH: http://www.meraferesources.co.za/wp-content/uploads /2012/03/chrome_ore_brochure.pdf.

Mayes, A.G. and Whitcombe, M.J. (2005), Synthetic strategies for the generation of molecularly imprinted organic polymers, *Advanced Drug Delivery Reviews*, **57**, pp. 1742-1778.

Meinrath, A., Schneider, P. and Meinrath, G. (2003), Uranium ores and depleted uranium in the environment - with a reference to uranium in the biosphere from

the Erzgebirge / Sachsen, Germany, *Journal of Environmental Radioactivity*, **64**, pp. 175-193.

Metilda, P., Gladis, J.M. and Rao, T.P. (2004), Influence of binary/ternary complex of imprint ion on the preconcentration of uranium(VI) using ion imprinted polymer materials, *Analytica Chimica Acta*, **512**, pp. 63-73.

Meunier, N., Drogui, P., Montan, C., Hausler, R., Mercier, G. and Blais, J. (2006), Comparison between electrocoagulation and chemical precipitation for metals removal from acidic soil leachate, *Journal of Hazardous Materials*, **B137**, pp. 581-590.

Mier, M.V., Callejas, R.L.P., Gehr, R., Cisneros, B.E.J.N. and Alvarez, P.J.J. (2001), Heavy metal removal with Mexican clinoptilolite: Multi-component ionic exchange, *Water Research*, **35**, pp. 373-378.

Milgram, S., Carrière, M., Thiebault, C., Malaval, L. and Gouget, B. (2008), Cytotoxic and phenotypic effects of uranium and lead on osteoblastic cells are highly dependent on metal speciation, *Toxicology*, **250**, pp. 62-69.

Milja, T.E, Prathish, K.P. and Rao, T.P. (2011), Synthesis of surface imprinted nanospheres for selective removal of uranium from simulants of Sambhar salt lake and ground water, *Journal of Hazardous Materials*, **188**, pp. 384-390.

Mining industry of South Africa Available from: http://en.wikipedia.org/wiki/Mining_industry_of_South_Africa#Chromium, Accessed on 12/01/2013.

Mirsky, V. and Yatsimirsky, A. (2011). Artificial receptors for chemical sensors. Wiley-VCH Verlag and Co. KGaA, pp. 402-403.

Mishra, R., Sinha, V., Kannan, A. and Upreti, R.K. (2012), Reduction of Chromium(VI) by Chromium Resistant Lactobacilli: A Prospective Bacterium for Bioremediation, *Toxicology International*, **19**, pp.25-30.

Mkandawire, M., Taubert, B. and Dudel E.G. (2004), Capacity of *Lemna gibba L*. (duckweed) for uranium and arsenic phytoremediation in mine tailing waters, *International Journal of Phytoremediation*, **6**, pp. 347-62.

Moad, G. and Solomon, D.H. (1995), The Chemistry of Free Radical Polymerization, Pergamon, Oxford.

Mohajeri, S.A., Karimi, G., Aghamohammadian, J. and Khansari, M.R. (2011), Clozapine Recognition *via* Molecularly Imprinted Polymers; Bulk Polymerization Versus Precipitation Method, *Journal of Applied Polymer Science*, **121**, pp. 3590-3595.

Mohapatra, M. and Anand, S. (2010), Synthesis and applications of nano-structured iron oxides/hydroxides-a review, *International Journal of Engineering, Science and Technology*, **2**, pp. 127-146.

Montgomery, C.W. (1995), Environmental geology, fourth edition, WCB Inc., Iowa, USA, pp. 344-345.

Moradi, O., Zare, K. and Yari. M. (2011), Interaction of some heavy metal ions with single walled carbon nanotube, *International Journal of Nano Dimension*, **1**, pp. 203-220.

Moreno-Bondi, M.C., Navarro-Villoslada, F., Benito-Peña, E. and Urraca, J.L. (2008), Molecularly Imprinted Polymers as Selective Recognition Elements in Optical Sensing, *Current Analytical Chemistry*, **4**, pp. 316-340.

Morrison, S.J. and Spangler, R.R. (1992), Chemical barriers for controlling groundwater contamination, *Environmental Progress*, **12**, pp. 175-181.

Mosbach, K. The Technique of Molecular Imprinting and Applications of the Imprinted Resulting Materials in Various Areas Molecular Imprinting-Principle Available from, http://www.klausmosbach.com/Principlemolecularimprinting .htm , Accessed on 11/01/2013.

Mosha, D.M.S. and Mkayula, L.L. (2005), Metal ion sequestration: An exciting dimension for molecularly imprinted polymer technique, *Tanzania Journal of Science*, **31**, pp. 91-98.

Murray, G.M. and Southard, G.E. (2002), Molecularly Imprinted lonomers, *Materials Research Society Symposium Proceedings*, **723**, pp. 67-76.

Naidoo, B. (2009), Acid mine drainage single most significant threat to South Africa's environment, Mining weekly. com. Available from: http://www.miningweekly.com/article/in-the-midst-of-a-disaster-2009-05-08, Accessed on 21/12/2011.

Naidoo, B. (2010), "Acid mine drainage single most significant threat to South Africa's environment" Mining Weekly, 8 May 2010, *http://www.miningweekly.com*.

Namasivayam, C. and Sureshkumar M.V. (2008), Removal of chromium(VI) from water and wastewater using surfactant modified coconut coir pith as a biosorbent, *Bioresource Technology*, **99**, pp. 2218-2225.

Nameni, M., Alavi, M. R. and Arami, M. (2008), Adsorption of hexavalent chromium from aqueous solutions by wheat bran, *International Journal of Environmental Science and Technology*, **5**, pp. 161-168.

Nan, A., Turcu, M.R., Bratu, I., Leostean, C., Chauvet, O., Gautron, E. and Liebscher, J. (2010), Novel magnetic core-shell Fe_3O_4 polypyrrole nanoparticles functionalized by peptides or albumin, *Greneral Papers*, *ARKIVOC*, pp. 185-198.

Nanostructured Materials and Interfaces, Lecture notes, Available from: http://www.chem.wisc.edu/courses/801/Spring00/chemlecnotes/chemln5.html, Accessed on 22/01/2013.

Nassar, N. and Husein, M. (2005), Preparation of iron oxide nanoparticle from $FeCl_3$ solid powder using microemulsions. *Poster presentation.*

NCRP (National Council on Radiation Protection and Measurements), 1999. Biological Effects and Exposure Limits for 'Hot Particles'. NCRP-Report 130.

Neagua, V. and Mikhalovsky, S. (2010), Removal of hexavalent chromium by new quaternized cross-linked poly(4-vinylpyridines), *Journal of Hazardous Materials*, **183**, pp. 533-540.

Nieboer, E. and Jusys, A.A. (1988), Biologic chemistry of chromium, In: Nriagu, J.O. and Nieboer, E. (Eds.), Chromium in Natural and Human Environments, (Wiley Interscience, New York), pp. 21-81.

Nishide, H., Deguchi, J. and Tsuchida, E. (1976), Selective adsorption of metal ions on cross-linked poly(vinylpyridine) resin prepared with a metal ion as a template, *Chemistry Letters*, **5**, pp. 169-174.

Niu, H., Wang, Y., Zhang, X., Meng, Z. and Cai, Y. (2012), Easy Synthesis of Surface-Tunable Carbon-Encapsulated Magnetic Nanoparticles: Adsorbents for Selective Isolation and Preconcentration of Organic Pollutants, *American Chemical Society Applied Materials and Interfaces*, **4**, pp. 286-95.

Nomanbhay, S.M. and Palanisamy, K. (2005), Removal of heavy metals from industrial wastewater using chitosan coated oil palm shell charcoal, **8**, *Environmental Biotechnology*, pp. 43-53.

Nuclear Cleanup Issues, Nuclear Waste Storage Issues, Available from: http://jan.ucc.nau.edu/~doetqpp/courses/env440/env440_2/lectures/lec4/lec4.ht, Accessed on 14/07/2012.

Ochieng, G.M., Seanego, E.S. and Nkwonta, E.I. (2010), Impacts of mining on water resources in South Africa, *Scientific Research and Essays*, **22**, pp. 3351-3357.

Ohmori, M. and Matijevic, E. (1992), Preparation and properties of uniform coated colloidal particles. VII. Silica on hematite, *Journal of Colloid and Interface Science*, **150**, pp. 594-598.

Olazabal., M.A., Nikolaidis, N.P., Suib, S.A. and Madariaga, J.M. (1997), Precipitation Equilibria of the Chromium(VI)/Iron(III) System and Spectrospcopic Characterization of the Precipitates, *Environmental Science and Technology*, **31**, pp. 2898-2902.

Oliveira, L.C.A., Petkowicz, D.I., Smaniotto, A. and Pergher, S.B.C. (2004), Magnetic zeolites: a new adsorbent for removal of metallic contaminants from water, *Water research*, **38**, pp. 3699-3704.

Ortiz-Palacios, J., Cardoso, J. and Manero, O. (2008), Production of Macroporous Resins for Heavy-Metal Removal. I. Nonfunctionalized Polymers, *Journal of Applied Polymer Science*, **107**, pp. 2203-2210.

Otton, J.K. (1992), The geology of radon. Washington, DC: US Geological Survey.

Pakade, V.E. (2012), Development and application of imprinted polymers selective adsorption of metal ions and flavonols in complex samples, A Thesis submitted to the Faculty of Science, University of the Witwatersrand, Johannesburg, in fulfilment of the requirements for the degree of Doctor of Philosophy.

Pakade, V.E., Cukrowska, E., Darkwa, J., Torto, N. and Chimuka, L. (2011), Selective removal of chromium(VI) from sulphates and other metal anions using an ion-imprinted polymer, *Water SA*, **37**, pp. 529-537.

Pakalns, P. (1980), Separation of uranium from natural waters on Chelex-100 resin, *Analytica Chimica Acta*, **120**, pp. 289-296.

Pan, J., Yao, H., Xu, L., Ou, H., Huo, P., Li, X. and Yan, Y. (2011), Selective Recognition of 2,4,6-Trichlorophenol by Molecularly Imprinted Polymers Based on Magnetic Halloysite Nanotubes Composites, *Journal of Physical Chemistry*, **115**, pp. 5440-5449.

Panichev, N., Mabasa, W., Ngobeni, P., Mandiwana, K. and Panicheva, S. (2008), The oxidation of Cr(III) to Cr(VI) in the environment by atmospheric oxygen during the bush fires, *Journal of Hazardous Materials*, **153**, pp. 937-941.

Pankhurst, Q.A., Connolly, J., Jones, S.K. and Dobson, J.J. (2003), Applications of magnetic nanoparticles in biomedicine, *Journal of Physics D: Applied Physics*, **36**, pp. R167-R181.

Park, J., Lee, E., Hwang, N.M., Kang, M., Kim, S.C., Hwang, Y., Park, J.G., Noh, H.J., Kim, J.Y., Park, J.H. and Hyeon, T. (2005), One-Nanometer-Scale Size-Controlled Synthesis of Monodisperse Magnetic Iron Oxide Nanoparticles, *Angewandte Chemie International Edition*, **44**, pp. 2872-2877.

Park, J.K. and Seo, J. (2002), Characteristics of Phenylalanine Imprinted Membrane Prepared by the Wet Phase Inversion Method, *Korean Journal of Chemical Engineering*, **19**, pp. 940-948.

Parka, D., Yun, Y., Joa, J.H. and Parka, J.M. (2005), Mechanism of hexavalent chromium removal by dead fungal biomass of *Aspergillus niger*, *Water Research*, **39**, pp. 533-540.

Paustenbach, D.J., Finley, B.L., Mowat, F.S. and Kerger, B.D. (2003), Human health risk and exposure assessment of chromium(VI) in tap water, *Journal of Toxicology and Environmental Health, Part A*, **66**, pp. 1295-1339.

Pavel, L.V., Cretescu, I. and Gavrilescu, M. (2009), Characterization and remediation of soils contaminated with uranium, *Journal of Hazardous Materials*, **163**, pp. 475-510.

Pavlović, J., Stopić, S., Friedrich, B. and Kamberović, Z. (2007), Selective removal of heavy metals from metal-bearing wastewater in a cascade line reactor, *Environmental Science and Pollution Research International*, **14**, pp. 518-522.

Pérez, N., Whitcombe, M.J. and Vulfson, E.N. (2000), Molecularly imprinted nanoparticles prepared by core-shell emulsion polymerization, *Applied Polymer Science*, **77**, pp. 1851-1859.

Petruzelli, D., Passino, R. and Tiravanti, G. (1995), Ion exchange process for chromium removal, recovery from tannery wastes, *Industrial and Engineering Chemistry Research*, **34**, pp. 2612-2617.

Philippova, O., Barabanova, A., Molchanov, V. and Khokhlov, A. (2011), Magnetic polymer beads: Recent trends and developments in synthetic design and applications, *European Polymer Journal*, **47**, pp. 542-559.

Pichon, V. and Chapuis-Hugon, F. (2008), Role of molecularly imprinted polymers for selective determination of environmental pollutants, *Analytica Chimica Acta*, **622**, pp. 48-61.

Polacco, G., Basile, C., Palla, M. and Semino, D. (2000), A simple technique for measuring particle size distributions during suspension polymerization, *Polymer Journal*, **32**, pp. 688-693.

Polti, M.A., García, R.O., Amoroso, M.J. and Abate, C.M. (2009), Bioremediation of chromium(VI) contaminated soil by *Streptomyces sp.* MC1, *Journal of Basic Microbiology*, **49**, pp. 285-292.

Pourbaix, M. (1966), Atlas of Electrochemical Equilibriua. Oxford: Pergamon Press.

Preetha. C.R., Gladis, J.M., Rao, T.P. and Venkateswaran, G. (2006), Removal of toxic uranium from synthetic nuclear power reactor effluents using uranyl ion imprinted polymer particles, *Environmental Science and Technology*, **140**, pp. 3070-3074.

Pyrzyńska, K. and Bystrzejewski, M. (2010), Comparative study of heavy metal ions sorption onto activated carbon, carbon nanotubes, and carbon-encapsulated

magnetic nanoparticles, *Colloids and Surfaces A: Physicochemical and Engineering Aspects*, **362**, pp. 102-109.

Qdaisa, H.A. and Moussab, H. (2004), Removal of heavy metals from wastewater by membrane processes: a comparative study, *Desalination*, **164**, pp. 105-110.

Qi, J., Li, X., Li, Y., Zhu, J. and Qiang, L. (2008), Selective removal of Cu(II) from contaminated water using molecularly imprinted polymer, *Frontiers of Chemical Engineering in China*, **2**, pp. 109-114.

Qi, P., Wang, J., Wang, L., Li,Y., Jin, J., Su, F., Tian, Y. and Chen, J. (2010), Molecularly imprinted polymers synthesized *via* semi-covalent imprinting with sacrificial spacer for imprinting phenols, *Polymer*, **51**, pp. 5417-5423.

Qian, Z., Zhang, Z. and Chen, Y. (2008), A novel preparation of surface-modified paramagnetic magnetite/polystyrene nanocomposite microspheres by radiation-induced miniemulsion polymerization, *Journal of Colloid and Interface Science*, **327**, pp. 354-361.

Radiation Effects - Effects by Radionuclides, Available from: http://hps.org/publicinformation/ate/q754.html, Accessed on 02/12/2010.

Ramakrishna, S., Fujihara, K., Teo, W., Yong, T., Ma, Z. and Ramaseshan, R. (2006), Electrospun nanofibres: *Solving Global Issues*, *Materials Today*, **9**, pp. 40-50.

Ramakrishnaiah, C.R. and Prathima, B. (2012), Hexavalent chromium removal from industrial watsewater by chemical precipitation method, *International Journal of Engineering Research and Research and Applications*, **2**, pp. 599-603.

Rana, M.S., Halim, M.A., Safiullah, S., Mollah, M.M., Azam, M.S., Goni, M.A., Hossain, M.K. and Rana, M.M. (2009), Removal of Heavy Metal from Contaminated Water by Biopolymer Crab Shell Chitosan, *Journal of Applied Sciences*, **9**, pp. 2762-2769.

Rao, T.P., Daniel, S. and Gladis, J.M. (2004), Tailored materials for preconcentration or separation of metals by ion-imprinted polymers for solid-phase extraction (IIP-SPE) *Trends in Analytical Chemistry*, **23**, pp. 28-35.

Rao, T.P., Kala, R. and Daniel, S. (2006), Review: Metal ion-imprinted polymers-Novel materials for selective recognition of inorganics, *Analytica Chimica Acta*, **578**, pp. 105-116.

Rao, T.P., Praveen, R.S. and Daniel, S. (2004), Styrene-Divinylbenzene Copolymers: Synthesis, Characterization, and Their Role in Inorganic Trace Analysis, *Critical Reviews in Analytical Chemistry*, **34**, pp. 177-193.

Raskin, I., Smith, R.D and Salt, D.E. (1997), Phytoremediation of metals: using plants to remove pollutants from the environment, *Current Opinion in Biotechnology*, **8**, pp. 221-226.

Ravikumar, C. and Bandyopadhyaya, R. (2011), Mechanistic Study on Magnetite Nanoparticle Formation by Thermal Decomposition and Coprecipitation Routes, *Journal of Physical Chemistry C*, **115**, pp. 1380-1387.

Rekacewic, P. (2005), Mining effects on rainfall drainage, Available from: http://www.grida.no/graphicslib/detail/mining-effects-on-rainfall-drainage_cac4, Accessed on 26/01/2013.

Revathi, K., Haribabu, T.E. and Sudha, P.N. (2011), Phytoremediation of chromium contaminated soil using Sorghum plant, *International Journal of Environmental Sciences*, **2**, pp. 417-428.

Richard, F.C. and Bourg, A.C.M. (1991), Aqueous geochemistry of chromium: a review, *Water Research*, **25**, pp. 807-816.

Richardson, C.J. (1988), Constructed wetland in water pollution progem press. New York, NY.605 p reports no 212.

Riley, R.G. and Zachara, J.M. (1992), U.S. Department of Energy, Office of Energy Research, *Subsurface Science Program*: Washington, DC, pp. 1-71.

Riva, B.L., Peric, I.V., Villegas, S. and Ruf, B. (2008), Binding of uranyl ions by water-insoluble polymers containing miltiligand groups, *Journal of the Chilean Chemical Society*, **53**, pp. 1356- 1359.

Roca, A.G., Niznansky, D., Poltierova-Vejpravova, J., Bittova, B., González-Fernández, M.A., Serna, C.J. and Morales, M.P. (2009), Magnetite nanoparticles with no surface spin canting, *Journal of Applied Physics*, **105**, 114309, pp. 1-7.

Roonasi, P. (2007), Adsorption and Surface Reaction Properties of Synthesized Magnetite Nano-Particles, Division of Chemistry Department of Chemical Engineering and Geosciences, Luleå University of Technology S-971 87 Luleå, Sweden.

Rosatzin, T., Andersson, L.T., Simon, W. and Mosbach, K. (1991), Preparation of Ca^{2+} selective sorbents by molecular imprinting using polymerizable ionophores, *Journal of the Chemical Society*, *Perkin Transactions 2*, **0**, pp. 1261-1265.

Saad, D.M.G., Cukrowska, E.M. and Tutu, H. (2012), Phosphonated cross-linked polyethylenimine for selective removal of uranium ions from aqueous solutions, *Water Science and Technology*, **66**, pp. 122-129.

Sadeghi, S. and Aboobakri, E. (2012), Magnetic nanoparticles with an imprinted polymer coating for the selective extraction of uranyl ions, *Microchimica Acta*, **178**, pp. 89-97.

Sadeghi, S. and Mofrad, A.A. (2007), Synthesis of a new ion imprinted polymer material for separation and preconcentration of traces of uranyl ions, *Reactive & Functional Polymers*, **67**, pp. 966-976.

Sandino, A. and Bruno, J. (1992), The solubility of $(UO_2)_3(PO_4)_2 \cdot 4H_2O(s)$ and the formation of U(VI) phospate complexes: Their influence in uranium speciation in natural waters, *Geochimica et Cosmochimica Acta*, **56**, pp. 4135-4145.

Sanga, Y., Lib, F., Gub, Q., Lianga, C. and Chena, J. (2008), Heavy metal-contaminated groundwater treatment by a novel nanofiber membrane, *Desalination*, **223**, pp. 349-360.

Sarangi, A.K. and Beri, K.K. (2000), Uranium mining by *in-situ* leaching. Presented and published in the proceedings of the International conference on "Technology management for mining, processing and environment", IIT, Kharagpur.

Say, R., Birlik, E., Ersöz, A., Yılmaz, F., Gedikbey, T. and Denizli, A. (2003), Preconcentration of copper ion-selective imprinted polymer microbeads, *Analytica Chimica Acta*, **480**, pp. 251-258.

Scheinost, A.C., Chavernas, A., Barron, V. and Torrent, J. (1998), Use and limitations of second-derivative diffuse reflectance spectroscopy in the visible to near infrared range to identify and quantify Fe oxide minerals in soils, *Clays and Clay Minerals*, **46**, pp. 528-536.

Schmidt, A.M. (2007), Thermoresponsive magnetic colloids, *Colloid and Polymer Science*, **285**, pp. 953-966.

Scorrano, S., Mergola, L., Sole, R.D. and Vasapollo, G. (2011), Synthesis of Molecularly Imprinted Polymers for Amino Acid Derivates by Using Different Functional Monomers, *International Journal of Molecular Sciences*, **12**, pp. 1735-1743.

Sellergre, B. (2003), Molecularly imprinted polymers man-made mimics of antibodies and their applications in analytical chemistry, second edition, *Elsevier Science B.V*, pp. 23-24.

Sellergren, B. and Allender, C.J. (2005), Molecularly imprinted polymers: A bridge advanced drug delivery, *Advanced Drug Delivery Reviews*, **57**, pp. 1733-1741.

Shaw, R.R. and Heasley, J.H. (1967), Superparamagnetic Behavior of $MnFe_2O_4$, and α-Fe_2O_3, Precipitated from Silicate Melts, *Journal of The American Ceramic Society*, **50**, pp. 297-302.

She, Y., Cao, W., Shi, X., Lv, X., Liu, J., Wang, R., Jin, F., Wang, J. and Xiao, H. (2010), Class-specific molecularly imprinted polymers for the selective extraction and determination of sulfonylurea herbicides in maize samples by high performance liquid chromatography–tandem mass spectrometry, *Journal of Chromatography B*, **878**, pp. 2047-2053.

Sherrington, D.C. and Hodge, P. (1988), Syntheses and Sepm.ats Uartg Functional Polymers, John Wiley, New York.

Shevade, S. and Ford, R.G. (2004), Use of synthetic zeolites for arsenate removal from pollutant water, *Water Research*, **38**, pp. 3197-3204.

Shin, D.C., Kim, Y.S., Moon, J.Y., Park, H.S., Him, J.Y. and Park, S.K. (2002), International Trends in Risk Management of Groundwater Radionuclides, *Journal of Environmental Toxicology*, **17**, pp. 273-284.

Shoemaker, S.H., Greiner, J.F. and Gillham, R.W. (1995), Permeable Reactive Barriers, In Assessment of Barrier Containment Technologies (ed. Rumer, R.R. and Mitchell, J.K.), *National Technical Information Service*, pp. 301-353.

Shupack, S.1. (1991), The Chemistry of Chromium and Some Resulting Analytical Problems, *Environmental Health Perspectives*, **92**, pp. 7-11.

Sidhu, P.S. (1988), Transformation of trace element-substituted maghemite to hematite, *Clays and Clay Minerals*, **36**, pp. 31-38.

Singh, D.K. and Mishra, S. (2009), Synthesis and characterization of UO_2^{2+}-ion imprinted polymer for selective extraction of UO_2^{2+}, *Analytica Chimica Acta*, **644**, pp. 42-47.

Slavov, L., Abrashev, M.V., Merodiiska, T., Gelev, C., Vandenberghe, R.E., Markova-Deneva, I. and Nedkov, I. (2010), Raman spectroscopy investigation of magnetite nanoparticles in ferrofluids, *Journal of Magnetism and Magnetic Materials*, pp. 1-8.

Sonmez, H.B. and Bicak, N. (2002), Quaternization of poly(4-vinylpyridine) beads with 2-chloroacetamide for selective mercury extraction, *Reactive and Functional Polymers*, **51**, pp. 55-60.

Souag, R., Touaibia, D., Benayada, B. and Boucenna, A. (2009), Adsorption of Heavy Metals (Cd, Zn and Pb) from Water Using Keratin Powder Prepared from Algerian Sheep Hoofs, *European Journal of Scientific Research*, **35**, pp. 416-425.

Spivak, D.A. and Sibrian-Vazquez, M. (2002), Development of Improved Crosslinking Monomers for Molecularly Imprinted Materials, *Materials Research Society Symposium Proceedings*, **723**, pp. 1-7.

Sun, S., Zeng, H., Robinson, D.B., Raoux, S., Rice, P.M., Wang, S.X. and Li, G.J. (2003), *Journal of the American Chemical Society*, **126**, pp. 273-279.

Sun, Y., Duan, L., Guo, Z., DuanMu, Y., Ma, M., Xu, L., Zhang, Y. and Gu, N. (2005), An improved way to prepare superparamagnetic magnetite-silica core-shell nanoparticles for possible biological application, *Journal of Magnetism and Magnetic Materials*, **285**, pp. 65-70.

Superparamagnetism, Available from: http://en.wikipedia.org/wiki/Superparamagnetism, Accessed on 17/09/2010.

Tamami, B. and Kiasat, A.R. (1997), Synthesis and Application of Quaternized Polyvinylpyridine Supported Dichromate As a New Polymeric Oxidizing Agent, *Iranian Polymer Journal*, **6**, pp. 273-279.

Tang, J., Myers, M., Bosnick, K.A. and Brus, L.E. (2003), Magnetite Fe_3O_4 Nanocrystals, Spectroscopic Observation of Aqueous Oxidation Kinetics, *Journal of Physical Chemistry B*, **107**, pp. 7501-7506.

Tartaj, P., Morales, M., Veintemillas-Verdaguer, S., Gonźalez-Carreno, T. and Serna, C.J. (2003), The preparation of magnetic nanoparticles for applications in biomedicine, *Journal of Physics D: Applied Physics*, **36**, pp. R182-R197.

Teprat, O., Vercouter, T., Ansobotlo, E., Fichet, P., Perret, P., Kurttio, P. and Salonen, L. (2009), Uranium Speciation in Drinking Water from Drilled Wells in Southern Finland and Its Potential Links to Health Effects, *Environmental Science and Technology*, **43**, pp. 3941-3946.

Thompson, G., Swain, J., Kay, M. and Forster, C.F. (2001), The treatment of pulp and paper mill effluent: a review, *Bioresource Technology*, **77**, pp. 275-286.

Thorek, D.L.J., Chen, A.K., Czupryna, J. and Tsourkas, A. (2006), Superparamagnetic Iron Oxide Nanoparticle Probes for Molecular Imaging, *Annals of Biomedical Engineering*, **34**, pp. 23-38.

Todorov, P. and Ilieva, E.N. (2004), Contamination with uranium from natural and anthropological sources, *Romanian Journal of Physics*, **51**, pp. 27-34.

Togashi, T., Takami, S., Kawakami, K., Yamamoto, H., Naka, T., Sato, K., Abe, K. and Adschiri, T. (2012), Continuous hydrothermal synthesis of 3,4-dihydroxyhydrocinnamic acid-modified magnetite nanoparticles with stealth-functionality against immunological response, *Journal of Materials Chemistry*, **22**, pp. 9041-9045.

Toral, M.I., González-Navarrete, J., Leiva, A., Ríos, H.E. and Urzúa, M.D. (2009), Chromium retention properties of N-alkyl quaternized poly(4-vinylpyridine), *European Polymer Journal*, **45**, pp. 730-737.

Torrent, J. and Barron, V. Diffuse reflectance spectroscopy of iron oxides.

Treyball, R.E. (1980), Mass transfer operations. 3rd ed, McGraw Hill, New York

Tsukagoshi, K., Yu, K.Y., Maeda, M. and Takagi, M. (1993), Metal Ion-Selective Adsorbent Prepared by Surface-Imprinting Polymerization, *Bulletin of the Chemical Society of Japan*, **66**, pp. 114-120.

Tsukagoshi, K., Yu, K.Y., Maeda, M., Takagi, M. and Miyajima, T. (19950), Surface Imprinting. Characterization of a Latex Resin and the Origin of the Imprinting Effect, *Bulletin of the Chemical Society of Japan*, **68**, pp. 3095-3103.

Tulla-Puche, J. and Albericio, F. (2008), The Power of Functional Resins in Organic Synthesis, Wiley-VCH Verlag GmbH and Co. KGaA, Weinheim, pp. 19.

Turiel, E. and Martín-Esteban, A. (2010), Molecularly imprinted polymers for sample preparation: A review, *Analytica Chimica Acta*, **668**, pp. 8799.

Udy, M.J. (1956), Chromium: Chemistry of Chromium and its Compounds, **1**, Reinhold Publishing Corporation, New York; Chapman & Hall Ltd. London.

Uezu, K., Goto, M. and Nakashio, F. (1998), Metal Ion-Imprinted Polymers Prepared by Surface Template Polymerization with Water-in-Oil Emulsions, Chapter 19, in *Molecular and Ionic Recognition with Imprinted Polymers*, pp. 278-289.

UNSCEAR (United Nations Scientific Committee on the Effects of Atomic Radiation). 1993, Report to the General Assembly, with scientific annexes, New York.

Uranium, Available from: http://en.wikipedia.org/wiki/Uranium, Accessed on 15/02/2012.

Uranium-U, Available from: http://www.lenntech.com/periodic/elements/u.htm#ixzz1q7U9leJL, Accessed on 06/09/2011.

Uranium Heap Leaching, (2011), Available from: http://www.wise-uranium.org/uhl.html, Accessed on 11/11/2011.

U.S. DOE. (1999), From Cleanup to Stewardship. U.S. D.O.E. Office Environ. Management.

US EPA, (1999), National Primary Drinking Water Regulation: Radon-222: Proposed Rule.

Voit, W., Kim, D.K., Zapka, W., Muhammed, M. and Rao, K.V. (2001), Magnetic behaviour of coated superparamagnetic iron oxide nanoparticles in ferrofluids, *Materials Research Society*, **676**, pp. Y7.8.1- Y7.8.6.

Wang, J., Bao, Z., Chen, S. and Yang, J. (2011), Removal of Uranium From Aqueous Solution by Chitosan and Ferrous Ions, *Journal of Engineering for Gas Turbines and Power*, **133**, pp. 1-3.

Wang, J., Peng, R., Yang, J., He, Q. and Liu, Y. (2011) Selective Adsorption of Uranium(VI) on U(VI) Ion-Imprinted Chitosan Composite Magnetic Microsphers, Computer Distributed Control and Intelligent Environmental Monitoring (CDCIEM), International Conference, pp. 1714-1717.

Wang, L.K., Tay, J., Tay, S.T.L. and Hung, Y. (2010), Handbook of Environmental engineering, Environmental Bioengineering, *Hamana Press*, **11**, pp. 377-379.

Wang, X.B., Zheng, Z.H., Ding, X.B., Cheng, X., Hu, X.H. and Peng, Y.X. (2006), Synthesis of Molecularly Imprinted Polymer Particles by Suspension Polymerization in Silicon Oil, *Chinese Chemical Letters*, **17**, pp. 1243-1246.

Wang, Y., Alsmeyer, D.C. and McCreery, R.L. (1990), Raman Spectroscopy of Carbon Materials: Structural Basis of Observed Spectra, *Chemistry of Materials*, **2**, pp. 557-563.

Wang, Q., Guan, Y., Liu, X., Ren, X. and Yang, M. (2012), High-capacity adsorption of hexavalent chromium from aqueous solution using magnetic microspheres by surface dendrimer graft modification, *Journal of Colloid and Interface Science*, **375**, pp. 160-166.

Weerasinghe, A., Ariyawnasa, S. and Weerasooriya, R. (2008), Phyto-remediation potential of Ipomoea aquatica for Cr(VI) mitigation, *Chemosphere*, **30**, pp. 521-524.

WHO, (2001), Depleted Uranium, Sources, Exposure and Health Effects, WHO, Geneva.

Wojtówicz, A. and Stokłosa, A. (2002), Removal of Heavy Metal Ions on Smectite Ion-Exchange Column, *Polish Journal of Environmental Studies*, **11**, pp. 97-101.

World Supply of Uranium,
Available on: www.purepoint.ca/abouturanium/worldsupply.php, Accessed on 04/11/2012.

Wu, G., Wang, G., Wang, J. and He, C. (2007), Hierarchically imprinted organic-inorganic hybrid sorbent for selective separation of mercury ion from aqueous solution, *Analytica Chimica Acta*, **582**, pp. 304-310.

Yang, C., Xing, J., Guan, Y., Liu, J. and Liu, H. (2004), Synthesis and characterization of superparamagnetic iron nanocomposites by hydrazine reduction, *Journal of Alloys and Compounds*, **385**, pp. 283-287.

Yao , X., Fu, Z., Zhao, Y., Wang, L., Fang, L. and Shen, H. (2012) Use of tetraethylenepentamine-functional Fe_3O_4 magnetic polymers for matrix solid

phase dispersion extraction and preconcentration of Cr(VI) in water samples at ultratrace levels, *Talanta*, **97**, pp. 124-130.

Ying, W.C., Dietz, E.A. and Woehr, G.C. (1990), Adsorptive capacities of activated carbon for organic constituents of waste waters, *Environmental Progress*, **9**, pp. 1-9.

Yoshizako, K., Hosoya, K., Iwakoshi, Y., Kimata, K. and Tanaka, N. (1998), Porogen Imprinting Effects, *Analytica Chimica Acta*, **70**, pp. 386-389.

Yu, J.C.C. and Lai, E.P.C. (2010), Molecularly Imprinted Polymers for Ochratoxin A Extraction and Analysis, *Toxins*, **2**, pp. 1536-1553.

Yue, Z., Bender, S.E., Wang, J. and Economy, J. (2009), Removal of chromium Cr(VI) by low-cost chemically activated carbon materials from water *Journal of Hazardous Materials*, **166**, pp. 74-78.

Zaheri, A., Moheb, A., Keshtkar, A.R. and Shirani, A.S. (2010), Uranium Seperation from Wastewater by Electrodialysis, *Iranian Journal of Environmental Health, Science and Engineering*, **7**, pp. 429-436.

Zeinali, F., Ghoreyshi, A.A. and Najafpour, G.D. (2010), Adsorption of Dichloromethane from Aqueous Phase Using Granular Activated Carbon: Isotherm and Breakthrough Curve Measurements, *Middle-East Journal of Scientific Research*, **5**, pp. 191-198.

Zhan, Y., Luo, X., Nie, S., Huang, Y., Tu, X. and Luo, S. (2011), Selective Separation of Cu (II) from Aqueous Solution with a Novel Cu (II) Surface Magnetic Ion-Imprinted Polymers, *Industrial and Engineering Chemistry Research*, **50**, pp. 6355-6361.

Zhang, X., Jiao, C., Wang, J., Liu, Q., Li, R., Yang, P. and Zhang, M. (2012), Removal of uranium(VI) from aqueous solutions by magnetic Schiff base: Kinetic and thermodynamic investigation, *Chemical Engineering Journal*, **198-199**, pp. 412-419.

Zhang, Y., Song, D., Lanni, L.M. and Shimizu, K.D. (2010), Importance of Functional Monomer Dimerization in the Molecular Imprinting Process, *Macromolecules*, **43**, pp. 6284-6294.

Zhao, D., SenGupta, A.K. and Stewart, L. (1998), Selective removal of Cr VI) oxyanions with a new anion exchanger, *Industrial and Engineering Chemistry research*, **37**, pp. 4383-4387.

Zhao, W.H., Sheng, N., Zhu, R., Wei, F.D., Cai, Z., Zhai, M.J., Du, S.H. and Hu, Q. (2010), Preparation of dummy template imprinted polymers at surface of silica microparticles for the selective extraction of trace bisphenol A from water samples, *Journal of Hazardous Materials*, **179**, pp. 223-229.

Zhao, Y.G., Shen, H.Y, Pan, S.D and Hu, M.Q (2010), Synthesis, characterization and properties of ethylenediamine-functionalized Fe_3O_4 magnetic polymers for removal of Cr(VI) in wastewater, *Journal of Hazardous Materials*, **182,** pp. 295-302.

Zhu, X., Cui, Y., Chang, X., Zou, X. and Li, Z. (2009), Selective solid-phase extraction of lead(II) from biological and natural water samples using surface-grafted lead(II)-imprinted polymers, *Microchimica Acta*, **164**, pp. 125-132.

Appendix

A.1 Calculation of the amount of γ-MPS on the surface of the magnetite using CHNS Analysis

Mass of the sample = 2 mg

C in the sample = 20.16%

Mass of carbon in the sample = 20.16% x 2

= 0.4032 mg

$$\text{Ligand concentration} = \frac{(0.4032 \times 10^{-3})}{12}$$

= 3.36 x 10^{-5} moles (in 2 mg-sample)

$$\text{Ligand concentration per g} = \frac{(3.36 \times 10^{-5})}{(2 \times 10^{-3})}$$

= 16.8 mmol C g^{-1}

The three other values for the ligand concentration per gram were similarily calculated and the values were both 15.8 mmol C g^{-1}.

Ligand concentration = (11) x (16.1)

= 177.1 mmol H g^{-1}

Mass of H per g = (177.1) x (1)

= 177.1 mg H g^{-1}

= 17.71%

A.2 Calculation of the amount of OA on the surface of the magnetite using CHNS Analysis

Mass of the sample = 2.05 mg

% C in the sample = 4.627%

Mass of carbon in the sample = 4.627% x 2.05

= 0.9485 mg

Ligand concentration $= \frac{(0.9485 \times 10^{-3})}{12}$

= 7.9 x 10^{-5} moles (in 2 mg-sample)

Ligand concentration per g $= \frac{(7.9 \times 10^{-5})}{(2.05 \times 10^{-3})}$

= 38.1 mmol C g^{-1}

Ligand concentration = (33) x (3.85)

= 42.35 mmol H g^{-1}

Mass of H per g = (42.35) x (1)

= 42.35 mg H g^{-1}

= 4.24%

A.3 PXRD analysis: Particle size analysis

$$\bar{D} = \frac{57.3 \cdot k \cdot \lambda}{\beta \cos\theta}$$

$$= \frac{57.3 \cdot k \cdot \lambda}{\beta \cos\theta}$$

$$= \frac{(57.3)(0.9)(1.5418)}{(0.7)(\cos 17.5)}$$

= 119.1 Å

= 11.9 nm

A.4 TEM micrograms of the uncoated and coated γ-MPS-magnetite

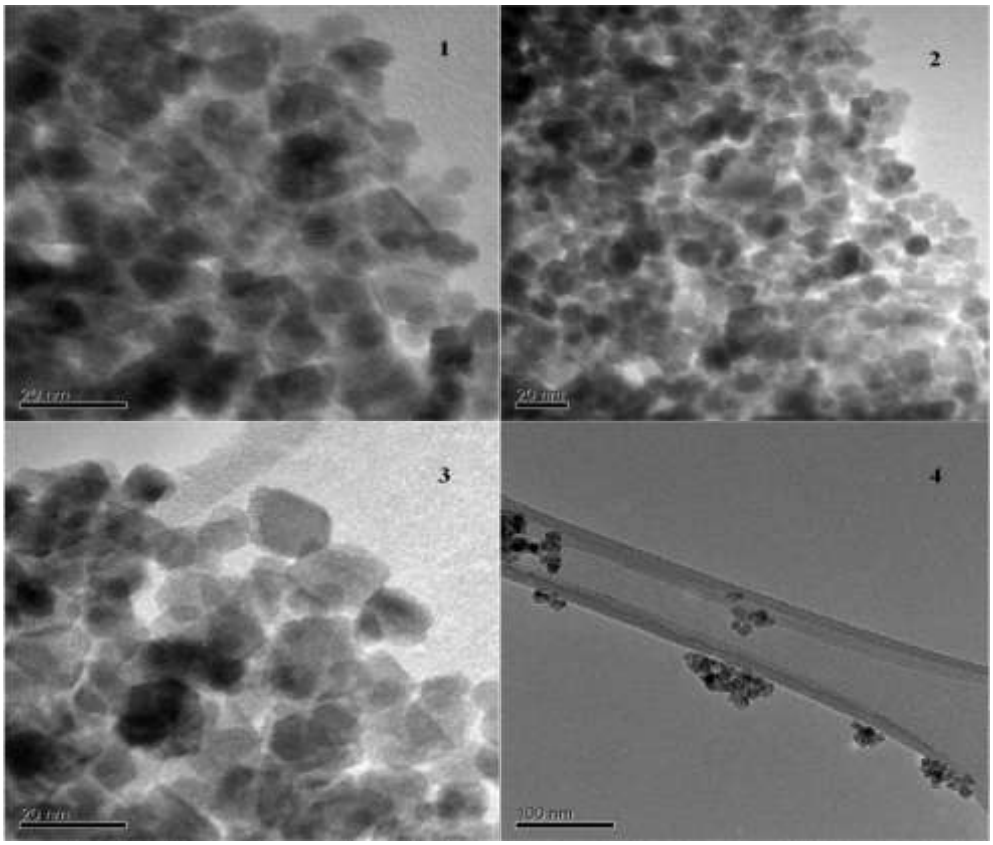


Figure A1: TEM micrograms of the uncoated magnetite

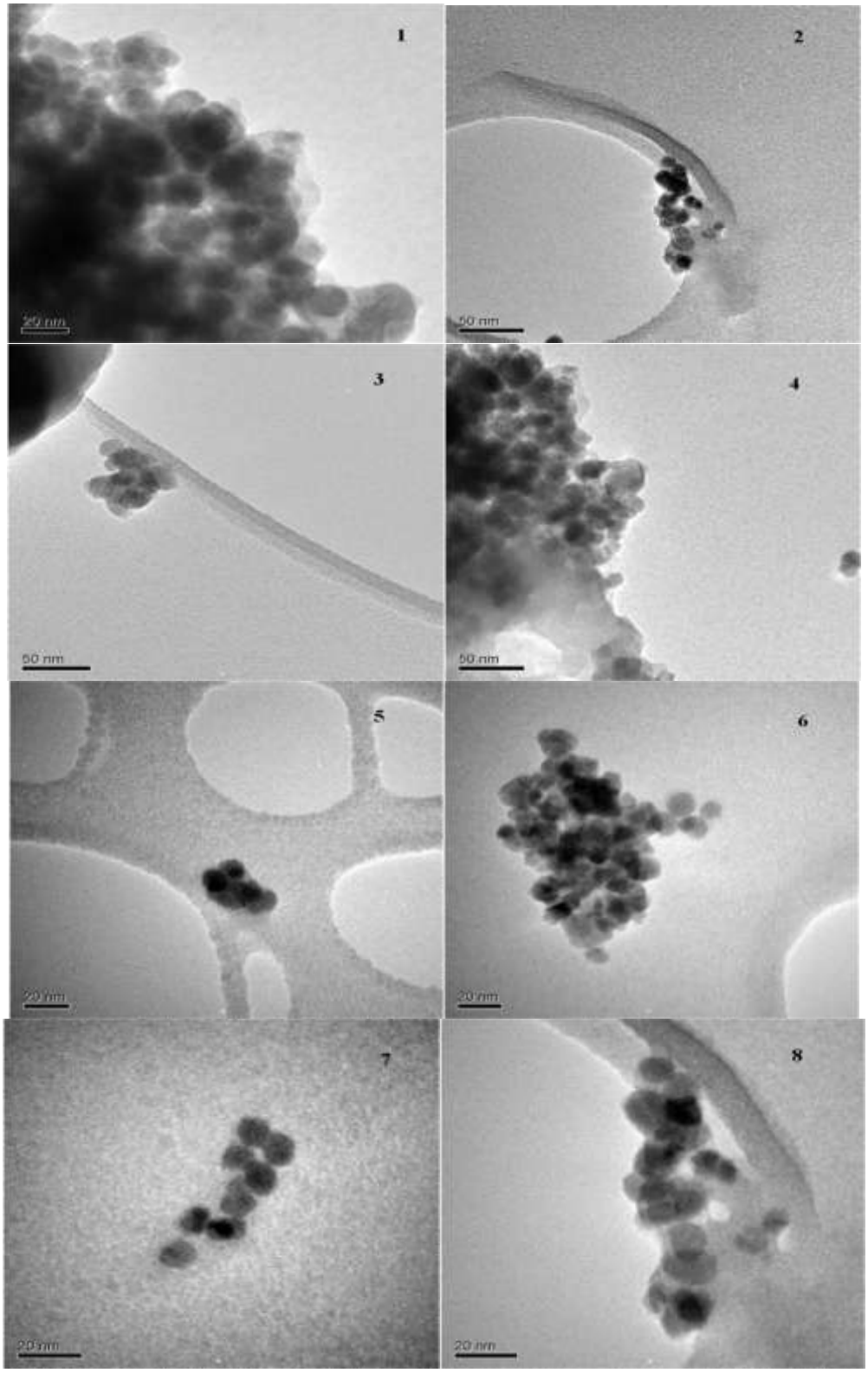


Figure A2: TEM micrograms of the coated γ-MPS-magnetite